

9-2013

# Discriminatory Bio-Adhesion Over Nano-Patterned Polymer Brushes

Saugata Gon

University of Massachusetts Amherst, saugata.gon@gmail.com

Follow this and additional works at: [https://scholarworks.umass.edu/open\\_access\\_dissertations](https://scholarworks.umass.edu/open_access_dissertations)



Part of the [Biomedical Engineering and Bioengineering Commons](#), [Chemical Engineering Commons](#), and the [Nanoscience and Nanotechnology Commons](#)

---

## Recommended Citation

Gon, Saugata, "Discriminatory Bio-Adhesion Over Nano-Patterned Polymer Brushes" (2013). *Open Access Dissertations*. 796.  
<https://doi.org/10.7275/fxcc-ec94> [https://scholarworks.umass.edu/open\\_access\\_dissertations/796](https://scholarworks.umass.edu/open_access_dissertations/796)

This Open Access Dissertation is brought to you for free and open access by ScholarWorks@UMass Amherst. It has been accepted for inclusion in Open Access Dissertations by an authorized administrator of ScholarWorks@UMass Amherst. For more information, please contact [scholarworks@library.umass.edu](mailto:scholarworks@library.umass.edu).

# **DISCRIMINATORY BIO-ADHESION OVER NANO-PATTERNED POLYMER BRUSHES**

A Dissertation Presented  
by  
**SAUGATA GON**

Submitted to the Graduate School of the  
University of Massachusetts Amherst in partial fulfillment of the  
requirement for the degree of

**DOCTOR OF PHILOSOPHY**

September 2013  
Department of Chemical Engineering

© Copyright by Saugata Gon 2013  
All Rights Reserved

# **DISCRIMINATORY BIO-ADHESION OVER NANO-PATTERNED POLYMER BRUSHES**

A Dissertation Presented

by

**SAUGATA GON**

Approved as to style and content by:

---

Maria M. Santore, Chair

---

Jeffrey M. Davis, Member

---

David M. Ford, Member

---

Harry Bermudez, Member

---

T. J. Mountziaris, Department Head  
Department of Chemical Engineering.

# **DEDICATION**

To my wife and my family members.

# ACKNOWLEDGEMENTS

It was a great experience working in the Santore lab at the PSE department at UMass Amherst. The work done in this thesis would not have been possible without active support and guidance by my advisor Prof. Maria M. Santore. Whenever I had any questions or needed anything in the lab I could just walk into her office and she was always there to help me out. I do not have enough words to thank her and I would not try it here.

Another person who helped me getting here today is Prof. Lakis Mountziaris, the departmental head of the Chemical Engineering dept. I would like to take this opportunity to thank Prof. Mountziaris for his encouraging advice and suggestions which were really helpful.

I want to thank the group members in the Santore group in Polymer Science and the Davis group in Chemical Engineering department. Their help, suggestions and friendship were instrumental in achieving the goal for this PhD thesis.

Next in the thank list are my friends in Amherst and in India. Without their presence and support this journey would have been really a boring one.

The support and company of my wife Somdatta throughout this journey made it a really enjoyable one. Her presence always motivated me to work harder and that made this goal reachable. At last I would like to mention about my parents, my brother, nephew, sister in law and all my family members in India whose caring words and faith in me helped me to reach the finish-line finally.

# **ABSTRACT**

## **DISCRIMINATORY BIO-ADHESION OVER NANO- PATTERNED POLYMER BRUSHES**

**SEPTEMBER 2013**

**SAUGATA GON, B. TECH. HIT INDIA**

**M.TECH., IIT BOMBAY, INDIA**

**M.S., UNIVERSITY OF MASSACHUSETTS AMHERST**

**PhD., UNIVERSITY OF MASSACHUSETTS AMHERST**

Directed by Professor Maria M. Santore

Surfaces functionalized with bio-molecular targeting agents are conventionally used for highly-specific protein and cell adhesion. This thesis explores an alternative approach: Small non-biological adhesive elements are placed on a surface randomly, with the rest of the surface rendered repulsive towards biomolecules and cells. While the adhesive elements themselves, for instance in solution, typically exhibit no selectivity for various compounds within an analyte suspension, selective adhesion of targeted objects or molecules results from their placement on the repulsive surface. The mechanism of selectivity relies on recognition of length scales of the surface distribution of adhesive elements relative to species in the analyte solution, along with the competition between attractions and repulsions between various species in the suspension and different parts of

the collecting surface. The resulting binding selectivity can be exquisitely sharp; however, complex mixtures generally require the use of multiple surfaces to isolate the various species: Different components will be adhered, sharply, with changes in collector composition. The key feature of these surface designs is their lack of reliance on biomolecular fragments for specificity, focusing entirely on physicochemical principles at the lengthscales from 1 – 100 nm. This, along with a lack of formal patterning, provides the advantages of simplicity and cost effectiveness.

This PhD thesis demonstrates these principles using a system in which cationic poly-L-lysine (PLL) patches (10 nm) are deposited randomly on a silica substrate and the remaining surface is passivated with a bio-compatible PEG brush. TIRF microscopy revealed that the patches were randomly arranged, not clustered. By precisely controlling the number of patches per unit area, the interfaces provide sharp selectivity for adhesion of proteins and bacterial cells. For instance, it was found that a critical density of patches (on the order of  $1000/\mu\text{m}^2$ ) was required for fibrinogen adsorption while a greater density comprised the adhesion threshold for albumin. Surface compositions between these two thresholds discriminated binding of the two proteins. The binding behavior of the two proteins from a mixture was well anticipated by the single- protein binding behaviors of the individual proteins.

The mechanism for protein capture was shown to be multivalent: protein adhesion always occurred for averages spacings of the adhesive patches smaller than the dimensions of the protein of interest. For some backfill brush architectures, the spacing between the patches at the threshold for protein capture clearly corresponded to the major dimension of the target protein. For more dense PEG brush backfills however, larger



adhesion thresholds were observed, corresponding to greater numbers of patches involved with the adhesion of each protein molecule. . The thesis demonstrates the tuning of the position of the adhesion thresholds, using fibrinogen as a model protein, using variations in brush properties and ionic strength. The directions of the trends indicate that the brushes do indeed exert steric repulsions toward the proteins while the attractions are electrostatic in nature.

The surfaces also demonstrated sharp adhesion thresholds for *S. Aureus* bacteria, at smaller concentrations of adhesive surfaces elements than those needed for the protein capture. The results suggest that bacteria may be captured while proteins are rejected from these surfaces, and there may be potential to discriminate different bacterial types. Such discrimination from protein-containing bacterial suspensions was investigated briefly in this thesis using *S. Aureus* and fibrinogen as a model mixture. However, due to binding of fibrinogen to the bacterial surface, the separation did not succeed. It is still expected, however, that these surfaces could be used to selectively capture bacteria in the presence of non-interacting proteins.

The interaction of these brushes with two different cationic species PLL and lysozyme were studied. The thesis documents rapid and complete brush displacement by PLL, highlighting a major limitation of using such brushes in some applications. Also unanticipated, lysozyme, a small cationic protein, was found to adhere to the brushes in increasing amounts with the PEG content of the brush. This finding contradicts current understanding of protein-brush interactions that suggests increases in interfacial PEG content increase biocompatibility.

# TABLE OF CONTENTS

	<b>Page</b>
ABSTRACT.....	vi
LIST OF TABLES .....	xiii
LIST OF FIGURES .....	xiv
<b>CHAPTER</b>	
<b>1. INTRODUCTION .....</b>	<b>1</b>
1.1 Surface heterogeneity and its role in adhesion .....	1
1.1.1 Specific and nonspecific interaction .....	3
1.2 Adhesion on tunable surface patterns .....	4
1.3 Effect of flow on adhesion .....	8
1.4 Surface patterning methods.....	10
1.5 Motivation and objective .....	12
1.5.1 Thesis objective .....	13
1.6 Research strategy .....	13
1.7 Thesis overview .....	15
1.8 References.....	18
<b>2. ARCHITECTURE AND STABILITIES OF PLL-PEG BRUSHES: CASE STUDIES WITH CATIONIC AND ANIONIC PROTEINS AND A STRONG CATIONIC POLYELECTROLYTE PLL .....</b>	<b>28</b>
2.1 Introduction.....	28
2.2 Synthesis and characterization of brushes .....	30
2.2.1 Brush synthesis .....	30
2.2.2 Brush characterization using NMR.....	31
2.3 Experimental methodology.....	32
2.4 Results.....	34
2.4.1 Calculation of brush height.....	34
2.4.2 Interaction with globular proteins .....	37
2.4.3 Interaction with PLL.....	42
2.5 Discussion .....	48
2.6 Conclusions.....	52
2.7 References.....	54

<b>3 MANIPULATING PROTEIN ADSORPTION USING A PATCHY PEG BRUSH</b> ....	59
3.1 Introduction.....	59
3.2 Experimental Methodology .....	62
3.3 Results.....	64
3.3.1 Features of patchy brush # 1 surfaces .....	64
3.3.1.1 PLL patches .....	64
3.3.1.2 PLL-PEG brushes .....	71
3.3.1.3 Patchy brushes .....	71
3.3.2 Fibrinogen adsorption on patchy surfaces .....	73
3.4 Discussion .....	75
3.5 Conclusions.....	80
3.6 References.....	81
<b>4 SINGLE COMPONENT AND SELECTIVE COMPETITIVE PROTEIN ADSORPTION AND SEPARATION USING A PATCHY POLYMER BRUSH</b> .....	86
4.1 Introduction.....	86
4.2 Experimental Methodology .....	90
4.3 Results.....	91
4.3.1 Features of patchy brush # 1 surfaces .....	91
4.3.2 Patchy brush.....	95
4.3.3 Protein adsorption over patchy brushes .....	96
4.3.3.1 Comparison of fibrinogen, albumin and alkaline phosphatase adhesion .....	96
4.3.3.2 Comparison of myoglobin adhesion with other proteins .....	100
4.3.4 Protein separation.....	101
4.4 Discussion .....	105
4.5 Conclusions.....	109
4.6 References.....	111
<b>5 STUDYING BRUSH HEIGHTS, GRAFTING RATIO AND IONIC STRENGTH VARIATION ON PROTEIN ADHESIONS: A CASE STUDY WITH FIBRINOGEN</b> 116	
5.1 Introduction.....	116
5.2 Background on brush and strategy.....	119
5.3 Materials and methods .....	124
5.4 Results.....	125
5.5 Discussion .....	132

5.6 Summary .....	136
5.7 References.....	138
<b>6 BACTERIAL ADHESION OVER PATCHY BRUSHES: A CASE STUDY WITH <i>S. AUREUS</i></b> .....	<b>143</b>
6.1 Introduction.....	143
6.2 Materials and methods .....	147
6.3 Results.....	152
6.4 Discussion .....	155
6.4.1 Role of adhesive flaws on bacterial and protein adhesion .....	156
6.4.2 Impact of steric repulsion from brush architecture on bacteria .....	158
6.4.3 Steric interaction of brushes with proteins.....	162
6.5 Conclusions.....	165
6.6 References.....	167
<b>7 CONCLUSION AND FUTURE DIRECTION OF RESEARCH</b> .....	<b>173</b>
7.1 Conclusion .....	173
7.1.1 New concept of patchy brush.....	173
7.1.2 Brush stability analysis with protein and polyelectrolyte addition .....	174
7.1.3 Tuning size based protein adhesion .....	175
7.1.4 Tuning protein adhesion by controlling brush height density and ionic strengths of buffer solution .....	176
7.1.5 Tuning bacterial adhesion .....	176
7.2 Future direction.....	177
7.2.1 Generation of myoglobin detection sensor .....	177
7.2.2 Generation of smart surfaces to effectively capture and kill bacteria..	177
7.2.3 Capture of cells from media.....	178
7.2.4 Separating different bacteria and cells .....	178
7.3 References.....	180
 <b>APPENDICES</b>	
<b>A EFFECT OF GRAFTING RATIO ON PROTEIN ADHESION OVER BRUSH # 1...</b> .....	<b>181</b>
<b>B NMR DATA FOR BRUSH # 1, 2 AND 3</b> .....	<b>182</b>

BIBLIOGRAPHY .....185

## LIST OF TABLES

Table	Page
2.1 Molecular Properties of different brushes .....	32
2.2 Brush architecture and zeta potentials, $\zeta$ .....	36
2.3 Protein adsorption at $\kappa^{-1} = 2$ nm, pH 7.4 (R = substantially reversible adsorption, E = Exchange (displacement) of previously adsorbed brush .....	38
3.1 Properties of saturated PLL and PLL-PEG Brush # 1 .....	65
4.1 Properties of proteins .....	92
4.2 Properties of PLL and PLL-PEG layers in pH 7.4 phosphate buffer, I=0.026 M. ....	95
6.1 Brush architectures.....	150
6.2 Brush Features Relevant to Steric Repulsion of Bacteria and Protein.....	160

## LIST OF FIGURES

<b>Figures</b>	<b>Page</b>
1.1 Definition of zone of influence and its radius, $R_{zi}$ .....	6
2.1 Schematic of polymer brush .....	35
2.2 Structure of the PEG tethers within the three brushes, calculated according to the Alexander deGennes treatment, showing graft spacing or brush persistence length, equal to the “blob” size. ....	37
2.3 Protein repellence characteristics of PEG brushes.....	39
2.4: Lysozyme adsorption onto three brushes at pH 7.4 and $k-1 = 2$ nm, followed by rinsing, near 20 minutes. (Brush adsorption portion of each run is not shown.).....	39
2.5 Fibrinogen adsorption on brushes for different ionic strengths. ....	41
2.6 Adsorption and PLL challenge of Brush #1 in buffer with $k-1 = 2$ nm. The original brush is exposed to 100 ppm albumin before and after the PLL challenge, using 100 ppm PLL solution.....	43
2.7 Adsorption of fluorescently labeled PLL, measured by TIRF onto a bare silica surface, and during the challenge of Brush #1. ....	43
2.8 Adsorption of fluorescent PLL on silica and during challenge experiments for three brushes .....	44
2.9 Close up of overshoot portion of reflectometry runs in which PLL challenges pre-adsorbed PLL-PEG brushes. ....	45
2.10: Amount of PLL-PEG adsorbing to silica after adsorption of small amounts of PLL, on the x-axis.....	46
2.11 Full reflectometry traces of runs in which PLL-PEG brushes are challenged by 100 ppm PLL solutions in buffer having $k-1 = 2$ nm.....	47
2.12 Mass decrease during PLL-challenge of the three brushes. Examining relaxation timescales.....	48
3.1 Schematic of patchy brush .....	61
3.2 Features of different interfacial brush components .....	66
3.3 TIRF microscopy images of PLL patches: Comparison of experimental data with theoretical calculations.....	69
3.4 Controlled PLL deposition to make cationic patches. ....	70
3.5 TIRF experiment for the adsorption of fluorescently-labeled PLL .....	70
3.6 Coverage of PLL-PEG and Fibrinogen over patchy brush.....	74
3.7 Summary of the impact of PLL patch density on (A) amount of PLL-PEG backfill (B) short term fibrinogen coverage and (C) initial fibrinogen adsorption rate. ....	76
4.1 Adsorption of bigger proteins over A) PLL saturated silica B) bare silica .....	93

4.2 Myoglobin adsorption over bare silica (glass) and PLL saturated layer .....	94
4.3 Example reflectometry data showing (A) albumin and (B) alkaline phosphatase adsorption traces on to surfaces having variations in the surface loading of cationic patches.....	97
4.4 Summary of protein (A) adsorbed amounts and (B) initial adsorption kinetics, as a function of the surface loading of PLL patches. ....	99
4.5 Comparison of myoglobin adhesion threshold with other proteins. ....	100
4.6 Adsorption kinetic traces for a mixture of fluorescent-albumin and untagged fibrinogen on a selective surface carrying 3400 PLL patches / $\mu\text{m}^2$ . ....	103
4.7 Adsorption kinetic traces measured by TIRF (sees only fluorescent albumin) for a mixture of fluorescent-albumin and untagged fibrinogen. A selective surface carrying 3400 PLL patches / $\mu\text{m}^2$ is compared to a non-selective control surface carrying 8000 PLL patches / $\mu\text{m}^2$ .....	103
4.8 Studies on a non-selective adhesive PLL surface: single protein solution adsorption (at 100 ppm protein) versus simultaneous co-adsorption of two proteins (each at 100 ppm) in a mixture.....	104
4.9 Possible near-patch brush structure. (A) Isolated versus (B) nearby patches.....	108
5.1 Schematics of different PEG brush structures. ....	121
5.2 Amount of PLL-PEG copolymer adsorbed against PLL patches .....	123
5.3 Reflectometry traces for fibrinogen adsorption over patchy Brush # 2 at 2 nm Debye length buffer strength .....	126
5.4 Summary of initial fibrinogen adsorption rates, comparing adsorption at different Debye lengths, for the three brushes in parts A, B, C.....	127
5.5 Summary of different adsorption rates focusing on different brush architecture for different Debye lengths in the different parts of the figure .....	130
5.6 Impact of Debye length on the adhesion thresholds for 20 k PLL patches in the three brushes .....	131
5.7 Adhesion threshold as a function of (A) the PEG content of the patchy brushes (B) the corrected brush height, (C) as a function of persistence length based on the backfill as shown in figure 5.2Abstract.....	133
6.1 Figure 6.1 The effect of the molecular weight of the PLL patches in Brush #2 on the bacterial capture efficiency, for 20,000 (gray diamonds) and 50,000 (black squares) PLL, plotted as a function of (A) patch number and (B) patch mass. ....	153
6.2 Figure 6.2 A) Bacterial capture efficiencies on three different brushes containing embedded 20,000 molecular weight poly-l-lysine patches. B) Fibrinogen adsorption on the same surfaces .....	154



6.3 Schematic of a bacteria contact with a patchy brush surface (A) defining the electrostatic interaction radius $r_f^{es}$ (B) defining the steric brushy interaction radius $r_p$ for brush height $h$ and brush compression $\delta$ .....	158
6.4 Side on fibrinogen adsorption, required for bridging multiple patches, likely requires brush penetration, especially because the narrow fibrinogen dimension is smaller than the brush height.....	163
A.1 Protein repellence for PLL-PEG with different grafting ratios .....	181
B.1 NMR data for Brush # 1 .....	182
B.2 NMR data for Brush # 2.....	183
B.3 NMR data for Brush # 3.....	184

# CHAPTER 1

## INTRODUCTION

Adhesion of proteins and cells on synthetic or biological surfaces is broadly assigned the term *bio-adhesion*. Depending on the application, it may be desirable or highly detrimental. While bio-adhesion can involve molecular adsorption or cell adhesion, it is generally accepted that protein adsorption is the precursor for cell adhesion.<sup>1</sup> Selective bio-adhesion on patterned surfaces has become a focus of scientific research due to its relevance in multiple areas such as bio-diagnostics, bio-sensor development, pharmaceutical separations, drug delivery, and tissue engineering.<sup>2-4</sup> Use of polymer coatings to facilitate selectivity (through elimination of non-specific adhesion) on synthetic surfaces is a common practice.<sup>5-10</sup> In most applications, however, selectivity is still accomplished through the incorporation of biomolecular fragments. This thesis addresses the use of nano-patterns within a bio-compatible polymer brush, to achieve bio-selectivity without incorporation of biomolecular fragments at the interface. The current chapter therefore presents a brief overview of bio-adhesion and its driving factors relevant to the development of entirely synthetic selective interfaces.

### 1.1 Surface heterogeneity and its role in adhesion

Most of the surfaces found in nature are chemically or topographically heterogeneous. This diversity can occur on the micron lengthscale, but often it is sub-micron. Heterogeneity contributes to colloidal forces and can often lead to adhesion in

unexpected circumstances: The presence of heterogeneities is well-established on minerals,<sup>11-14</sup> polymers,<sup>15-17</sup> and biological cells.<sup>18-21</sup> While some impurities on mineral surfaces are known to cause aggregation,<sup>22-25</sup> chemical heterogeneity in polymers can dominate the contact angle and wetting characteristics.<sup>26-28</sup>

Biological surfaces, especially those of cells are also heterogeneous. While spatial and temporal heterogeneity is observed in polysaccharides of plant cell walls,<sup>29-31</sup> the lipid rafts of biological membranes exemplify heterogeneous distributions of phospholipids and proteins.<sup>32-34</sup> Such compositional variations are hypothesized to be related to bio-functionality, for instance enhanced recognition specificity of targeting, or improved efficiency biochemical reactions initiating on a cell's surface. Separately, topographical features of bacteria can also be considered to constitute surface heterogeneity. For example, some bacteria have pili (protrusions as long as 100 nm that concentrate cell adhesion molecules on their tips) on the outer cell surface. Other bacteria, for instance *Escherichia coli*, have different net electrostatic charges on their sides versus on their poles.<sup>35-37</sup>

While it is not conventional to view the ligand-receptor interactions at on cellular surfaces as a heterogeneous component of surface forces, this classification is useful from the perspective of interfacial design. Colloidal interactions are classically described on planar or curved interfaces by a mean-field formalism. By contrast, the discrete nature of biomolecular interactions and the dependence of these interactions on the distributions of molecules over a surface gives results that fundamentally differ from a mean field approach. Important, then to the notion of developing synthetic surfaces with discrete

functionality is the fact that the receptor sites in cell membrane are of the order of couple of angstroms to a few nanometers in size.

### **1.1.1 Specific and Non-Specific Interactions**

Biological “binding” interactions are driven by bio-molecular recognition are typically referred to as *specific* interactions. While these interactions occur throughout cells, specific interactions occurring on the surfaces of cells are of central importance to the concepts developed in this thesis. Cell adhesion molecules (CAMs) on outer membranes of cells can provide specific binding capability to other cells or to the extracellular matrix. These specific binding interactions take place within the background field of other cell surface molecules, including glycoproteins.<sup>38</sup> Important examples include the RGD-integrin interaction for adhesion of different cells to the extracellular matrix.<sup>39</sup> This usually constitutes fairly strong bonds that are irreversible on short timescales. By contrast, lectin-selectin associations between white blood cells and the vascular endothelium are weak and reverse rapidly, facilitating cell rolling.<sup>40</sup> Another important interaction, extreme in its binding tightness, is the biotin-streptavidin interaction,<sup>41</sup> often used as a building block for bio-molecular presentation and structures. While the biotin-streptavidin interaction has the capacity for specificity, the specificity is often undermined by hydrogen bonding interactions between the avidin and other species, necessitating the use of modified avidins and creating other technical challenges. Another workhorse of the bio-diagnostic and pharmaceutical industries is the interactions between antigens and antibodies.<sup>42</sup> Attached to surfaces, antibodies facilitate assays for molecular and cellular targets alike. Particularly in the case of cellular targets, other

interactions besides the antibody-antigen interaction must be accounted for in the design of the diagnostic device. In both cases, though, it is critical to eliminate non-specific interactions through sophisticated surface treatments of the materials involved.

Besides the specific bio-molecular interactions discussed above, non-specific forces such as van der Waals attractions, electrostatic interactions, hydrophobic interactions, and donor-acceptor interactions can also drive biological interactions or dominate specific bio-molecular interactions.<sup>38</sup> The relative strength and range of nonspecific interactions must be therefore be taken into account in biomaterial design. Even when non-specific interactions, such as electrostatic or van der Waals forces, are weak compared with those of bio-molecular origin, non-specific interactions may play the major role in the phenomena of interest. Indeed, this fact has led to the exploitation of electrostatic and steric interactions in the design and passivation of biomaterial interfaces. Conversely, the nonspecific interactions that tend to occur between biomolecules or cells and synthetic surfaces can overwhelm the intended specific interactions undercutting technological performance. For this reason, elimination of undesired non-specific interactions has been a major activity in the development of biomaterial surfaces.<sup>5-7, 9, 38, 42</sup> At the same time, it is interesting to note that in nature, these non-specific interactions are appropriately managed to maintain precisely-functioning surfaces and interfaces.

## 1.2 Adhesion on tunable surface patterns

Biological surfaces often interact through pattern recognition. This occurs on two lengthscales. At the angstrom-level, unique mating between complimentary functionality (hydrophobic, van der Waals, electrostatic, acid-base and polar) on opposing molecular surfaces produces the specificity of ligands and receptors such as the antibody-antigen interaction. On longer length scales, however, there is mounting evidence for additional pattern recognition-type mechanisms that are related to sophisticated bio-functionality. The organization of the cellular membrane into nanoscale rafts that concentrate functionality increases the binding affinity and avidity of the receptors involved. Spatial arrangements likewise are thought to affect cellular sensitivity to the concentrations of receptors on the surface of a partnering cell. These longer-lengthscale pattern recognition behaviors are critical to cell signaling and are potentially recreated in synthetic systems that achieve patterning on nanoscopic lengths scales. This thesis extends early work on this concept, developed previously in the Santore lab for non-biological systems,<sup>43-50</sup> to the bio-arena.

Kozlova and Santore<sup>49</sup> introduced a simple system consisting of a silica surface onto which cationic PDMAEMA (poly dimethylaminoethyl methacrylate) polymer coils, of the order of 10 nm in size, were irreversibly (on experimental timescales) and randomly adsorbed. These patchy collectors, when exposed to freely-flowing silica microparticles, showed distinct adhesion thresholds, a critical density of patches needed to capture the microparticles. It was noted that the silica particles adhered substantially to the heterogeneous collectors when their average charge was negative, contrary to

expectations from classical DLVO theory. The obvious explanation was that the patches formed localized attractive areas for silica particles, despite the repulsive background and the average repulsive character of the collector surface. Kozlova and Santore<sup>49</sup> reported the dependence of microparticle adhesion on the average patch spacing. A key concept, “the zone of influence,” was established as the amount of lateral area seen by the approaching particles. The zone of influence was calculated as a function of the particle size and the Debye length of the solution. Figure 1.1 illustrates the zone of influence as described by Kozlova and Santore.<sup>49</sup>

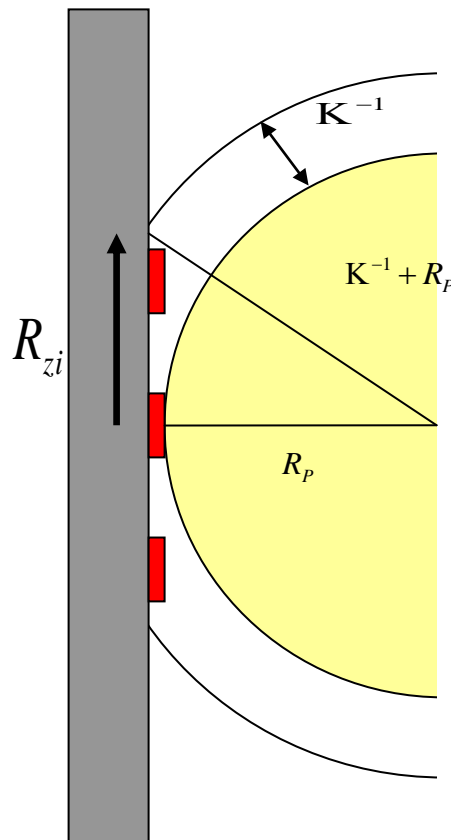


Figure 1.1 Definition of zone of influence and its radius,  $R_{zi}$ . The sphere radius is  $R_p$  and the Debye length is  $\kappa^{-1}$ .  $R_{zi}$  is calculated according to right triangles.

Critical to the design of these collectors were length scales intrinsic to their functionality, despite the random distribution of the patches. This was evident in the observation that as the average patch spacing approach the radius of the zone of influence, the capture rate of the spheres become significant. The effect of the spatial distribution of patches on the capture rate of silica particles, established by Kozlova and Santore,<sup>49</sup> was further extended to a demonstration of particle separation. Different collector surfaces targeting different elements within an analyte solution (each with its own contact length scale for interactions with the collector) could be sharply separated. While Kozlova demonstrated a size and curvature specificity for collectors containing cationic pDMAEMA coils, the same principle was developed for nano-particle-containing collectors.<sup>51</sup> The idea is extended to biological targets in the current thesis, using surfaces specifically designed to minimize non-specific attractions with biomolecule and cells.

Preceding the current thesis on abiotic surface designs for biological targeting, Kalasin in the Santore group extended the work of Kozlova and Santore<sup>49</sup> to a pilot study on bacterial (*S. aureus*) adhesion.<sup>44</sup> Here patchy surfaces with sparse cationic nano-functionality were created by randomly adsorbing small amounts of pDMAEMA on fully adsorbed layers of bovine serum albumin (BSA). The BSA was used to reduce non-specific bacteria adhesion, while PDMAEMA patches were used as the attractive zones. A key observation by Kalasin *et al.*<sup>44</sup> was engagement of multiple cationic patches to capture individual bacterial cells at an adhesion threshold. This multivalent capture of flowing objects was earlier reported for silica particles.<sup>49</sup> Manipulating electrostatic interactions, achieved by varying the ionic strength, enabled the position of the threshold



(the valency and the number density of pDMAEMA patches at the threshold) to be precisely tuned. The work was complimented by the studies of Fang *et al.*<sup>52</sup> that also demonstrated an effect of ionic strength on the adhesion threshold for bacterial capture, albeit in the opposite direction: moving from higher ionic strength to lower ionic strength increased the Debye length and the adhesive strength of the collector for *S. aureus* bacteria. These observations are put into perspective by the work of Bunt *et al.*<sup>53</sup> in which, in a different environment, *E.coli* adhesion in a hydrocarbon bath increased with increase in ionic strength. In the work of Fang, the bacteria surface interactions were dominated by bacterial attractions to cationic nanoparticles, giving a parallel effect. The ionic strength effect in Kalasin's system,<sup>44</sup> had the opposite effect due to domination of bacteria-surface interactions by the electrostatic repulsion with the albumin on the background surface. These differences emphasize the importance of the remainder of the surface in controlling seeming specific bacterial-surface interactions.

### **1.3 Effect of flow on adhesion**

Flow conditions have been found to strongly influence adhesion of particles, proteins, and cells. Klapper *et al.*<sup>54</sup> suggested that structure and performance of a biofilm formed by bacterial deposition can depend on shear stress. At higher shear stress the detachment force is greater and the number of adherent bacterial becomes smaller<sup>55-57</sup> as the detachment force overwhelms the adhesion. Separately, it was reported that increases in shear stress can make biofilms denser and thinner.<sup>58</sup> However contrary to common findings Nilsson *et al.*<sup>59</sup> reported that shear stress enhanced reduction of bacterial

detachment for the fimbrial FimH-mannose-mediated surface adhesion of *E. Coli*.<sup>60</sup> Shear is also expected to influence the adhesion of particles and cells exhibiting adhesion thresholds on heterogeneous collectors.

The influence of flow on adhesion in systems exhibiting a threshold in the density of adhesive surface elements can be complex. For a heterogeneously-charged surface with specific localized regions of attractive sites, the attractions between the patches and the analyte particles are opposed by hydrodynamic drag forces in addition to background repulsive surface forces. At the same time an increase in flow will increase the transport flux of the analyte particles towards the capturing surface and thereby increase the rate of capture.

Not surprisingly, therefore, two different regimes are observed for capture of particles on heterogeneous surfaces in a laminar flow cell, of the type commonly employed for adhesion studies. An increase in particle capture rate with increases in the surface loading of attractive elements is the hallmark of the surface-limited capture regime. Flow reduces the particle capture rate in this regime through its opposition to adhesive interactions. For surfaces containing more than a critical number of attractive elements (not to be confused with the formal adhesion threshold), the particle capture rate becomes insensitive to the surface features. This is the mass transport regime. For the laminar flow chambers employed for this thesis, the mass particle capture rate is described by the Leveque equation.

$$\frac{d\Gamma}{dt} = \frac{1}{\Gamma(4/3)9^{1/3}} \left( \frac{\gamma}{DL} \right)^{1/3} DC$$

Here,  $\frac{d\Gamma}{dt}$  is the capture rate,  $C$  is the bulk solution particle concentration,  $D$  is free solution particle diffusivity,  $L$  is the length from the solution inlet to the point of observation,  $\gamma$  is the wall shear rate.

At mass transport-limited conditions, the flow assists the capture. The critical number of patches where the particle capture switches from aid being aided by flow to being inhibited by flow was identified by Kalasin hydrodynamic crossover.<sup>46</sup> Kalasin and Santore demonstrated hydrodynamic cross over for silica particles with patchy silica surfaces. Notably, microparticle capture rates and crossovers corresponded almost exactly to similar crossover behavior reported by others for the capture of flowing *S. aureus* on collagen.<sup>61</sup> While the turnover in bacterial capture was attributed to complicated dynamic physics of the *S. aureus* receptor for collagen, the findings of Kalasin suggest a mere hydrodynamic crossover as the simpler explanation. The quantitative parallels also suggest similar binding energies and dynamics between the cationic surface elements in Kalasin's work and some biological adhesion molecules on cells, but in vitro.

## 1.4 Surface patterning methods

In order to create a patterned surface with functionality length scales similar to those on a cell surface, a common strategy has been to immobilize bio-specific capture molecules and to passivate rest of the surface. Surface modification can, itself, be a challenge and thus there exist diverse approaches, depending on the specific application. Surface functionalization is often coupled with patterning on the micron length scale,

including self-assembly,<sup>62, 63</sup> micro-contact printing,<sup>64-66</sup> or combined nano-imprint lithography and molecular self-assembly.<sup>67, 68</sup> Other than conventional UV-lithography, various nanofabrication procedures such as E-beam lithography, nano-imprint lithography, colloidal lithography, focused ion beam lithography etc. are being used to create surface patterns from a few micrometers to tens of nanometers. All these processes require multiple steps. They are all costly and time consuming and, even with these sophisticated approaches, reliably achieving sub-10 nm pattern length scales remains a challenge.

The primary motivation for micro- and nano- patterning is to create devices that screen for multiple targets on a single readable surface. Notably, the sophisticated recognition processes in biology, which go far beyond a simple yes-no readout of target adhesion, proceed without any regular patterning and exploit length scales intrinsic to the density of functionality on the cell surface.

Creation of cationic patchy surfaces based on deposition from dilute polycation solutions, for instance flowing past a silica surfaces inside a laminar chamber, (an approach developed in the Santore lab<sup>49</sup>), is used extensively in this thesis. The approach creates surfaces with controlled density of targeted functionality (and therefore precisely tuned surface length scales in the range 10-300 nm) relatively quickly and inexpensively. The adsorption approach lacks the ability to produce ordered arrays, which can be created through the methods discussed above. The order of the heterogeneous functionality turns out not to be entirely necessary for the biomimetic technological targets addressed here.

To reduce non-specific adhesion, coating the surface with a material that resists to bio-attachment is a critical step. Decades of fundamental and applied work have

advanced a variety of low fouling coatings, with none of them being entirely resistant to proteins and cells long term and under a variety of exposure and storage conditions. Most passivating materials are polymers that are non-ionic and hydrophilic.<sup>7</sup> Many are brush-like in nature, with chains end-tethered to the surface and solvation forces causing the chains to stretch normal to the surface several times their free solution diameter. “Polymer brushes,” a formal term in the polymer physics discipline, that can be used for surface passivation include polyvinyl alcohol (PVA),<sup>69</sup> polyacrylamide,<sup>70</sup> hyaluronic acid,<sup>71</sup> dextran,<sup>72</sup> polyethylene glycol (PEG).<sup>9, 73-75</sup> Also adsorption of bovine serum albumin and self-assembled monolayers of oligo(ethylene glycol) alkane thiols (EG-SAMs) have been reported for surface passivation.<sup>76-78</sup>

PEG in particular has garnered much interest among researchers because of its unique bio-compatibility. Immobilization of PEG on surfaces to reduce non-specific protein adhesion is a preferred approach. Incorporation of PEG into a copolymer with a second absorbing component is a common method to anchor PEG on a surface. Useful chemistries used for anchoring blocks include 3,4 dihydroxyphenylealanine (DOPA),<sup>73, 74</sup> poly propylene sulfide (PPS),<sup>79</sup> poly-L-lysine (PLL),<sup>80</sup> and poly-ethylene-imine (PEI),<sup>81</sup> depending on the substrate of interest.

## **1.5 Motivation and Objective**

The Santore group has conducted extensive studies that addressed the impact of various physical forces and sub-micron surface heterogeneity on particle adhesion. These studies laid the ground work for the current thesis. The limitation of the surfaces studied

by Kalasin *et al.*<sup>44-48</sup> was that they were not bio-compatible. Bare glass surfaces provided the background electrostatic repulsion forces needed for manipulation of negatively charged silica particle analytes, while a pilot study with BSA illustrated the possibilities for bacterial interaction through the reduction of non-specific interactions with *S. aureus*. At this point, the challenge remains to develop nano-patterned attractive moieties in a bio-compatible repulsive background. Additionally, a requirement is that the relative length scales of the attractive heterogeneous surface features should match the dimension of proteins and cells. These challenges form the subject of this thesis.

### **1.5.1 Thesis Objective**

Our aim in this research is to create biocompatible surfaces with well-characterized tunable attractive heterogeneities and to study the molecular interactions of proteins and cells with these collectors. A particular thrust is the development of highly selective surfaces that adhesively discriminate different proteins and cells in a mixture.

## **1.6 Research Strategy**

We have implemented a graft poly-ethylene glycol (PEG) poly-L-lysine (PLL-PEG) copolymer whose PEG side chains form a protein-repellant polymer brush. The steric interactions from this brush set up a conceptual parallel in this thesis with the electrostatic repulsions in the work of Kalasin. The use of PLL-PEG for surface passivation was first demonstrated by Sawhney and Hubbell.<sup>82</sup> X-ray photoelectron spectroscopy (XPS) by Huang *et al.*<sup>80</sup> suggested that, once PLL-PEG is exposed to metal

oxide surfaces a monolayer of PLL binds to the negative metal oxide and the hydrated PEG chains extend away from the surface forming a brush structure. In a good solvent if the separation distance ( $d$ ) between the PEG anchoring points is less than twice the Flory radius  $r_f$  ( $d < 2r_f$ ) the so called “brush” regime is invoked.<sup>74</sup> As a result of the osmotic pressure generated by the good solvent, segmental repulsions stretch the polymer chain normal to the interface and can prevent close approach of proteins or other brushy objects.

While other groups employing PLL-PEG brushes focused on eliminating nonspecific protein adsorption<sup>74</sup> or on the specific biofunctionalization of the brush itself (usually at the free chain ends),<sup>9</sup> we relied on the unfunctionalized PLL-PEG brush to produce a repulsive field against which embedded attractive cationic elements compete. The selection of homopolymer PLL as the attractive cationic element or patch was based on the fact that PLL is widely known as a polymer that can enhance mammalian cell adhesion to solid surfaces. Moreover PLL has been shown to enhance microbial cell adhesion<sup>83</sup> and is being widely used for surface patterning for biofilm development.<sup>84</sup> PLL has been used to form layer-by-layer thin film assembly for thin film biomaterials and is known to enhance protein adhesion for fibronectin<sup>3, 85</sup> which made it a suitable choice for our study. The PLL patches form the nanoscale elements within the PLL-PEG copolymer brush. The accessibility of these patches to targets in solution was probed in this thesis.

## 1.7 Thesis Overview

This thesis explored the capabilities of nano scale heterogeneities embedded within a PEG brush to achieve selective adhesion of different proteins and cells. Polyethylene glycol (PEG) graft poly-L-lysine (PLL) copolymers were used to create the PEG brush on silica surfaces. The cationic PLL backbone anchor within the copolymer maintains the brush on the surface through electrostatic attractions to the negatively charged silica substrate. PEG chain lengths and grafting ratios were varied to study their role in bio-adhesion. Three different PEG brushes were studied for this thesis. Cationic homopolymer PLL coils were used as patches and were embedded within the brush providing a nano patterned PEG brush.

**Chapter 2** focuses on the stability of three PLL-PEG brushes on silica surfaces upon exposure to different anionic and cationic proteins, in addition to free (cationic) PLL itself. While all three brushes were found to almost completely resist the adhesion of anionic proteins, lysozyme was found to be adsorb loosely to the outer PEG layer, with the amount of retained lysozyme roughly proportional to the PEG content of the interface. By contrast, free homopolymer PLL was found to penetrate the PEG brush and displace the it from the silica substrate.

**Chapter 3** details the ability of a 2000-molecular weight PEG brush, containing cationic PLL patches, to tune adhesion of a model protein, fibrinogen. A sharp protein adhesion threshold for fibrinogen adhesion is reported.



**Chapter 4** extends the principle of fibrinogen adhesion to other proteins: albumin, alkaline phosphatase and myoglobin, varying in size but possessing similar pKas. The adhesion thresholds were found to rank with protein size, demonstrating a molecular ruler effect. Highly selective capture of fibrinogen (exceeding 99%) from fibrinogen – albumin mixtures was achieved at a surface that had intermediate patch density between the adhesion thresholds of fibrinogen and albumin.

**Chapter 5** explores the effect of brush height, brush grafting density and variation of buffer ionic strength over fibrinogen adhesion. It was demonstrated how protein adhesion can be tuned by varying the brush architecture and ionic strength. Selective capture and release of proteins at different ionic strengths over the brushes was demonstrated.

**Chapter 6** extends the protein-selectivity of the three patchy brushes to cellular lengthscales using *S. aureus* adhesion as a model. Distinct adhesion thresholds for *S. aureus* capture were found for all three brushes. It was further discovered that bacterial adhesion thresholds preceded protein adhesion for all of the brushes. An effort was made to separate *S. aureus* from a mixture of the protein and the bacteria at an intermediate patchy Brush 2 surface. It was found that the particular protein fibrinogen altered the bacterial outer membrane and bacterial separation was hindered. This turned out to be a poor choice to demonstrate bacterial separations, but still results were suggested success with other systems.

**Chapter 7** contains the concluding points for this thesis and elaborated on future research directions.

## 1.8 References:

- 1.) Kasemo, B. (2002). Biological surface science. *Surface Science*, 500(1-3), 656-677.
- 2.) Gupta, R., & Kumar, A. (2008). Molecular imprinting in sol-gel matrix (Retracted article. See vol. 28, pg. 939, 2010). [Review]. *Biotechnology Advances*, 26(6), 533-547.
- 3.) Meyer, A., Auemheimer, J., Modlinger, A., & Kessler, H. (2006). Targeting RGD recognizing integrins: Drug development, biomaterial research, tumor imaging and targeting. *Current Pharmaceutical Design*, 12(22), 2723-2747.
- 4.) Wright, A. T., & Anslyn, E. V. (2006). Differential receptor arrays and assays for solution-based molecular recognition. *Chemical Society Reviews*, 35(1), 14-28.
- 5.) VandeVondele, S., Voros, J., & Hubbell, J. A. (2003). RGD-Grafted poly-l-lysine-graft-(polyethylene glycol) copolymers block non-specific protein adsorption while promoting cell adhesion. *Biotechnology and Bioengineering*, 82(7), 784-790.
- 6.) Chen, H., Yuan, L., Song, W., Wu, Z. K., & Li, D. (2008). Biocompatible polymer materials: Role of protein-surface interactions. *Progress in Polymer Science*, 33(11), 1059-1087.
- 7.) Lutz, J. F. (2008). Polymerization of oligo(ethylene glycol) (meth)acrylates: Toward new generations of smart biocompatible materials. *Journal of Polymer Science Part a-Polymer Chemistry*, 46(11), 3459-3470.
- 8.) Mahmud, G., Huda, S., Yang, W., Kandere-Grzybowska, K., Pilans, D., Jiang, S. Y., & Grzybowski, B. A. (2011). Carboxybetaine Methacrylate Polymers Offer Robust, Long-Term Protection against Cell Adhesion. *Langmuir*, 27(17), 10800-10804.
- 9.) NoppI Simson, D. A., & Needham, D. (1996). Avidin-biotin interactions at vesicle surfaces: Adsorption and binding, cross-bridge formation, and lateral interactions. *Biophysical Journal*, 70(3), 1391-1401.

- 10.) Wei, Y., Ji, Y., Xiao, L. L., & Jian, J. A. (2010). Construction of biomimetic polymer surface for endothelial cell selectivity. *Acta Polymerica Sinica*(12), 1474-1478.
- 11.) Kortright, J. B., Kim, S. K., Denbeaux, G. P., Zeltzer, G., Takano, K., & Fullerton, E. E. (2001). Soft-x-ray small-angle scattering as a sensitive probe of magnetic and charge heterogeneity. *Physical Review B*, 64(9), 2401-2404.
- 12.) Tombacz, E., & Szekeres, M. (2006). Surface charge heterogeneity of kaolinite in aqueous suspension in comparison with montmorillonite. *Applied Clay Science*, 34(1-4), 105-124.
- 13.) Gun'ko, V. M., Leboda, R., Turov, V. V., Villieras, F., Skubiszewska-Xieba, J., Chodorowski, S., & Marciniak, M. (2001). Structural and energetic nonuniformities of pyrocarbon-mineral adsorbents. *Journal of Colloid and Interface Science*, 238(2), 340-356.
- 14.) Mahnke, J., Stearnes, J., Hayes, R. A., Fornasiero, D., & Ralston, J. (1999). The influence of dissolved gas on the interactions between surfaces of different hydrophobicity in aqueous media Part I. Measurement of interaction forces. *Physical Chemistry Chemical Physics*, 1(11), 2793-2798.
- 15.) Lubarsky, G. V., Davidson, M. R., & Bradley, R. H. (2004). Elastic modulus, oxidation depth and adhesion force of surface modified polystyrene studied by AFM and XPS. *Surface Science*, 558, 135-144.
- 16.) Song, J., Duval, J. F. L., Stuart, M. A. C., Hillborg, H., Gunst, U., Arlinghaus, H. F., & Vancso, G. J. (2007). Surface ionization state and nanoscale chemical composition of UV-irradiated poly(dimethylsiloxane) probed by chemical force microscopy, force titration, and electrokinetic measurements. *Langmuir*, 23(10), 5430-5438.
- 17.) Brant, J. A., Johnson, K. M., & Childress, A. E. (2006). Characterizing NF and RO membrane surface heterogeneity using chemical force microscopy. *Colloids and Surfaces a-Physicochemical and Engineering Aspects*, 280(1-3), 45-57.

- 18.) Mendez-Vilas, A., Diaz, J., Donoso, M. G., Gallardo-Moreno, A. M., & Gonzalez-Martin, M. L. (2006). Ultrastructural and physico-chemical heterogeneities of yeast surfaces revealed by mapping lateral-friction and normal-adhesion forces using an atomic force microscope. *Antonie Van Leeuwenhoek International Journal of General and Molecular Microbiology*, 89(3-4), 495-509.
- 19.) Dorobantu, L. S., Bhattacharjee, S., Foght, J. M., & Gray, M. R. (2008). Atomic force microscopy measurement of heterogeneity in bacterial surface hydrophobicity. *Langmuir*, 24(9), 4944-4951.
- 20.) Dufrene, Y. F. (2003). Recent progress in the application of atomic force microscopy imaging and force spectroscopy to microbiology. *Current Opinion in Microbiology*, 6(3), 317-323.
- 21.) Camesano, T. A., & Abu-Lail, N. I. (2002). Heterogeneity in bacterial surface polysaccharides, probed on a single-molecule basis. *Biomacromolecules*, 3(4), 661-667.
- 22.) Plaksin, I. N., & Shafeev, R. S. (1958). The Influence of the Electrochemical Heterogeneity of the Sulfide Mineral Surface on the Xanthate Distribution under the Conditions of Flotation. *Doklady Akademii Nauk Sssr*, 121(1), 145-148.
- 23.) Bartoli, F., Burtin, G., & Guerif, J. (1992). Influence of Organic-Matter on Aggregation in Oxisols Rich in Gibbsite or in Goethite .2. Clay Dispersion, Aggregate Strength and Water-Stability. *Geoderma*, 54(1-4), 259-274.
- 24.) Wang, Z., Hemmer, S. L., Friedrich, D. M., & Joly, A. G. (2001). Anthracene as the origin of the red-shifted emission from commercial zone-refined phenanthrene sorbed on mineral surfaces. *Journal of Physical Chemistry A*, 105(25), 6020-6023.
- 25.) Priest, C., Stevens, N., Sedev, R., Skinner, W., & Ralston, J. (2008). Inferring wettability of heterogeneous surfaces by ToF-SIMS. *Journal of Colloid and Interface Science*, 320(2), 563-568.

- 26.) Strobel, M., Jones, V., Lyons, C. S., Ulsh, M., Kushner, M. J., Dorai, R., & Branch, M. C. (2003). A comparison of corona-treated and flame-treated polypropylene films. *Plasmas and Polymers*, 8, 61-95.
- 27.) Fang, C. P., & Drelich, J. (2004). Theoretical contact angles on a nano-heterogeneous surface composed of parallel apolar and polar strips. *Langmuir*, 20(16), 6679-6684.
- 28.) Sharma, A., Konnur, R., & Kargupta, K. (2003). Thin liquid films on chemically heterogeneous substrates: self-organization, dynamics and patterns in systems displaying a secondary minimum. *Physica a-Statistical Mechanics and Its Applications*, 318(1-2), 262-278.
- 29.) Jauneau, A., Quentin, M., & Driouich, A. (1997). Micro-heterogeneity of pectins and calcium distribution in the epidermal and cortical parenchyma cell walls of flax hypocotyl. *Protoplasma*, 198(1-2), 9-19.
- 30.) McCann, M. C., Wells, B., & Roberts, K. (1992). Complexity in the spatial localization and length distribution of plant cell-wall matrix polysaccharides. *Journal of Microscopy-Oxford*, 166, 123-136.
- 31.) Obel, N., Erben, V., Schwarz, T., Kuhnel, S., Fodor, A., & Pauly, M. (2009). Microanalysis of Plant Cell Wall Polysaccharides. *Molecular Plant*, 2(5), 922-932.
- 32.) Hancock, J. F. (2006). Lipid rafts: contentious only from simplistic standpoints. *Nature Reviews Molecular Cell Biology*, 7(6), 456-462.
- 33.) Mayor, S., & Rao, M. (2004). Rafts: Scale-dependent, active lipid organization at the cell surface. *Traffic*, 5(4), 231-240.
- 34.) Pike, L. J. (2004). Lipid rafts: heterogeneity on the high seas. *Biochemical Journal*, 378, 281-292.
- 35.) Jacobs, C., & Shapiro, L. (1999). Bacterial cell division: A moveable feast. *Proceedings of the National Academy of Sciences of the United States of America*, 96(11), 5891-5893.

- 36.) Jones, J. F., Feick, J. D., Imoudu, D., Chukwumah, N., Vigeant, M., & Velegol, D. (2003). Oriented adhesion of *Escherichia coli* to polystyrene particles. *Applied and Environmental Microbiology*, 69(11), 6515-6519.
- 37.) Shapiro, L., McAdams, H. H., & Losick, R. (2002). Generating and exploiting polarity in bacteria. *Science*, 298(5600), 1942-1946.
- 38.) Hammer, D. A., & Tirrell, M. (1996). Biological adhesion at interfaces. [Review]. *Annual Review of Materials Science*, 26, 651-691.
- 39.) Ruoslahti, E. (1996). RGD and other recognition sequences for integrins. *Annual Review of Cell and Developmental Biology*, 12, 697-715.
- 40.) Mehta, P., Patel, K. D., Laue, T. M., Erickson, H. P., & McEver, R. P. (1997). Soluble monomeric P-selectin containing only the lectin and epidermal growth factor domains binds to P-selectin glycoprotein ligand-1 on leukocytes. *Blood*, 90(6), 2381-2389.
- 41.) Holmberg, A., Blomstergren, A., Nord, O., Lukacs, M., Lundeberg, J., & Uhlen, M. (2005). The biotin-streptavidin interaction can be reversibly broken using water at elevated temperatures. *Electrophoresis*, 26(3), 501-510.
- 42.) Elbert, D. L., & Hubbell, J. A. (1996). Surface treatments of polymers for biocompatibility. *Annual Review of Materials Science*, 26, 365-394.
- 43.) Duffadar, R., Kalasin, S., Davis, J. M., & Santore, M. M. (2009). The impact of nanoscale chemical features on micron-scale adhesion: Crossover from heterogeneity-dominated to mean-field behavior. *Journal of Colloid and Interface Science*, 337(2), 396-407.
- 44.) Kalasin, S., Dabkowski, J., Nusslein, K., & Santore, M. M. (2010). The role of nanoscale heterogeneous electrostatic interactions in initial bacterial adhesion from flow: A case study with *Staphylococcus aureus*. *Colloids and Surfaces B-Biointerfaces*, 76(2), 489-495.

- 45.) Kalasin, S., Martwiset, S., Coughlin, E. B., & Santore, M. M. (2010). Particle Capture via Discrete Binding Elements: Systematic Variations in Binding Energy for Randomly Distributed Nanoscale Surface Features. *Langmuir*, 26(22), 16865-16870.
- 46.) Kalasin, S., & Santore, M. M. (2008). Hydrodynamic crossover in dynamic microparticle adhesion on surfaces of controlled nanoscale heterogeneity. *Langmuir*, 24(9), 4435-4438.
- 47.) Kalasin, S., & Santore, M. M. (2009). Non-specific adhesion on biomaterial surfaces driven by small amounts of protein adsorption. *Colloids and Surfaces B-Biointerfaces*, 73(2), 229-236.
- 48.) Kalasin, S., & Santore, M. M. (2010). Sustained Rolling of Microparticles in Shear Flow over an Electrostatically Patchy Surface. *Langmuir*, 26(4), 2317-2324.
- 49.) Kozlova, N., & Santore, M. M. (2006). Manipulation of micrometer-scale adhesion by tuning nanometer-scale surface features. *Langmuir*, 22(3), 1135-1142.
- 50.) Santore, M. M., & Kozlova, N. (2007). Micrometer scale adhesion on nanometer-scale patchy surfaces: Adhesion rates, adhesion thresholds, and curvature-based selectivity. *Langmuir*, 23(9), 4782-4791.
- 51.) Santore, M. M., Zhang, J., Srivastava, S., & Rotello, V. M. (2009). Beyond Molecular Recognition: Using a Repulsive Field to Tune Interfacial Valency and Binding Specificity between Adhesive Surfaces. *Langmuir*, 25(1), 84-96.
- 52.) Fang, B., Gon, S., Park, M., Kumar, K. N., Rotello, V. M., Nusslein, K., & Santore, M. M. (2011). Bacterial adhesion on hybrid cationic nanoparticle-polymer brush surfaces: Ionic strength tunes capture from monovalent to multivalent binding. *Colloids and Surfaces B-Biointerfaces*, 87(1), 109-115.
- 53.) Bunt, C. R., Jones, D. S., & Tucker, I. G. (1993). The effects of pH, ionic-strength and organic-phase on the bacterial adhesion to hydrocarbons (bath) test. *International Journal of Pharmaceutics*, 99(2-3), 93-98.



- 54.) Klapper, I., Rupp, C. J., Cargo, R., Purvedorj, B., & Stoodley, P. (2002). Viscoelastic fluid description of bacterial biofilm material properties. *Biotechnology and Bioengineering*, 80(3), 289-296.
- 55.) Katsikogianni, M., Amanatides, E., Mataras, D., & Missirlis, Y. F. (2008). Staphylococcus epidermidis adhesion to He, He/O-2 plasma treated PET films and aged materials: Contributions of surface free energy and shear rate. *Colloids and Surfaces B-Biointerfaces*, 65(2), 257-268.
- 56.) Katsikogianni, M., Spiliopoulou, I., Dowling, D. P., & Missirlis, Y. F. (2006). Adhesion of slime producing Staphylococcus epidermidis strains to PVC and diamond-like carbon/silver/fluorinated coatings. *Journal of Materials Science-Materials in Medicine*, 17(8), 679-689.
- 57.) Katsikogianni, M. G., & Missirlis, Y. F. (2010). Interactions of bacteria with specific biomaterial surface chemistries under flow conditions. *Acta Biomaterialia*, 6(3), 1107-1118.
- 58.) Chang, H. T., Rittmann, B. E., Amar, D., Heim, R., Ehlinger, O., & Lesty, Y. (1991). Biofilm detachment mechanisms in a liquid-fluidized bed. *Biotechnology and Bioengineering*, 38(5), 499-506.
- 59.) Nilsson, L. M., Thomas, W. E., Sokurenko, E. V., & Vogel, V. (2006). Elevated shear stress protects Escherichia coli cells adhering to surfaces via catch bonds from detachment by soluble inhibitors. *Applied and Environmental Microbiology*, 72(4), 3005-3010.
- 60.) Thomas, W., Forero, M., Yakovenko, O., Nilsson, L., Vicini, P., Sokurenko, E., & Vogel, V. (2006). Catch-bond model derived from allostery explains force-activated bacterial adhesion. *Biophysical Journal*, 90(3), 753-764.
- 61.) Mohamed, N., Rainier, T. R., & Ross, J. M. (2000). Novel experimental study of receptor-mediated bacterial adhesion under the influence of fluid shear. *Biotechnology and Bioengineering*, 68(6), 628-636.
- 62.) Blawas, A. S., & Reichert, W. M. (1998). Protein patterning. *Biomaterials*, 19(7-9), 595-609.

- 63.) Kane, R. S., Takayama, S., Ostuni, E., Ingber, D. E., & Whitesides, G. M. (1999). Patterning proteins and cells using soft lithography. *Biomaterials*, 20(23-24), 2363-2376.
- 64.) Casimirus, S., Flahaut, E., Laberty-Robert, C., Malaquin, L., Carcenac, F., Laurent, C., & Vieu, C. (2004). Microcontact printing process of individual for the patterned growth CNTs. *Microelectronic Engineering*, 73-4, 564-569.
- 65.) Malaquin, L., Carcenac, F., Vieu, C., & Mauzac, M. (2002). Using polydimethylsiloxane as a thermocurable resist for a soft imprint lithography process. *Microelectronic Engineering*, 61-2, 379-384.
- 66.) Thibault, C., LeBerre, V., Casimirus, S., Trevisiol, E., Francois, J., & Vieu, C. (2005). Direct microcontact printing of oligonucleotides for biochip applications. *Journal of Nanobiotechnology*, 3(1), 1-12.
- 67.) Falconnet, D., Csucs, G., Grandin, H. M., & Textor, M. (2006). Surface engineering approaches to micropattern surfaces for cell-based assays. *Biomaterials*, 27(16), 3044-3063.
- 68.) Falconnet, D., Pasqui, D., Park, S., Eckert, R., Schiff, H., Gobrecht, J., Barbucci, R., & Textor, M. (2004). A novel approach to produce protein nanopatterns by combining nanoimprint lithography and molecular self-assembly. *Nano Letters*, 4(10), 1909-1914.
- 69.) Amanda, A., & Mallapragada, S. K. (2001). Comparison of protein fouling on heat-treated poly(vinyl alcohol), poly(ether sulfone) and regenerated cellulose membranes using diffuse reflectance infrared Fourier transform spectroscopy. *Biotechnology Progress*, 17(5), 917-923.
- 70.) Park, S., Bearer, J. P., Lautenschlager, E. P., Castner, D. G., & Healy, K. E. (2000). Surface modification of poly(ethylene terephthalate) angioplasty balloons with a hydrophilic poly(acrylamide-co-ethylene glycol) interpenetrating polymer network coating. *Journal of Biomedical Materials Research*, 53(5), 568-576.

- 71.) Matsuda, T., Moghaddam, M. J., Miwa, H., Sakurai, K., & Iida, F. (1992). Photoinduced prevention of tissue adhesion. *ASAIO journal (American Society for Artificial Internal Organs : 1992)*, 38(3), M154-157.
- 72.) Holland, N. B., Qiu, Y. X., Ruegsegger, M., & Marchant, R. E. (1998). Biomimetic engineering of non-adhesive glycocalyx-like surfaces using oligosaccharide surfactant polymers. *Nature*, 392(6678), 799-801.
- 73.) Dalsin, J. L., Hu, B. H., Lee, B. P., & Messersmith, P. B. (2003). Mussel adhesive protein mimetic polymers for the preparation of nonfouling surfaces. *Journal of the American Chemical Society*, 125(14), 4253-4258.
- 74.) Dalsin, J. L., Lin, L. J., Tosatti, S., Voros, J., Textor, M., & Messersmith, P. B. (2005). Protein resistance of titanium oxide surfaces modified by biologically inspired mPEG-DOPA. *Langmuir*, 21(2), 640-646.
- 75.) Zalipsky, S. (1995). Chemistry of polyethylene-glycol conjugates with biologically-active molecules. *Advanced Drug Delivery Reviews*, 16(2-3), 157-182.
- 76.) Kerrigan, J. J., McGill, J. T., Davies, J. A., Andrews, L., & Sandy, J. R. (1998). The role of cell adhesion molecules in craniofacial development. *Journal of the Royal College of Surgeons of Edinburgh*, 43(4), 223-229.
- 77.) Park, S., Kim, H. C., & Chung, T. D. (2007). Site-specific anti-adsorptive passivation in microchannels. *Biochip Journal*, 1(2), 98-101.
- 78.) Sweryda-Krawiec, B., Devaraj, H., Jacob, G., & Hickman, J. J. (2004). A new interpretation of serum albumin surface passivation. *Langmuir*, 20(6), 2054-2056.
- 79.) Feller, L. M., Cerritelli, S., Textor, M., Hubbell, J. A., & Tosatti, S. G. P. (2005). Influence of poly(propylene sulfide-block-ethylene glycol) di- and triblock copolymer architecture on the formation of molecular adlayers on gold surfaces and their effect on protein resistance: A candidate for surface modification in biosensor research. *Macromolecules*, 38(25), 10503-10510.

- 80.) Huang, N. P., Michel, R., Voros, J., Textor, Marcus, Hofer, R., Rossi, A., Elbert, D. L., et al. (2001). Poly(L-lysine)-g-poly(ethylene glycol) Layers on Metal Oxide Surfaces: Surface-Analytical Characterization and Resistance to Serum and Fibrinogen Adsorption. *Langmuir*, 17(2), 489-498.
- 81.) Bergstrand, A., Rahmani-Monfared, G., Ostlund, A., Nyden, M., & Holmberg, K. (2009). Comparison of PEI-PEG and PLL-PEG copolymer coatings on the prevention of protein fouling. *Journal of Biomedical Materials Research Part A*, 88A(3), 608-615.
- 82.) Sawhney, A. S., & Hubbell, J. A. (1992). Poly(ethylene oxide)-graft-poly(l-lysine) copolymers to enhance the biocompatibility of poly(l-lysine)-alginate microcapsule membranes. *Biomaterials*, 13(12), 863-870.
- 83.) Verschoor, J. A., Meiring, M. J., Vanwyngaardt, S., & Weyer, K. (1990). Polystyrene, poly-l-lysine and nylon as adsorptive surfaces for the binding of whole cells of mycobacterium-tuberculosis h37 rv to elisa plates. *Journal of Immunoassay*, 11(4), 413-428.
- 84.) Cowan, S. E., Liepmann, D., & Keasling, J. D. (2001). Development of engineered biofilms on poly-L-lysine patterned surfaces. *Biotechnology Letters*, 23(15), 1235-1241.
- 85.) Wittmer, C. R., Phelps, J. A., Saltzman, W. M., & Van Tassel, P. R. (2007). Fibronectin terminated multilayer films: Protein adsorption and cell attachment studies. *Biomaterials*, 28(5), 851-860.

# **CHAPTER 2**

## **ARCHITECTURE AND STABILITIES OF PLL-PEG BRUSHES: CASE STUDIES WITH CATIONIC AND ANIONIC PROTEINS AND A STRONG CATIONIC POLYELECTROLYTE PLL**

### **2.1 Introduction**

This chapter covers the architecture and stabilities of the different PEG brushes studied for this thesis. The impact of different protein and polyelectrolyte over such brushes is further described here. Much of this chapter is reproduced from a recently published work.<sup>37</sup>

Despite advances that enable growth of covalently-attached brushes from surface-bound initiators, economic considerations drive continued interest in brush formation from the adsorption of PEG (polyethylene glycol)-containing copolymers. For hydrophobic surfaces, amphiphilic co-polymers are an obvious choice to create PEG-tethered surfaces from aqueous formulations; however, complications can arise from micelles in solution and on surfaces. For negative surfaces, copolymers of PEG and polycations are a useful route to produce surfaces with PEG tethers. Here, the adsorbing polycation is self-repellant and avoids the aggregation and micellization-based complications that occur with polymer amphiphiles. Indeed, several labs have developed libraries of PEG-PLL (PEG-Poly-l-lysine)<sup>1-4</sup> and PEG-PEI (PEG-poly(ethylene imine))<sup>5,6</sup> copolymers, containing at least some members that are exceptionally protein resistant,

adsorbing 0.01mg/m<sup>2</sup> or less from serum. Also, Messersmith has pioneered the creation of DOPA (3,4-dihydroxyphenylalanine)-containing PEG, most appropriate as a protein-resistant coating for TiO<sub>2</sub> implants.<sup>7</sup> A close comparison between the best PLL-PEG copolymers and the PEG-DOPA polymers reveals a slight superiority of the former's protein resistance *in-vitro*,<sup>8</sup> while the significance of this difference for *in-vivo* applications is unclear. Indeed, current indicators suggest that in the long run, the DOPA-based anchors, though appropriate for only limited substrate chemistries, are the better choice *in-vivo*.<sup>7</sup>

Beyond the chemical instability of PEG, a problem for any physisorbed copolymer-based brush is its potential for displacement by competing species. While biomedical studies have not revealed exactly which proteins may be responsible, arguments from polymer physics suggest that cationic proteins, polymers, and polypeptides can destabilize PEG brushes anchored by cationic chains on negative substrates. High molecular weight homopolymers will displace, ultimately, low molecular weight chains of identical chemistry,<sup>9,10</sup> while densely charged polyelectrolytes will displace chains of lower charge density but similar length.<sup>11</sup>

These rules of thumb apply to the anchoring constituent of PEG-polycation adsorbed brushes. Thus, efficient cationic challengers for brush displacement could include the PLL-homopolymer itself, since functionalization of PLL with PEG chains reduces the cationic functionality of the backbone, and since the PLL anchor of the copolymer must also pay the entropic "cost" of stretching its PEG tethers.<sup>12</sup> The question, then, is to what extent can cationic challengers, such as positively charged proteins or PLL itself, penetrate the PEG corona and displace the PLL anchors. Since

brushes with about  $\sim 1 \text{ mg/m}^2$  of PEG tethers have been documented to be protein-resistant,<sup>2,8,13</sup> it is interesting to ask whether this resistance translates to an impermeability towards challenging species, at least ones that are peptide-based. Indeed, if a brush is thick enough to shield the underlying substrate from approaching proteins, then it may be stable against exchange for very long periods, despite a driving force favoring exchange.

This chapter examines brushes formed from PLL-PEG copolymers physisorbed on silica. Following the literature from the Hubbell, Voros, and Textor groups, this study focuses on architectures which have been previously established to be highly protein resistant, adsorbing less than  $0.01 \text{ mg/m}^2$  of serum protein at physiological pH and ionic strength.<sup>8,13</sup> These brushes are thicker (8-16 nm) than the range of electrostatic interactions. We reproduce the stability of these surfaces against adsorption of albumin, fibrinogen and other negative proteins, but observe that cationic protein adsorption occurs and that brushes can be destroyed by exposure to cationic polypeptides. The observations prompt reconsideration of the general assumption of protein-PEG repulsions, and the ability of polypeptides to penetrate relatively thick PEG brushes.

## **2.2 Synthesis and Characterization of Brushes**

The synthesis and characterization processes of PLL-PEG brushes are described in this section.

### **2.2.1 Brush Synthesis**

The general brush synthesis procedure followed the technique described by the Hubbell group<sup>14-15</sup>. However due to unavailability of the PEG reactive group as employed by the former group we used a slightly different PEG compound as described by (Gon et al., 2010)<sup>16</sup>. Poly-L-lysine hydrobromide (PLL) with a nominal molecular weight of 20,000 from Sigma-Aldrich was dissolved in 50 mM pH 9.1 sodium borate buffer. Two different PEG molecular weights were employed, either 2000 or 5000. For copolymers containing 2K PEG, the N-hydroxysuccinimidyl ester of methoxypoly(ethylene glycol) acetic acid (Layson Bio Inc.) was added, and the solution was stirred for 6h. For copolymers containing 5K PEG, this reactive compound was not available and PEG sodium valeric acid (PEG-SVA) was employed instead. After reaction, the mixture was dialyzed against pH 7.4 phosphate-buffered saline for 24h, dialyzed against DI water for another 24 h, and then freeze dried and stored at -20°C. The relative amounts of PEG and PLL were varied, with the grafting ratio defined to be the number of PLL monomer per PEG side chain. This is inversely proportional to the percent functionalization of the PLL by PEG.




### **2.2.2 Brush characterization using NMR**

Purified copolymers were characterized in D<sub>2</sub>O using <sup>1</sup>H NMR on a Bruker 400 MHz instrument. The grafting ratio was determined from the relative areas of the lysine side-chain peak (-CH<sub>2</sub>-N-) at 2.909 ppm and the PEG peak (-CH<sub>2</sub>-CH<sub>2</sub>-) at 3.615 ppm. Table 2.1 summarizes the molecular properties of the three samples employed in this study. While other molecular architectures were synthesized as described in Appendix A, these particular three samples were studied further because the brushes they formed on



adsorption to silica eliminated the adsorption of key serum proteins, consistent with prior literature.<sup>13</sup> NMR data for the three polymers are given in Appendix B.

Table 2.1 Molecular Properties of different brushes

	<b>Polymer I</b>	<b>Polymer II</b>	<b>Polymer III</b>
			
	PLL-(2.7)PEG(2K)	PLL-(2.2)PEG(5K)	PLL-(4.7)PEG(5K)
PEG MW	2,000	5,000	5,000
Grafting Ratio	2.7	2.24	4.5
% PLL Functionalization	37%	45%	22%
Molecular Weight	136,000	367,000	188,000

PLL- 20K  
(157 repeats) 

## 2.3 Experimental methodology

Polymer brushes were formed by adsorbing copolymers from flowing phosphate buffered solution (0.008 M Na<sub>2</sub>HPO<sub>4</sub> and 0.002M KH<sub>2</sub>PO<sub>4</sub>, pH 7.4 with Debye length  $\kappa^{-1}$  = 2 nm, 100 ppm copolymer) over acid-etched microscope slides (these surfaces are silica) in slit shear laminar flow cells at gentle flow conditions (wall shear rate = 5.0 s<sup>-1</sup>) for 20 minutes. This was followed by continued flow of the same buffer for another 20 minutes. Optical reflectometry,<sup>17</sup> run *in-situ*, was used to track the adsorption process

and determine the ultimate mass of adsorbed copolymer. When needed, total internal reflectance fluorescence (TIRF) was employed to track the adsorption or desorption of a fluorescently-tagged species during competitive challenge experiments. This instrument was described <sup>18</sup> previously and, notably, employs the same flow chamber as the reflectometer.

The polymers and proteins used to challenge the adsorbed PLL-PEG brushes were purchased from Sigma Aldrich and used as-is. These included hen egg white lysozyme (L6876), bovine serum albumin A (7511-10G), bovine fibrinogen (F8630-1G, fraction 1, type 1S), equine skeletal muscle myoglobin (M0630-1G), and alkaline phosphatase (P7640-1G). Notably the PLL homopolymer used to challenge the brush was the same PLL employed as the anchoring group of the copolymer. In cases where TIRF was employed to track PLL adsorption, it was made fluorescent by labeling with fluorescein-isothiocyanate (FITC isomer I, F250-2 from Aldrich). Labeling and purification were conducted as described by (Wertz and Santore, 1999)<sup>19</sup>. Challenge experiments were conducted in the same flow chamber used to deposit brushes, with continuous flow of the various solutions and buffers, and the same flow rate. Studies at Debye lengths other than 2 nm were done either in dilute (overall concentration of 0.005M for  $\kappa^{-1} = 4\text{nm}$ ) or concentrated buffer for  $\kappa^{-1} = 1\text{ nm}$ .

In some studies, small amounts of PLL were adsorbed to bare silica surfaces prior to the adsorption of the PLL-PEG brush. This was carried out as a sequence of carefully-timed adsorption steps in a single flow chamber. Control of the particular small PLL amount was achieved through the use of dilute PLL solution (5 ppm) and careful timing of PLL flow and reinjection of buffer, so that controlled deposition, not full surface

saturation, occurred. Subsequent adsorption of the brush was carried out by flowing PLL-PEG solution for a time appropriate to saturate the surface. Buffer was reinjected only after a clear plateau was demonstrated. This procedure has been documented in detail previously.<sup>16</sup> It was additionally shown that (1) initial PLL adsorption did not produce surface aggregates and that PLL chains were well-distributed about the surface; and (2) initially adsorbed PLL was not displaced by subsequently adsorbing PLL-PEG.<sup>16</sup>

Zeta potential measurements, intended to gauge the electrostatic features of planar brush-bearing surfaces, were conducted using 50 ppm suspensions of 1-micron silica spheres (from GelTech, Orlando) as a model for the planar silica surfaces. Polymers were adsorbed to the particles to create PLL- or brush-covered silica, using an amount of polymer appropriate to saturate the surface and known the specific area of the microparticles. Particles were incubated overnight prior to measurement of their zeta potential in a Malvern Zeta Sizer Nano ZS instrument.

## **2.4 Results**

### **2.4.1 Calculation of brush height**

The calculation of the brush heights were calculated following the “blob” approach put forth by Alexander and DeGennes<sup>20-21</sup>, in which sections of the chain, each possessing about a  $kT$  of energy, termed “blobs,” extend normal to the surface (Figure 2.1). The brush height is the blob diameter times the number of blobs:

$$\text{Height} = (N / N_{\text{blob}}) d_{\text{blob}} \quad (2.1)$$

The number of blobs in a chain is equal to the number of statistical segments in a chain divided by the number statistical segments in a blob,  $N/N_{\text{blob}}$ . The blob diameter corresponds to the spacing of the PEG anchors, which is calculated from the experimentally adsorbed amount of PLL-PEG coverage at saturation.

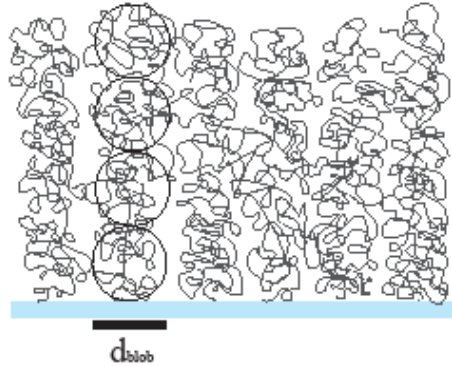


Figure 2.1 Schematic of polymer brush

The PEG statistical segment length,  $b$ , was determined as 0.57 nm and the molecular weight of a statistical segment was found to be 59. Therefore a 2000 molecular weight PEG chain contains 34 statistical segments while  $N_{\text{blob}}$  is calculated by blob diameter =  $b N_{\text{blob}}^{3/5}$ .

An assumption of  $N^{3/5}$  (good solvent) scaling of the chain inside each blob (at distances less than a persistence length) allows calculation of the number of blobs in the brush, as previously described.<sup>16,22</sup> From Equation 2.1 we can calculate the brush height which is reported in Table 2.2. Most notably, the PLL content of all three brushes (presumably at the brush base) is substantially less than a saturated PLL layer of the same molecular weight, while the graft spacing of the PEG tethers is smaller than the calculated free coil diameter, 3.3 nm for 2K PEG and 6.1 nm for 5K PEG. This suggests

that the PEG tethers are stretched normal to the surface, as required in brushes. The calculation of the brush height follows the determination of the average spacing between tethers, giving the brush's persistence length. Notably, Brush #1 is shorter than the others but still substantially thicker than the 2nm Debye length in the main study, while the two thicker brushes are nearly similar in height but differ in their PEG/PLL content and in the effective number of “blobs” per tether. These estimates are conceptualized in the Figure 2.2.

Table 2.2 Brush architecture and zeta potentials,  $\zeta$

	<b>PLL</b>	<b>Brush #1</b>	<b>Brush #2</b>	<b>Brush #3</b>
	Homopoly 20K	PLL-(2.7) PEG(2K)	PLL-(2.2) PEG(5K)	PLL-(4.7) PEG(5K)
Saturated adsorption	0.4 mg/m <sup>2</sup>	1.1 mg/m <sup>2</sup>	0.9	1.3
Adsorbed PEG	0	0.94 mg/m <sup>2</sup>	.85	1.16
Adsorbed PLL	0.4 mg/m <sup>2</sup>	0.16 mg/m <sup>2</sup>	0.05	0.14
Area / Copolymer	83 nm <sup>2</sup>	206 nm <sup>2</sup>	680	247
Area / PEG tether		3.6 nm <sup>2</sup>	9.6	7.2
“Blob” Diameter, or tether spacing		1.9 nm	3.1	2.7
Number of Blobs		4.7	5.1	6.4
Brush Height, nm		9 nm	15.5	17.2
$\zeta$ (1 nm) [ $\zeta_{\text{SiO}_2} = -57\text{mV}$ ]	2 $\pm$ 5 mV	-4 $\pm$ 3 mV	-11 $\pm$ 3 mV	-4 $\pm$ 3 mV
$\zeta$ (2 nm) [ $\zeta_{\text{SiO}_2} = -73\text{mV}$ ]	6 $\pm$ 3 mV	-9 $\pm$ 3 mV	-19 $\pm$ 3 mV	-10 $\pm$ 3 mV
$\zeta$ (4 nm) [ $\zeta_{\text{SiO}_2} = -84\text{mV}$ ]	4 $\pm$ 3 mV	-21 $\pm$ 3 mV	-34 $\pm$ 3 mV	-25 $\pm$ 3 mV

While the literature suggests that electrostatic effects should be unimportant at the 2 nm Debye length of this study, an assessment of the electrokinetic surface character is useful. The lower part of Table II reveals, via zeta potential, a net negative interface for

all brushes. That the surfaces have an underlying negative charge is not surprising: The silica substrate is substantially negative and a PLL layer adsorbed to saturation ( $0.4 \text{ mg/m}^2$ ) only slightly overcompensates the underlying surface charge. The brushes, with their PLL content less than that of a fully saturated PLL layer, will therefore be negatively charged in region where the PEG is anchored. That the negative interfacial potential can be sensed hydrodynamically via zeta potential suggests that the shear plane penetrates the brush somewhat. The zeta potential is still substantially reduced (in magnitude) for these brush-containing surfaces compared with surfaces with similar PLL loading but no PEG. The extent to which proteins can sense the negative interfacial environment (do they penetrate the brush more or less than the shear plane?) is addressed below.

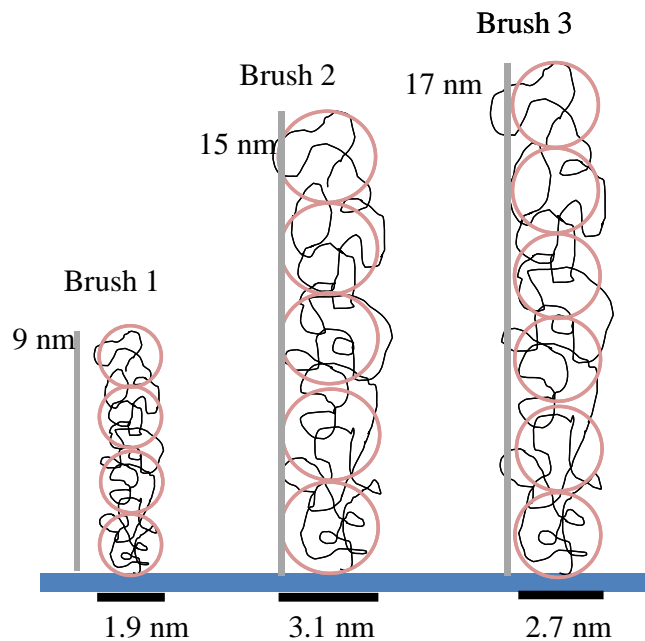


Figure 2.2 Structure of the PEG tethers within the three brushes, calculated according to the Alexander deGennes treatment, showing graft spacing or brush persistence length, equal to the “blob” size. Also shown is the number of blobs in each brush.

## 2.4.2 Interaction with globular proteins

Table 2.3 summarizes the adsorption of several proteins on the three brushes at a Debye length of 2 nm. In general, proteins with a net negative charge, regardless of size or shape, do not adsorb to the brushy surfaces, while cationic proteins and polypeptides do adhere. In the case of lysozyme with a net charge of 9+, substantial adsorption is observed for the thicker brushes, with the greatest adsorption on Brush #2, which contains the greatest mass of PEG. Notably, the efficient elimination of negative protein adsorption (albumin, fibrinogen, and others) on these brushy surfaces reproduces reports in the literature for of a lack of adsorption from serum.<sup>13-15</sup> Indeed the lack of serum adsorption was the basis our choice of these brush architectures (and in particular the grafting ratio). Figure 2.3 shows the experimental results of challenging these proteins over different brushes.

Table 2.3 Protein adsorption at  $\kappa^{-1} = 2$  nm, pH 7.4 (R = substantially reversible adsorption, E = Exchange (displacement) of previously adsorbed brush

		MW	Dimensions nm x nm x nm	Charge, pI	Protein mg/m <sup>2</sup>	Adsorption,	
					#1	Brush # #2	#3
Fibrinogen, serum	bovine	340,000	4.5 x 4.5 x 47	-8 - -10 <sup>23</sup> , 5.8 <sup>24</sup>	0 – 0.02	0	0
Albumin, serum	bovine	68,000	4 x 4 x 14	-9, 4.8 <sup>25</sup> -5.1	0	0	0
Myoglobin		17,000	4.4 x 4.4 x 2.5	-, 6.8-7.0 <sup>26</sup>	0 – 0.02	-	-
Alkaline Phosphatase, Monomer (bovine)		81,000	9 x 4 x 4	-, 5.7 <sup>27</sup>	0	-	-
Lysozyme, white	hen egg	14,300	3 x 3 x 5	+7, 11 <sup>26,28</sup>	0.05R	1.0R	0.2R
Poly-l-lysine		20,000	Random coil	+++	0.4 E	0.4E	0.4E

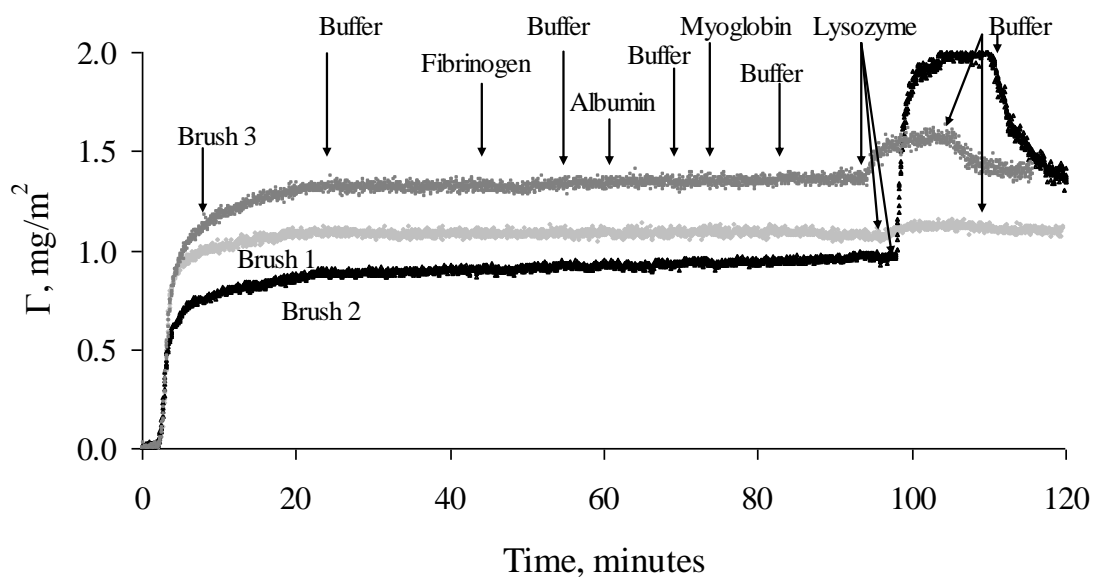


Figure 2.3 Protein repellence characteristics of PEG brushes.

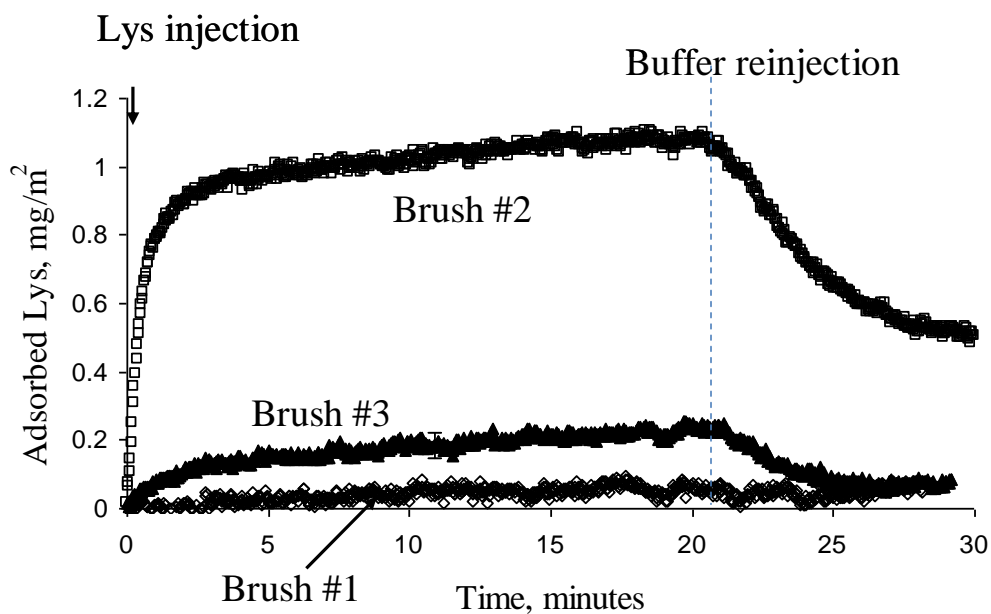


Figure 2.4: Lysozyme adsorption onto three brushes at pH 7.4 and  $k-1 = 2$  nm, followed by rinsing, near 20 minutes. (Brush adsorption portion of each run is not shown.)



The adsorption traces for lysozyme on the three brushes are detailed in Figure 2.4, and run contrary to current thinking about protein-brush interactions. First, it is generally accepted that protein repellence occurs when brushes are sufficiently thick to screen electrostatic and van der Waals attractions. Indeed a comprehensive study employing libraries of PLL-PEG and DOPA-PEG polymers suggests that the most important feature of a brush is the tethered PEG mass: If it is about  $1 \text{ mg/m}^2$  or greater, good resistance to serum proteins is observed, independent of PEG chain length or grafting density (for PEG lengths in the range from 1-5K).<sup>8</sup> Figure 2.4 shows the opposite. The thinnest brush, #1, adsorbs practically no lysozyme, while the thicker brushes adhere more lysozyme. This suggests, first, that the attractions between lysozyme and the interface are between the protein and the PEG, not between the protein and the underlying substrate. (Notably lysozyme –substrate interactions are electrostatically attractive, but apparently well-screened by the thinnest of the brushes, # 1.) Instead, the increasing protein retention with PEG content suggests specific interactions between PEG and lysozyme, not available to the other proteins.

The claim that lysozyme adsorption does not result from electrostatic attractions to the underlying silica must be substantiated by a similar lack of interaction between the anionic protein and the brush-covered silica. Figure 2.5 considers the influence of Debye length on the adsorption of fibrinogen, chosen as a model negative protein because it is well studied and known to adsorb onto positive<sup>29</sup> and negative surfaces (including silica at pH 7.4).<sup>30-32</sup> On negative surfaces, electrostatic attractions involve fibrinogen's cationic groups, evidenced by the impact of ionic strength.<sup>30,31</sup> Figure 2.5 demonstrates

that for  $\kappa^{-1} = 4\text{nm}$ , fibrinogen adsorbs onto Brush #1 but not Brush #2 or #3. This suggests an attraction between fibrinogen and the underlying substrate, screened by the thicker brushes. That this attraction is electrostatic in origin is further supported, in Figure 2.5, by the observed lack of fibrinogen adsorption to all three brushes at  $\kappa^{-1}$  of 1 and 2 nm, conditions where the steric brush repulsions screen electrostatic interactions. The argument is further strengthened by the reversibility of the fibrinogen adsorption on Brush #1 with changing ionic strength. Long range electrostatic attractions at 4 nm may draw fibrinogen to the brush periphery, but without stronger interactions the silica or train layer, fibrinogen is immediately and completely released when the ionic strength is raised. The fast rate of protein release suggests fibrinogen adsorption (at 4 nm) on top of the brush.

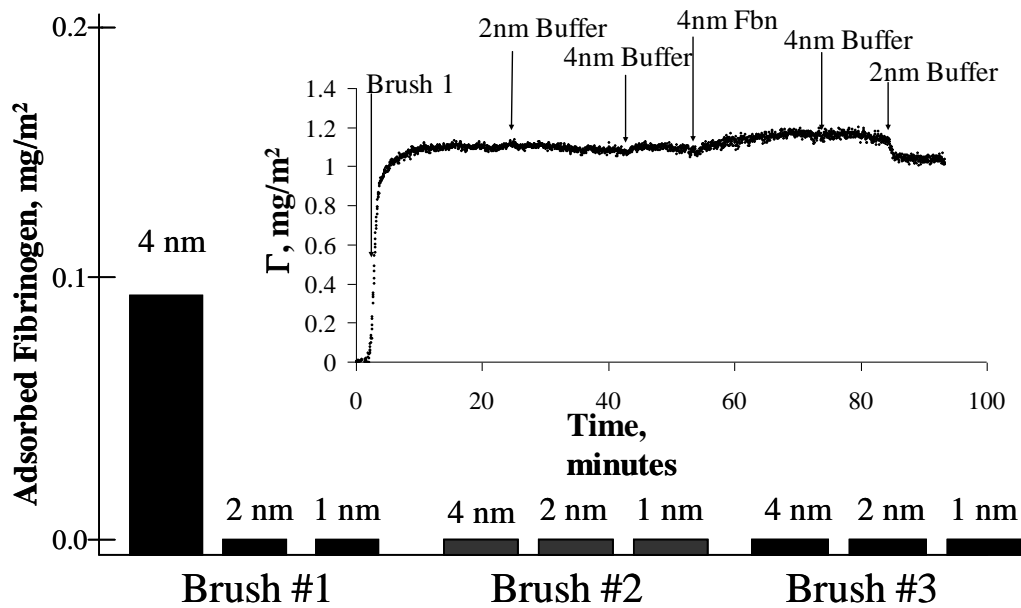


Figure 2.5 Fibrinogen adsorption on brushes for different ionic strengths. Note reversible adsorption on Brush #1 when the ionic strength is switched (inset) from the mildly adsorbing conditions at  $\kappa^{-1} = 4\text{ nm}$  down to 2 nm.

Thus, we deduce that at 2 nm, the conditions for most of this study, the brushes fully screen electrostatic interactions between the proteins and silica. Therefore, the net-negative character of the non-adsorbing proteins in Table 2.3 is not directly (through electrostatic repulsions) responsible for their lack of adsorption.

### **2.4.3 Interaction with PLL**

Table 2.3 notes that PLL solutions displace PLL-PEG from the silica. An example of PLL challenge of Brush #1 is shown in Figure 2.6, a reflectometry trace including multiple steps: initial adsorption of PLL-(2.7) PEG-2K to form Brush #1; its retention on the surface during rinsing in pH 7.4  $\kappa^{-1}=2$  nm buffer; challenge by albumin solution (in the same buffer, nothing happens); and subsequent challenge by PLL solution (100 ppm). Brush exposure to PLL causes the surface coverage to decrease from 1.1 mg/m<sup>2</sup> to 0.4 mg/m<sup>2</sup>. The latter is characteristic of a saturated PLL layer on silica, and indeed, when albumin is exposed again to the surface, it adsorbs rapidly. The gray data set on the same graph show the adsorption of PLL on a bare silica surface and subsequent albumin adsorption. The latter is kinetically identical to albumin adsorption on a surface initially containing a PLL-PEG brush (#1), after PLL challenge. This suggests that the brush is completely displaced by PLL as though the brush were never present. The technical implications of the subsequent protein adsorption are clear.

The rapid kinetics of the PLL / PLL-PEG exchange process are striking. The loss of PLL-PEG from the silica is clear in Figure 2.6, but adsorption of PLL into the brush is equally fast, in Figure 2.7.

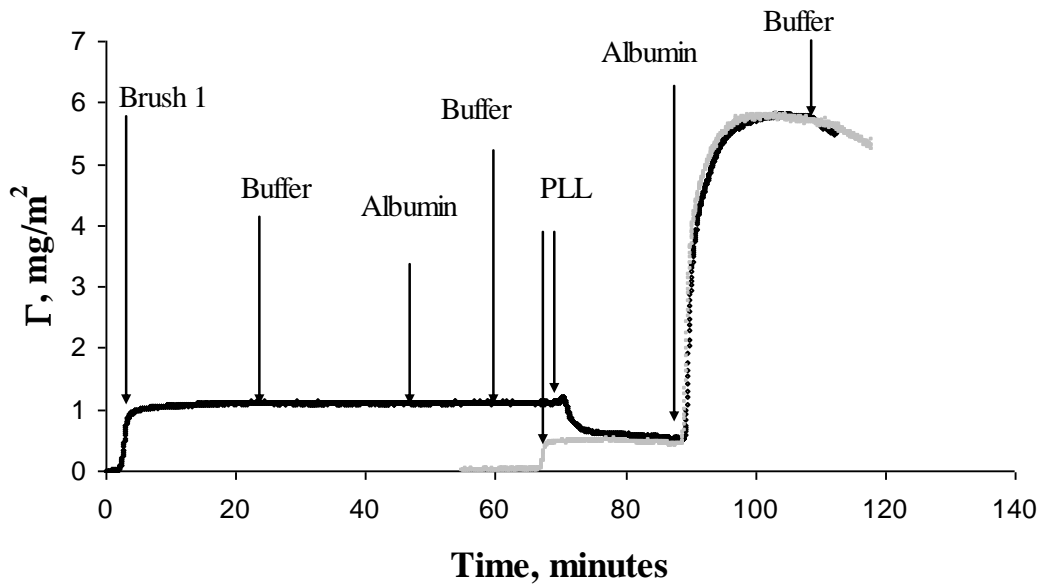


Figure 2.6 Adsorption and PLL challenge of Brush #1 in buffer with  $k-1 = 2$  nm. The original brush is exposed to 100 ppm albumin before and after the PLL challenge, using 100 ppm PLL solution.

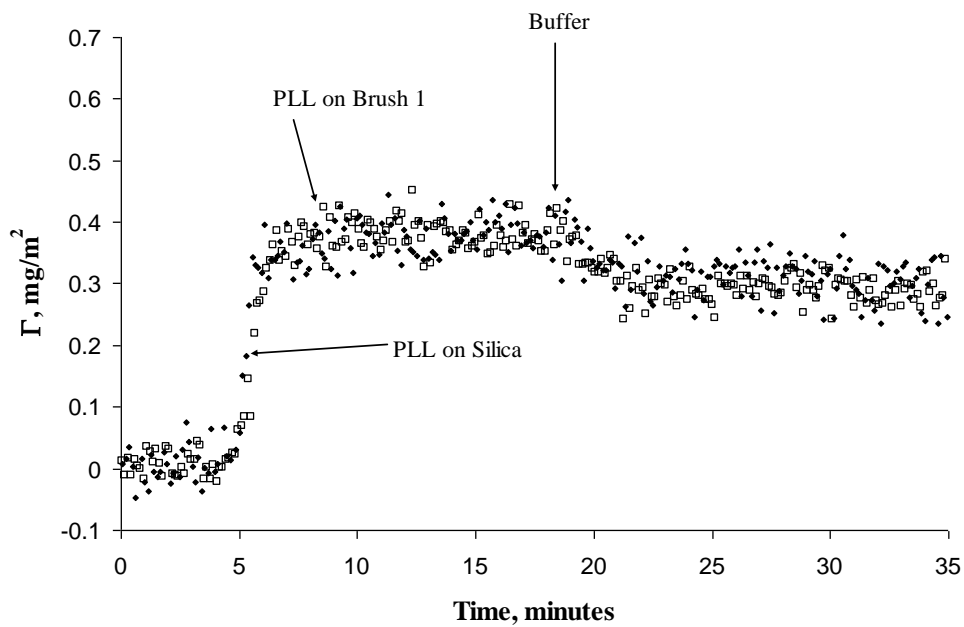


Figure 2.7 Adsorption of fluorescently labeled PLL, measured by TIRF onto a bare silica surface, and during the challenge of Brush #1. In the latter, the behavior of PLL-PEG chains are not seen since they are not fluorescently tagged.

Figure 2.7 demonstrates identical kinetics for PLL adsorption on bare silica and PLL adsorption (measured via TIRF with FITC-tagged PLL) into Brush #1. Brush #1 presents no kinetic barrier to the penetration of PLL, and apparently the segmental exchange at the base of the brush is rapid. Fast PLL adsorption kinetics is also depicted for PLL challenges on Brushes #2 and #3. Although PLL adsorption over Brush # 2 and # 3 seem to be slightly slower than observed for Brush #1, with  $0.4 \text{ mg/m}^2$  of PLL established in under 2 minutes as observed in Figure 2.8.

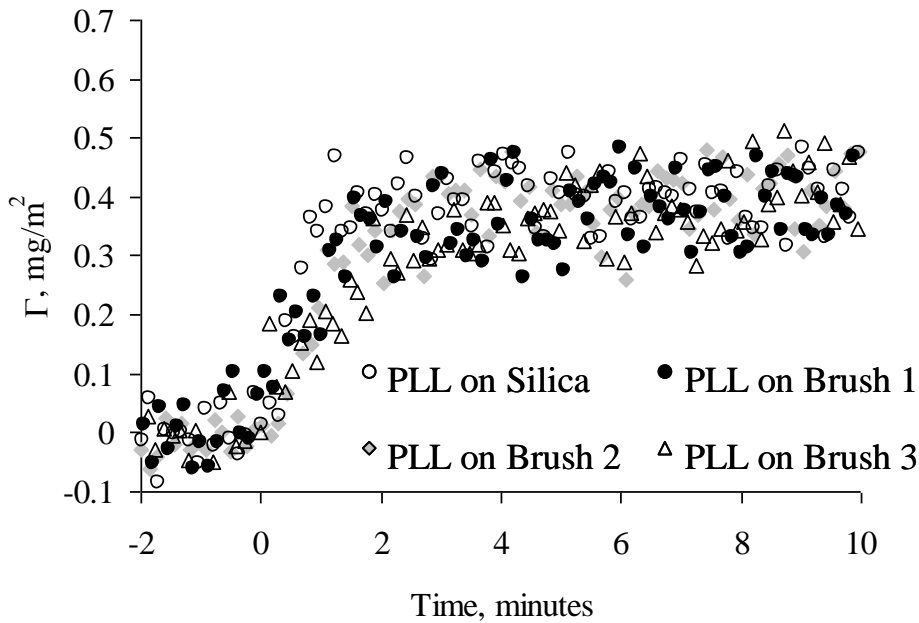


Figure 2.8 Adsorption of fluorescent PLL on silica and during challenge experiments for three brushes.

Figure 2.6 documents a small but interesting overshoot (near 70 minutes) in the total interfacial mass during PLL challenge of PLL-PEG brushes. This feature is seen, in

Figure 2.9, for all 3 brushes, though it varies quantitatively. The overshoot suggests that a small amount, 0.03-0.08 mg/m<sup>2</sup>, of PLL adsorbs on the silica before the PLL-PEG starts to be displaced. The possibility of this incremental adsorption is reinforced by Table II: The amount of PLL anchored at the base of these brushes, 0.05-0.16 mg/m<sup>2</sup>, is considerably less than the PLL saturation coverage on a bare silica surface, 0.4 mg/m<sup>2</sup>.

Also interesting, in Figure 2.7, PLL adsorbs continuously during the overshoot and subsequent PLL-PEG displacement processes, near the transport-limited PLL adsorption rate.

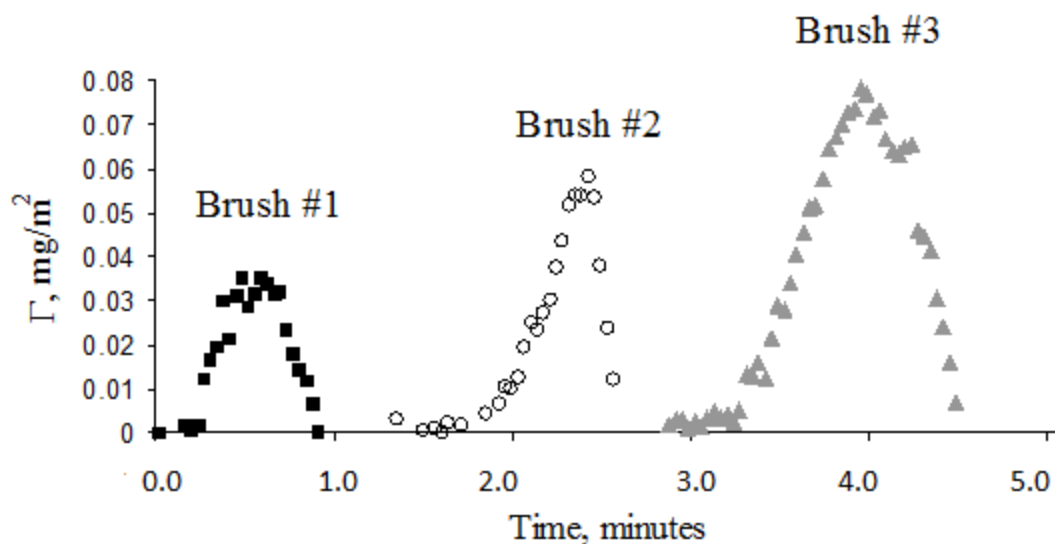


Figure 2.9 Close up of overshoot portion of reflectometry runs in which PLL challenges pre-adsorbed PLL-PEG brushes. The time axis for the different runs is shifted to facilitate a comparison of the overshoot seen for the different brushes.

Figure 2.10 argues, based on a different type of experiment, that some PLL can be accommodated at the base of an adsorbed PLL-PEG brush. Here, small amounts of PLL were adsorbed to a bare silica surface, followed by adsorption of a saturated PLL-PEG brush on the remaining surface. Figure 2.10 summarizes the amount of PLL-PEG accommodated after PLL preadsorption: Small amounts of PLL do not affect the PLL-PEG coverage, and are tolerated at the base of the brush. However, there is a maximum amount (depending on the particular PLL-PEG sample) of PLL that can be accommodated before PLL-PEG adsorption is reduced, indicated by the vertical bars, whose width indicates the level of uncertainty. Notably, for the three different PLL-PEG architectures, the amount of pre-adsorbed PLL that can be accommodated without compromise of a subsequently adsorbed brush is similar to that which can be adsorbed into an existing brush before the PLL-PEG is displaced. The latter is given by the overshoots in Figure 2.9.

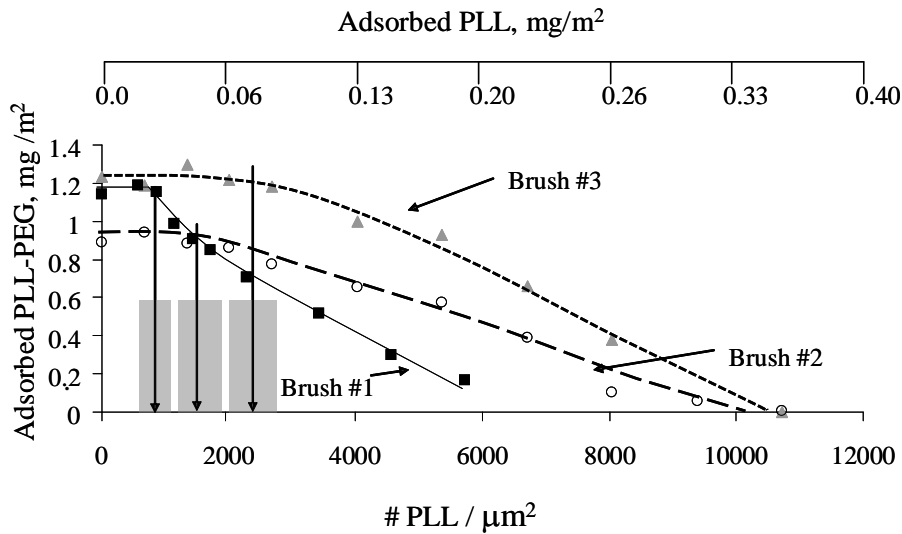


Figure 2.10: Amount of PLL-PEG adsorbing to silica after adsorption of small amounts of PLL, on the x-axis. Gray bars indicate uncertainty in determining the x-axis values where the data start to turn down.

Desorption kinetics of three brushes as illustrated in Figure 2.11 point out the competition between the PLL in the solution and the PLL anchored at the base of these brushes. The steric repulsion from the PEG brushes and the electrostatic attraction between the surface and the PLL anchors oppose each other. In the absence of a strong polyelectrolyte like PLL the electrostatic attraction of the PLL anchors at the base of the brushes win over the steric repulsion generated by the PEG segments of the brushes. However, as the brushes are challenged with PLL solution the electrostatic attraction of the anchors face a two front attack. First PLL coils in the solution find some defects in the brush and starts adhering over the silica substrate after penetrating the brush. These PLL coils have more  $-NH_2$  on their surface and hence more positive charge. The PLL anchors at the base of the brush start to feel the electrostatic repulsion from the anchored PLL coils. Secondly the steric repulsion generating from the PEG brushes enhances altogether desorption of the brushes from the surface.

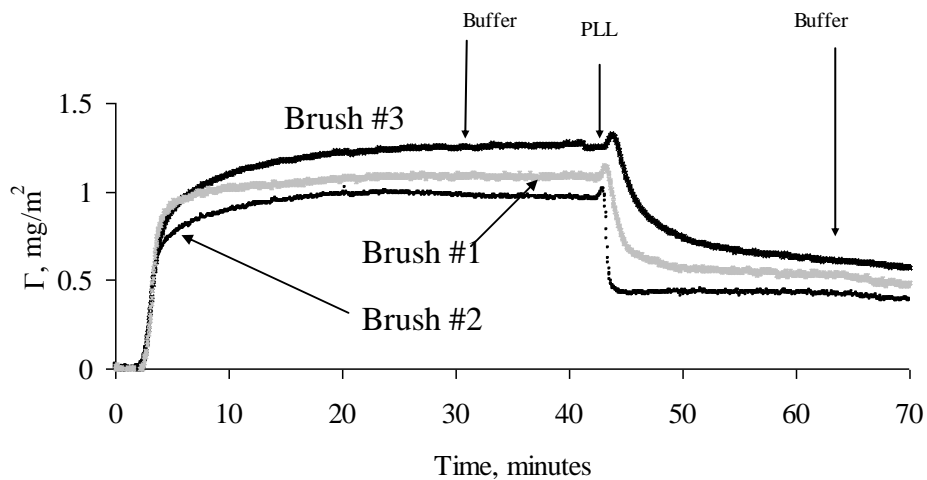


Figure 2.11 Full reflectometry traces of runs in which PLL-PEG brushes are challenged by 100 ppm PLL solutions in buffer having  $k-1 = 2$  nm.



A mass decrease plot is generated from Figure 2.11 and illustrated in Figure 2.12. From Figure 2.12 it is evident that Brush # 2 has the fastest desorption among the three brushes followed by Brush #1 and # 3. The grafting ratios of these three brushes show highest PEG loading per L-lysine repeat units in Brush # 2 followed by Brush # 1 and # 3. Hence we can expect highest steric repulsion from PEG segments in Brush # 2 followed by # 1 and # 3. Thus brush desorption kinetics support our former argument about steric force of PEG segments playing a crucial role here.

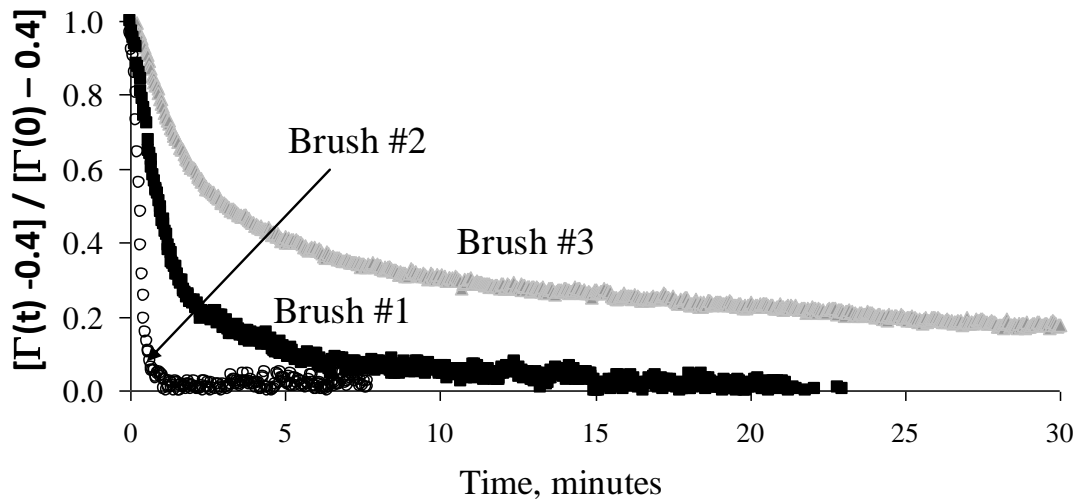


Figure 2.12 Mass decrease during PLL-challenge of the three brushes. Examining relaxation timescales.

## 2.5 Discussion

Of the proteins studied, those with negative charge did not adhere to brushy surfaces, while those with net positive charge were attracted to the brushes or to the underlying negative substrates. The observed correlation between adsorption and the

sign of the protein charge implicates electrostatic protein-surface interactions, with the negative proteins being repelled from the underlying negative substrates. The increased fibrinogen adhesion at lowered ionic strengths (Figure 2.5) only on the thinnest Brush #1, however, clarifies that electrostatic repulsions from the silica could not be responsible for the non-adherence of the negative proteins at  $\kappa^{-1} = 2$  nm. Indeed Figure 2.5 parallels findings from the literature with serum proteins, for the effects of brush thickness and ionic strength.<sup>1</sup> It was necessary to reproduce this trend with our own materials to ensure the conformance of our brushes to the literature. The importance of this result, lies (1) in its reaffirmation (for our materials) of the substantially greater brush thicknesses compared with the 2 nm Debye length (eliminating electrostatic protein-substrate interactions), and (2) in the contrasting behaviors of negative proteins and of lysozyme and PLL. Thus the surprising influence of the net protein charge on protein interactions with brushy surfaces cannot be attributed to electrostatic protein-substrate (silica or train layer) interactions.

It is interesting to note the negative zeta potentials of the brushy surfaces, significant for two reasons: First, it may seem counterintuitive that Brush #1 had more mildly negative zeta potentials than thicker Brushes #2 or #3. All other things constant, the magnitude of the zeta potentials should decrease with increasing brush thickness because the thicker brushes push the shear plane further out from the surface.<sup>12</sup> Table 2.2 reveals, however, differing amounts of PLL at the base of these brushes, altering the effective surface potential in the train layer of the brush. For instance, while Brush #1 is thinner than Brush #2, Brush #1 also contains more PLL at its base. Therefore the surface potential beneath Brush #1 will be less negative than Brush #2. A second

important point is that while the zeta potentials reveal the electrostatic environment at some point inside the PEG brush (due to some penetration of the shear plane into the brush), globular proteins seem not to access this electrostatic environment at  $\kappa^{-1} = 1$  or 2 nm. That is, the shear plane during a zeta potential measurement penetrates the brush more than globular proteins.

An observation which was not previously documented, to our knowledge, is the adhesion of lysozyme to relatively thick PEG brushes. (While Pasche has studied lysozyme interactions with PLL-PEG on Nb<sub>2</sub>O<sub>5</sub> surfaces, those copolymers contained 2K PEG tethers and all but one system were thin brushes that did not completely screen the electrostatic potential from the underlying substrate.<sup>1</sup> Indeed, current results with PLL(2.7)-PEG-2K (similar to one protein-resistant specimen within the Pasche study) produce very slight lysozyme adsorption in agreement with that their findings.) Figure 2 argues in favor of PEG-lysozyme attractions, a possibility which runs contrary to mainstream thinking that PEG ubiquitously repels globular proteins through steric (osmotic) interactions, as a result of the (1) the lack of charge on PEG, (2) its tendency to be well-solvated in water, with a net repulsion towards other molecules that are also water-solvated and (3) its hydrogen-bond accepting capacity (with no donor capacity).<sup>33</sup> We do not generally find, in the literature a discussion of PEG being adhesive towards some globular proteins and repulsive towards others. We note however, the Fraden lab's report of a negative second (cross) virial coefficient between PEG and lysozyme in free solution, based on light scattering.<sup>34</sup> This measure of PEG-lysozyme attractions supports our interpretation of Figure 2.4. Notably, these attractions may cause some penetration of

the lysozyme into the PEG layer, but lysozyme penetration through the brush layer to the silica substrate is not indicated or necessary to produce our observations.

A third behavior, the penetration of random PLL coils into PEG-PLL brushes and their subsequent displacement, in Figure 2.6 and 2.7 is technologically important because it dramatically compromises the protein resistance. These figures demonstrate that an established brush can be completely removed from the surface in less than five minutes, a surprising observation if one expects the PEG corona to osmotically shield the surface from PLL, or if one expects kinetically trapped states at in the adsorbed PLL layer to hinder exchange at the base of the brush.<sup>11,35,36</sup> Our study demonstrates arrival of PLL to the interface to be the rate limiting step: the adsorbed PLL-PEG brushes are in this sense extremely fragile.

It is worth pointing out that PLL was the only macromolecule tested that was able to penetrate the PEG brushes and proceed with brush displacement. This observation points toward the importance of protein / polypeptide structure in brush interactions. Apparently the dense globular nature of folded proteins is a key component of their exclusion from PEG brushes. The rapid displacement of adsorbed PLL-PEG by PLL suggests a lack of steric repulsions between hydrated PEG tethers and random-coil PLL chains. With PLL able to rapidly penetrate the otherwise protein-repelling brushes, electrostatic attractions to the base of the brush drive PLL adsorption.

The observation of rapid PLL-PEG displacement by PLL further argues that the anchoring PLL sequences are highly dynamic on the silica substrate. While some studies of polyelectrolyte exchange between solution and an interface reveal sluggish kinetics,<sup>11,35,36</sup> the PLL anchors of the current study are aided in their removal from the

surface by the entropy gain of the PEG tethers when the anchoring sections are released from the substrate. Without these tethers, short PLL train sections might re-adsorb as rapidly as they desorb, so that the entire PLL chain remains bound despite its dynamic fluctuations: A high density of PEG tethers make local PLL desorption events (involving a few segments) within the trains longer-lasting, facilitating adsorption of homopolymer PLL challengers.

## **2.6 Conclusions**

This chapter examined the interactions of cationic proteins and polypeptides with cationically-anchored PEG brushes whose architectures were previously reported and confirmed here to eliminate adhesion of key serum proteins. The study focused on ionic strength conditions where electrostatic interactions with the negative underlying substrate were screened by the brush.

The work revealed a strong correlation between the sign of the net protein charge and interactions with the brushy surfaces: Negative proteins did not adsorb, while positive proteins / polypeptides were attracted to and retained at the interface. Additional control studies re-affirmed the lack of electrostatic interactions between globular proteins and the underlying substrate, focusing attention on specific interactions between globular proteins and the hydrated PEG tethers. In the case of lysozyme, the greatest adsorption occurred to the brushes having the greatest amount of tethered PEG, a finding running contrary to the literature for general protein repellency of PEG brushes. While the specific mechanism for PEG-lysozyme attractions remains unclear, it is found that

cationic lysozyme behaves differently from anionic serum proteins in its interactions with PEG. This finding is contrary to conventional thinking which treats all globular proteins as similar in their interactions with nonionic brushes. These results point to the importance of the interactions between hydrated PEG brushes and globular proteins, which can be highly varied. Apparently there is a sensitivity of this interaction to nature of each protein, a possibility which is generally overlooked in the literature which, based on frequently studied protein models, always assumes domination by steric repulsions between PEG and globular proteins.

Beyond adhesion of the cationic protein lysozyme to the PEG brush corona, the study revealed that cationic random-coil polypeptides, for instance PLL, can rapidly penetrate a hydrated PEG brush, electrostatically interacting with the underlying substrate and displacing the brush. For moderately dense PEG brushes with tethers in the 2000 – 5000 MW range, such displacement processes are dominated by the arrival rate of PLL to the interface, identical to that for the adsorption of PLL on bare silica. The immediate displacement of the PEG brush demonstrates a potential failure mechanism of these interfaces *in-vivo*, and motivates permanent attachment of PEG chains to the substrate.

This work prompts reconsideration of specific PEG-protein interactions, and the nature of the anchoring of PEG groups in the presence of random-coil cationic polyelectrolytes. The findings demonstrate that, even if the PEG tethers were covalently bound to a substrate, cationic proteins and homopolymers can penetrate and adhere to the brush, or the substrate. Their retention in the brush potentially renders the interface bioadhesive to other proteins and cells, even without displacement of the PEG tethers.

## 2.7 References

- 1.) Pasche, Stéphanie, Vörös, J., Griesser, H. J., Spencer, N. D., & Textor, Marcus. (2005). Effects of Ionic Strength and Surface Charge on Protein Adsorption at PEGylated Surfaces. *The Journal of Physical Chemistry B*, 109(37), 17545-17552.
- 2.) Michel, R., Pasche, Stephanie, Textor, Marcus, & Castner, D. G. (2005). Influence of PEG Architecture on Protein Adsorption and Conformation. *Langmuir*, 21(26), 12327-12332.
- 3.) Yang, Z., Zhou, F., Yuan, J., Ma, L., Zhai, C., & Cheng, S. (2006). Preparation of PLL-PEG-PLL and its application to DNA encapsulation. *Science in China Series B: Chemistry*, 49(4), 357-362.
- 4.) Harris, L. G., Tosatti, S., Wieland, M., Textor, M., & Richards, R. G. (2004). Staphylococcus aureus adhesion to titanium oxide surfaces coated with non-functionalized and peptide-functionalized poly(L-lysine)-grafted-poly(ethylene glycol) copolymers. *Biomaterials*, 25(18), 4135-4148.
- 5.) Bergstrand, A., Rahmani-Monfared, G., Ostlund, A., Nydén, M., & Holmberg, K. (2009). Comparison of PEI-PEG and PLL-PEG copolymer coatings on the prevention of protein fouling. *Journal of Biomedical Materials Research. Part A*, 88(3), 608-615.
- 6.) Dinçer, S., Türk, M., Karagöz, A., & Uzunalan, G. (2011). Potential c-myc antisense oligonucleotide carriers: PCI/PEG/PEI and PLL/PEG/PEI. *Artificial Cells, Blood Substitutes, and Immobilization Biotechnology*, 39(3), 143-154.
- 7.) Dalsin, J. L., Hu, B.-H., Lee, B. P., & Messersmith, P. B. (2003). Mussel Adhesive Protein Mimetic Polymers for the Preparation of Nonfouling Surfaces. *Journal of the American Chemical Society*, 125(14), 4253-4258.
- 8.) Dalsin, J. L., Lin, L., Tosatti, Samuele, Vörös, J., Textor, Marcus, & Messersmith, P. B. (2005). Protein resistance of titanium oxide surfaces modified by biologically inspired mPEG-DOPA. *Langmuir: The ACS Journal of Surfaces and Colloids*, 21(2), 640-646.

- 9.) Dijt, J. C., Cohen, S., & Fleer, G. J. (1994). Competitive Adsorption Kinetics of Polymers Differing in Length Only. *Macromolecules*, 27(12), 3219-28.
- 10.) Fu, Z., & Santore, M. M. (1998). Kinetics of Competitive Adsorption of PEO Chains with Different Molecular Weights. *Macromolecules*, 31(20), 7014-7022.
- 11.) Sukhishvili, S. A., & Granick, S. (1998). Kinetic regimes of polyelectrolyte exchange between the adsorbed state and free solution. *Journal of Chemical Physics*, 109(16), 6869-6878.
- 12.) Milner, S. T. (1991). Polymer brushes. *Science (New York, N.Y.)*, 251(4996), 905-914.
- 13.) Pasche, Stephanie, De, P., Voeroes, J., Spencer, N. D., & Textor, Marcus. (2003). Poly(L-lysine)-graft-poly(ethylene glycol) assembled monolayers on Niobium Oxide surfaces: a quantitative study of the influence of polymer interfacial architecture on resistance to protein adsorption by ToF-SIMS and in situ OWLSu OWLS. *Langmuir*, 19(22), 9216-9225.
- 14.) Huang, N.-P., Michel, R., Voros, J., Textor, Marcus, Hofer, R., Rossi, A., Elbert, D. L., et al. (2001). Poly(L-lysine)-g-poly(ethylene glycol) Layers on Metal Oxide Surfaces: Surface-Analytical Characterization and Resistance to Serum and Fibrinogen Adsorption. *Langmuir*, 17(2), 489-498.
- 15.) Kenausis, G. L., Voeroes, J., Elbert, D. L., Huang, N., Hofer, R., Ruiz-Taylor, L., Textor, Marcus, et al. (2000). Poly(L-lysine)-g-Poly(ethylene glycol) Layers on Metal Oxide Surfaces: Attachment Mechanism and Effects of Polymer Architecture on Resistance to Protein Adsorption. *Journal of Physical Chemistry B*, 104(14), 3298-3309.
- 16.) Gon, S., Bendersky, M., Ross, J. L., & Santore, M. M. (2010). Manipulating Protein Adsorption using a Patchy Protein-Resistant Brush. *Langmuir*, 26(14), 12147-12154.
- 17.) Fu, Z., & Santore, M. M. (1998b). Poly(ethylene oxide) adsorption onto chemically etched silicates by Brewster angle reflectivity. *Colloids and Surfaces, A: Physicochemical and Engineering Aspects*, 135(1-3), 63-75.



- 18.) Kelly, M. S., & Santore, M. M. (1995). The role of a single end group in poly(ethylene oxide) adsorption on colloidal and film polystyrene: complimentary sedimentation and total internal reflectance fluorescence studies. *Colloids and Surfaces, A: Physicochemical and Engineering Aspects*, 96(1/2), 199-215.
- 19.) Wertz, C. F., & Santore, M. M. (1999). Adsorption and Relaxation Kinetics of Albumin and Fibrinogen on Hydrophobic Surfaces: Single-Species and Competitive Behavior. *Langmuir*, 15(26), 8884-8894.
- 20.) Alexander, S. (1977). Adsorption of chain molecules with a polar head a scaling description. *Journal de Physique (Paris)*, 38(8), 983-7.
- 21.) de Gennes, P. G. (1976). Scaling theory of polymer adsorption. *Journal de Physique (Paris)*, 37(12), 1445-1452.
- 22.) Gon, S., & Santore, M. M. (2011). Single Component and Selective Competitive Protein Adsorption in a Patchy Polymer Brush: Opposition between Steric Repulsions and Electrostatic Attractions. *Langmuir*, 27(4), 1487-1493.
- 23.) Wasilewska, Monika, Adamczyk, Zbigniew, & Jachimska, B. (2009). Structure of Fibrinogen in Electrolyte Solutions Derived from Dynamic Light Scattering (DLS) and Viscosity Measurements. *Langmuir*, 25(6), 3698-3704.
- 24.) Tsapikouni, T. S., & Missirlis, Y. F. (2007). pH and ionic strength effect on single fibrinogen molecule adsorption on mica studied with AFM. *Colloids and Surfaces, B: Biointerfaces*, 57(1), 89-96.
- 25.) Böhme, U., & Scheler, U. (2007). Effective charge of bovine serum albumin determined by electrophoresis NMR. *Chemical Physics Letters*, 435(4-6), 342-345.
- 26.) Arai, T., & Norde, W. (1990). The behavior of some model proteins at solid-liquid interfaces. 1. Adsorption from single protein solutions. *Colloids and Surfaces*, 51, 1-15.

- 27.) de, Backer, M., McSweeney, S., Rasmussen, H. B., Riise, B. W., Lindley, P., & Hough, E. (2002). The 1.9 Å crystal structure of heat-labile shrimp alkaline phosphatase. *Journal of Molecular Biology*, 318(5), 1265-1274.
- 28.) Kuehner, D. E., Engmann, J., Fergg, F., Wernick, M., Blanch, H. W., & Prausnitz, J. M. (1999). Lysozyme Net Charge and Ion Binding in Concentrated Aqueous Electrolyte Solutions. *Journal of Physical Chemistry B*, 103(8), 1368-1374.
- 29.) Kalasin, S., & Santore, M. M. (2009). Non-specific adhesion on biomaterial surfaces driven by small amounts of protein adsorption. *Colloids and Surfaces. B, Biointerfaces*, 73(2), 229-236.
- 30.) Deshmukh, V., Britt, D. W., & Hlady, V. (2010). Excess fibrinogen adsorption to monolayers of mixed lipids. *Colloids and Surfaces. B, Biointerfaces*, 81(2), 607-613.
- 31.) Adamczyk, Z, Nattich, M., Wasilewska, M, & Sadowska, M. (2011). Deposition of colloid particles on protein layers: fibrinogen on mica. *Journal of Colloid and Interface Science*, 356(2), 454-464.
- 32.) Ortega-Vinuesa, J. L., Tengvall, P., & Lundstrom, I. (1998). Molecular packing of HSA, IgG, and fibrinogen adsorbed on silicon by AFM imaging. *Thin Solid Films*, 324(1,2), 257-273.
- 33.) Ostuni, E., Chapman, R. G., Holmlin, R. E., Takayama, S., & Whitesides, G. M. (2001). A Survey of Structure-Property Relationships of Surfaces that Resist the Adsorption of Protein. *Langmuir*, 17(18), 5605-5620.
- 34.) Bloustone, J., Virmani, T., Thurston, G. M., & Fraden, S. (2006). Light Scattering and Phase Behavior of Lysozyme-Poly(Ethylene Glycol) Mixtures. *Physical Review Letters*, 96(8),
- 35.) Hansupalak, N., & Santore, M. M. (2004). Polyelectrolyte Desorption and Exchange Dynamics near the Sharp Adsorption Transition: Weakly Charged Chains. *Macromolecules*, 37(4), 1621-1629.

- 36.) Santore, M. M. (2005). Dynamics in adsorbed homopolymer layers: Understanding complexity from simple starting points. *Current Opinion in Colloid & Interface Science*, 10(3,4), 176-183.
- 37.) Gon, S., Fang, B., & Santore, M. M. (2011). Interaction of Cationic Proteins and Polypeptides with Biocompatible Cationically-Anchored PEG Brushes. *Macromolecules*, 44(20), 8161-8168.

# CHAPTER 3

## MANIPULATING PROTEIN ADSORPTION USING A PATCHY PEG BRUSH

### 3.1 Introduction

The focus in this chapter is to develop patchy polymer brushes as a means of controlling adhesive protein contact. Much of this chapter has been reproduced from a recently published work<sup>45</sup>.

The design of surfaces for the control of protein adsorption has been a scientific and industrial endeavor for the past several decades, with the goals ranging from complete avoidance of protein adsorption (and cell adhesion) for some implants, to selective reversible protein binding for pharmaceutical separations, and addressable specific-targeting elements in protein chip arrays and diagnostics. Common strategies include immobilization of bio-specific (“affinity”) capture molecules and passivation of the remaining surface. Often, lithographic methods enable controlled placement of adhesive and non-adhesive moieties, enabling addressability. As pattern length scales often exceed protein dimensions proteins are found clustered over patterned surfaces. While this may be useful in some applications such study can not focus on molecular level interaction of proteins with patterned media.

Many proteins spread and denature substantially on large areas of adhesive surfaces.<sup>1-8</sup> It follows, then, that limiting protein-surface contact is a potential means of

achieving protein adhesion without denaturing. This challenge, however, requires the fine tuning of binding energies and contact areas to ensure protein retention at the same time avoiding unfolding. Steps have been made in this direction employing nanoparticles.<sup>9-12</sup> For instance, it has been reported that albumin is more stable to denaturing when adsorbed onto small rather than large gold nanoparticles.<sup>13</sup> Related to these findings and providing further motivation for immobilization of small numbers of proteins is the observation that the edges of a 2D lysozyme pattern are more accessible to antibody binding than the proteins in the main area of the pattern.<sup>14</sup>

By way of background, hydrated polymer brushes such as PEG (polyethylene glycol)<sup>15-19</sup> or certain zwitterionic polymers<sup>20, 21</sup> have been used for prevention of non-specific bio-adhesion. By strict definition in the polymer physics community, a brush is produced when polymer chains are end-grafted to an interface in a good solvent, with the grafting spacing smaller than the characteristic free coil size, by about an order of magnitude.<sup>22-24</sup> As a result of the osmotic pressure generated by the good solvent, segmental repulsions stretch the polymer chain normal to the interface and can prevent close approach of proteins or other brushy objects. It is noted however that in most cases of bioinertness and near-perfect protein repellency, the brush density and height fall substantially short of the rigorous definition.<sup>25-28</sup> Thus it is the case, especially in the biomaterial community, that the term “brush” is used loosely, as we do here. (Indeed, until the advent of surface initiated polymerizations, the adsorption method of depositing brushes always fell short of the coverages of true brush.<sup>28</sup> Adsorption continues, however, to be a preferred method of brush placement, due to its economic and processing advantages.)

This chapter explores the use of “patchy brushes” as materials for the manipulation of protein adsorption, potentially for protein separation or biomaterial applications. These surfaces contain relatively flat nanoscale adhesive regions surrounded by a polymer protein-resistant polymer brush, shown schematically in Figure 3.1. Brush # 1 as described in the previous chapter is the focus here. While the adhesive elements or “patches” could be any arbitrary chemistry, here they are cationic. The current patchy brushes are modeled after the electrostatically-patchy surfaces previously studied in detail by the Santore group,<sup>29-31</sup> but the current surfaces employ brushes on the main surface region as opposed to negative charge of the prior body of work. The size of the adhesive regions, 10 nm or less, is small relative to the protein size, limiting protein contact with the surface.

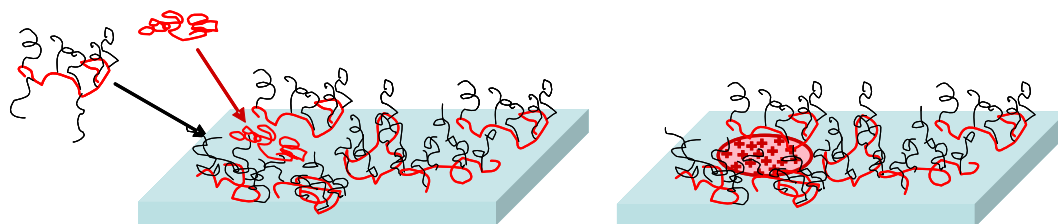


Figure 3.1 Schematic of patchy brush

This chapter reports the interaction of these patchy brush surfaces with fibrinogen, which was chosen because of its importance in different applications and its tendency to adhere to many different surface types. This is a result of its substantial hydrophobicity and electrostatic heterogeneity: Fibrinogen’s central e-domain is positively charged while the protein charge is overall net negative.<sup>32</sup> Also though fibrinogen is relatively

large, roughly  $47 \times 4.5 \times 4.5 \text{ nm}^3$ ,<sup>33</sup> it has been shown to adhere to relatively small surface features, for instance the interstices of a saturated adsorbed albumin layer, ie after no further albumin would adhere.<sup>34</sup>

This chapter demonstrates a simple method for creation of patchy brushes and reports their basic behavior in terms of protein interactions. Here we demonstrate that patches can be made sufficiently small / weakly binding that single patches are not able to adsorb protein. When the surface density of the patches becomes sufficiently high that fibrinogen can interact with multiple patches at once, limited adsorption occurs. The work demonstrates how flaws or contaminants can be accommodated in a polymer brush without altering its structure, and then goes on to demonstrate how these flaws or adhesive regions potentially lead to bioadhesion.

## **3.2 Experimental Methodology**

Synthesis and characterization of Brush # 1 has been described in chapter 2. Poly-L-lysine hydrobromide, PLL, with a nominal molecular weight of 20,000 was purchased from Sigma-Aldrich. Bovine serum fibrinogen (fraction I, type 1-s) was purchased from Sigma (F8630-1G). In the runs in the published figures, which employed optical reflectometry, the protein was used as received. The adsorption substrates for this study were acid-etched microscope slides. In our procedure, overnight soaking in concentrated sulfuric acid, followed by copious rinsing in DI (de-ionized water) leaches metal ions from the soda-lime glass to produce a pure silica surface, as characterized by XPS.<sup>33</sup>

As described in Chapter 2 Polymer and protein adsorption were conducted in a laminar slit shear flow cell<sup>35</sup> with a wall shear rate of  $5 \text{ s}^{-1}$ , using polymers dissolved in 0.01M pH 7.4 phosphate buffer. In the main portion of the study, adsorption was monitored with near-Brewster optical reflectometry, a method sensitive to the refractive index of the layer, and which requires no labeling of the adsorbing molecules. In our instrument,<sup>36</sup> a parallel-polarized HeNe laser impinges on the liquid solid interface from the solid side. Near the Brewster condition, the back reflected beam is vanishingly small, arising primarily from the etched silica layer on the microscope slide. As adsorption proceeds, however, the intensity grows in a fashion that can be adequately quantified using a step profile optical model. For the different interfacial layers (polymer and protein) in the current study, the overall mass is sufficiently small that this treatment works well, though different refractive indices potentially apply to the polymer and protein layers.<sup>36</sup>

Control runs were performed using total internal reflectance fluorescence with the same flow chamber.<sup>37</sup> By labeling either the PLL or the fibrinogen with fluorescein or rhodamine b isothiocyanate,<sup>34</sup> (ITC) we were able to establish that PLL and PLL-PEG molecules were not displaced during fibrinogen adsorption. A rhodamine-b-ITC labeled PLL sample was employed in single fluorophore imaging studies of the distribution of PLL chains on the surface.

Total internal reflection fluorescence imaging of polymer-coated surfaces was performed with a home-build laser system (488 nm and 532 nm) built around a Nikon Ti-E inverted microscope using through the lens illumination (60x objective, NA 1.49). Images were recorded on a Cascade (Roper Scientifics) electron-multiplier CCD camera



with a 1 second exposure time using an EM gain set at 3564. Data was analyzed in ImageJ by selecting individual particles after thresholding and measuring the intensity.

Zeta potentials for saturated layers of PLL and PLL-PEG on silica were determined using 1  $\mu\text{m}$  silica spheres from GelTech (Orlando, FL), onto which varying amounts of these polymer had been adsorbed. The ionic strength conditions for adsorption and zeta potential measurement corresponded to those used in the corresponding portions of the main study. A Malvern Zeta Sizer Nano ZS instrument was employed.

### **3.3 Results**

#### **3.3.1 Features of patchy Brush # 1 surfaces**

Some properties of the patchy brush surfaces can be deduced from the interfacial properties of the component polymers, summarized in Table 3.1.

##### **3.3.1.1 PLL Patches**

Features of the PLL patches can be inferred from properties of PLL layers, in Figure 3.2A. In Table 3.1, PLL having a nominal molecular weight of 20,000 forms saturated layers with coverages of  $0.4 \text{ mg/m}^2$ , typical of other densely charged cationic polymers on silica at pH 7.4.<sup>38</sup> Coverage is independent of free solution concentration over a large range, as a result of the substantial segment-surface binding energy.

In general, when densely charged cationic polymers adsorb on a negative substrate, the backbone lies flat to the surface.<sup>39</sup> This is particularly true at coverages well below saturation, pertinent to the current isolated cationic patches. Consistent with this scenario is the mildly positive zeta potential of saturated PLL layers, on silica. The mild overcompensation of charge by saturated PLL layers suggests that isolated PLL chains adsorbed at low coverages will also be locally positively charged. Patches can also be expected to be relatively flat.<sup>29</sup>

Table 3.1 Properties of saturated PLL and PLL-PEG Brush # 1

	PLL	PLL-PEG (Brush # 1)
Nominal molecular weight, g/mol	20,000	147,100
Free solution hydrodynamic radius, nm	7	-----
Saturated layer coverage, mg/m <sup>2</sup>	0.4 ± 0.02	1.1 ± 0.1
Effective chain footprint, nm <sup>2</sup>	83 ± 10	220 ± 22
Zeta potential of saturated layer, mV	+ 5	-9 ± 3

The net positive charge on the PLL chains gives rise to modest patch-patch repulsions on the surface that limit the ultimate PLL coverage. Near neutral pH when the ionic strength is raised from 0.01M to 0.1M, the PLL coverage increases by about 20%.<sup>40</sup> This is consistent with the reduction of the Debye length from 3 to just under 1 nm. With the 2nm Debye length at conditions for our patch deposition (ionic strength I= 0.026M for a phosphate buffer concentration of 0.01M), no patch ordering or other special long range effects of patch-patch interactions are expected in our studies. It is worth noting,

however, that the documented presence of repulsions between adsorbing PLL chains and the impact of these repulsions on the PLL adsorption on silica argues against any surface aggregation of the PLL.

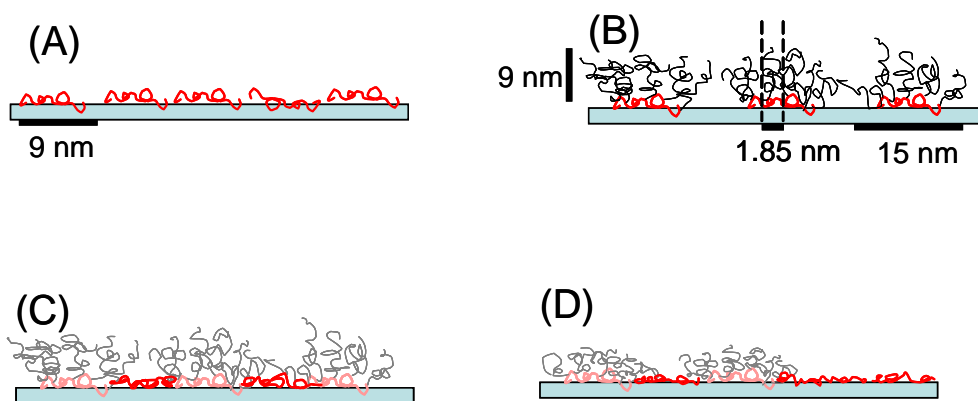


Figure 3.2 Features of interfacial brush components. A) A saturated PLL layer showing the diameter of excluded footprint B) A saturated diameter of Brush # 1 showing the diameter of the excluded footprint of PLL-PEG and the effective diameter of a PEG tether. C) Inclusion of PLL patches in the brush. Graft copolymers are shown in fade pink to highlight patches. D) Greater PLL loading reduces brush coverage thus reducing crowding and PEG chain stretching.

One metric of the patch size of adsorbed PLL derives from its free solution hydrodynamic coil diameter,  $d_h = 7$  nm from dynamic light scattering. A second measure of the adsorbed coil size derives from the excluded footprint of a chain in a saturated PLL layer. Dividing the molecular weight by the adsorbed amount in a saturated layer, and converting units reveals a footprint of  $83 \text{ nm}^2$ , giving a diameter (of “gyration” a statistical measure)  $d_g = 9.1$  nm. The free solution hydrodynamic diameter is consistent with this value, as it is generally accepted that polyelectrolytes at moderate and high ionic

strengths act like neutral chains. Then, a non-draining model relates the hydrodynamic to the statistical size:  $d_h = 0.676 d_g$ .<sup>41</sup>

As demonstrated previously with other systems<sup>29, 33, 42</sup> for PLL, using a shear flow cell with well-characterized mass transport, we are able to deposit PLL in controlled amounts down to extremely low coverages, where individual coils are randomly isolated on the surface. The patch deposition by varying flow time of PLL solution is illustrated in Figure 3.4. Previous study of pDMAMEA (poly[dimethylaminoethyl methacrylate]) polycation adsorption has demonstrated the near-random arrangement of polycations adsorbed in this fashion on silica, especially in the dilute range of patch loading relevant to the current work.<sup>31</sup> Additionally, we have found that the tight binding of polycations on a negative surface prevents chain translation along the surface that would tend to reduce order.

The random distribution of the adsorbed patches is further strongly supported by Figure 3.3. Figure 3A shows a micrograph of a patchy PLL layer containing 500 chains / $\mu\text{m}^2$  as established by the controlled deposition. In fabricating this specimen, a PLL sample containing an average of 0.6 rhodamine tags per PLL chain was diluted into an unlabeled PLL solution and exposed in steady flow to the substrate under tightly controlled timing to produce a surface having with 1.5 rhodamine tags / $\mu\text{m}^2$  with 500 PLL chains total / $\mu\text{m}^2$ . The intent of this surface composition was to produce an image containing diffraction-limited spots for the individual fluorophores. (One fluorophore on each of 500 chains /  $\mu\text{m}^2$  would have produced a layer too densely labeled to resolve individual labels.) Given the scale of the micrograph, one expects roughly 1500 fluorophores in the image. 1300 spots are actually counted, indicating that some of the

diffraction-limited spots, each 250 nm in diameter contain 2 or more fluorophores, as expected for a random distribution (and for the finite probability of 2 labels on some of the chains.) Indeed, Figure 3B, a simulated image of the randomly positioned spots in the same field looks similar in randomness to the micrograph, confirming the overall random distribution of our patches and a lack of PLL aggregation on the surface. Figure 3C addresses the fact that less than 1% of the chains in Figure 3A carry fluorescent labels. Here the distribution of intensities per spot indicates that some spots contain multiple fluorophores. As the amount of fluorescent PLL is increased, while keeping the total PLL patch loading constant, the distribution shifts proportionately to the right, indicating a greater incidence of spots with multiple fluorophores.

In summary, the features of saturated PLL layers along with other data suggest that when individual PLL chains are sparsely adsorbed on silica, the resulting patches are about 9 nm in size, lie flat to the surface, are randomly arranged, and locally present positive charge. Figure 3.5 demonstrates that the PLL patches resist desorption in pH 7.4 buffer while and withstand challenge by PLL-PEG and fibrinogen. Prior work suggests they do not diffuse laterally on the surface on timescales relevant to our study.<sup>29,43,44</sup>

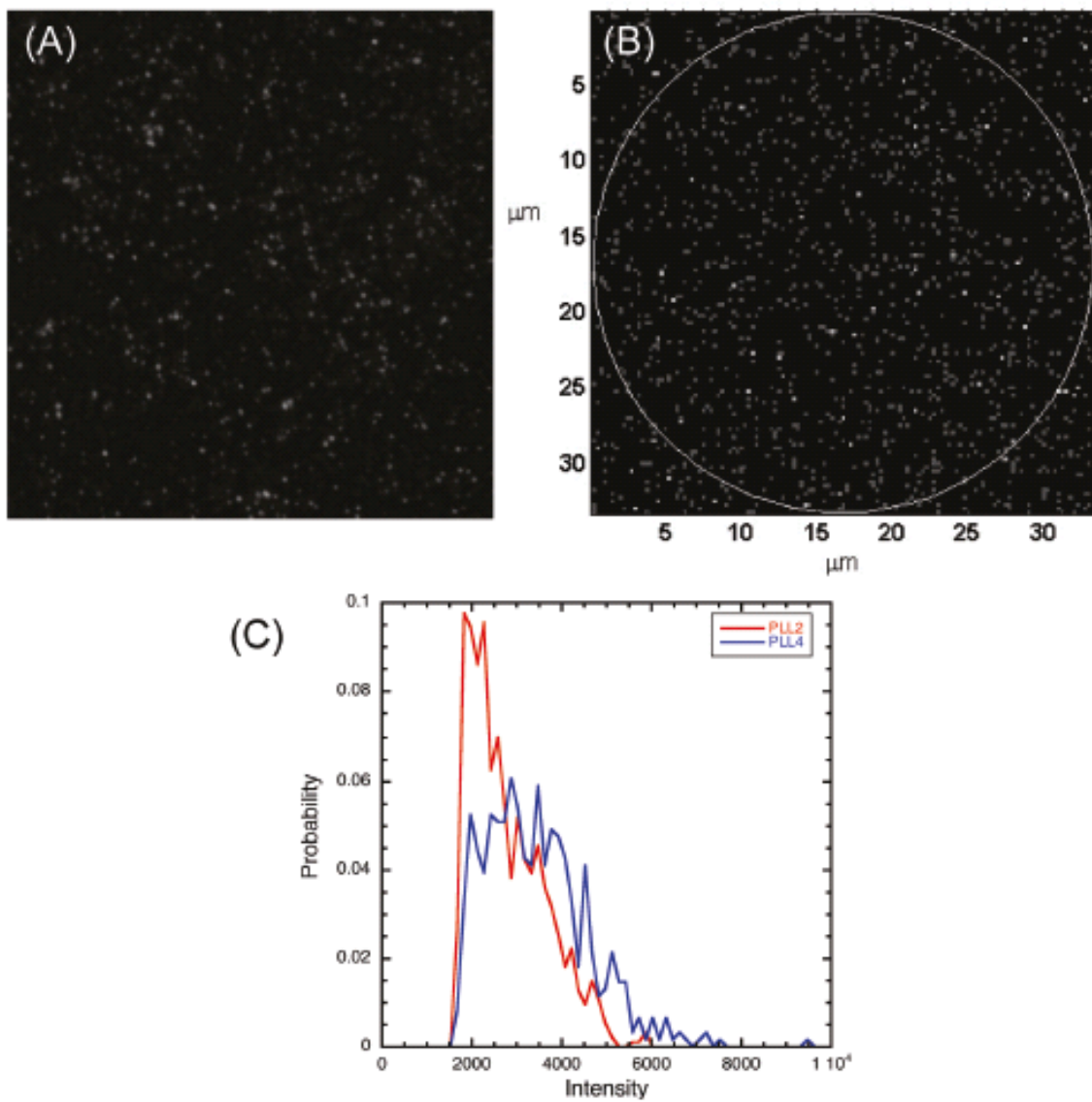


Figure 3.3 TIRF microscopy images of PLL patches A)  $33\ \mu\text{m} \times 33\ \mu\text{m}$  micrograph containing  $500\ \text{PLL}/\mu\text{m}^2$ , a trace amount of which is fluorescently labeled to give  $1.5\ \text{fluorophores}/\mu\text{m}^2$  corresponding to 1500 illuminated spots, some of which might overlap. B) Image simulated in Matlab with 1500 spots distributed randomly in the same area. Here doubles appear brighter. C) Distribution of spot intensities for two surfaces like in A with 1.5 and 3 labels per  $\mu\text{m}^2$ .

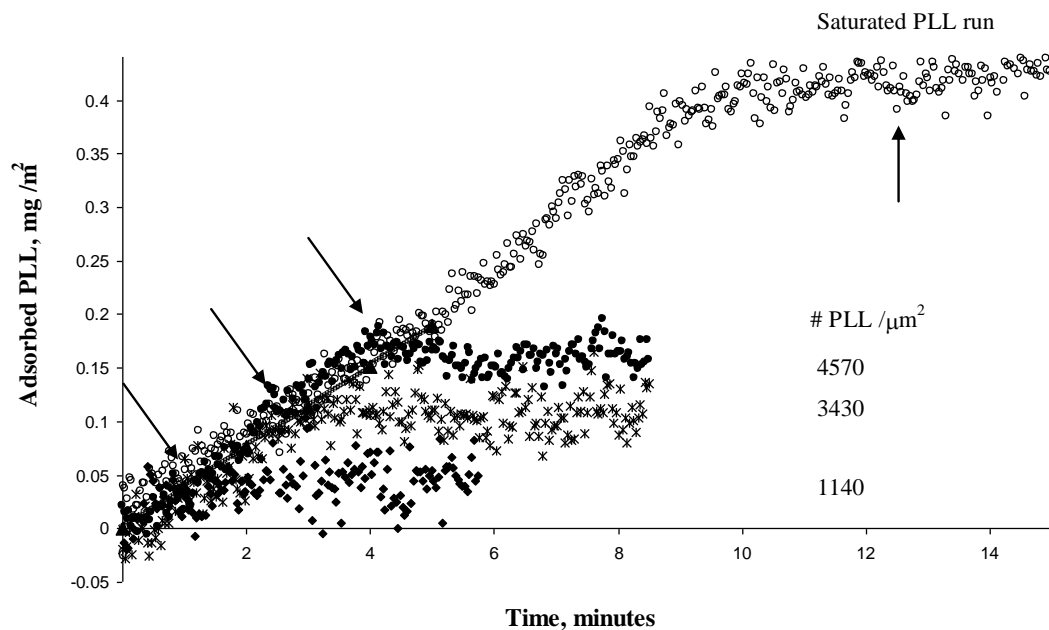


Figure 3.4 Controlled PLL deposition to make cationic patches. Buffer injection at arrows limits the amount of PLL deposited. Buffer injection at the arrow for the saturated run demonstrates good retention of the fully saturated layer

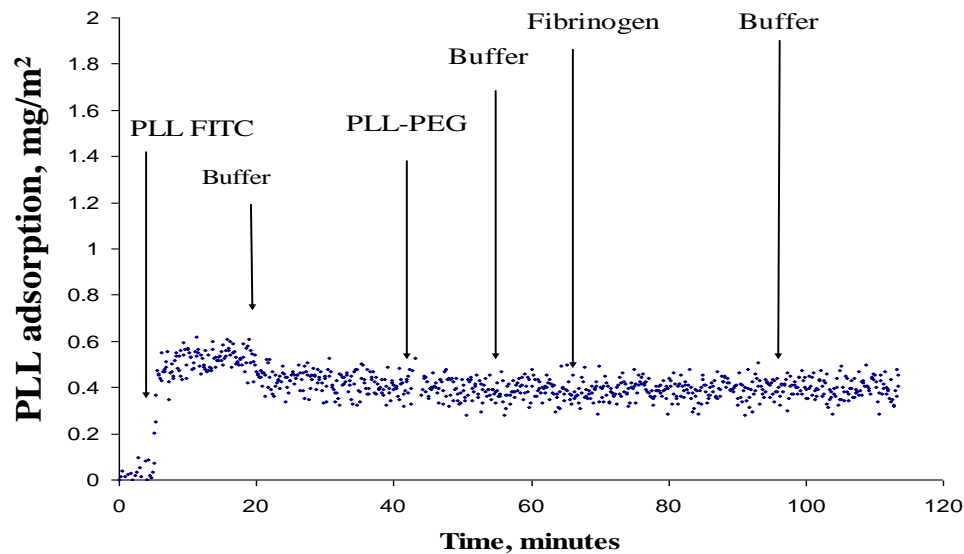


Figure 3.5 TIRF experiment for the adsorption of fluorescently-labeled PLL, subsequently challenged by flowing buffer, PLL-PEG, and fibrinogen. The PLL-PEG and fibrinogen are unlabeled and therefore not visible in the experiment, which shows the retention of the labeled PLL.

### 3.3.1.2 PLL-PEG Brushes

The saturation coverage of  $1.1 \pm 0.1 \text{ mg/m}^2$  for PLL-PEG on bare silica (in Table 3.1, and Figure 3.6 A) provides quantitative insight into the features of the PEG brush: With a grafting ratio of 2.8 and a PEG molecular weight of 2000, this saturation coverage corresponds to  $220 \pm 20 \text{ nm}^2$  per adsorbed PLL-PEG molecule, and  $3.4 \text{ nm}^2$  per interfacial PEG chain, or a 1.85 nm diameter footprint for a tether. These dimensions are shown schematically in Figure 3.2 B. The calculated unperturbed (theta solvent) end-end distance of a 2000 molecular weight PEG chain is 3.35 nm (radius = 1.67 nm) or, with classic 3/5-power law scaling of molecular weight expected in a good solvent, the maximum coil radius might be as large as 2.4 nm. Therefore the PEG chains tethered to our surfaces by PLL anchors are just sufficiently closely tethered to be forced to stretch normal to the surface. A brush height of 9 nm is estimated as described in chapter 2.

The larger excluded footprint ( $220 \text{ nm}^2$ ) of chains within a pure saturated PLL-PEG layer compared with those within a pure saturated PLL layer ( $83 \text{ nm}^2$ ) in Table 3.1 is significant. This difference indicates that in the PLL-PEG layer, it is the PEG rather than the PLL backbone that limits the brush coverage. The lower content of PLL backbones within the PLL-PEG layer, per Figure 3.2A and B is also consistent with the negative zeta potential of the saturated PLL-PEG surfaces.

### 3.3.1.3 Patchy Brushes

Patchy brushes were created by first depositing controlled amounts of PLL from dilute flowing solution, (as shown in Figure 3.4) and, following a buffer rinse, backfilling with PLL-PEG. (Control studies using fluorescently-labeled PLL have demonstrated full retention of the PLL patches throughout this process as demonstrated in Figure 3.5.)



Figure 3.6 A presents reflectometry data for the PLL-PEG backfilling portion of the process for surfaces containing different densities of preadsorbed PLL patches. With no PLL pre-adsorbed, the saturation coverage for PLL-PEG on bare silica is  $1.1 \pm 0.1$  mg/m<sup>2</sup>, and its initial adsorption onto silica is transport limited. As the amount of pre-adsorbed PLL is increased, the ultimate PLL-PEG coverage decreases; however, the adsorption kinetics are mostly unaffected. The flat signal following buffer reinjection demonstrates the stability of the composite layers at these conditions.

Figure 3.7 A summarizes the data in Figure 3.6 A by plotting the amount of PLL-PEG backfill as a function of the initially adsorbed PLL patch density. This representation demonstrates that small amounts of PLL, below 900 chains /  $\mu\text{m}^2$ , can be accommodated at the interface without reducing overall brush density, shown schematically in Figure 3.2 C. The mechanism derives from the smaller excluded footprint of PLL compared with PLL-PEG in pure saturated layers, in Table 3.1 and Figure 3.2 A-B. The lower backbone content of the saturated PLL-PEG layers, compared with a saturated layer of pure PLL provides an opportunity for limited PLL incorporation at the base of the brush. At the point where the maximum amount of PLL chains have been incorporated into the base of the brush, there are about 5400 PLL chains /  $\mu\text{m}^2$  on the surface, either as part of PLL-PEG chains (4500 /  $\mu\text{m}^2$ ) or as PLL patches (900 /  $\mu\text{m}^2$ ). This is far less than the 12,000 PLL chains /  $\mu\text{m}^2$  in a pure saturated PLL layer. The difference provides evidence for the lack of mobility of the adsorbed chains. Were chains sufficiently mobile on the surface, they might rearrange to accommodate a greater density of PLL at the base of the brush.

When PLL patch densities exceed  $0.03 \text{ mg/m}^2$  ( $900 \text{ chains /um}^2$ ), additional PLL patches reduce the amount of PLL-PEG needed for backfilling. Over most of this regime, each PLL patch added to the surface reduces the PLL-PEG backfill by one chain. (We note however, that the decay has some curvature so the effective chain exchange percentage is initially higher. Our point here is, however that the displacement occurs near the order of a 1-1 chain swapping.) Ultimately a saturated layer of PLL completely excludes PLL-PEG. As the numbers of PEG tethers decrease with increases in the PLL patches, the overall average quality of the brush is reduced (ie the average chain becomes less extended normal to the surface because the tethers are progressively less crowded), in Figure 3.2 D.

### **3.3.2 Fibrinogen adsorption on patchy surfaces**

For each run in Figure 3.6 A, after PLL-PEG backfilling and exposure to flowing buffer for several minutes, the surfaces were exposed to 100 ppm solutions of flowing fibrinogen, with the resulting kinetic traces in Figure 4B corresponding to the runs in Figure 4A. Here, without any PLL patches, a PLL-PEG brush adsorbs virtually no fibrinogen. As the PLL-patch content of the brushy surface is increased, the fibrinogen adsorption also increases. For small amounts of PLL patches, the fibrinogen kinetic traces rise slowly and become level. With greater amounts of PLL patches (order  $0.12 \text{ mg/m}^2$  or  $3500 \text{ patches / um}^2$ ), fibrinogen adsorption is initially rapid, with a rate approaching that seen on a saturated PLL layer in the inset. After some time, however, the fibrinogen adsorption slows.

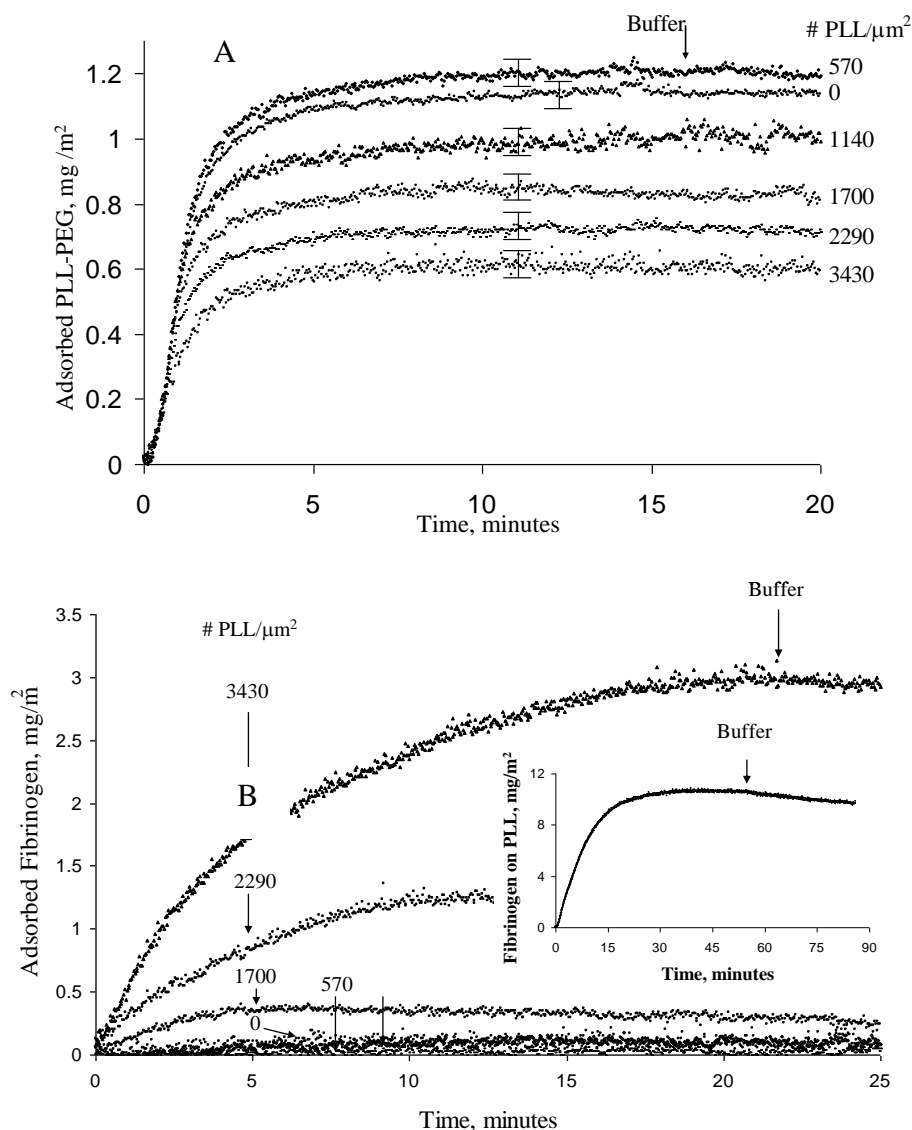


Figure 3.6 Coverage of PLL-PEG and Fibrinogen over patchy brush. A) PLL-PEG adsorption following different preloaded PLL coverages. B) Fibrinogen coverage over different patchy brushes.

The inset of Figure 3.6 B emphasizes the extensive adsorption of fibrinogen on vast areas of surface made cationic by the adsorption of a saturated PLL-layer. Here the saturated fibrinogen coverage, approaching 5 mg/m<sup>2</sup>, exceeds the coverages of fibrinogen on surfaces containing as much as 4000 PLL chains / μm<sup>2</sup>.

In Figures 3.6 B and C, fibrinogen adsorption on the patchy brush surface is summarized in terms of the ultimate fibrinogen coverage, and also in terms of its initial binding rate. The two representations are necessitated by the protracted fibrinogen binding kinetics at long times on the more densely patchy surfaces, in Figure 3.6 B. Regardless of the choice of metric for fibrinogen adsorption, an important point becomes clear: There is a threshold in the density of patches that must be achieved before fibrinogen will adsorb to the surface. Beyond this threshold, fibrinogen coverage (and its binding rate) increase with increasing cationic patch density, though coverage can be quite low. Conversely, when the PLL patch density is on the order of  $4000/\mu\text{m}^2$ , fibrinogen adsorption approaches (within a factor of 2 or so) the levels seen on purely PLL surfaces, in the inset of Figure 3.6 B. The diagonal line in Figure 3.7 B marks fibrinogen adsorption levels that would correspond to one per cationic patch.

### **3.4 Discussion**

The threshold in patch density for fibrinogen adsorption in Figures 3.7 B and C occurs near  $1500 \text{ patches } / \mu\text{m}^2$ , which we believe to be greater (within the significance of experimental error) than the onset of reduced brush coverage at  $900 \text{ PLL patches } / \mu\text{m}^2$  in Figure 3.7 A.

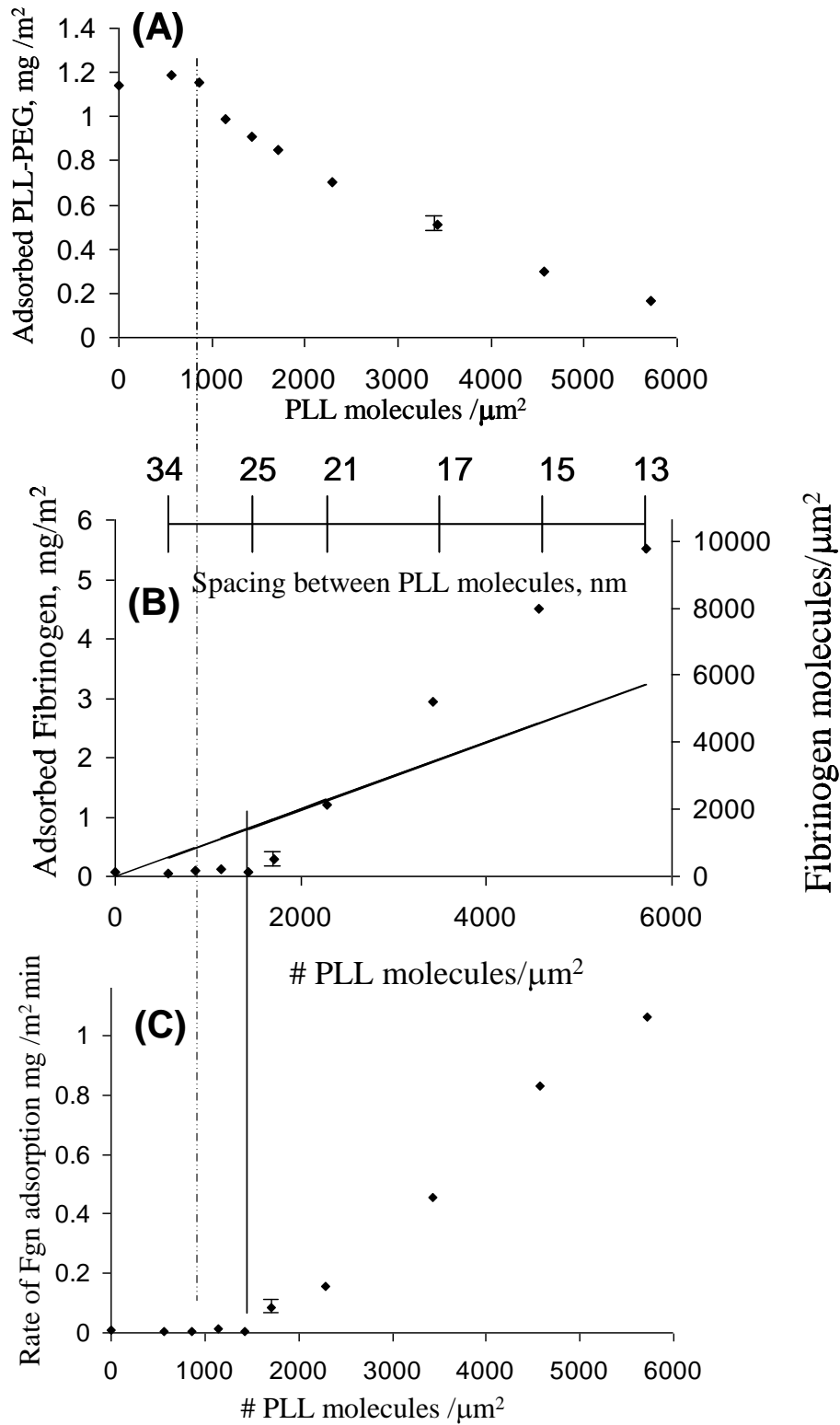


Figure 3.7 Summary of the impact of PLL patch density on (A) amount of PLL-PEG backfill (B) short term fibrinogen coverage and (C) initial fibrinogen adsorption rate.

Therefore we conclude that the effect of the PLL patches on PLL-PEG backfilling is different from their effect on fibrinogen adsorption. Indeed, if the two thresholds were to occur at the same PLL patch density, one would conclude simply that PLL patches at the base of the brush were entirely shielded by the PEG corona and any reduction in the PEG corona (reduced backfilling), caused by the PLL patches, would immediately lead to fibrinogen adsorption. Instead Figures 3.7 B and C shows that even with some overall reduction in the PEG brush relative to full saturation, resistance to fibrinogen persists. The subsequent limited fibrinogen adsorption just above the threshold motivates consideration of the PLL patches and brush structure near the patches, rather than discussion of the overall or average properties of the brush.

First, it is worth noting that the presence of a threshold patch density for fibrinogen adsorption implies that individual isolated PLL patches are unable to capture and hold fibrinogen molecules. Instead two or more patches are involved in fibrinogen capture. It may be the case that at the lowest patch densities, below  $900 / \mu\text{m}^2$ , the patches are simply buried within the brush and completely shielded by the corona. Indeed, it is interesting to consider whether a 9 nm patch can be entirely shielded by the particular PEG brushes in this study. When the PLL-PEG coverage is near the saturation level of  $1.1 \text{ mg}/\text{m}^2$ , we expect a PEG chain extension or brush height of 9 nm, as calculated in the supplemental material. Near a patch, some of these stretched PEG tethers will spill sideways and obstruct the patch, in Figure 3.2 C, reducing its accessible area and fibrinogen binding energy. Indeed, with a brush height of 9 nm, and a similar lengthscale for the sideways extension of PEG tethers over PLL patches, it becomes a possibility that PLL patches are completely hidden from approaching proteins. (Patch

accessibility will also depend on the conditions for protein exposure, for instance the relative exposure and brush relaxation times.)

In the dilute patch limit above, widely spaced PLL patches are sufficiently hidden in a saturated PLL-PEG brush that they cannot individually bind fibrinogen. At higher patch loadings, fibrinogen likely adsorbs by bridging multiple patches. At some point, however, the binding energy per patch will increase relative to the dilute patch limit because the brush structure around the patches becomes compromised. Bridging and further “revealing” of patches are mechanisms which must ultimately act in concert to facilitate protein capture.

Two distinct mechanisms for brush compromise at elevated PLL patch loadings will act together in statistical proportion: First, above 900 PLL patches /  $\mu\text{m}^2$ , PLL-PEG coverage is reduced because of the net reduction in surface area available for further copolymer adsorption. (Here, the PLL patches are still far enough apart, 33 nm on average that the likelihood of PLL exclusion between neighboring pairs of patches is small.) The reduced PLL-PEG adsorption gives rise to a smaller extension of the PEG chains and a less robust brush. This in turn compromises the ability of the PEG brush to obscure isolated PLL patches, increasing the binding energy and probability for fibrinogen adsorption. A second mechanism for brush compromise will become important at higher PLL patch loadings when two adsorbed patches lie sufficiently close that PLL-PEG chains might be excluded between them. (Whether this actually occurs depends on whether the cationic backbone of the adsorbing chain can sufficiently uncoil to fill the narrow region of surface between two patches. If backbone chain deformation on adsorption occurs appreciably, than this surface exclusion mechanism will not occur.)

Such exclusion might only occur when the patch centers are smaller than roughly 15 nm in separation. With a Poisson distribution for the arrangement of random patches on a surface, one finds that only 5% of the patches could exclude a brush between pairs when there are 900 patches / $\mu\text{m}^2$ . At the threshold for fibrinogen adsorption, 1500 PLL patches/ $\mu\text{m}^2$ , 11% of the patches will be paired so as to potentially exclude a brush and be an effectively larger fibrinogen patch.

A final point about fibrinogen adsorption onto the surfaces, in light of the small adhesive patches and the relatively large fibrinogen size: 47 nm x 4.5 nm x 4.5 nm. It is not obvious that fibrinogen would adhere to as few as 2-3 small adhesive regions, as we argue above. Our interpretation of Figures 3.7 B and C is, however, consistent with previous reports of fibrinogen binding in small exposed areas between previously adsorbed proteins near saturation coverages.<sup>34</sup> Indeed, we previously demonstrated that fibrinogen could adhere tightly with an effective footprint of 120 nm<sup>2</sup> or less, even approaching the footprint of lysozyme (12.6 nm<sup>2</sup>) on the same surfaces.<sup>8</sup> Adhesive regions the same size as the protein itself are not a prerequisite for protein binding. In light of fibrinogen's ability to bind small regions of surface, and from our inferences about the structure of the patchy brush, we conclude that complete obscuring of patches in a brush is not necessary to avoid protein adsorption: Wide separation of partially obscured elements will avoid protein adsorption if the binding energy per patch is sufficiently weak. The compromise of the brush at increased patch density further favors protein adsorption.



### 3.5 Conclusions

This work has demonstrated the creation of patchy brush surfaces that are useful for protein manipulation. The study also illustrates general principles for structure and performance of polymer brushes whose tethered chains are modestly stretched normal to the substrate.

While proteins such as fibrinogen generally adsorb to most surface chemistries including the cationic polymer layers in the current study, protein capture becomes impossible when adhesive elements of the same chemistry are widely spaced and sufficiently small or substantially shielded by a nonadhesive polymer brush. The PEG “brushes” of the current study are typical of “pegylated” protein resistant biomaterials: This study emphasizes that protein resistance is maintained even when the PEG tethers form marginal brushes compared with rigorously defined brushes in the polymer physics literature. The study further demonstrates that these marginal brushes are effective to conceal substantial amounts of buried adhesive moieties from proteins which are otherwise highly adhesive. Ultimately it was demonstrated that protein adhesion occurred when the adsorbing protein could make multiple surface contacts, and when the local PEG tether concentration was sufficiently low that brush formation was compromised.

### 3.6 References

- 1.) Chang, B.S., Kendrick, B.S., & Carpenter, J.F. (1996). Surface-induced denaturation of proteins during freezing and its inhibition by surfactants. *Journal of pharmaceutical sciences*, 85(12), 1325-1330.
- 2.) Bos, M. A., & van, V. T. (2001). Interfacial rheological properties of adsorbed protein layers and surfactants: a review. *Advances in colloid and interface science*, 91(3), 437-471.
- 3.) Agnihotri, A., & Siedlecki, C. A. (2004). Time-Dependent Conformational Changes in Fibrinogen Measured by Atomic Force Microscopy. *Langmuir*, 20(20), 8846-8852.
- 4.) Dickinson, E. (1999). Adsorbed protein layers at fluid interfaces: interactions, structure and surface rheology. *Colloids and Surfaces, B: Biointerfaces*, 15(2), 161-176.
- 5.) Haynes, C. A., & Norde, W. (1995). Structures and stabilities of adsorbed proteins. *Journal of Colloid and Interface Science*, 169(2), 313-328.
- 6.) Norde, W. (1995). Adsorption of proteins at solid-liquid interfaces. *Cells and Materials*, 5(1), 97-112.
- 7.) Wertz, C. F., & Santore, Maria M. (2002). Fibrinogen Adsorption on Hydrophilic and Hydrophobic Surfaces: Geometrical and Energetic Aspects of Interfacial Relaxations. *Langmuir*, 18(3), 706-715.
- 8.) Santore, Maria M., & Wertz, C. F. (2005). Protein Spreading Kinetics at Liquid-Solid Interfaces via an Adsorption Probe Method. *Langmuir*, 21(22), 10172-10178.
- 9.) Billsten, P., Wahlgren, M., Arnebrant, T., McGuire, J., & Elwing, H. (1995). Structural changes of T4 lysozyme upon adsorption to silica nanoparticles measured by circular dichroism. *Journal of Colloid and Interface Science*, 175(1), 77-82.

- 10.) Cedervall, T., Lynch, I., Lindman, S., Berggard, T., Thulin, E., Nilsson, H., Dawson, K. A., & Linse, S. (2007). Understanding the nanoparticle-protein corona using methods to quantify exchange rates and affinities of proteins for nanoparticles. *Proceedings of the National Academy of Sciences of the United States of America*, *104*(7), 2050-2055.
- 11.) Karajanagi, S. S., Vertegel, A. A., Kane, R. S., & Dordick, J. S. (2004). Structure and Function of Enzymes Adsorbed onto Single-Walled Carbon Nanotubes. *Langmuir*, *20*(26), 11594-11599.
- 12.) Shang, L., Wang, Y., Jiang, J., & Dong, S. (2007). pH-Dependent Protein Conformational Changes in Albumin:Gold Nanoparticle Bioconjugates: A Spectroscopic Study. *Langmuir*, *23*(5), 2714-2721.
- 13.) Teichroeb, J. H., Forrest, J. A., & Jones, L. W. (2008a). Size-dependent denaturing kinetics of bovine serum albumin adsorbed onto gold nanospheres. *European Physical Journal E: Soft Matter*, *26*(4), 411-415.
- 14.) Gao, P., & Cai, Y. (2008). The Boundary Molecules in a Lysozyme Pattern Exhibit Preferential Antibody Binding. *Langmuir*, *24*(18), 10334-10339.
- 15.) Kenausis, G. L., Voeroes, J., Elbert, D. L., Huang, N., Hofer, R., Ruiz-Taylor, L., Textor, Marcus, et al. (2000). Poly(L-lysine)-g-Poly(ethylene glycol) Layers on Metal Oxide Surfaces: Attachment Mechanism and Effects of Polymer Architecture on Resistance to Protein Adsorption. *Journal of Physical Chemistry B*, *104*(14), 3298-3309.
- 16.) McPherson, T., Kidane, A., Szleifer, I., & Park, K. (1998). Prevention of Protein Adsorption by Tethered Poly(ethylene oxide) Layers: Experiments and Single-Chain Mean-Field Analysis. *Langmuir*, *14*(1), 176-186.
- 17.) Sofia, S. J., Premnath, V., & Merrill, E. W. (1998). Poly(ethylene oxide) Grafted to Silicon Surfaces: Grafting Density and Protein Adsorption. *Macromolecules*, *31*(15), 5059-5070.

- 18.) Mrksich, M., Chen, C. S., Xia, Y., Dike, L. E., Ingber, D. E., & Whitesides, G. M. (1996). Controlling cell attachment on contoured surfaces with self-assembled monolayers of alkanethiolates on gold. *Proceedings of the National Academy of Sciences of the United States of America*, 93(20), 10775-10778.
- 19.) Stolnik, S., Illum, L., & Davis, S. S. (1995). Long circulating microparticulate drug carriers. *Advanced Drug Delivery Reviews*, 16(2,3), 195-214.
- 20.) Ladd, J., Zhang, Z., Chen, S., Hower, J. C., & Jiang, S. (2008). Zwitterionic Polymers Exhibiting High Resistance to Nonspecific Protein Adsorption from Human Serum and Plasma. *Biomacromolecules*, 9(5), 1357-1361.
- 21.) Chen, S. F., Zheng, J., Li, L., & Jiang, S. (2005). Strong Resistance of Phosphorylcholine Self-Assembled Monolayers to Protein Adsorption: Insights into Nonfouling Properties of Zwitterionic Materials. *Journal of the American Chemical Society*, 127(41), 14473-14478.
- 22.) Milner, S. T. (1991a). Polymer brushes. *Science (Washington, DC)*, 251(4996), 905-914.
- 23.) de Gennes, P. G. (1976). Scaling theory of polymer adsorption. *Journal de Physique (Paris)*, 37(12), 1445-1452.
- 24.) Alexander, S. (1977). Polymer adsorption on small spheres. A scaling approach. *Journal de Physique (Paris)*, 38(8), 977-981.
- 25.) Dalsin, J. L., Lin, L., Tosatti, Samuele, Voeroes, J., Textor, Marcus, & Messersmith, P. B. (2005). Protein Resistance of Titanium Oxide Surfaces Modified by Biologically Inspired mPEG-DOPA. *Langmuir*, 21(2), 640-646.
- 26.) Dalsin, J. L., Hu, B. H., Lee, B. P., & Messersmith, P. B. (2003). Mussel Adhesive Protein Mimetic Polymers for the Preparation of Nonfouling Surfaces. *Journal of the American Chemical Society*, 125(14), 4253-4258.

- 27.) Kent, M. S., Lee, L. T., Factor, B. J., Rondelez, F., & Smith, G. S. (1995). Tethered chains in good solvent conditions: an experimental study involving Langmuir diblock copolymer monolayers. *Journal of Chemical Physics*, 103(6), 2320-2342.
- 28.) Brittain, W. J., & Minko, S. (2007). A structural definition of polymer brushes. *Journal of Polymer Science, Part A: Polymer Chemistry*, 45(16), 3505-3512.
- 29.) Kozlova, N., & Santore, Maria M. (2006). Manipulation of Micrometer-Scale Adhesion by Tuning Nanometer-Scale Surface Features. *Langmuir*, 22(3), 1135-1142.
- 30.) Kalasin, S., & Santore, M. M. (2008). Hydrodynamic Crossover in Dynamic Microparticle Adhesion on Surfaces of Controlled Nanoscale Heterogeneity. *Langmuir*, 24(9), 4435-4438.
- 31.) Duffadar, R., Kalasin, Surachate, Davis, J. M., & Santore, Maria M. (2009). The impact of nanoscale chemical features on micron-scale adhesion: Crossover from heterogeneity-dominated to mean-field behavior. *Journal of Colloid and Interface Science*, 337(2), 396-407.
- 32.) Feng, L., & Andrade, J. D. (1994). *Proteins at Interfaces II: Fundamentals and Applications*. Horbett, T. A., Brash, J. L. Eds. American Chemical Society: Washington DC, 602, 66-79.
- 33.) Toscano, A., & Santore, Maria M. (2006). Fibrinogen Adsorption on Three Silica-Based Surfaces: Conformation and Kinetics. *Langmuir*, 22(6), 2588-2597.
- 34.) Wertz, C. F., & Santore, Maria M. (1999). Adsorption and Relaxation Kinetics of Albumin and Fibrinogen on Hydrophobic Surfaces: Single-Species and Competitive Behavior. *Langmuir*, 15(26), 8884-8894.
- 35.) Shibata, C. T., & Lenhoff, A. M. (1992). TIRF of salt and surface effects on protein adsorption. II. Kinetics. *Journal of Colloid and Interface Science*, 148(2), 485-507.

- 36.) Fu, Z., & Santore, Maria M. (1998). Poly(ethylene oxide) adsorption onto chemically etched silicates by Brewster angle reflectivity. *Colloids and Surfaces, A: Physicochemical and Engineering Aspects*, 135(1-3), 63-75.
- 37.) Rebar, V. A., & Santore, M. M. (1996). History-Dependent Isotherms and TIRF Calibrations for Homopolymer Adsorption. *Macromolecules*, 29(19), 6262-6272.
- 38.) Hansupalak, N., & Santore, Maria M. (2003). Sharp Polyelectrolyte Adsorption Cutoff Induced by a Monovalent Salt. *Langmuir*, 19(18), 7423-7426.
- 39.) Shin, Y., Roberts, J. E., & Santore, Maria M. (2002). Influence of charge density and coverage on bound fraction for a weakly cationic polyelectrolyte adsorbing onto silica. *Macromolecules*, 35(10), 4090-4095.
- 40.) Jiang, M., Popa, I., Maroni, P., & Borkovec, M. (2010). Adsorption of poly(-lysine) on silica probed by optical reflectometry. *Colloids and Surfaces, A: Physicochemical and Engineering Aspects*, 360(1-3), 20-25.
- 41.) Yamakawa, H. (1971). *Modern Theory of Polymer Solutions*. Harper and Row. New York
- 42.) Zhang, J., Srivastava, S., Duffadar, R., Davis, J. M., Rotello, V. M., & Santore, Maria M. (2008). Manipulating Microparticles with Single Surface-Immobilized Nanoparticles. *Langmuir*, 24(13), 6404-6408.
- 43.) Santore, Maria M. (2005). Dynamics in adsorbed homopolymer layers: Understanding complexity from simple starting points. *Current Opinion in Colloid & Interface Science*, 10(3,4), 176-183.
- 44.) Hansupalak, N., & Santore, Maria M. (2004). Polyelectrolyte Desorption and Exchange Dynamics near the Sharp Adsorption Transition: Weakly Charged Chains. *Macromolecules*, 37(4), 1621-1629.
- 45.) Gon, S., Bendersky, M., Ross, J. L., & Santore, M. M. (2010). Manipulating Protein Adsorption using a Patchy Protein-Resistant Brush. *Langmuir*, 26(14), 12147-12154.

# **CHAPTER 4**

## **SINGLE COMPONENT AND SELECTIVE COMPETITIVE PROTEIN ADSORPTION AND SEPARATION USING A PATCHY POLYMER BRUSH**

### **4.1 Introduction**

It has been shown that using a patchy polymer brush (Brush # 1 in the present study) we were able to tune fibrinogen adhesion. This chapter explores this concept for various proteins. Most of this chapter has been reproduced from work published recently.<sup>1</sup> It is generally thought that, regardless of the PEG anchoring chemistry (direct surface grafting from the surface, or tacking to the surface by an adsorption of a PEG containing block copolymer), surfaces must contain more than about 1 mg/m<sup>2</sup> of PEG in order to ensure proteins, which facilitate the binding of bacteria and cells, do not themselves adsorb.<sup>2</sup> (In this rule of thumb it is assumed that any anchoring component of an adsorbed block of a copolymer does not extend off the surface into the brush or into solution, where it could easily be adhered by approaching protein molecules.) The criterion for the PEG coverage associated with protein resistance is thought to be independent of the particular choice of PEG molecular weight, at least within some workable range on the order of 1000 g/mol. As long as the combination of grafting

density and PEG chain length gives the appropriate total amount of anchored PEG, protein adsorption is observed to be reduced to 0.05 mg/m<sup>2</sup> or less.

When the surface loading of PEG falls below 1.0 mg/m<sup>2</sup>, moderate protein adsorption occurs.<sup>2</sup> This behavior is often explained in terms of a thinner hydrated polymer brush, which allows proteins to experience electrostatic and van der Waals attractions with the underlying substrate and, ultimately, adsorb.<sup>3</sup> An alternate explanation, surely appropriate for a subset of systems, involves impurities on the substrate that interfere locally with brush placement. If enough bare patches are present at the base of a brush, protein adsorption could become appreciable.<sup>4</sup> Related fundamental questions are cast in terms of the physics of solvated polymer brushes and protein-brush interactions. For instance, when a defect or region of surface containing no grafted chains exists within a brush, to what extent do hydrated brush chains “spill” laterally to obstruct the defect, and how does this depend on the average brush grafting density and molecular weight? Further, given the existence of such defects, what protein properties dictate the interactions between proteins and patches?

Such questions about heterogeneous brush structure have not, our knowledge, been addressed in the context of protein adsorption.<sup>5</sup> A limited number of studies do, however, provide insight into the ability of proteins to adhere to small adhesive regions on an otherwise less or non-adhesive surface (sometimes, but not necessarily brush-like,) though there is no general consensus.<sup>6-8</sup> One study demonstrated single and clustered protein adsorption on nano-scale metal clusters on graphite<sup>9</sup> and, indeed, blood protein adsorption was increased by the presence of nano-pyramids on germanium.<sup>10</sup> Previous



work with surfaces nearly saturated with protein suggests that protein adsorption can occur in small surface interstices between previously adsorbed proteins, and that these interstices, in some instances can be smaller than the average protein dimension.<sup>11</sup> In the particular case of fibrinogen which is long (47 nm) and thin (4.5 nm dia), access of the narrow protein tip to a small empty region of a hydrophobic surface was sufficient to facilitate strong adsorption. Access to the surface by the entire side or face of fibrinogen was unnecessary. While the results from different labs with different proteins and surfaces achieve no general consensus, at least some of the results suggest that certain proteins may be able to access and adhere to nanoscale small flaws or adhesive patches smaller than the average protein dimension. This further suggests that such binding may take place on small bald patches at the base of a brush.

The observation of protein-dependent adhesion to nanoscale surface regions (and, also potentially to flaws within a brush) suggests applications involving protein manipulation, selective binding, separation, and diagnostics. For instance, the limited protein adsorption on small adhesive surface patches suggests that on different surfaces, the proteins adsorbed near the edges of large adhesive features may be configured more or less densely,<sup>6,12-14</sup> or with more or less bioactivity<sup>9,15</sup> than those away from the pattern edges. Also, the protein size-dependence of adhesion on nano-scale features suggests adhesive selectivity for separation and diagnostics.

The current chapter investigates the ability of different proteins to adhere to controlled but randomly placed adhesive “flaws” in otherwise protein-repellant PEG brushes. The study sheds light on both the mechanisms for protein interactions with

imperfect brushes and on the use of such “patchy” brush interfaces as vehicles for affecting sharp protein separations.

The system of patchy brush # 1 as discussed in the previous chapter and described in detail earlier<sup>16</sup> is the subject of further study here. The ability of proteins to adsorb to patchy brushes depends on the competition between electrostatic attractions between negative regions on the protein and positive surface patches, and steric repulsions between the PEG surface brush and the body of the protein.<sup>17</sup> While our initial study of these patchy brushes focused on patchy brush architecture and implications for the adsorption of a single protein (fibrinogen),<sup>16</sup> the current chapter explores different proteins adsorbing to the same brush and demonstrates a mechanism for highly selective protein binding from a mixture. We argue that the basis for the selectivity is ability of different proteins to bind multiple patches (a multivalency effect<sup>18, 19</sup>) which is a combination of protein size and charge. In the absence of great charge differences, differences in the ability of proteins to span and bind multiple patches translates to sharp differences in binding.

The patchy PEG brushes in this study differ from mixed brushes:<sup>20-22</sup> The latter may also exhibit localized regions of different chemistry, however, the current surfaces are well-characterized in terms of their overall compositions and their local random structure has been previously established.<sup>16</sup> The concept of embedding functionality at the base of a protein-resistant brush also differs substantially from the classical approach of tethering biofunctionality on the brush chain ends.<sup>23-25</sup>

## 4.2 Experimental Methodology

PLL-PEG Brush # 1 as described in chapter 2 was studied here. Poly-L-lysine hydrobromide (20,000 MW) purchased from Sigma was used for patch generation. Silica surfaces of microscope slides were used as substrates after etching overnight in concentrated sulfuric acid as described in previous chapters. Patchy brush surfaces were created *in-situ* in a slit shear chamber containing the acid-etched slide, first flowing pH 7.4 phosphate buffer (0.008M Na<sub>2</sub>HPO<sub>4</sub> and 0.002M KH<sub>2</sub>PO<sub>4</sub>, Debye length  $\kappa^{-1} = 2$  nm), then flowing a 5 ppm PLL solution in the same buffer for a controlled time and reintroducing buffer to halt adsorption at the desired surface density of patches. A 100 ppm buffered solution PLL-g-PEG was then introduced to backfill the remaining surface with the brush. Protein solutions were subsequently introduced in the same buffer and their adsorption monitored. Previous studies demonstrated that surface area occupied by PLL patches did not adsorb PLL-g-PEG copolymer.<sup>16</sup> Near Brewster angle reflectometry<sup>26</sup> was used for studying adsorption of polymer and proteins.

This study compared the adsorption of 4 proteins, bovine serum fibrinogen (fraction-I, type 1-s, F8630-1G), bovine serum albumin (A3809-10G), bovine alkaline phosphatase (P7640-1G), and equine skeletal muscle myoglobin (M0630-1G) all purchased from Sigma and used as received. For studies involving protein mixtures, the reflectometry measurements were complemented by TIRF experiments<sup>27</sup> in the same flow chamber (but not run simultaneously.) In this work, fluorescein-tagged labeled albumin, labeled at 0.9 tags / molecule, was labeled and purified as previously described.<sup>28</sup>

Zeta potentials were measured using a Malvern Zeta Sizer Nano ZS instrument and a model system consisting of 1-micron silica spheres (Gel Tech), onto which the materials of interest were adsorbed. In order to direct adsorption to the particle surfaces, a sphere concentration of 50 ppm was employed and, in some cases, the walls of the containers holding the suspensions were pre-treated with PLL to avoid adsorption of PLL, intended for the particles, to other surfaces. We found no evidence of loss of PLL from the vessel walls, and the loss of microspheres to the vessel walls had negligible influence on their bulk concentration.

## **4.3 Results**

### **4.3.1 Protein properties**

Electrostatic interactions play an important role in protein adsorption on the brush-modified silica surfaces in this study. It is therefore instructive to consider the protein properties and the ability of the proteins to adhere to relatively homogenous cationic and anionic surfaces. Adsorption on the cationic surface (a saturated PLL layer) provides insight into how proteins could interact with patches. Adsorption on the anionic surface (bare silica), provides perspective on protein interactions with any negatively charged areas at the base of the brush, the relevance of which will become clear below.

Table 4.1 summarizes the properties of the proteins. Fibrinogen, albumin and alkaline phosphatase have major dimensions larger than individual patch size and they are the main focus of this chapter. Of note, the dimensional and molecular weight information for alkaline phosphatase here are taken from the Research Collaboratory for

Structural Bioinformatics Protein DataBank and correspond to the monomer. The material we purchased from Sigma is a stable dimer with a molecular weight of 160,000.

Table 4.1 Properties of proteins

	Albumin, bovine serum	fibrinogen, bovine serum	Alkaline phosphatase, bovine	Myoglobin, horse skeletal muscle
Dimensions, nm x nm x nm	4 x 4 x 14	4.5 x 4.5 x 47	9 x 4 x 4 (monomer)	4.4 x 4.4 x 2.5
Molecular weight	68,000	340,000	81198 (monomer)	17,000
Diffusivity, cm <sup>2</sup> /s	4.8 x 10 <sup>-7</sup> ref 29	2 x 10 <sup>-7</sup> ref 30	9 x 10 <sup>-8</sup>	1.2 x 10 <sup>-7</sup> ref 31
pI	4.8 ref 29 – 5.1	5.8 ref 32	5.7	6.8-7.4 ref 34
Number charges, pH 7.4	-8, ref 29 -7 to -10 ref 33	-8 to -10 ref 30	unknown	Neutral ref 35
Adsorption on Cationic Surface				
Plateau*	5 mg/m <sup>2</sup>	12 mg/m <sup>2</sup>	4.8 mg/m <sup>2</sup>	2.0 mg/m <sup>2</sup>
kinetics	Transport-limited	Transport-limited	Transport-limited	Not transport limited
Adsorption on Anionic Surface				
plateau*	2 mg/m <sup>2</sup>	9 mg/m <sup>2</sup>	0.75 mg/m <sup>2</sup>	1.0 mg/m <sup>2</sup>
kinetics	Slow	Transport-limited	Slow	Slow

\*Plateau coverage measured at 20-25 minutes, for bulk solution of 100 ppm, and wall shear of 5 s<sup>-1</sup>

Myoglobin is the smallest protein and its size (4.4 nm x 4.4 nm x 2.5 nm ) is significantly smaller than the patch size of random PLL coils (10 nm). Additionally it's smallest dimension is very close to the persistence length of Brush 1, 2 nm. Myoglobin is almost neutral at our pH condition. Hence comparison of adhesion characteristics of myoglobin with the other three proteins is presented later.

None of these proteins adsorb onto PLL-g-PEG brushes without PLL patches. Importantly, at pH 7.4 all four proteins carry a net negative charge, but vary in size. All adsorb onto positively- or negatively-charged uniform surfaces. Figure 4.1 shows

adsorption of three bigger proteins over bare silica and PLL saturated layer. Myoglobin adsorption over saturated PLL and bare silica surface is presented in Figure 4.2. Like the bigger proteins, myoglobin adsorbs significantly over both of these surfaces.

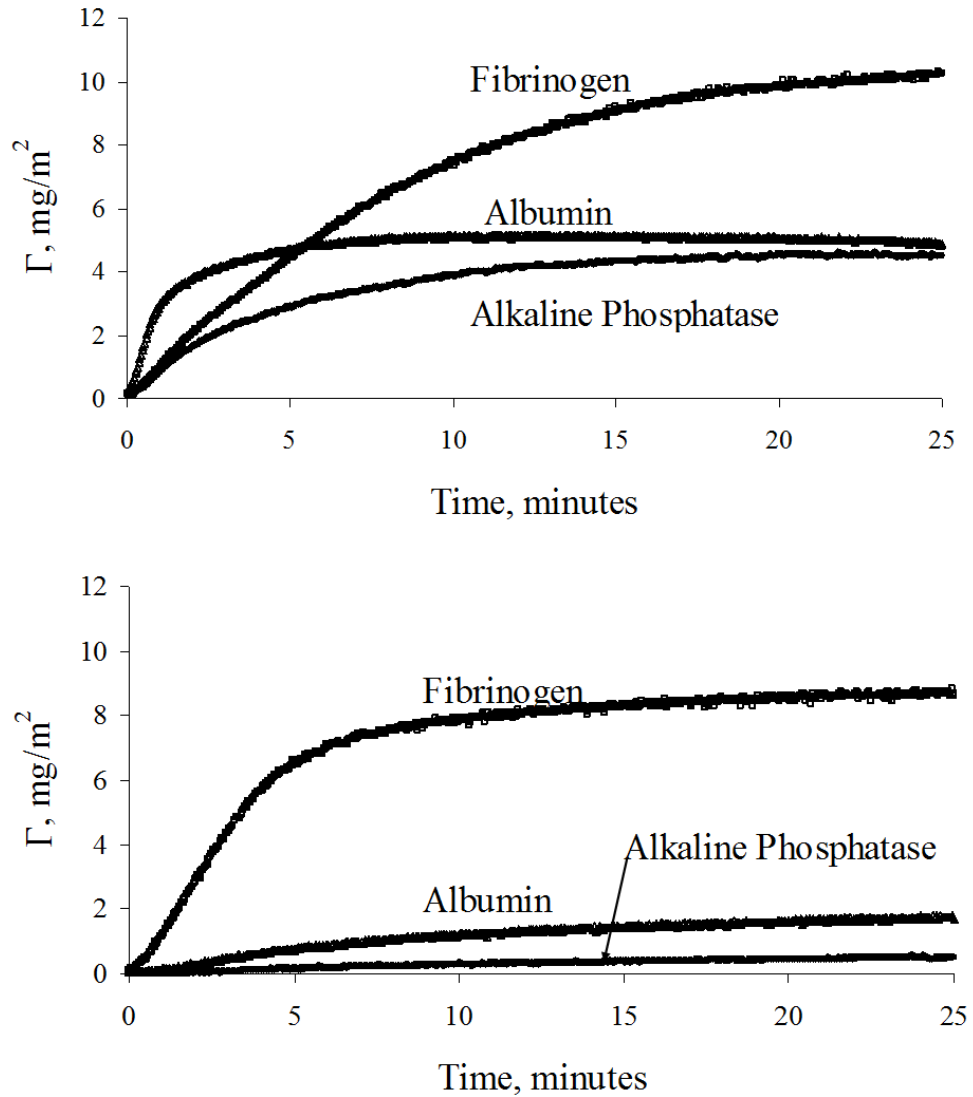


Figure 4.1 Adsorption of bigger proteins over A) PLL saturated silica B) bare silica

The ultimate protein coverages in Table 4.1, after 20-25 minutes, reflect the protein size, with the higher molecular weight fibrinogen giving greatest surface coverage, presumably as a result of a thicker layer.

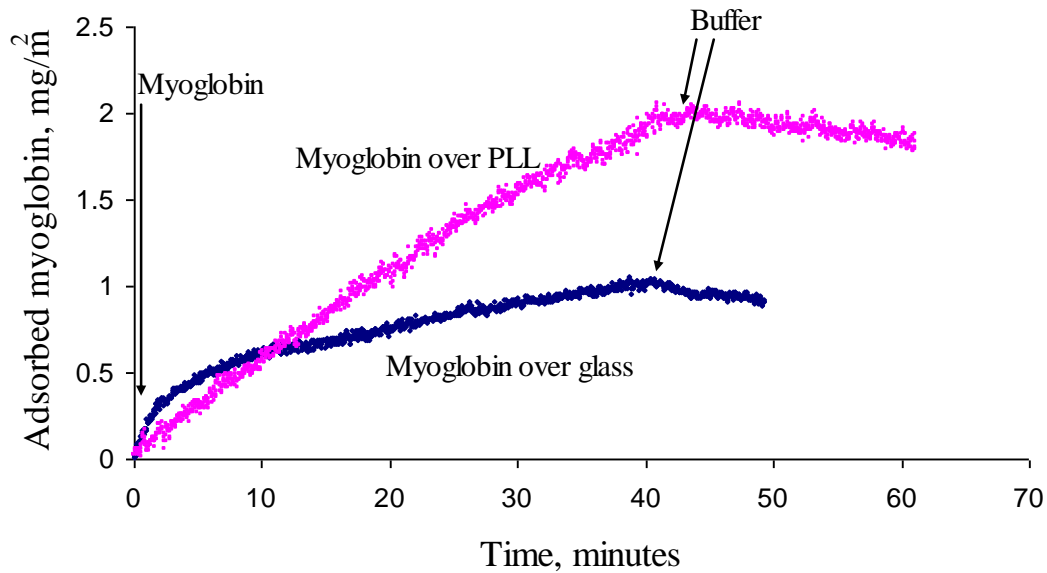


Figure 4.2 Myoglobin adsorption over bare silica(glass) and PLL saturated layer

Proteins generally adsorb at / near their transport-limited rates and are well-retained upon rinsing with buffer, indicating strong binding. The exceptions are albumin, alkaline phosphatase and myoglobin adsorption on the negative silica and myoglobin adsorption over PLL. Here protein adsorption is slow. In the case of albumin, adsorption on silica depends on ionic strength, suggesting that negative charges on albumin contribute a barrier against adsorption. This negative albumin charge favors adsorption on uniform positive surfaces and is expected to promote adhesion to the positive patches.

As myoglobin is neutral at pH 7.4 the absence of electrostatic repulsion makes it adsorb in higher amounts compared to albumin and alkaline phosphatase. Fibrinogen adsorption was substantial on both positive and negative surfaces, suggesting that positive and negative groups on the proteins can facilitate adsorption. Another explanation for protein adsorption on surfaces of the same net charge is charge regulation.<sup>36</sup>

### 4.3.2 Patchy Brush

The features of Brush # 1 have been discussed in detail in Chapter 2, but are included here for continuance in Table 4.2.

Table 4.2 Properties of PLL and PLL-PEG Brushes in pH 7.4 phosphate buffer, I=0.026 M

	PLL	PLL-PEG
Nominal MW, g/mol	20,000	147,100
Saturated layer coverage, $\Gamma_{\text{sat}}$ mg <sup>2</sup>	0.4 ± 0.02	1.1 ± 0.1
Effective chain footprint, nm <sup>2</sup> (=MW/ $\Gamma_{\text{sat}}$ )	83 ± 10	220 ± 22
PLL in saturated layer, mg/m <sup>2</sup>	0.4	0.15
PEG in saturated layer, mg/m <sup>2</sup>	0	0.95
Zeta potential of saturated layer	+ 5 mV	-9±3 mV

The brush thickness estimated from initial coverage of Brush # 1 over silica was found to be 9 nm. Regardless of the actual brush thickness, one surmises that the surface charge beneath a saturated PLL-PEG brush is somewhat negative (motivating control studies of protein adsorption on negative surfaces, in Table 4.1). This is consistent with the low PLL content of saturated PLL-PEG brushes, 0.15 mg/m<sup>2</sup>, which is less than the saturated homopolymer PLL coverage (0.4 mg/m<sup>2</sup>). Additionally, about 1/3 of the PLL in the PLL-PEG copolymer is reacted to form an amide, and has lost its positive charge.



From the observation that fibrinogen does not adsorb to saturated PLL-PEG brushes but it does adsorb on negative surfaces, we infer that the saturated brush holds proteins further from the surface than the shear plane. The lack of protein adsorption on these brushes is further consistent with the PEG mass near  $1.0 \text{ mg/m}^2$  within the saturated brush, the rule of thumb suggested for protein resistance.<sup>2</sup> Finally, with the modest adsorption of albumin and alkaline phosphatase and myoglobin on the negative surfaces, we would not expect their adsorption on the brush regions of the patchy surfaces.

Also worth reemphasizing are our previous findings concerning these surfaces:<sup>16</sup> PLL and PLL-PEG are retained on silica during flow of pH 7.4  $I=0.026 \text{ M}$  buffer or protein solutions. Additionally, fluorescence studies revealed the random arrangement of PLL patches which was unaltered by PLL-PEG backfilling.

### **4.3.3 Protein adsorption over patchy brushes**

Adhesion of fibrinogen, albumin and alkaline phosphatase is discussed in detail below. Myoglobin adhesion characteristics differ from the other three proteins.

#### **4.3.3.1 Comparison of fibrinogen, albumin and alkaline phosphatase adhesion**

Figure 4.3 presents example reflectometry data for albumin and alkaline phosphatase adsorption onto a series of surfaces containing different loadings of PLL patches (with the rest of the surface backfilled with PLL-g-PEG Brush # 1 prior to exposure of protein solution.) The lowest data set, essentially a flat line, demonstrates rejection of protein from a saturated PLL-g-PEG brush. As PLL patches are initially added to this brush, the protein adsorption is difficult to discern; however, as the PLL

patch density is increased, protein adsorption is clear. The PLL patch density ultimately controls both the ultimate protein coverage (that observed after about 20 minutes), and the initial rate of protein adsorption.

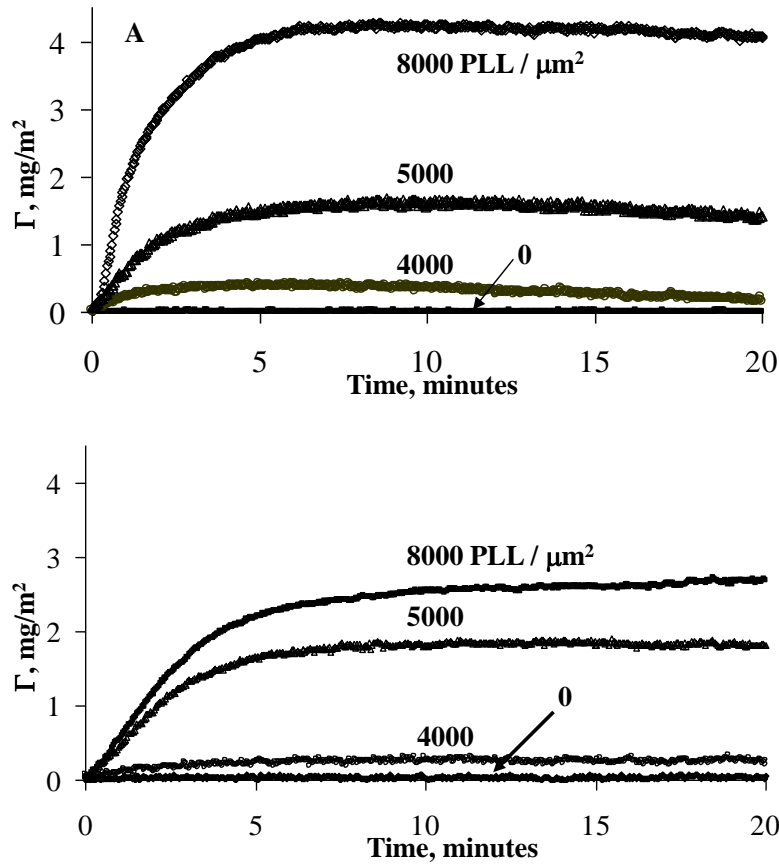


Figure 4.3 Example reflectometry data showing (A) albumin and (B) alkaline phosphatase adsorption traces on to surfaces having variations in the surface loading of cationic patches.

In Figure 4.4, adsorption for the 3 proteins is compared as a function of the density of PLL patches in the brush. Figure 4.4A shows the ultimate protein coverage after about 20 minutes when the adsorbed amount of protein had leveled off, while Figure 4.4B focuses on the initial protein adsorption rates, indicative of pairwise protein-substrate interactions.

Independent of whether one considers the adsorption rate or amount, important features of the protein adsorption are apparent. First, the cationic patches at the base of the brush do indeed adsorb protein, as was the intention with this surface design: greater patch surface loadings produce more rapid and more extensive protein adsorption. A feature common to the adsorption of all 3 proteins is that they do not adhere to saturated PLL-g-PEG layers (without patches) and they also do not adhere to PLL-g-PEG layers containing a small amount of patches. Instead, only above a threshold patch density, protein adsorption commences. Importantly, the threshold patch density for adsorption depends on the particular protein.

Typically the existence of a threshold signals capture of target species on multiple rather than single patches. If individual patches were capable of adhering individual targets, the data would intersect the origin. The requirement that multiple patches engage each adsorbing protein molecule further suggests that the binding energy between each patch and a protein is insufficient to overcome protein translational entropy, and any entropy loss associated with the compression of PEG tethers in the vicinity of the protein. The energetic argument concerning the physics of the threshold was recently validated using adhesive cationic patches on an entirely negative non-brushy surface in studies of particle capture.<sup>37</sup>

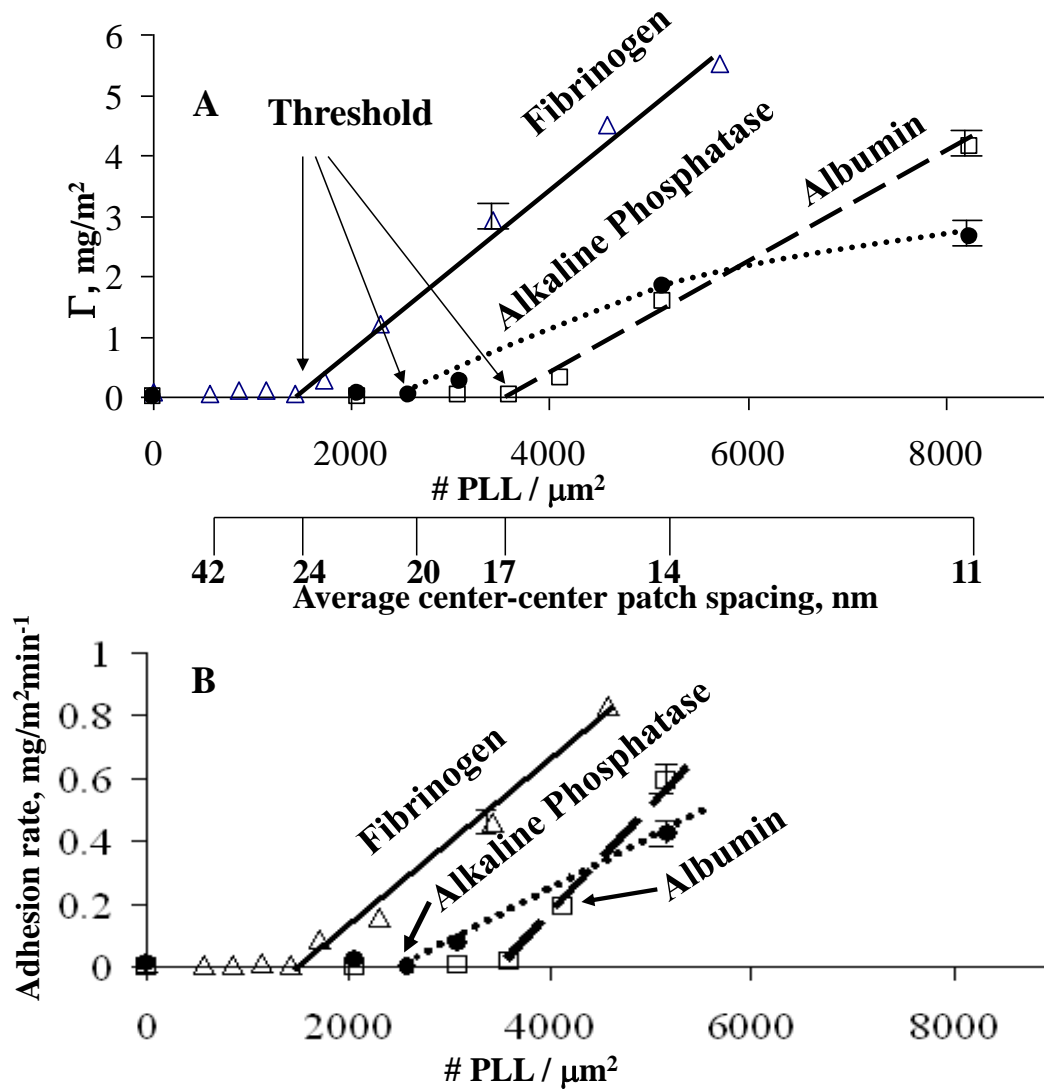


Figure 4.4 Summary of protein (A) adsorbed amounts and (B) initial adsorption kinetics, as a function of the surface loading of PLL patches.

The dependence of the threshold on the individual proteins is also interesting. The largest threshold  $\sim 3700$  patches/ $\mu\text{m}^2$ , is found for the smallest protein, albumin. Indeed, the secondary x-axis suggests a rough correlation between protein size and the

average patch spacing at the threshold. Only when the average patch spacing is sufficiently small that a protein can bridge at least 2 patches can adsorption occur, supporting the multivalency interpretation.

### 4.3.3.2 Comparison of myoglobin adhesion with other proteins

Myoglobin adhesion over the patchy brushes shows a different trend from the behavior of fibrinogen, albumin, and alkaline phosphatase. The argument that a protein needs to bridge the average patch spacing in order to effectively capture itself over a patchy brush requires average patch spacing to be less than 4.4 nm for effective capture of myoglobin. Being the smallest protein among the four proteins discussed here myoglobin would then require highest number of patches over the surface to be captured.

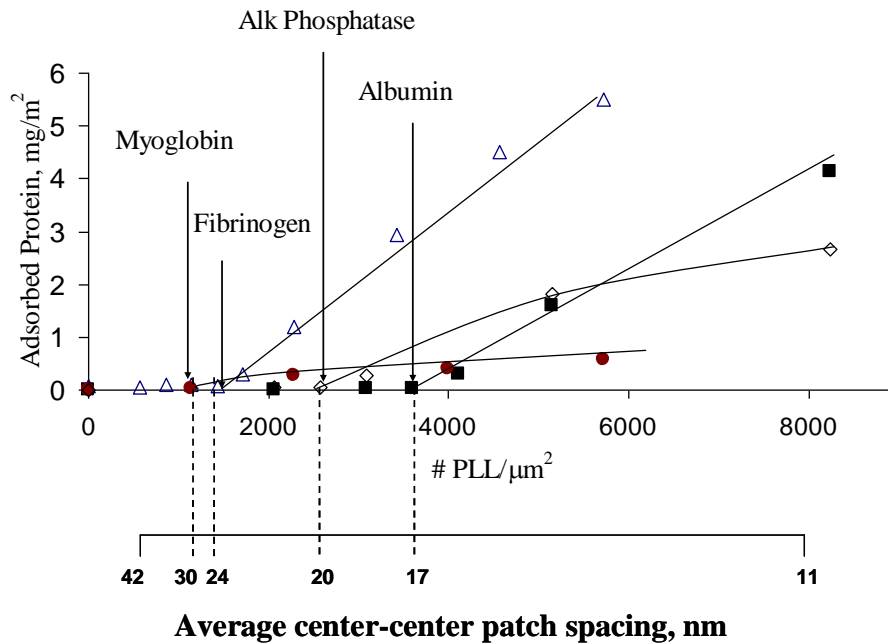


Figure 4.5 Comparison of myoglobin adhesion threshold with other proteins

Contrary to these expectations, Figure 4.5 shows myoglobin adhesion threshold is smaller than that of the other three proteins. The myoglobin threshold comes to an average patch spacing of 30 nm with PLL loading of  $\sim 1000$  patches/ $\mu\text{m}^2$ . Hence it can be inferred that myoglobin adsorption is univalent in nature rather than multivalent. Figure 4.5 suggests that some compromise of brush structure is required before myoglobin can effectively bind to the patches. Referring to Figure 2.10 we find that at 1000 patches/ $\mu\text{m}^2$  the brush coverage is 1.1 mg/ $\text{m}^2$ . Figure 2.10 further project the brush threshold at the same patch density as that of myoglobin threshold. Myoglobin can also feel reduced steric repulsion from the brushes because of its smaller size and is expected to be more sensitive to local brush structure, especially near the patches, compared with the larger proteins. All of these factors make myoglobin adsorption an interesting topic in this study.

#### **4.3.4 Protein separation**

The protein dependence of the binding threshold suggests that patchy brush surfaces could serve as separation media, if appropriately engineered. The key is the choice of patch density between the thresholds of proteins of interest. For instance, based on Figure 4.4, a surface with  $\sim 3400$  PLL patches/ $\mu\text{m}^2$  should adhere fibrinogen and reject albumin. This hypothesis is tested in Figure 4.6 for mixtures of albumin and fibrinogen, in a weight ration of 1:1, where albumin is fluorescently labeled and fibrinogen is not. In Figure 4.6 the protein mixture, exposed to a surface containing 3400 patches /  $\mu\text{m}^2$ , shows no protein adsorption in TIRF, while the same experiment conducted in the reflectometer shows a visible signal. These observations indicate that only fibrinogen adsorbs on this surface while albumin is completely rejected. The absence of a TIRF

adsorption signal indicates a complete lack of albumin adsorption but does not provide information about the adsorption of the unlabeled fibrinogen. The finite reflectometry signal indicates substantial protein adsorption and, since albumin adsorption was ruled out in the TIRF experiment, the adsorption must be due entirely to fibrinogen.

This behavior contrasts with simultaneous albumin and fibrinogen adsorption on control surfaces with cationic patch densities exceeding the thresholds of both species, in Figure 4.7. Here, TIRF data are compared for labeled albumin adsorption from the same mixture, on the test surface of Figure 4A and a control surface having 8000 PLL chains /  $\mu\text{m}^2$ , above both thresholds. Substantial albumin adsorption on the control surface is expected and observed but is lower than that for albumin alone (from a single-species solution), due to partial surface occupation by adsorbing fibrinogen.

Figure 4.8 addresses the additivity of albumin and fibrinogen adsorption from a mixture, using a saturated PLL surface. This surface was chosen because it strongly adsorbs both proteins and is expected to give the greatest interference between competing species, ie worst case scenario for separation applications. In Figure 4.6, single-species adsorption traces for albumin and fibrinogen, each at 100 ppm, are presented, along with data for a mixture of the two proteins (200 ppm total, the same individual concentrations as in the single-component runs). Superposed on this is a curve for the sum of the individual species.

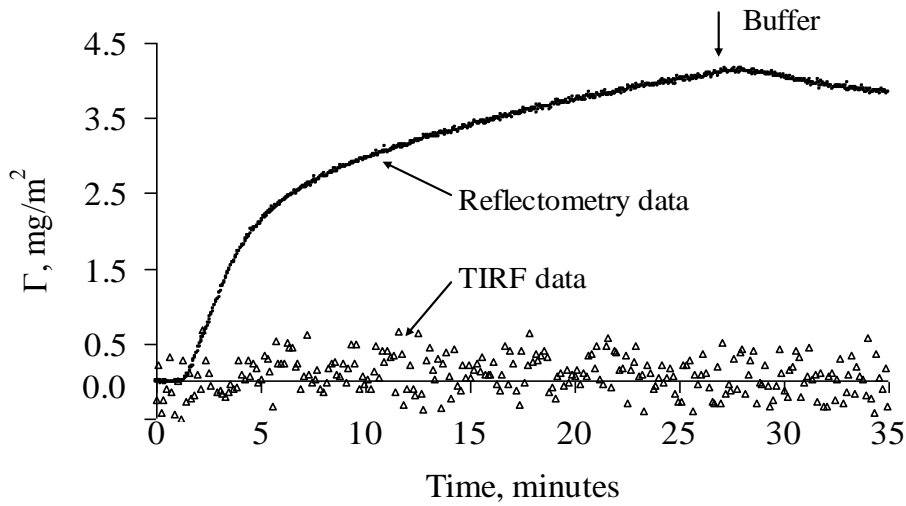


Figure 4.6 Adsorption kinetic traces for a mixture of fluorescent-albumin and untagged fibrinogen on a selective surface carrying 3400 PLL patches /  $\mu\text{m}^2$ . TIRF data show only the albumin coverage while the reflectometry data show the total protein adsorption.

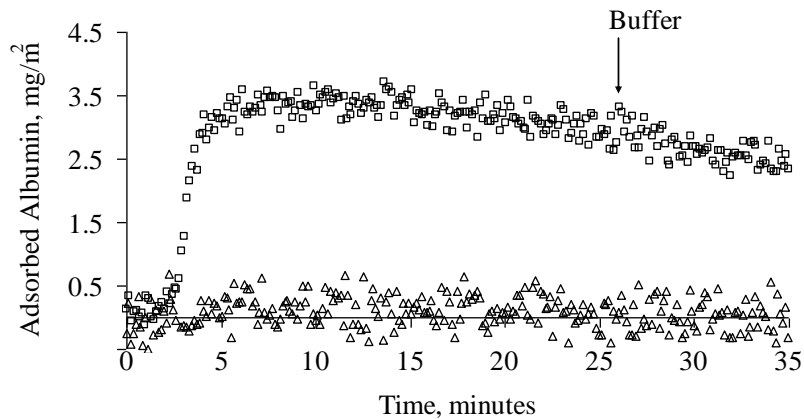


Figure 4.7. Adsorption kinetic traces measured by TIRF (sees only fluorescent albumin) for a mixture of fluorescent-albumin and untagged fibrinogen. A selective surface carrying 3400 PLL patches /  $\mu\text{m}^2$  is compared to a non-selective control surface carrying 8000 PLL patches /  $\mu\text{m}^2$ .



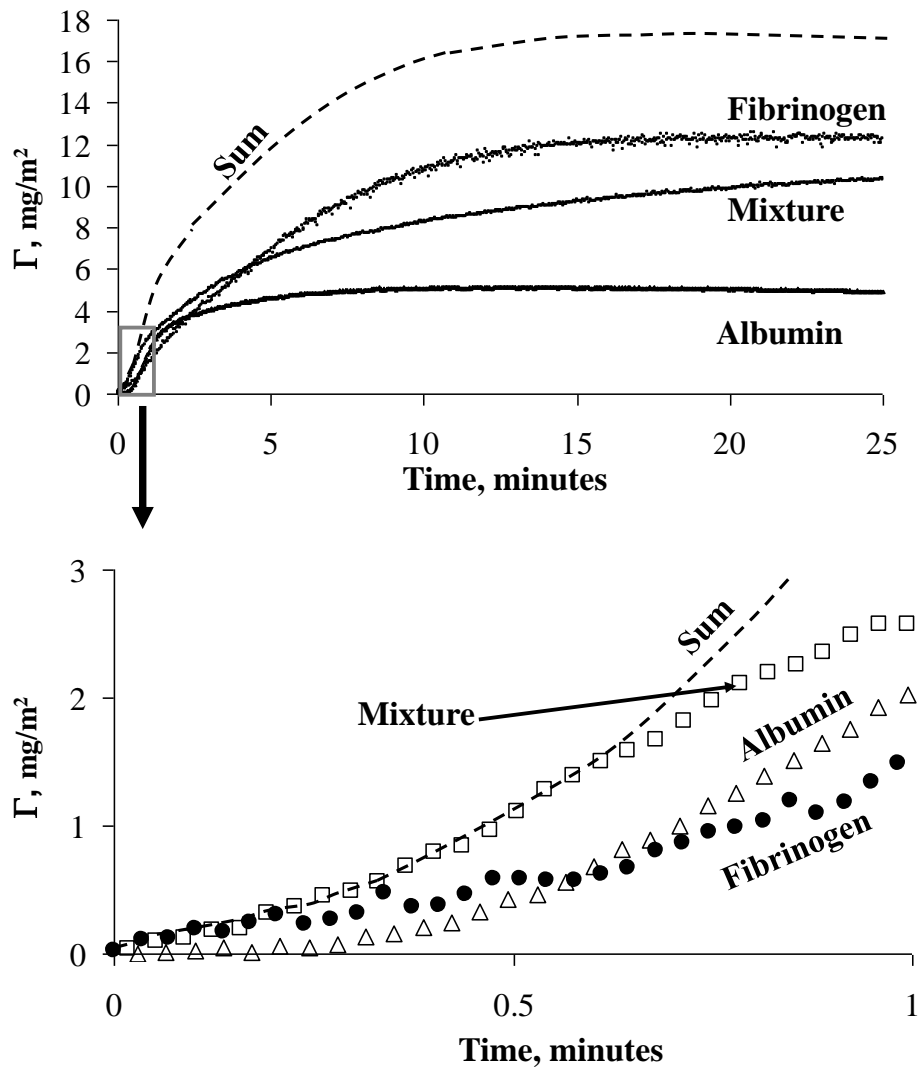


Figure 4.8. Studies on a non-selective adhesive PLL surface: single protein solution adsorption (at 100 ppm protein) versus simultaneous co-adsorption of two proteins (each at 100 ppm) in a mixture. Also drawn is the sum of the two data sets for single species adsorption, to test additivity of the co-adsorption mixture run.

One observes that, at low surface coverages, the protein mixture adsorbs at the rate expected from the sum of the two single-component experiments. This indicates a lack of competition between proteins on a nearly empty surface. The adsorption of the mixture slows above  $1.8 \text{ mg/m}^2$  total, as the surface begins to look crowded to approaching proteins. Notably, in the single species run, the albumin adsorption rate begins to turn over at this same coverage. It therefore may be the case that a reduced albumin adsorption rate, in particular, is responsible for the slowing of the mixture adsorption. Notably the single species fibrinogen adsorption run is still nearly linear at this coverage, suggesting that in the mixture, fibrinogen may also continue to adsorb unimpeded at this surface condition. Overall these data, along with those in Figure 4.4, suggest that up to moderate surface loadings, the single species adsorption behavior of proteins is a good predictor of protein adsorption from a mixture. This simple additivity is relevant to the regime of interest, near the adhesion thresholds where surfaces would be engineered for separation applications.

## **4.4 Discussion**

This chapter demonstrates that the previously reported adhesion threshold for fibrinogen on patchy brush surfaces<sup>16</sup> is a behavior that also occurs with other proteins, varying only in quantitative detail. The average patch separation at the threshold correlates with, but is not exactly equal to the largest protein dimension. This is most apparent for fibrinogen, where the average patch spacing at the threshold is 25 nm while the longest protein dimension is 47 nm. (For alkaline phosphatase, the adsorption of the

dimer is larger than albumin but smaller than fibrinogen, though the alkaline phosphatase monomer (in the first 2 entries of Table 4.1) more closely approaches the albumin size.) These observations suggest that the protein binding mechanism is not simply protein bridging between two surface patches, but instead involves protein interactions with an appropriate number of surface sites, necessary to produce adequate binding energy. The thresholds therefore rank roughly in order of protein size but will also be influenced by the charge density and distribution on the protein itself. Three of the proteins in this study are negative with similar isoelectric points in Table 4.1 and one (myoglobin) is neutral. With similarities in the negative characters of the three proteins, protein size becomes the primary factor in setting the adhesion threshold as long as the major dimensions of the proteins are larger than the patch size.

A point worth mentioning is that, as the surface is loaded with increasing numbers of PLL patches, the surrounding brush structure is potentially altered. In the limit of sparse PLL patches, one should continue to think of the brush structure as being similar to that of a brush containing no patches, with the exception of the tethers nearest the patches. These neighboring tethers may not extend as far perpendicular to surface as those in the main body of the brush because tethers near the patches may be relaxed to partially (or completely) obstruct the patches. However, as the PLL patch density is increased, the probability of finding PLL patches near each other is increased: When a small number of PLL-g-PEG copolymers are adsorbed between closely situated PLL patches in Figure 5, the brush in this region will be less extended than the brush on a saturated surface. The localized compromised brush could extend over the full region of

surface between two nearby patches, creating an adhesive area perhaps 40 nm in linear dimension.

We believe that, for surface compositions near the protein adsorption thresholds, this kind of compromise of brush structure is generally not occurring, and that patches are acting discretely with mostly local influence on the brush structure. At the fibrinogen threshold of  $\sim 1500$  PLL patches /  $\mu\text{m}^2$ , the PLL-g-PEG backfill density is roughly 85% of saturation, arguing against the potential mechanism in the previous paragraph. (With 1500 PLL patches per each square micron, about 12% of the surface is covered with PLL so one might expect a similar reduction in the backfill.) Likewise for the alkaline phosphatase threshold of  $\sim 2500$  PLL /  $\mu\text{m}^2$ , the PLL-g-PEG coverage is 70% of saturation, and for the albumin threshold the PLL-g-PEG coverage is 60% of saturation. In the latter cases, thinner brushes might still resist protein adhesion, given the minimal albumin and alkaline phosphatase adsorption on glass. One can therefore argue in favor of discrete patch action for protein capture, rather than a more mean field reduction in interfacial protein resistance. Conversely, since the size of proteins approach the brush persistence length, its adsorption depends on the brush structure and it becomes univalent.

If patches act discretely in their interactions with proteins, one then can think of the thresholds (for instance in Figure 4.4, producing the separations in Figure 4.6) as resulting from local patch arrangements accessible to single protein molecules. The presence of thresholds indicates a multivalency mechanism for protein binding: Two or more patches must engage in the capture of each protein, and therefore the protein dimension becomes an important lengthscale in establishing protein adhesion. The other

important factor is the effective binding energy of each patch, which is influenced by the local structure of the brush near the patch. PEG tethers may obstruct the PLL patches, but any lateral expansion of brush chains near patches leaves a locally compromised brush within a few nanometers of each isolated PLL patch. Therefore the binding energy associated with each patch in the dilute surface limit is the sum of the electrostatic binding energy of partially obstructed patches, plus any attractions between the protein and the negative substrate in the region of the compromised brush, per Figure 4.9.

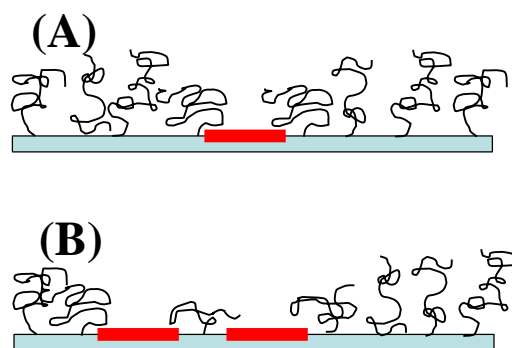


Figure 4.9. Possible near-patch brush structure. (A) Isolated versus (B) nearby patches

While in our other work, we have been able to estimate the number of patches involved in the capture of spheres approaching a patchy surface, we do not hazard the estimate in this case. Prior studies exploited systematic changes, via ionic strength, in the contact area between the approaching particles and the engineered substrate. This is accomplished loosely in the current study through variations in protein size amount the 3 test proteins, however, not only is the protein shape (aspect ratio) impossible to hold constant, the local charge density of the adsorbing face of the protein may not be constant. Therefore, even though the effective “contact areas” between the protein and the substrate may be estimated here, the protein binding energy per cationic patch is

unknown and not necessarily fixed (though we chose proteins with similar pI's to approximate this effect).

The adhesion characteristics of myoglobin present an interesting counter example to this discussion here. Myoglobin has two major difference with other three proteins considered. First the major dimension of myoglobin is smaller than the patch size (10 nm) approaching the brush persistence length. Second myoglobin is net neutral at our operating pH of 7.4. The myoglobin threshold corresponded to an average patch spacing, which is greater than the major dimension of myoglobin. This suggested that myoglobin adhered to single patches in order to get captured over the surface. Myoglobin's small size near the brush persistence length may facilitate its adhesion. The smaller size of myoglobin compared to a single patch size further facilitate its univalent adhesion on patches. Indeed the myoglobin threshold may be affected by the slightly compromised brush structure in the vicinity of the patches.

## **4.5 Conclusions**

This chapter demonstrated an adhesion threshold in the surface density of cationic patches needed to produce protein adsorption into/onto an otherwise protein-resistant 2000- molecular weight PEG brush. The study found that this behavior, which was previously reported for fibrinogen, is qualitatively similar for 2 other proteins, albumin and alkaline phosphatase. The three proteins, however, exhibited quantitatively different thresholds that ranked in order of protein size / molecular weight, with the adhesion threshold inversely proportional to protein size, and the patch spacing at the threshold

similar to the protein dimension. These observations suggested that multivalent interactions are responsible for protein capture: multiple patches must interact with each protein to cause it to adsorb. Individual patches are too weakly binding, as a result of their fundamentally small size with limited accessibility of cationic groups and a result of the entropic cost of compressing nearby regions of the PEG brush as the protein approaches.

The work also demonstrated the utility of surfaces engineered with patch loadings between the thresholds of competing adsorbing proteins from a mixture. On adhesive control surfaces above all thresholds, all proteins adsorb in proportion to their concentration and transport properties. Surface compositions between protein thresholds reject some proteins (those with high adsorption thresholds) and strongly adsorb others. The separation is extremely sharp and would be useful in technologies where staged operations, or those with multiple theoretical plates are undesirable.

## 4.6 References

- 1.) Gon, S., & Santore, M. M. (2011). Single Component and Selective Competitive Protein Adsorption in a Patchy Polymer Brush: Opposition between Steric Repulsions and Electrostatic Attractions. *Langmuir*, 27(4), 1487-1493.
- 2.) Dalsin, J. L., Lin, L., Tosatti, Samuele, Voeroes, J., Textor, Marcus, & Messersmith, P. B. (2005). Protein Resistance of Titanium Oxide Surfaces Modified by Biologically Inspired mPEG-DOPA. *Langmuir*, 21(2), 640-646.
- 3.) Bartucci, R., Pantusa, M., Marsh, D., & Sportelli, L. (2002). Interaction of human serum albumin with membranes containing polymer-grafted lipids: spin-label ESR studies in the mushroom and brush regimes. *Biochimica et Biophysica Acta, Biomembranes*, 1564(1), 237-242.
- 4.) Alang Ahmad, S., Hucknall, A., Chilkoti, A., & Leggett, G. J. (2010). Protein Patterning by UV-Induced Photodegradation of Poly(oligo(ethylene glycol) methacrylate) Brushes. *Langmuir*, 26(12), 9937-9942.
- 5.) Halperin, A., Buhot, A., & Zhulina, E. B. (2005). Brush effects on DNA chips: Thermodynamics, kinetics, and design guidelines. *Biophysical Journal*, 89(2), 796-811.
- 6.) Huang, Y.-W., & Gupta, V. K. (2004). A SPR and AFM study of the effect of surface heterogeneity on adsorption of proteins. *Journal of Chemical Physics*, 121(5), 2264-2271.
- 7.) Slater, J. H., & Frey, W. (2008). Nanopatterning of fibronectin and the influence of integrin clustering on endothelial cell spreading and proliferation. *Journal of Biomedical Materials Research. Part A*, 87(1), 176-195.
- 8.) Wolfram, T., Belz, F., Schoen, T., & Spatz, J. P. (2007). Site-specific presentation of single recombinant proteins in defined nanoarrays. *Biointerphases*, 2(1), 44-48.



- 9.) Collins, J. A., Xirouchaki, C., Palmer, R. E., Heath, J. K., & Jones, C. H. (2004). Clusters for biology: immobilization of proteins by size-selected metal clusters. *Applied Surface Science*, 226(1-3), 197-208.
- 10.) Riedel, M., Muller, B., & Wintermantel, E. (2001). Protein adsorption and monocyte activation on germanium nanopyramids. *Biomaterials*, 22(16), 2307-2316.
- 11.) Santore, Maria M., & Wertz, C. F. (2005). Protein Spreading Kinetics at Liquid-Solid Interfaces via an Adsorption Probe Method. *Langmuir*, 21(22), 10172-10178.
- 12.) Fang, J., & Knobler, C. M. (1996). Phase-separated two-component self-assembled organosilane monolayers and their use in selective adsorption of a protein. *Langmuir*, 12(5), 1368-1374.
- 13.) de las Heras Alarcón, C., Farhan, T., Osborne, V. L., Huck, W. T. S., & Alexander, C. (2005). Bioadhesion at micro-patterned stimuli-responsive polymer brushes. *Journal of Materials Chemistry*, 15(21), 2089.
- 14.) Sanford, M. S., Charles, P. T., Commisso, S. M., Roberts, J. C., & Conrad, D. W. (1998). Photoactivatable Cross-Linked Polyacrylamide for the Site-Selective Immobilization of Antigens and Antibodies. *Chemistry of Materials*, 10(6), 1510-1520.
- 15.) Miller, R., Guo, Z., Vogler, E. A., & Siedlecki, C. A. (2005). Plasma coagulation response to surfaces with nanoscale chemical heterogeneity. *Biomaterials*, 27(2), 208-215.
- 16.) Gon, S., Bendersky, M., Ross, J. L., & Santore, M. M. (2010). Manipulating Protein Adsorption using a Patchy Protein-Resistant Brush. *Langmuir*, 26(14), 12147-12154.
- 17.) Halperin, A., & Kroger, M. (2009). Ternary Protein Adsorption onto Brushes: Strong versus Weak. *Langmuir*, 25(19), 11621-11634.

- 18.) Pluckthun, A., & Pack, P. (1997). New protein engineering approaches to multivalent and bispecific antibody fragments. *Immunotechnology*, 3(2), 83-105.
- 19.) Tweedle, M. F. (2006). Adventures in multivalency the Harry S. Fischer Memorial Lecture CMR 2005; Evian, France. *Contrast Media & Molecular Imaging*, 1(1), 2-9.
- 20.) Minko, S., Muller, M., Usov, D., Scholl, A., Froeck, C., & Stamm, M. (2002). Lateral versus perpendicular segregation in mixed polymer brushes. *Physical review letters*, 88(3), 035502.
- 21.) Draper, J., Luzinov, I., Minko, Sergiy, Tokarev, I., & Stamm, Manfred. (2004). Mixed Polymer Brushes by Sequential Polymer Addition: Anchoring Layer Effect. *Langmuir*, 20(10), 4064-4075.
- 22.) Uhlmann, P., Houbenov, N., Brenner, N., Grundke, K., Burkert, S., & Stamm, Manfred. (2007). In-Situ Investigation of the Adsorption of Globular Model Proteins on Stimuli-Responsive Binary Polyelectrolyte Brushes. *Langmuir*, 23(1), 57-64.
- 23.) Gautrot, J. E., Huck, W. T. S., Welch, M., & Ramstedt, M. (2010). Protein-Resistant NTA-Functionalized Polymer Brushes for Selective and Stable Immobilization of Histidine-Tagged Proteins. *ACS Applied Materials & Interfaces*, 2(1), 193-202.
- 24.) Tosatti, S., Schwartz, Z., Campbell, C., Cochran, D. L., VandeVondele, S., Hubbell, J.A., Denzer, A., et al. (2004). RGD-containing peptide GCRGYGRGDSPG reduces enhancement of osteoblast differentiation by poly(L-lysine)-graft-poly(ethylene glycol)-coated titanium surfaces. *Journal of biomedical materials research. Part A*, 68(3), 458-472.
- 25.) Tosatti, S., De, P., Askendal, A., VandeVondele, S., Hubbell, J. A., Tengvall, P., & Textor, M. (2003). Peptide functionalized poly(L-lysine)-g-poly(ethylene glycol) on titanium: resistance to protein adsorption in full heparinized human blood plasma. *Biomaterials*, 24(27), 4949-4958.

- 26.) Fu, Z., & Santore, Maria M. (1998). Poly(ethylene oxide) adsorption onto chemically etched silicates by Brewster angle reflectivity. *Colloids and Surfaces, A: Physicochemical and Engineering Aspects*, 135(1-3), 63-75.
- 27.) Rebar, V. A., & Santore, M. M. (1996). A total internal reflectance fluorescence nanoscale probe of interfacial potential and ion screening in polyethylene oxide layers adsorbed onto silica. *Journal of Colloid and Interface Science*, 178(1), 29-41.
- 28.) Wertz, C. F., & Santore, Maria M. (1999). Adsorption and Relaxation Kinetics of Albumin and Fibrinogen on Hydrophobic Surfaces: Single-Species and Competitive Behavior. *Langmuir*, 15(26), 8884-8894.
- 29.) Böhme, U., & Scheler, U. (2007). Effective charge of bovine serum albumin determined by electrophoresis NMR. *Chemical Physics Letters*, 435(4-6), 342-345.
- 30.) Wasilewska, M., Adamczyk, Z., & Jachimska, B. (2009). Structure of Fibrinogen in Electrolyte Solutions Derived from Dynamic Light Scattering (DLS) and Viscosity Measurements. *Langmuir*, 25(6), 3698-3704.
- 31.) Jürgens, K. D., Peters, T., & Gros, G. (1994). Diffusivity of myoglobin in intact skeletal muscle cells. *Proceedings of the National Academy of Sciences of the United States of America*, 91(9), 3829-3833.
- 32.) Tsapikouni, T. S., & Missirlis, Y. F. (2007). pH and ionic strength effect on single fibrinogen molecule adsorption on mica studied with AFM. *Colloids and Surfaces, B: Biointerfaces*, 57(1), 89-96.
- 33.) Desfougeres, Y., Croguennec, T., Lechevalier, V., Bouhallab, S., & Nau, F. (2010). Charge and Size Drive Spontaneous Self-Assembly of Oppositely Charged Globular Proteins into Microspheres. *Journal of Physical Chemistry B*, 114(12), 4138-4144.
- 34.) Graf, M., Galera, G. H., & Wätziq, M. (2005). Protein adsorption in fused-silica and polyacrylamide-coated capillaries. *Electrophoresis*, 26(12), 2409-2417

- 35.) Schillemans, J. P., Hennink, W. E., & van Nostrum, C. F. (2010). The effect of network charge on the immobilization and release of proteins from chemically crosslinked dextran hydrogels. *European Journal of Pharmaceutics and Biopharmaceutics*, 76(3), 329-335.
- 36.) de, V., Leermakers, F. A. M., de, K., Cohen, S., & Kleijn, J. M. (2010). Field Theoretical Analysis of Driving Forces for the Uptake of Proteins by Like-Charged Polyelectrolyte Brushes: Effects of Charge Regulation and Patchiness. *Langmuir*, 26(1), 249-259.
- 37.) Kalasin, S., Martwiset, S., Coughlin, E. B., & Santore, Maria M. (2010). Particle Capture via Discrete Binding Elements: Systematic Variations in Binding Energy for Randomly Distributed Nanoscale Surface Features. *Langmuir*, 26(22), 16865-16870.

## CHAPTER 5

# SENSITIVITY OF PROTEIN ADSORPTION TO ARCHITECTURAL VARIATIONS IN A PROTEIN- RESISTANT POLYMER BRUSH CONTAINING ENGINEERED NANO-SCALE ADHESIVE SITES

### 5.1 Introduction

The current chapter focuses on how protein adsorption can be manipulated based on the architectural variation of a PEG brush. Most of this chapter has been reproduced from our recent paper.<sup>1</sup> A popular strategy for imparting biocompatibility is the modification of surfaces with polymer brushes that sterically repel approaching proteins. For brushes to be effective, both their chemistry and interfacial architecture must be appropriate. The polymer itself must be hydrophilic and well-solubilized in water, charge-neutral, and a hydrogen bond acceptor.<sup>2</sup> Polyethylene glycol (PEG) is one of a handful of polymers meeting these criteria, making it a popular choice for the creation of protein-resistant brushes. The brush must further have an appropriate architecture to screen the full range of Van der Waals and electrostatic interactions between proteins and the underlying substrate.<sup>3</sup> This latter criterion has been usually interpreted to mean that the brush extension must exceed the range of substrate-protein attractions; however, it is understood that proteins must not penetrate or compress the brush.<sup>3</sup> A tall but

insufficiently dense brush may not be fully effective. Indeed, some reports suggest that the mass of the tethered polymer (such as PEG) is a better predictor of brush performance than the calculated brush height.<sup>3,4</sup> In the case of PEG chains tethered to surfaces by different anchoring chemistries, a PEG chain mass exceeding  $1.1 \text{ mg/m}^2$  led to almost complete repulsion of serum proteins, independent of the length of the tethers themselves, in the range from 2,000 to 10,000 molecular weight.<sup>4</sup> The ease by which brush architecture can be altered (both in terms of tether length and density), make polymer brushes an attractive choice for manipulating the initial encounters of proteins with surfaces. Functionalization of the free brush ends has traditionally allowed tuning of bio-adhesion.<sup>5</sup>

A second materials-based strategy to manipulate protein adsorption is control over the area of protein-surface contact. With an eye towards constraining protein denaturing<sup>6,7</sup> or tuning the adsorbing sites,<sup>8</sup> a few groups have created interfaces where the protein-attracting regions are small and the remaining surface is neutral or repulsive. Restricted contact areas have been potentially achieved employing phase-separated polymer<sup>9</sup> and silane ligands,<sup>10,11</sup> surface-immobilized or suspended nanoparticles,<sup>12-16</sup> and other strategies.<sup>17</sup> (Antibody-based and receptor capture of targeted proteins represents a special case outside the current scope.) Varied observations regarding adsorption (or lack of it) on surfaces whose adhesive elements are similar to the protein size has not produced a consensus on the importance of the relative sizes of proteins and adhesive islands. Some argue that the adsorption site must be at least as large as the protein;<sup>18</sup> however, counter examples exist.<sup>19</sup> The philosophy in the Santore lab, generally, is that the energy rather than the size of the initial contact is critical.<sup>20</sup> While increased contact

area will generally provide an opportunity for strengthened interactions, sufficiently strong attractions might result from contact regions smaller than the size of the target. For example, we demonstrated that micron-scale silica spheres could be captured and held in flow by electrostatic attractions to single surface-immobilized 10 nm nanoparticles.<sup>21,22</sup> More recently we demonstrated bacterial capture by single nanoparticles on a weakly-repulsive surface.<sup>23</sup>

The current chapter focuses on surfaces containing protein-adhesive cationic elements or “patches,” about 10 nm in size (roughly the same as the protein), randomly positioned at the base of a PEG brush whose steric repulsion limits patch-protein interactions. This approach opposes the conventional wisdom of placing attractive functionality on a brush periphery.<sup>5</sup> While tethered ligands can selectively bind targets via biomolecular specificity, the adhesive elements buried within patchy brushes bind targets with sharp selectivity, as a result of competing steric repulsion from the brush and attractions to the adhesive elements.<sup>24</sup> Without prerequisite biofunctional specificity, patchy brushes can be fabricated at smaller expense and tend to be more robust.

Previous studies of patchy brushes revealed a threshold in the patch surface loading necessary for protein adsorption.<sup>25</sup> That is, if the PEG brush contained less than the critical surface concentration of patches, no protein adsorption occurred. This was preliminary evidence for multivalent binding. It was speculated that a protein needed to adhere to multiple patches simultaneously in order to be retained. In a second work,<sup>24</sup> the utility of patchy brushes with protein adsorption thresholds was demonstrated. The thresholds for a series of proteins correlated with their size, further supporting the hypothesis of multivalent protein capture. Additionally, surfaces engineered between the

two thresholds of the competing species in a protein mixture could selectively adhere one protein. Sharp selectivities exceeding 100 (the ratio of the surface to bulk composition) were demonstrated for proteins with similar charge.

In the previous chapters we have examined the influence of cationic patches on protein capture in only one type of brush and at a single ionic strength.<sup>24,25</sup> The current study, employing fibrinogen as a model protein (chosen because it is well studied on a variety of surfaces and because its dimensions are similar in magnitude to the patch size) varies the relative ranges of electrostatic attractions and steric repulsions, via systematic variation in ionic strength and brush architecture. Given the complexity of the results, further variations in the patch composition and size are addressed separately. The current study reveals how variations in electrostatic and steric forces shift the adhesion thresholds in ways that might be engineered to fine-tune selectivity. Additionally, the work provides fundamental perspective into the properties of polymer brushes: the ability of tethered chains to extend laterally on a surface and the accessibility of bare protein-sized spots, spatial fluctuations, or flaws as the base of a brush to proteins in solution.

## **5.2 Background on brush and strategy**

The patchy brushes in this study, represented schematically in Figure 5.1, were created as documented previously in Chapter 2. Tightly-controlled amounts of a cationic polymer, poly-L-lysine (PLL), were adsorbed on a silica surface at well-characterized mass transport conditions so the surface loading is limited well below saturation. With



PLL coverage sufficiently low that adsorbed coils are isolated, each coil acts as a randomly-situated cationic patch, about 10 nm in size, an estimate based on its free solution size from light scattering. (Though ionic strength was varied during the protein adsorption portions of the study, all patches and brushes were deposited at uniform conditions, in pH 7.4 phosphate buffer of ionic strength 0.026 M, having a Debye length of 1.96 nm. These electrostatically screened conditions impart flexibility to the PLL backbone so that it is in a random coil conformation, rather than a rigid rod. Indeed the observed 10 nm radius is consistent with a well-solvated random coil rather than a rod.) The remaining surface was backfilled via adsorption from solution, with a PLL-PEG graft copolymer to prevent protein adsorption on the bare silica. Key in this approach, the PLL component of the patches was the same as the anchoring part of the PLL-PEG backfill brush. This led to exclusion of PLL-PEG from the regions where PLL is already adsorbed. Notable features of these interfaces<sup>25</sup> are described below.

- 1) A net positive charge on a saturated layer of PLL on silica ( $0.4 \text{ mg/m}^2$ ), suggesting a local positive charge in the vicinity of the isolated patches of the current study,
- 2) Retention of patches on the surface during backfilling and subsequent use of the surfaces at the conditions of these studies, with the backfill brushes also being robust at the conditions of interest<sup>26</sup>.
- 3) Substantial fibrinogen adsorption onto saturated PLL layers on silica, suggesting protein-patch attractions, at least in the absence of the brushy backfill.

The copolymers (Polymer I, Polymer II, Polymer III) from which these brushes were created has been discussed in detail in Chapter 2. Other brush properties, such as

brush height and persistence length, were calculated according to the Alexander-DeGennes model,<sup>27,28</sup> as described previously<sup>25</sup>.

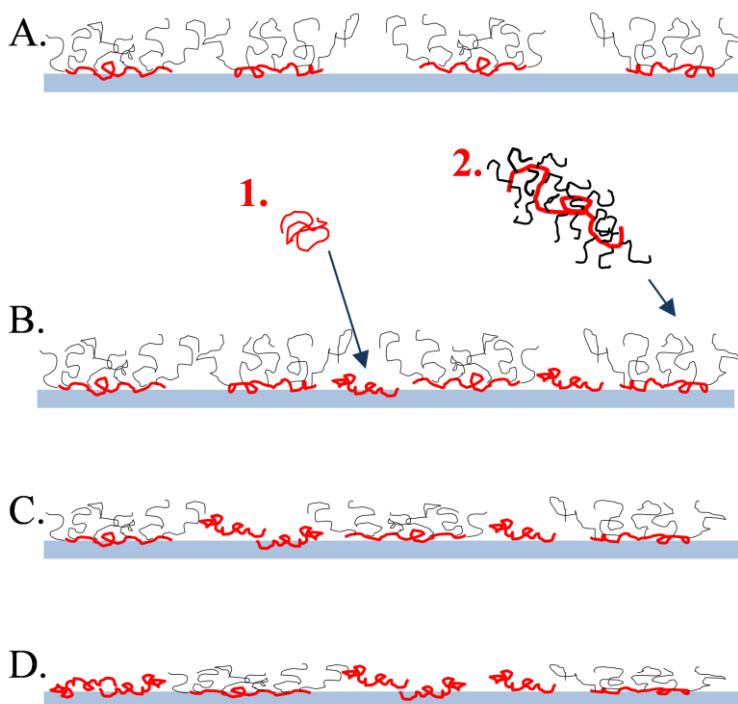


Figure 5.1 Interfacial structure with increased patch loading, (A) Full brush containing no patches, (B) Full brush containing buried patches, (C) Increased patches reducing backfill, (D) Substantial patch loading causing patches to lose identity while brush structure is lost (mushroom brush)

The Alexander-DeGennes brush model<sup>28</sup>, while unrealistic in its treatment of the brush as a sharply-defined (step-function) region having a constant polymer solution concentration, is powerful in its nearly accurate predictions of key brush properties, as reviewed by Milner.<sup>29</sup> The parabolic brush treatment, thought to give a more accurate

description of brush features including the interfacial concentration profile of segments (and estimating a nominal brush height to be about 25% greater than the Alexander-DeGennes treatment), has been shown by Kent<sup>30</sup> to be achieved only in rare experimental instances where the loading of chains at the interface is much greater than what we achieved in the current work. The significance of this for the current work is that the description of our brushes is imprecise because of the lack of an appropriate model. On the other hand, the three brushes presented in this work are distinct in their architectures, protein interactions and, separately, their dynamics.<sup>26</sup>

The brushes as described in Chapter 2, without the incorporation of PLL patches, completely resist the adsorption of serum proteins such as fibrinogen and albumin (within detectible limits of 0.01 mg/m<sup>2</sup>), and related brushes have been shown to eliminate protein adsorption from serum below the detectible limits.<sup>31,32</sup> The nearly perfect protein resistance of the brushes themselves is a key element in this work. The current study focuses on the ability of the patches to interact with and adsorb proteins in the presence of protein-repelling brushes. The only exception to the nearly perfect protein resistance is Brush #1 (Polymer I) which, when  $\kappa^{-1} = 4$  nm, adsorbs 0.08 mg/m<sup>2</sup> of fibrinogen. This adsorption is, however, reversible, with fibrinogen washing off the surface (giving coverage below 0.01 mg/m<sup>2</sup>) when the ionic strength is increased. This suggests that only with shorter Brush #1, when the ionic strength allows electrostatic interactions with the base of the brush to be felt by proteins at the periphery, does slight and weak protein adsorption occur on the outside of the brush. For thicker Brushes #2 (Polymer II) and #3 (Polymer III), and for higher ionic strengths, all brushes screen electrostatic and other protein substrate interactions.

As a general rule, adsorbed PLL patches occupy the negative silica and reduce the amount of PLL-PEG backfill necessary to saturate the interface. The details of the progressive reduction in backfill with increasing PLL patches are presented in Figure 5.2, reproduced from a recent paper on brush-protein interaction physics.<sup>26</sup>

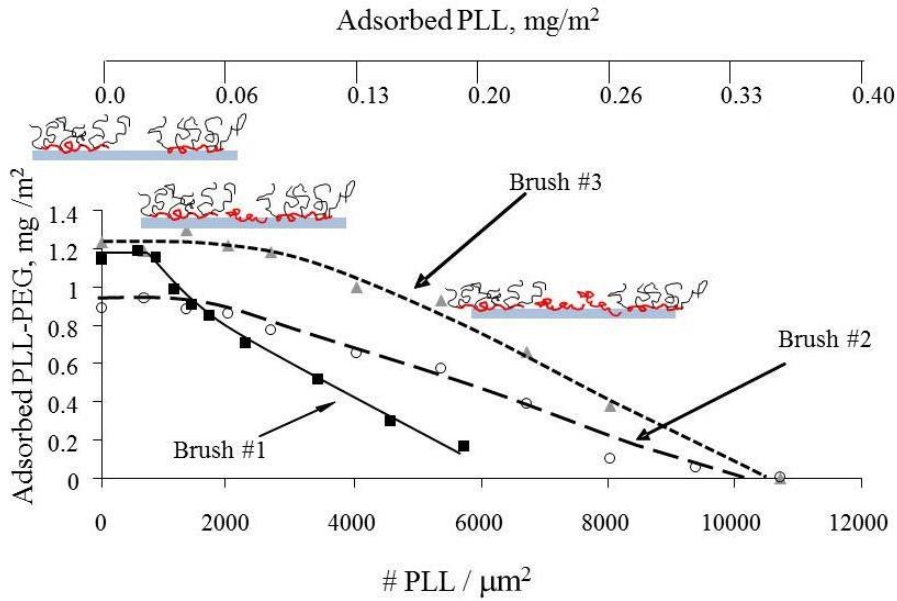


Figure 5.2: Amount of PLL-PEG copolymer adsorbed against PLL patches<sup>30</sup>

An interesting recent finding is that low levels of PLL patches do not alter the brush; however, at above some level of PLL coverage, the amount of PLL-PEG needed to saturate the surface is reduced substantially. The amount of PLL that can be incorporated at fixed PLL-PEG loading and the degree to which PLL-PEG backfill is reduced depends on the PLL-PEG architecture and the brush itself, varying substantially among the three samples in our system. Since brushes without patches contain limited amounts of PLL anchoring groups on the silica beneath the brush relative to a saturated PLL layer (0.4

mg/m<sup>2</sup>), small amounts of homopolymer PLL can be accommodated before the backfill is affected.

### 5.3 Materials and methods

The PEG brushes were synthesized and characterized as described in Chapter 2. Acid-etched (overnight in concentrated sulfuric acid, and well-rinsed in DI water) microscope slides (Fisher Finest) were used as the adsorption substrate. XPS has revealed these to have a silica surface<sup>33</sup>. Polymer and protein adsorption were carried out in a laminar slit shear flow cell at a wall shear rate of 5 s<sup>-1</sup> using polymers dissolved in 0.01 M pH 7.4 phosphate buffer (0.002M KH<sub>2</sub>PO<sub>4</sub> and 0.008M Na<sub>2</sub>HPO<sub>4</sub>). Notably, all patchy brushes were created in this buffer, and for protein adsorption studies at other ionic strengths, the buffer was switched subsequently, a process which did not alter the originally-formed patchy brushes. This buffer has a Debye length,  $\kappa^{-1} = 2\text{nm}$ . Buffers with  $\kappa^{-1} = 4\text{ nm}$  or  $1\text{ nm}$  were created by diluting to an overall concentration of 0.005M or operating at a greater concentration. Patchy brushes were created by flowing a 5 ppm PLL solution over the surface for a specific amount of time, allowing only the desired amount of PLL to adsorb and be retained before the flow was switched back to buffer. Then a 100 ppm buffered solution of the particular PLL-PEG of interest was flowed to backfill the remaining surface before the flow was again switched to buffer. This procedure has been documented and studied in detail,<sup>24,25</sup> including a study of the brush

stability.<sup>26</sup> The buffer was then switched to that of the protein adsorption study, and fibrinogen introduced at 100 ppm in the buffer of interest for 20-30 minutes, prior to switching back to buffer.

Adsorption of polymer and protein was observed using a custom-built near-Brewster optical reflectometry instrument in which 633 nm parallel-polarized laser light impinges on the interface from the substrate side<sup>34</sup>. The reflected intensity is proportional to the square of the adsorbed interfacial mass, with the calibration constant determined from the optical properties of the solution and the adsorbed layer, or from an appropriate kinetic-based calibration. Notably, slightly different calibration constants apply to polymer and protein adsorption portions of the runs.

## 5.4 Results

Figure 5.3 presents a series of raw reflectometry data for fibrinogen adsorption onto different surfaces with varying amounts of PLL patches in a PLL-PEG brush. This example, with Brush #2, is typical of all the data obtained with the other brushes. Most importantly, without any patches at the base of the brush, there is no protein adsorption.

With increasing amounts of PLL patches, fibrinogen adsorbs more readily, both in terms of the initial rate and the coverage after approximately 20 minutes (at which time buffer was re-injected). Indeed with 10,700 patches /  $\mu\text{m}^2$ , the fibrinogen coverage approaches that on a saturated PLL layer without PLL-PEG.<sup>24</sup> The 0.4 mg/m<sup>2</sup> of PLL at

saturation on silica translates to 12,000 patches / $\mu\text{m}^2$ . The nearly linear initial data in Figure 5.3 allow determination of the initial protein adsorption rate, providing insight into single protein-surface encounters at short times.

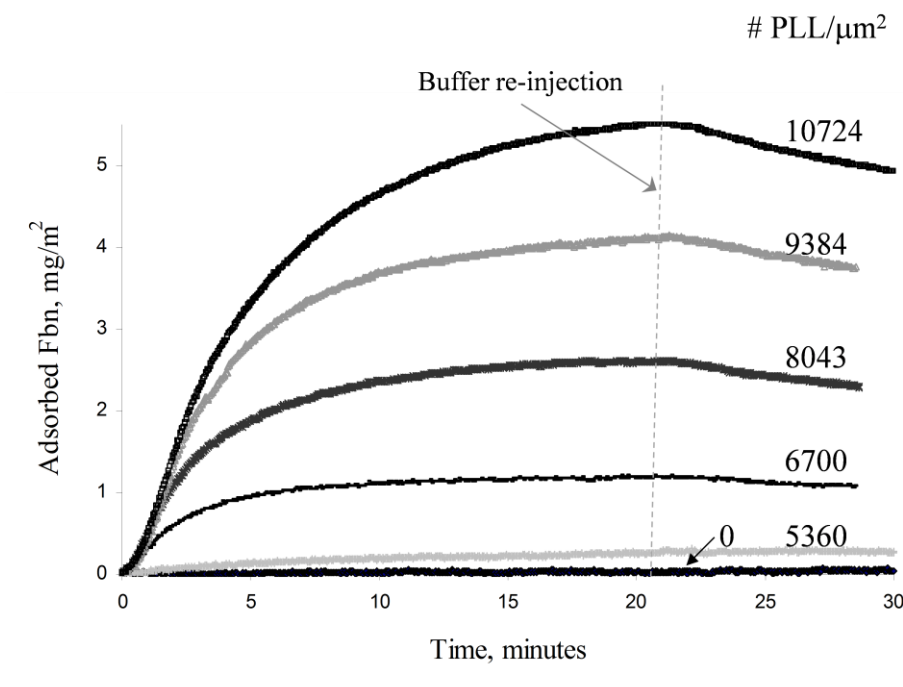


Figure 5.3 Reflectometry traces for fibrinogen adsorption over patchy Brush # 2 at 2 nm Debye length buffer strength

The data from Figure 5.3, along with other data for Brushes #1 and #3 and data at different ionic strengths, are summarized in Figure 5.4, which plots the initial fibrinogen adsorption rate as a function of PLL patch density within each brush. Each part of Figure 5.4 summarizes data for a different brush, highlighting the influence of the Debye length. The main feature of each data set is its extrapolation to a finite x-intercept. This x-intercept is termed the “adhesion threshold,” the minimum surface loading of adhesive patches needed to produce protein adhesion.

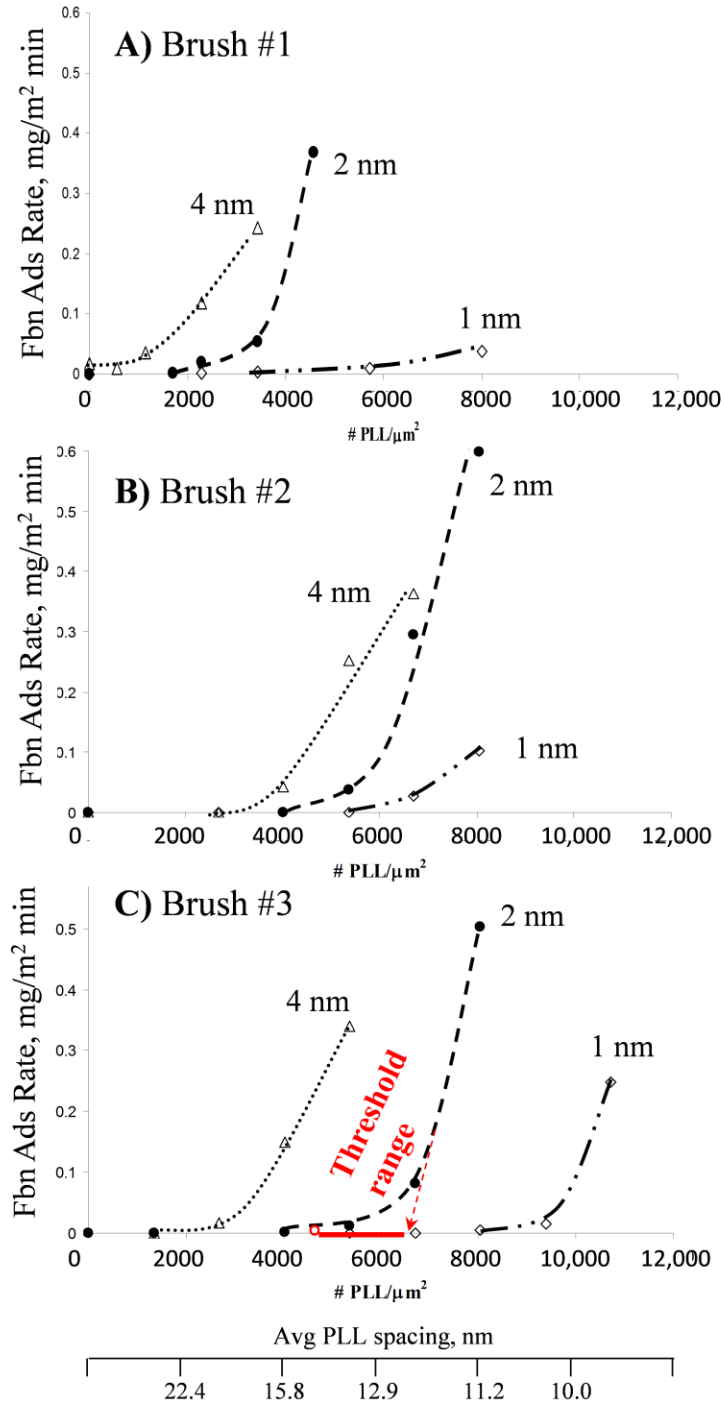


Figure 5.4 Summary of initial fibrinogen adsorption rates, comparing adsorption at different Debye lengths, for the three brushes in parts A, B, C. One example of threshold quantification is illustrated in red.



Previous studies of the fibrinogen adhesion threshold in a brush similar to Brush #1 at  $\kappa^{-1} = 2$  nm supported the interpretation that the threshold is indicative of multivalent protein capture. Because they are buried within the brush, individual patches are too weakly binding to each adhere fibrinogen. For several patches to simultaneously engage a protein (providing the requisite binding energy), surfaces must be loaded with sufficient patch density, so that the 47 nm length of the fibrinogen molecule exceeds the average patch spacing. This interpretation, which was reasonable for brushes like Brush #1, might also hold for Brushes #2 and #3, discussed below.

Figure 5.4 examines the impact of Debye length on the fibrinogen adsorption rates for the three different brush types. As a general trend, a particular brush is most adhesive at low salt conditions where the Debye length is 4 nm and least adhesive at higher ionic strengths where the Debye length is 1 nm. This is a result of the range and strength of electrostatic attractions from the PLL patches towards fibrinogen. While there may be some interpretation as to the exact value of each threshold (for instance illustrated in Figure 5.4C), it is remarkable that a 3 nm change in Debye length shifts the position of the threshold by several thousand patches /  $\mu\text{m}^2$  for any particular brush. For instance, in the case of Brush # 1 in Figure 4A, the threshold shifts from near 1000 patches /  $\mu\text{m}^2$  at  $\kappa^{-1} = 4$  nm to around 5000 patches /  $\mu\text{m}^2$  or greater when  $\kappa^{-1} = 1$  nm. The effect is even greater for the thicker Brushes, #2 and #3. This range of threshold shifts corresponds to about 50% of the possible range of surface composition or capacity for patches. Adhesion onto patchy brushes is therefore highly sensitive to ionic strength, likely a result of the comparable ranges of Debye lengths and brush thicknesses in this study.

Fibrinogen adsorption is slight when the Debye length is 1 nm: with hardly any adsorption up to 8000 patches /  $\mu\text{m}^2$ . This patch density was generally the maximum tested because 8000 patches /  $\mu\text{m}^2$  comprise two thirds of a fully saturated PLL layer. Adsorbed PLL coils are not positioned as isolated adhesive islands at high PLL coverages and, further, the polymer brush is not well-established because the backfill amount has become small. In Figure 4C, nonetheless, we extended the range of study slightly, because even with 8000 PLL/  $\mu\text{m}^2$  there was no evidence for fibrinogen adsorption on Brush #3. The observations of negligible fibrinogen adsorption for  $\kappa^{-1} = 1$  nm, with as many as 8000 or 9000 PLL patches /  $\mu\text{m}^2$  (and as little as 0.15 mg/m<sup>2</sup> of PLL –PEG brush,) are unexpected, given the lack of an established PEG brush in this regime. Even though the electrostatic attractions between fibrinogen and PLL are short range at  $\kappa^{-1} = 1$  nm, the attractions are still expected to be substantial.

Figure 5.5 recapitulates the data from Figure 5.4, providing a perspective on the impact of the brush choice on the fibrinogen capture rate. For a fixed Debye length in a single panel of the figure, the trends are generally clear. For instance at a Debye length of  $\kappa^{-1} = 2$  nm, the threshold increases with increases in the brush thickness, with the thresholds and brush numbers ranking in order: #1, #2, #3. The ranking of the thresholds is different, however, at 4 nm: the threshold order is Brush #1, Brush #3, and Brush #2. While there are complexities in the ranking of the thresholds at different ionic strengths, the basis for discussion in the next section, there is a zero-order ranking of the thresholds with the brush thickness: Brush #1 always has the smallest thresholds. Brush #2 and #3, which exhibit slight differences in height, have greater thresholds than Brush #1.

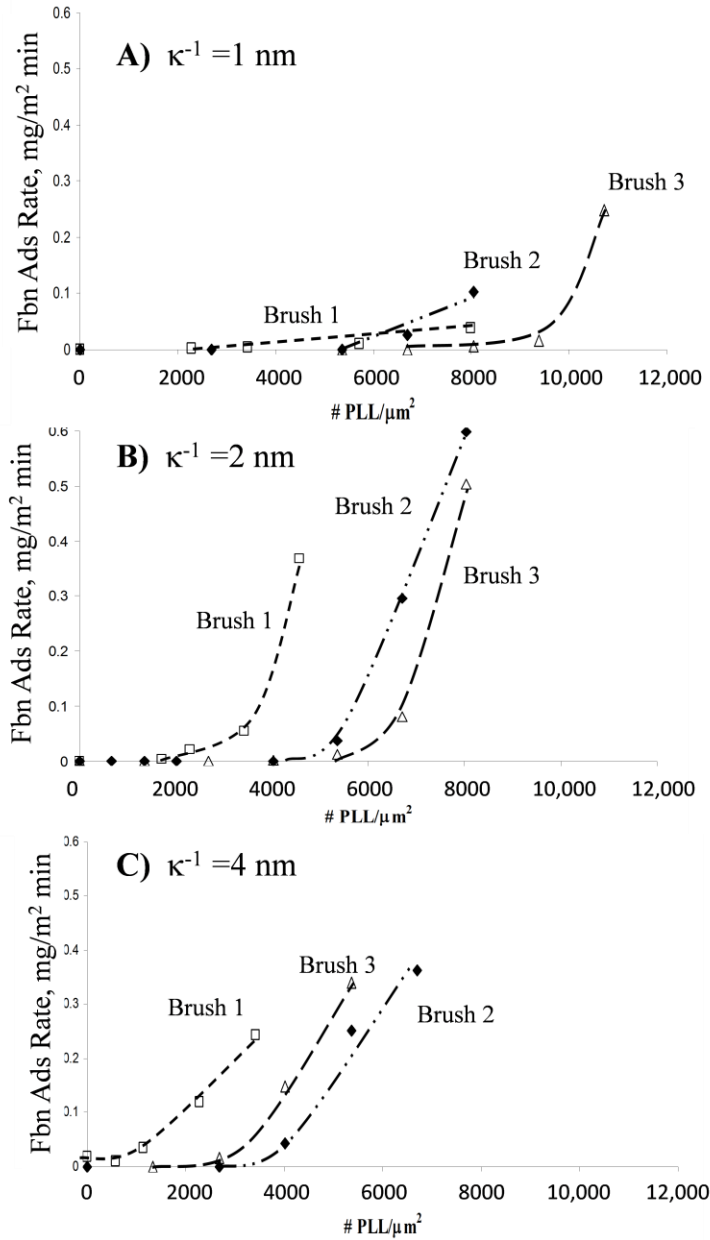


Figure 5.5 Summary of different adsorption rates focusing on different brush architecture for different Debye lengths in the different parts of the figure

Figure 5.6 summarizes the impact of Debye length on the thresholds for the three brushes. The two data sets for each brush (with the curves through the data set drawn only to guide the eye) demonstrate the range of PLL loadings at the threshold, depending

on the particular criterion for the threshold. The upper data sets represent extrapolations of the linear part of the data to the x-axis. The lower data sets represent the PLL coverage when fibrinogen adsorption first becomes noticeable, shown in Figure 5.4C. The difference between the two varies with conditions.

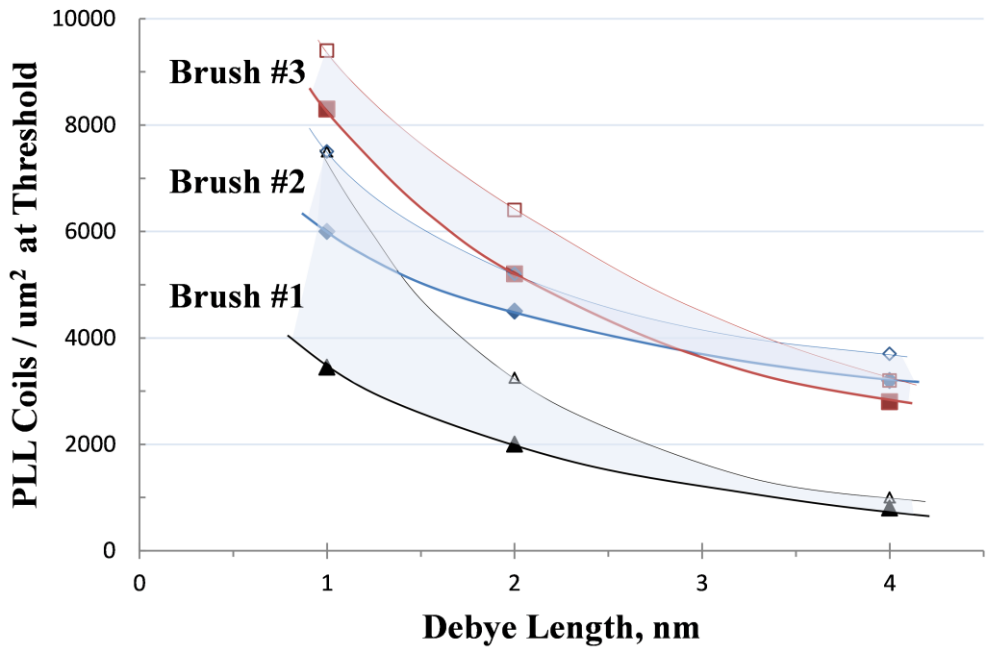


Figure 5.6 Impact of Debye length on the adhesion thresholds for 20 k PLL patches in the three brushes

Important to note, the crossing of the data for Brushes #2 and #3 is modest if one consistently employs a single criterion for the threshold (linear extrapolation or rigorous onset of protein adsorption). Figure 5.3 suggests a decay-type functionality for the impact of Debye length. However, with a practical limited range (1-4 nm) in the Debye length, speculating on the functional form is premature.

## 5.5 Discussion

To attempt a quantitative interpretation of the protein capture mechanism and the impact of steric forces, this study considered systematic variations in brush architecture. Because the brushes are created by adsorption, governed by the competition between entropic stretching of the tethers and the enthalpic binding of the anchors, a non-linear relationship links the adsorbed amount of the brush and the molecular parameters of the graft copolymers. This translates to simultaneous variation in some brush properties. For instance, the brush heights and their persistence lengths are different from their PEG content. Prior studies suggest that either brush height or the amount of PEG in a brush correlates well with protein resistance.<sup>3,4</sup> That this classical perspective would apply to patchy brushes is unclear: All three brushes in this study were chosen because of their protein repellence before the incorporation of adhesive patches.<sup>26,31,32</sup> Adhering proteins are directed onto patchy “flaws.”

Figure 5.5 suggests, at first glance, that the protein adsorption thresholds rank with brush height, rather than PEG content. As discussed in Chapter 2, Brush #1, with its 2K molecular weight tethers is by far the thinnest brush, though it ranks between Brushes #2 and #3 in terms of the amount of PEG it contains. Complicating the correlation is the fact, in Figure 5.2 that, as the amount of patches increases, the amount of PLL-PEG backfill is reduced, reducing the brush thickness. The proper way to consider the impact of brush parameters is to document the condition of the brush at each threshold, rather than the brush height without the addition of patches. Figure 5.7 therefore summarizes the adhesion thresholds (both the high and low limits as presented in Figure 5.6) in terms

of the calculated brush thickness, PEG content, and brush persistence length (average tether spacing), based on the amount of backfill, from Figure 5.2, at each threshold.

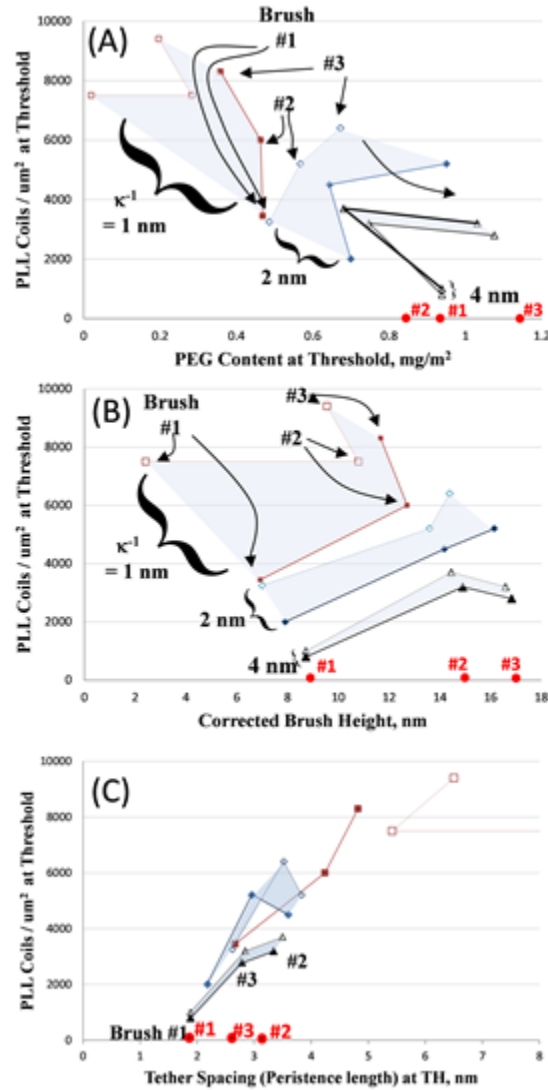


Figure 5.7 Adhesion threshold as a function of (A) the PEG content of the patchy brushes (B) the corrected brush height, (C) as a function of persistence length based on the backfill as shown in figure 5.2

In Figure 5.7A, with the thresholds for each Debye length presented as a function of the PEG content of the brush at each threshold, in Figure 5.7B where thresholds are

presented as a function of brush height at each threshold, and in Figure 5.7C which tests dependence on persistence length, there appear different behaviors at different Debye lengths. At Debye lengths of 2 and 4 nm, the data exhibit the most nearly clear functionality on brush height in Figure 5.7B. For the data set with  $\kappa^{-1} = 1$  nm in any part of Figure 5.7, the data turn back on themselves (if the data are connected in the same sequence as the ordering for the longer Debye lengths). Alternately, if the data are considered in the order of the brush feature (ie rank #1, #3, #2) then the data are non-monotonic in brush height or PEG content, and sometimes reverse their ordering at different Debye lengths.

It was observed that, for  $\kappa^{-1} = 4$  nm, the electrostatic attractions between the patches and the fibrinogen are the strongest. As a result of the thresholds occurring at relatively low PLL loadings, with  $\kappa^{-1} = 4$  nm, the amounts of adsorbed PLL-PEG at these thresholds are similar to the adsorbed amounts in the “full” brushes of Table II, also on the x-axes of Figure 5.7. This suggests that while individual patches attract fibrinogen (at  $\kappa^{-1} = 4$  nm) too weakly to hold fibrinogen onto a single patch, they are still able, from their positions at the base of the brush, to exert weak attractions towards fibrinogen. While one patch cannot capture fibrinogen, several of them can, as evidenced by the existence of a threshold. Thus, at  $\kappa^{-1} = 4$  nm, fibrinogen adsorption near the threshold follows the intended patchy brush concept and can be modeled simply by plain brush parameters and a PLL-loading-independent fibrinogen-patch attraction.

At the other extreme, with  $\kappa^{-1} = 1$  nm, the fibrinogen-patch interactions are weak, and in the limit of low patch loadings (backfilled by the full brushes), the attractions may

be completely screened. Protein adsorption occurs only when there is so much PLL that the brushes are severely compromised compared with their “full properties”. In most cases, there is so little interfacial PEG that tethers are likely configured as non-stretched chains or “mushrooms.” This loss of brushy character suggests data at  $\kappa^{-1} = 1$  nm be omitted from any attempt at a correlation on physical brush features. The data are retained in the graphs because of their potential practical utility in protein separations.

In Figure 5.7 for  $\kappa^{-1} = 2$  or 4 nm that, regardless of whether one considers PEG loading, brush height, or persistence length at the fibrinogen capture threshold, there is not an obvious correlation between the threshold and brush architecture. The trend with brush height is, however, better than those with PEG surface loading or brush persistence length. Brush height screens protein-substrate interactions in the absence of patches, and it also determines the extent to which small adhesive islands can be accessed. The forces driving chain stretching perpendicular to the substrate also determine lateral chain stretching to obstruct patches.

The illustrations in Figure 5.1 schematically interpret how PLL-PEG loading, via brush height, could influence the ability of fibrinogen to access patches. The schematics consider a series of surfaces in which the PLL patch density is increased and the remaining surface is backfilled with one choice of PLL-PEG. At low PLL amounts, the effective binding energy per isolated PLL patch is constant. (Both the brush height and its ability to obstruct patches are unchanged.) As more PLL is added to the interface, however, the amount of PLL-PEG which can subsequently adsorb is reduced, causing the effective binding energy per patch to increase as the patches become more exposed. A



quantitative analysis of the fibrinogen binding energy per patch requires an understanding of the brush structure near the patch, for instance the extent to which chains extend laterally over the patch. This level of detail is beyond the current scope.

## 5.6 Summary

This chapter examined the impact of ionic strength and brush architecture on the ability of a model protein, fibrinogen, to adsorb onto 10-nm cationic patches at the base of a protein-repellant PEG brush. Beyond confirming the general expectation that taller/denser brushes more effectively hide the buried “stickers,” interesting and technologically useful behaviors were revealed:

- 1) In all cases fibrinogen capture was multivalent, involving from 2-5 patches or patch-protein interactions,
- 2) At  $\kappa^{-1} = 4$  nm where the electrostatic patch-protein interactions were strongest, protein adsorption started at conditions where the brush structure was uninfluenced by the presence of patches, leading to a fixed binding energy / patch.
- 3) At  $\kappa^{-1} = 1$  nm where the protein-patch interaction energy was weakest, the protein adsorption thresholds occurred at high PLL surface loadings where the amount of backfill brush was reduced, strengthening the weak binding energy.

4) While ionic strength and brush structure profoundly affected the protein adsorption thresholds, producing a range of thresholds that covered half the possible surface loadings of PLL patches, the impact of these parameters on the numbers of patches actually engaged in protein capture was smaller: 2-5 patches were needed for capture. This was a result of competing effects of ionic strength and steric repulsions due to altered brush structure and the adhesion thresholds.

A clear correlation on brush height, PEG surface loading at the threshold, or brush persistence length was not discovered. For instance, there was no single brush height or PEG surface loading below which the patches were sufficiently accessible to produce adsorption. Likewise, analysis such as that in Figure 5.7 did not motivate collapse of data using the ratio of the brush height to the Debye length. This complexity is likely a result of the multivalent mechanism of protein capture, which depends on the binding energy of single patches along with the probability of finding several of them in close proximity. One might speculate that, in the case of univalent capture of proteins onto single patches, critical brush parameters might be revealed. Notably, the current investigation revealed that brush height is a more important factor than the amount of PEG at the interface in controlling multivalent protein binding onto buried patches. This finding opposes the importance of PEG surface loading for the adsorption of serum proteins onto uniform (non-patchy) brushes.

## 5.7 References

- 1.) Gon, S., & Santore, M. M. (2011). Sensitivity of Protein Adsorption to Architectural Variations in a Protein-Resistant Polymer Brush Containing Engineered Nanoscale Adhesive Sites. *Langmuir*, 27(24), 15083-15091.
- 2.) Ostuni, E., Chapman, R. G., Holmlin, R. E., Takayama, S., & Whitesides, G. M. (2001). A survey of structure-property relationships of surfaces that resist the adsorption of protein. *Langmuir*, 17(18), 5605-5620.
- 3.) Szleifer, I. (1997). Polymers and proteins: Interactions at interfaces. *Current Opinion in Solid State & Materials Science*, 2(3), 337-344.
- 4.) Pasche, S., De Paul, S. M., Voros, J., Spencer, N. D., & Textor, M. (2003). Poly(L-lysine)-graft-poly(ethylene glycol) assembled monolayers on niobium oxide surfaces: A quantitative study of the influence of polymer interfacial architecture on resistance to protein adsorption by ToF-SIMS and in situ OWLS. *Langmuir*, 19(22), 9216-9225.
- 5.) Lin, J. J., Bates, F. S., Hammer, D. A., & Silas, J. A. (2005). Adhesion of polymer vesicles. *Physical Review Letters*, 95(2).
- 6.) Teichroeb, J. H., Forrest, J. A., & Jones, L. W. (2008). Size-dependent denaturing kinetics of bovine serum albumin adsorbed onto gold nanospheres. *European Physical Journal E*, 26(4), 411-415.
- 7.) Teichroeb, J. H., Forrest, J. A., Ngai, V., & Jones, L. W. (2006). Anomalous thermal denaturing of proteins adsorbed to nanoparticles. *European Physical Journal E*, 21(1), 19-24.
- 8.) Dutta, D., Sundaram, S. K., Teegarden, J. G., Riley, B. J., Fifield, L. S., Jacobs, J. M., Addleman, S. R., Kaysen, G. A., Moudgil, B. M., & Weber, T. J. (2007). Adsorbed proteins influence the biological activity and molecular targeting of nanomaterials. *Toxicological Sciences*, 100(1), 303-315.
- 9.) Lau, K. H. A., Bang, J., Kim, D. H., & Knoll, W. (2008). Self-assembly of Protein Nanoarrays on Block Copolymer Templates. *Advanced Functional Materials*, 18(20), 3148-3157.

- 10.) Hodgkinson, G., & Hlady, V. (2005). Relating material surface heterogeneity to protein adsorption: the effect of annealing of micro-contact-printed OTS patterns. *Journal of Adhesion Science and Technology*, 19(3-5), 235-255.
- 11.) Miller, R., Guo, Z., Vogler, E. A., & Siedlecki, C. A. (2006). Plasma coagulation response to surfaces with nanoscale chemical heterogeneity. *Biomaterials*, 27(2), 208-215.
- 12.) Linse, S., Cabaleiro-Lago, C., Xue, W. F., Lynch, I., Lindman, S., Thulin, E., Radford, S. E., & Dawson, K. A. (2007). Nucleation of protein fibrillation by nanoparticles. *Proceedings of the National Academy of Sciences of the United States of America*, 104(21), 8691-8696.
- 13.) Lundqvist, M., Stigler, J., Elia, G., Lynch, I., Cedervall, T., & Dawson, K. A. (2008). Nanoparticle size and surface properties determine the protein corona with possible implications for biological impacts. *Proceedings of the National Academy of Sciences of the United States of America*, 105(38), 14265-14270.
- 14.) Asuri, P., Karajanagi, S. S., Vertegel, A. A., Dordick, J. S., & Kane, R. S. (2007). Enhanced stability of enzymes adsorbed onto nanoparticles. *Journal of Nanoscience and Nanotechnology*, 7(4-5), 1675-1678.
- 15.) Fischer, N. O., McIntosh, C. M., Simard, J. M., & Rotello, V. M. (2002). Inhibition of chymotrypsin through surface binding using nanoparticle-based receptors. *Proceedings of the National Academy of Sciences of the United States of America*, 99(8), 5018-5023.
- 16.) Hong, R., Fischer, N. O., Verma, A., Goodman, C. M., Emrick, T., & Rotello, V. M. (2004). Control of protein structure and function through surface recognition by tailored nanoparticle scaffolds. *Journal of the American Chemical Society*, 126(3), 739-743.
- 17.) Muller, B., Riedel, M., Michel, R., De Paul, S. M., Hofer, R., Heger, D., & Grutmacher, D. (2001). Impact of nanometer-scale roughness on contact-angle hysteresis and globulin adsorption. *Journal of Vacuum Science & Technology B*, 19(5), 1715-1720.

- 18.) Wolfram, T., Belz, F., Schoen, T., & Spatz, J. P. (2007). Site-specific presentation of single recombinant proteins in defined nanoarrays. *Biointerphases*, 2(1), 44-48.
- 19.) Slater, J. H., & Frey, W. (2008). Nanopatterning of fibronectin and the influence of integrin clustering on endothelial cell spreading and proliferation. *Journal of Biomedical Materials Research Part A*, 87A(1), 176-195.
- 20.) Santore, M. M., & Wertz, C. F. (2005). Protein spreading kinetics at liquid-solid interfaces via an adsorption probe method. *Langmuir*, 21(22), 10172-10178.
- 21.) Zhang, J., Srivastava, S., Duffadar, R., Davis, J. M., Rotello, V. M., & Santore, M. M. (2008). Manipulating microparticles with single surface-immobilized nanoparticles. *Langmuir*, 24(13), 6404-6408.
- 22.) Santore, M. M., Zhang, J., Srivastava, S., & Rotello, V. M. (2009). Beyond Molecular Recognition: Using a Repulsive Field to Tune Interfacial Valency and Binding Specificity between Adhesive Surfaces. *Langmuir*, 25(1), 84-96.
- 23.) Fang, B., Gon, S., Park, M., Kumar, K. N., Rotello, V. M., Nusslein, K., & Santore, M. M. (2011). Bacterial adhesion on hybrid cationic nanoparticle-polymer brush surfaces: Ionic strength tunes capture from monovalent to multivalent binding. *Colloids and Surfaces B: Biointerfaces*, 87, 109-115.
- 24.) Gon, S., & Santore, M. M. (2011). Single Component and Selective Competitive Protein Adsorption in a Patchy Polymer Brush: Opposition between Steric Repulsions and Electrostatic Attractions. *Langmuir*, 27(4), 1487-1493.
- 25.) Gon, S., Bendersky, M., Ross, J. L., & Santore, M. M. (2010). Manipulating Protein Adsorption using a Patchy Protein-Resistant Brush. *Langmuir*, 26(14), 12147-12154.
- 26.) Gon, S., Fang, B., & Santore, M. M. (2011). Interaction of Cationic Proteins and Polypeptides with Biocompatible Cationically-Anchored PEG Brushes. *Macromolecules*, 44(20), 8161-8168.

- 27.) de Gennes, P. G. (1976). *J. Phys. (Paris)*, 38, 1443.
- 28.) Alexander, S. (1977). ADSORPTION OF CHAIN MOLECULES WITH A POLAR HEAD A-SCALING DESCRIPTION. *Journal De Physique*, 38(8), 983-987.
- 29.) Milner, S. T. (1991). POLYMER BRUSHES. *Science*, 251(4996), 905-914.
- 30.) Kent, M. S. (2000). A quantitative study of tethered chains in various solution conditions using Langmuir diblock copolymer monolayers. *Macromolecular Rapid Communications*, 21(6), 243-270.
- 31.) Huang, N. P., Michel, R., Voros, J., Textor, M., Hofer, R., Rossi, A., Elbert, D. L., Hubbell, J. A., & Spencer, N. D. (2001). Poly(L-lysine)-g-poly(ethylene glycol) layers on metal oxide surfaces: Surface-analytical characterization and resistance to serum and fibrinogen adsorption. *Langmuir*, 17(2), 489-498.
- 32.) Kenausis, G. L., Voros, J., Elbert, D. L., Huang, N. P., Hofer, R., Ruiz-Taylor, L., Textor, M., Hubbell, J. A., & Spencer, N. D. (2000). Poly(L-lysine)-g-poly(ethylene glycol) layers on metal oxide surfaces: Attachment mechanism and effects of polymer architecture on resistance to protein adsorption. *Journal of Physical Chemistry B*, 104(14), 3298-3309.
- 33.) Toscano, A., & Santore, M. M. (2006). Fibrinogen adsorption on three silica-based surfaces: Conformation and kinetics. *Langmuir*, 22(6), 2588-2597.
- 34.) Fu, Z. G., & Santore, M. M. (1998). Poly(ethylene oxide) adsorption onto chemically etched silicates by Brewster angle reflectivity. [Article]. *Colloids and Surfaces a-Physicochemical and Engineering Aspects*, 135(1-3), 63-75.
- 35.) Duffadar, R., Kalasin, S., Davis, J. M., & Santore, M. M. (2009). The impact of nanoscale chemical features on micron-scale adhesion: Crossover from heterogeneity-dominated to mean-field behavior. *Journal of Colloid and Interface Science*, 337(2), 396-407.

- 36.) Santore, M. M., & Kozlova, N. (2007). Micrometer scale adhesion on nanometer-scale patchy surfaces: Adhesion rates, adhesion thresholds, and curvature-based selectivity. *Langmuir*, 23(9), 4782-4791.

## CHAPTER 6

# BACTERIAL ADHESION OVER PATCHY BRUSHES: A CASE STUDY WITH *S. AUREUS*

### 6.1 Introduction

Bacterial adhesion and the design of surfaces to control cell-scale bioadhesion is a large area covering a range of disciplines including marine science, plant and soil science, the food industry, and the biomedical field. In the previous chapters, protein adhesion to nano-patterned PEG brushes has been described. The current chapter focuses on the adhesion of *S. aureus* bacteria on three different types of patchy PEG brushes (Brush # 1, Brush # 2 and Brush # 3). Those brushes are described in detail in Chapter 2. Much of this chapter has been reproduced from a recently published article.<sup>1</sup> Solvated polymer brushes, for instance tethered polyethylene glycol (PEG), are commonly placed on surfaces to inhibit bio-fouling by proteins and cells.<sup>2,3</sup> Key to the bioadhesion-resistance of these interfaces (beyond choosing a polymer chemistry that is fundamentally protein-repellant: neutral, hydrophilic, well-hydrated, and hydrogen bond accepting<sup>4</sup>) is the physical design of the brush. Its height must exceed the range of electrostatic<sup>5</sup> and van der Waals attractions<sup>6,7</sup> and its density must be sufficient to avoid penetration by small proteins.<sup>7,8</sup> Classic in the literature, surface forces experiments on solvated brushes generally confirm the expected force-distance profiles that tend to be strongly repulsive and long in range,<sup>9-16</sup> while atomic force microscopy indicates less



repulsion due to tip penetration into the brush.<sup>10</sup> A recent study of PEG brushes with colloidal force microscopy demonstrated the relative ranges of steric and electrostatic interactions.<sup>17</sup> The latter have proven useful in anticipating which brush architectures will resist fouling.<sup>5</sup> With the advent of well-characterized brushes, protein adsorption studies focused on the fundamental brush parameters of tether length and spacing, corroborating physical models of brush-protein interactions.<sup>6-8,13,14,18-23</sup> At the same time, however, careful studies with well-characterized brushes supported a rule of thumb that about  $1\text{mg}/\text{m}^2$  of end-grafted PEG is sufficient to eliminate bioadhesion *in-vitro*.<sup>19-21,24</sup> This observation was independent of tether length and spacing over a relatively broad range. It has been vexing, however, that protein-resistant PEG brushes (based on *in-vitro* characterization) still support non-specific bio-adhesion in applied and animal studies.<sup>3,25</sup>

Perfectly designed brushes can be difficult to implement. Even with the proper tether chemistry for the application, appropriate anchoring, and judicious choice of chain length and tether spacing, impurities can locally block brush deposition (or growth), creating flaws and heterogeneities as small as tens of nanometers.<sup>10</sup> While such tiny isolated bare patches on the substrate tend to be obstructed by the lateral expansion of the tethers, they are still locally less repulsive (and even attractive) to objects in solution compared with the “perfect” brush. Our lab has developed a controlled method to distribute such isolated flaws randomly on a brushy surface, and we have demonstrated that these “synthetic flaws” are useful in understanding the engineering challenges of brush fabrication.<sup>26</sup> We have additionally demonstrated the utility of flaws, as a motif for the design of functional brushes.<sup>27</sup> Embedding discrete functionality at the base of a brush rather than placing it on extended tethers sets up competition between local attractions

and the steric forces of the brush which leads to highly selective capture on the molecular level, for instance for proteins from solution.<sup>27</sup>

The flawed or “patchy” brushes, are based on a convenient PEG anchoring scheme originally developed in the Hubbell and Textor labs.<sup>28,29</sup> With poly-l-lysine (PLL)-PEG graft copolymers adsorbing on silica primarily by their main cationic backbones, the PEG tethers extend into solution to form the brush. It has been demonstrated that by random adhesion of PLL patches prior to PLL-PEG adsorption, the patches (PLL is more strongly adsorbing than the PLL-PEG) are retained during PLL-PEG backfill and that both the PLL and PLL-PEG are retained on the surface over and beyond the conditions (protein bacterial exposure and ionic strength variations).<sup>30</sup> In the current study, isolated PLL coils at the base of the brush not only provide nano-scale tether-free imperfections, they localize dense cationic functionality that is electrostatically attractive to negative proteins and bacteria, including *S. aureus*. These PLL coils carry greater positive charge than the PLL backbone of the PLL-PEG copolymer, since PEG grafting (on the PLL backbone of the copolymer) occurs at the sites of amines.

It is important to note that the brushes used for this study (as described in Chapter 2), before the incorporation of PLL patches, completely resist protein and *S. aureus* adhesion (to within  $0.01 \text{ mg/m}^2$ )<sup>30</sup> and were among the most protein- and bacteria-repellant architectures in the large library of “bottle brush” copolymers developed by Textor and Hubbell.<sup>28,29</sup> While it was observed and later explained with self consistent field models,<sup>31</sup> that some molecular architectures (especially those with large PEG functionalization of the PLL backbone) produced adsorbed layers which failed to form

classical brushes or to repel proteins, our study starts with brushes that avoid primary,<sup>7</sup> secondary,<sup>7</sup> and tertiary<sup>32</sup> protein adhesion and introduces well- characterized electrostatically adhesive “flaws” in a controlled fashion. Further, our choices of molecular architectures range from 25-50% in PEG functionalization, and have been shown to behave similarly, in their protein resistance, to single PEG chains anchored individually at appropriate densities,<sup>21</sup> as is the case for a classical polymer brush. We have not detected any suggestion that the specific PLL-PEG graft copolymer architectures we have chosen produce lateral heterogeneities in the brush and that instead, the interesting features of the brush adhesiveness in our studies arise from the homopolymer PLL patches we intentionally place on the substrate. This further substantiates the use of classical brush models for this study.

The impact of the polymer brush architecture on protein adsorption,<sup>26,27,30,33</sup> has been described in previous chapters. Current chapter focuses on *Staphylococcus aureus* capture at the same interfaces and reveals information about the brush compression during initial bacterial capture that compliments the classical literature on PEG brush compression.<sup>9,12,13,33</sup> Our emphasis on initial capture focuses on physico-chemical interactions and avoids longer-time processes such as viscoelastic relaxation of the bacteria’s shape or “living” responses of the bacteria. (The choice of *S. aureus* bacteria allows focus on the simplest spherical shape. The study does not address complexities associated with bacterial protrusions.)

Important distinctions in how steric forces potentially play out for micron-scale and molecular-scale objects have been further highlighted in this chapter. In this study, the flaws or PLL “patches” are used as a measure of the brush compression energy during

bacterial capture: The brushes themselves (without flaws) are robust against bacteria (and protein capture). The adhesive patches at the base of the brush, when present in sufficient numbers, pull *S. Aureus* bacteria (negatively charged 1  $\mu\text{m}$  spheres in the initial instants of their capture) to the interface, and are opposed by the steric repulsions from the brush on the remaining contact area. Thus the number of patches needed for bacterial capture provides a measure of the relative energy of brush compression, reported in this paper for three brushes which vary in height and PEG content.

Additionally in this chapter, the *S. aureus* adhesion is compared with previous studies of protein capture on the same surfaces,<sup>27,33</sup> to reveal potential differences between-micron-scale and molecular-scale steric interactions on these brushes. The latter provide insights into the failure of *in vitro* studies with serum proteins to predict the fouling of materials in implant studies.

## 6.2 Materials and methods

Poly-L-lysine hydrobromide (PLL) samples with molecular weights of 20,000 and 50,000 were purchased from Sigma and used as the adhesive cationic patches in these studies. Additionally, the 20,000 molecular weight PLL served as the anchoring component of the three copolymer brushes in this study.

Three graft copolymers, synthesized and purified as described in Chapter 2, were used to create the brushes in this study. They were all based on 20,000 molecular weight PLL but vary the length and density of their PEG side chains. These particular copolymers were chosen because the brushes they form upon adsorption to negative

surfaces almost completely eliminate adhesion of serum proteins<sup>28,29</sup> and bacteria.<sup>35</sup> The brush architecture was modified by varying the PEG tether length and the grafting ratio. The “grafting ratio” is defined as the number of PLL units per PEG side chain. This quantity is the inverse of the fraction of PLL units functionalized, but is reported here for consistency with prior convention.<sup>28,29</sup> The grafting ratio of the copolymers dissolved in D<sub>2</sub>O was determined using <sup>1</sup>H NMR on a Bruker 400 MHz instrument, based on the relative areas of the lysine side-chain peak (-CH<sub>2</sub>-N-) at 2.909 ppm and the PEG peak (-CH<sub>2</sub>-CH<sub>2</sub>-) at 3.615 ppm.

The surfaces of interest were formed by sequential adsorption of PLL and PLL-PEG from flowing pH 7.4 phosphate buffered solutions (phosphate buffer is 0.008M Na<sub>2</sub>HPO<sub>4</sub> and 0.002M KH<sub>2</sub>PO<sub>4</sub> having Debye length  $\kappa^{-1} = 2$  nm) on acid etched microscope slides, also described previously.<sup>26,33</sup> These substrates, Fisher Finest, were soaked overnight in concentrated sulfuric acid and rinsed with DI water to remove the metal ions from the near-surface region, leaving a nearly pure silica surface. The slides were then placed in a slit shear flow chamber and buffer was introduced into the fluid space. Flowing buffer, at a gentle wall shear rate of 5 s<sup>-1</sup>, was followed by 5 ppm PLL solution for a targeted amount of time to limit the adsorption of PLL chains below that of a saturated PLL layer. Buffer was then reintroduced, followed by a 100 ppm solution of the PLL-PEG of interest to backfill the remaining silica surface with a PEG brush. The amount of time necessary to deposit the desired amount of PLL was originally determined by monitoring the adsorption process using near-Brewster reflectometry.<sup>26</sup> In most of the current studies, especially those of bacterial capture, the surface fabrication was run “blind” based on previous calibrations for adsorption times. Studies of

fibrinogen adsorption (Sigma, F8630-1G, used as supplied) employed near-Brewster reflectometry,<sup>36</sup> and here it was possible to monitor the polymer deposition to create each surface just before the protein adsorption studies in the same flow chamber. In the fibrinogen adsorption studies, 100 ppm protein solution in pH 7.4 phosphate buffer was flowed over the surface of interest for 20-30 minutes and the reflectivity signal monitored. Buffer was subsequently reintroduced.

Table 6.1 summarizes the properties of the three brushes without adhesive patches. These parameters which describe the brush structures, were calculated from measurements of the adsorbed PLL-PEG mass and knowledge of the PEG content in each copolymer, as described in Chapter 2. Parameters, such as the average spacing between grafting sites, follow without any assumptions for a particular model of the brush. Other properties, such as the number of “blobs” in the brush, its height, and its energy are model-specific. Here, the “Flory” brush from Alexander and DeGennes and the semidilute brush model of DeGennes are compared and found to be in good agreement.<sup>37,38</sup> The height calculations based on the Alexander-DeGennes treatment carry second and third virial coefficients measured by osmometry (Advanced Instruments) for PEO solutions (8000 molecular weight, Polysciences) up to 17 wt%. These values were found to adequately predict measured depletion forces in a separate work.<sup>39</sup> Notable in Table 6.1 is that Brushes 1 and 2 are similar in PEG content while Brushes 2 and 3 are similar in height, allowing the importance of these parameters to be tested.

Table 6.1. Brush Architectures

	<b>Brush #1</b>	<b>Brush #2</b>	<b>Brush #3</b>
	PLL-(2.7) PEG(2K)	PLL-(2.2) PEG(5K)	PLL-(4.7) PEG(5K)
Saturated adsorption, mg/m <sup>2</sup>	1.1	0.9	1.3
<b>Adsorbed PEG, mg/m<sup>2</sup></b>	<b>0.94</b>	<b>0.85</b>	<b>1.16</b>
Area /Copolymer, nm <sup>2</sup>	206	680	247
Area /PEG tether, nm <sup>2</sup>	3.6	9.6	7.2
<b>Tether Spacing, <math>\sigma^{-1/2}</math>, nm<sup>*1</sup></b>	<b>1.9</b>	<b>3.1</b>	<b>2.7</b>
Number of Blobs	4.7	5.1	6.4
<b>Brush Height, h<sub>0</sub>, nm<sup>*2</sup></b>	<b>7.5 -9</b>	<b>14.5 - 15.5</b>	<b>16.5 - 17.2</b>

\*1. Tether spacing is equivalent to the blob diameter, also called the brush persistence length;  $\sigma$  = areal density of tethers

\*2. Brush heights show the range calculated for the Alexander-DeGennes treatment of the Flory brush and the semidilute brush of blobs. Calculations for both are detailed in the Supporting Information.

*S. aureus* (ATCC 25923) was chosen for this study because of its spherical shape and negative charge. The particular strain was originally a clinical isolate, and has become widely used in standardized tests of bacterial antibiotic susceptibility. This particular strain was additionally chosen for its nonpathogenic behavior, while still closely resembling strains found in hospital infections. Bacteria were grown according to standard procedure in Luria-Bertani (LB) medium. Cultures were incubated aerobically overnight at 37 °C, shaking at 200 rpm. Bacteria were harvested after a total of 24h during logarithmic growth. Bacteria were subsequently centrifuged at 100 x g and re-suspended in phosphate buffer twice. This rinsing procedure was shown to remove protein and other molecules which might potentially contaminate the surfaces. All bacteria were studied within 24h of preparation and stored in a refrigerator near 4°C. The nominal target bacterial concentration was 5 x 10<sup>5</sup>/ ml during the runs.

In studies of bacterial adhesion, bacteria suspensions were flowed over test surfaces in a custom-built “lateral” microscope. This instrument orients test surfaces perpendicular to the floor so that no gravitational forces contribute to or detract from bacteria-surface interactions. Bacteria capture was monitored on video and, using ImageJ software, the numbers of bacteria in each frame were determined, enabling the bacterial capture kinetics to be plotted. Bacterial accumulation was typically linear in time for at least 10 minutes, allowing the initial bacterial capture rates to be determined. These initial capture rates, which do not reflect bacteria-bacteria interactions at the surface, provide information about the interactions of individual bacteria with the substrates. Procedures follow those of prior studies in our lab for other surfaces.<sup>40-42</sup>

This chapter reports bacterial capture efficiencies. The capture efficiency is the initial bacterial capture rate on a test surface, normalized by the transport-limited (maximum possible) capture rate for the same suspension. The latter is measured on a surface that is strongly and rapidly adhesive towards bacteria. This analysis method is necessary because different batches of bacteria measured on different days contain slightly different bacterial concentrations, which are difficult to quantify with the necessary precision.<sup>40</sup> Measuring the transport-limited bacterial capture rates for each batch of bacteria suspension and presenting data in the form of bacterial capture efficiencies facilitate quantitative comparisons of different bacterial batches on different test surfaces. A saturated adsorbed PLL layer, which is densely positively charged, was employed as the strongly attractive surface. Transport limited bacterial capture on this type of surface, for the range of adsorption conditions studied here has been previously established.<sup>26</sup>



### 6.3 Results

For two different patch molecular weights, 20,000 and 50,000 in Brush 2, Figure 6.1A summarizes the adhesion or capture efficiencies of *S. aureus* from flowing phosphate buffer. Because brushes completely resist bacterial adhesion, in Figure 6.1A patches must be present within the brushes to produce bacterial capture. The onset of bacterial capture occurs at patch surface loadings or “thresholds” rather than the data passing through the origin.

Adhesion thresholds are indicators of multivalent bacterial capture,<sup>43</sup> that is, the involvement of several patches in the capture of each bacterial cell. This interpretation becomes clear when one considers that the surfaces containing fewer than the threshold density of adhesive patches are incapable of adhering bacteria. Thus, while single patches may attract bacteria, individual attractions are too weak to capture and hold single bacterial cells, even in gentle flow.

The shifting of the thresholds to smaller patch loadings (to the left) for larger 50K patches in Figure 6.1A is consistent with the expectation that higher molecular weight patches will have stronger attractions towards bacteria. With fewer large patches needed for bacterial capture (compared with a greater number of small patches) the threshold for large patches lies to the left of that for the small patches. In the limit of very strong patch-bacteria interactions, bacteria can be captured and held by surface species, and data extrapolate to the origin rather than a finite x-intercept.<sup>40</sup>

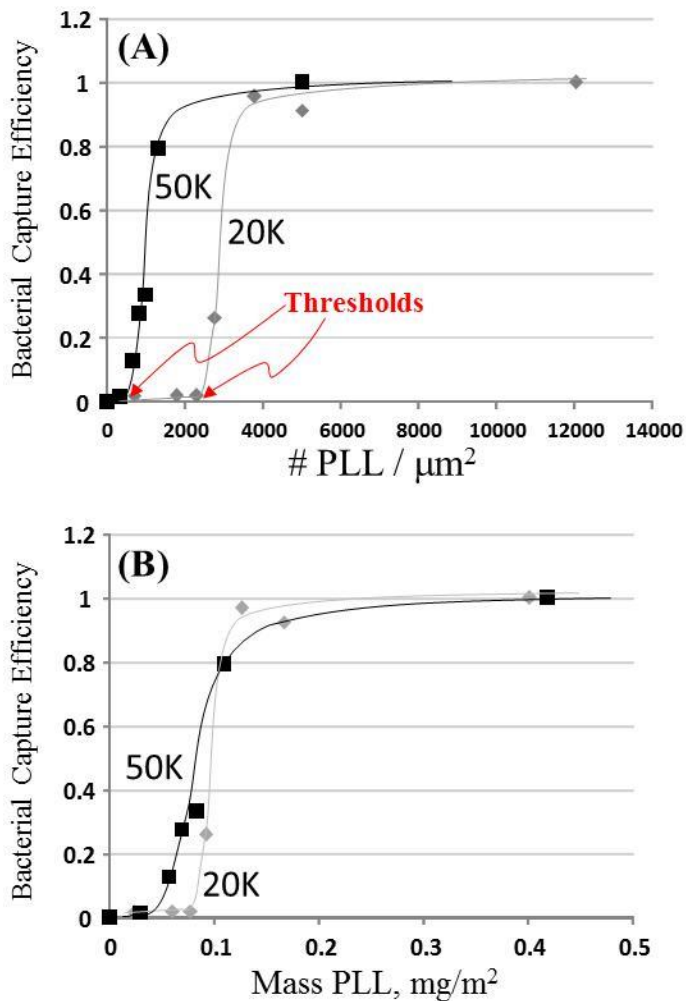


Figure 6.1 The effect of the molecular weight of the PLL patches in Brush #2 on the bacterial capture efficiency, for 20,000 (gray diamonds) and 50,000 (black squares) PLL, plotted as a function of (A) patch number and (B) patch mass.

Figure 6.2 explores the impact of the brush architecture on bacterial capture for PLL patches of 20,000 molecular weight. Part B of Figure 6.2, previously published,<sup>33</sup> facilitates a direct comparison to fibrinogen adsorption for the same series of surfaces, in the discussion below. In Figure 6.2, the threshold concentrations of adhesive patches for bacterial capture increases with brush height, since the range of steric repulsions increases accordingly.

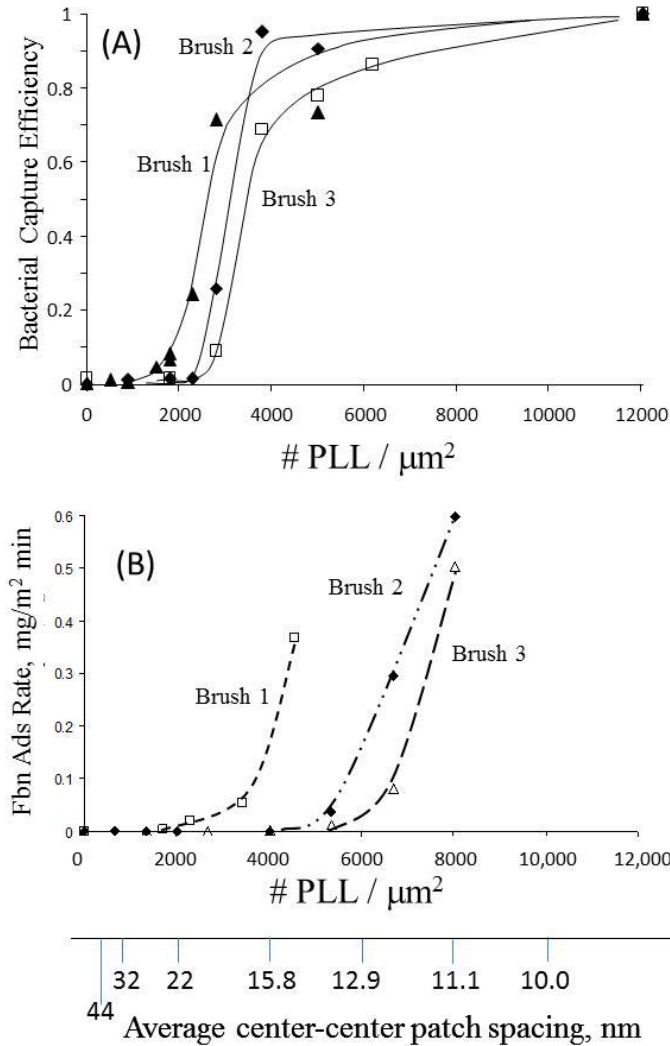


Figure 6.2 A) Bacterial capture efficiencies on three different brushes containing embedded 20,000 molecular weight poly-l-lysine patches. Adsorption is from flow at  $\gamma = 5 \text{ s}^{-1}$  and an ionic strength of 0.026 M corresponding to  $\kappa^{-1} = 2 \text{ nm}$ . B) Fibrinogen adsorption on the same surfaces for  $\kappa^{-1} = 2 \text{ nm}$ , from reference 33.

A comparison of parts A and B of Figure 6.2 reveals several interesting observations. First, thresholds for fibrinogen capture occur at much higher patch concentrations than the thresholds for bacteria. The observation of fibrinogen thresholds suggests weak patch-protein interactions: Fibrinogen adheres by bridging two or more adhesive surface sites.<sup>33</sup> This interpretation is consistent with the average patch spacing at

the fibrinogen thresholds (12-22 nm), which is less than fibrinogen's 45 nm length. Since proteins are relatively small, then, the surface loading of these randomly-arranged patches must be relatively large to ensure statistically significant numbers of protein-sized surface regions in which multiple adhesive sites are closely situated. Since the bacterial cells are larger than proteins, multivalent bacterial capture can potentially occur at lower patch loadings, consistent with the scale of the second x-axis (average patch spacing) in Figure 6.2. The actual bacterial thresholds will depend on the particular numbers of patches needed for capture and the bacterial-surface contact area, discussed below.

A second important observation in Figure 6.2 is that the sensitivity of the threshold position to the brush architecture is greater for the proteins than it is for *S. aureus*. That is, we observe a greater shifting in the protein thresholds in part B for Brushes 1-3 compared with the spread of the data in Figure 6.2 A. This observation has the technologically-useful benefit that brushes could be chosen to tune the relative adhesion of proteins and cells on these surfaces.

## 6.4 Discussion

While it has long been known that the brushy biocompatible surfaces which avoid protein adhesion are also useful in repelling cells such as bacteria,<sup>3</sup> the remarkable size range (3 orders of magnitude from molecular to cellular-scale) of the objects that can be manipulated by steric forces has historically been taken for granted. Figures 2 and 3 reveal important similarities and differences in how brushy steric repulsions come into

play for bacteria versus proteins experiencing localized attractions. If one views the adhesive “patches” as synthetic receptors or, at least, technologically-useful constructs for manipulation of biological entities, it is remarkable that the same brushy interfaces with the same adhesive “elements” produce parallel behaviors at the molecular and cellular level. On the other hand, if one views the cationic patches as (quantifiable models for) flaws in an otherwise bio-resistant brush, we have the striking observation that such small flaws (individually too adhesively weak to immobilize much of anything), are far more catastrophic in that they more readily facilitate unwanted cell adhesion compared to protein adhesion. (Of the several proteins we have studied on these brushes,<sup>27,30</sup> fibrinogen is the largest [4.5 nm x 4.5 nm x 47 nm] and correspondingly most adhesive, with other proteins such as albumin adhering only at even higher patch loadings.<sup>27</sup>) For most surfaces, even engineered surfaces, protein adsorption is typically thought to be a precursor for cellular adhesion.<sup>2,3</sup> On the “flawed” brushes in this study, cells adhere directly without prerequisite protein adsorption. We are aware of one other study documenting a similar trend on PEG-coated steel.<sup>25</sup>

#### **6.4.1 Role of adhesive flaws on bacterial and protein adhesion**

A basic quantity at the core of understanding *S. aureus* versus protein capture is the numbers of adhesive patches (the “valency”) required for their capture. Even without understanding the physics of the brushes or the patch-bacteria interaction, it is possible to estimate the valency. A statistical treatment that was published previously<sup>43</sup> was used to understand the patch distribution. The model assumes only (1) a random arrangement of adhesive sites on the surface, described by a Poisson distribution (a material feature

which has been previously established<sup>26</sup>) and (2) a known area between the surface and the target over which the attractive forces act. *S. aureus* is approximated as a simple sphere, a simplification which provides an estimate of the contact area, but which might more seriously break down for other bacterial strains with protrusions such as pili that might penetrate the brush rather than compress it. The treatment predicts the normalized capture probability as a function of the overall loading of patches. The latter is the quantity on the x-axis of Figures 6.1 and 6.2. The capture probability is roughly proportional to the capture rate or efficiency on the y-axis of these figures.<sup>43</sup> A prior work, which accessed a regime of monovalent bacterial capture on more strongly adhesive elements, presented a scheme to translate capture probability to efficiency.<sup>41</sup> This conversion translates to other systems with weaker adhesive elements such as the current study. In presenting the predictions of the statistical model, we include both scales on the y-axes.

Figure 6.3A provides perspective on the area over which *S. aureus*-surface attractions act. When a bacterium, approximated as a sphere of radius  $R_p = 500$  nm, first touches the surface, the area over which attractive (electrostatic) forces act is defined by the overlap of the electrostatic double layers of the sphere and the collector. The radius of this electrostatic force zone follows from geometry,  $(r_f^{es})^2 + (R_p - \kappa^{-1})^2 = (R_p + \kappa^{-1})^2$  or  $r_f^{es} = 2(R_p \kappa^{-1})^{1/2}$ . Here the Debye length,  $\kappa^{-1}$ , is 2 nm. For a 1-micron spherical bacterium  $r_f^{es} = 63.25$  nm, and the electrostatic area,  $(r_f^{es})^2$ , is 4000 nm<sup>2</sup>.

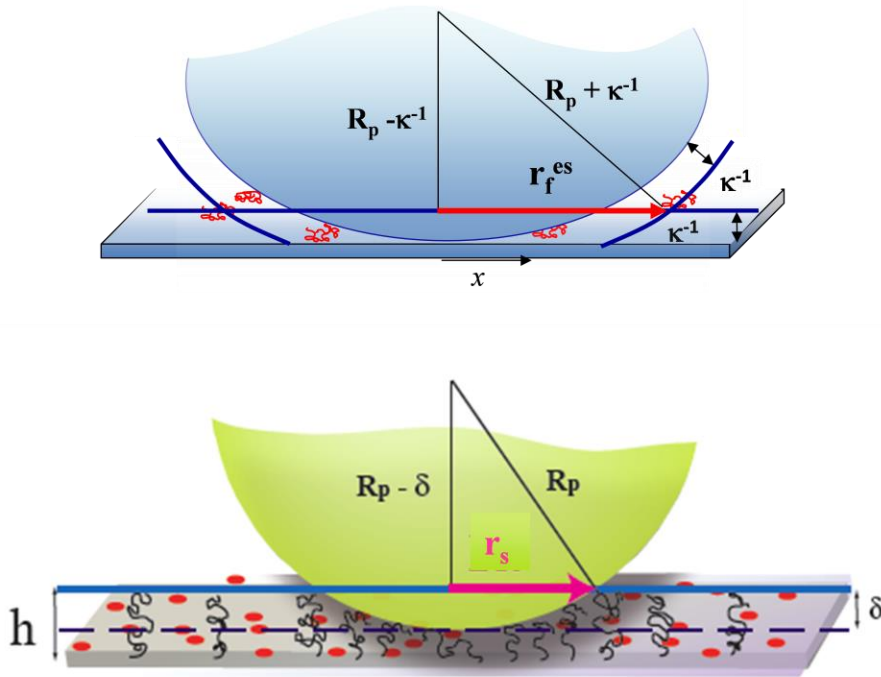


Figure 6.3 Schematic of a bacteria contact with a patchy brush surface (A) defining the electrostatic interaction radius  $r_f^{es}$  (B) defining the steric brushy interaction radius  $r_p$  for brush height  $h$  and brush compression  $\delta$ .

#### 6.4.2 Impact of Steric Repulsion from brush architecture on bacteria

The multiple attractions from the adhesive patches offset the different amounts of steric repulsion between the different brushes and a bacterium (or protein). In understanding this repulsion, two aspects must be considered: (1) the area over which the repulsion acts and (2) the physics of the repulsion: compression or penetration.

During bacterial capture, different steric interaction areas (of radius  $r_s$ ) for the different brushes result from the brush-dependence of the range of steric forces. In a first approximation illustrated in Figure 6.3B, a spherical bacterium of radius  $R_p = 500$  nm compresses the brush, of initial height  $h$  to final separation  $h'$ , so that the bacterial surface comes within about a Debye length ( $h' = \kappa^{-1} = 2$  nm) of the charged patches. The brush

deformation,  $\delta$ , follows as  $h - 2$  nm. Then from geometrical arguments motivated by Figure 4B,  $r_s^2 + (R_p - \delta)^2 = R_p^2$ , so that  $r_s = (\delta^2 + 2\delta R_p)^{1/2}$ . For instance for Brush 1 with  $\delta = 7$  nm, one obtains an approximate interaction radius,  $r_s \sim 84$  nm, and a total steric interaction area of about  $7000 \text{ nm}^2$ . Larger steric areas result for Brushes 2 and 3, still with  $h' = 2$  nm, summarized in Table 6.2 as published recently<sup>1</sup>. To a first approximation, the total steric repulsion should scale as the steric contact area. Proportionate numbers of adhesive elements, as calculated in the previous section, are expected to be needed within the electrostatic contact area to produce bacterial capture. Notably, the definitions of steric and electrostatic areas differ fundamentally. The steric area varies with differences in the brush, but the electrostatic interaction area depends on Debye length.

We estimate, as a first approximation, that bacteria-brush interactions resemble brush compression by an impenetrable wall, neglecting complexities of the bacterial surface which are insufficiently known to develop a more sophisticated picture. We proceed with this approach, as the use of brush compression models for cell interactions has shown recent success for the adhesion and release of mammalian cells which may be softer than bacteria.<sup>49</sup> The work brush of compression depends on the brush architecture, primarily through the parameters  $N$  and  $\sigma$ , the statistical number of segments per tether and areal density of tethers, respectively as summarized in Table 6.1.



Table 6.2. Brush Features Relevant to Steric Repulsion of Bacteria and Protein

	<b>Brush 1</b>	<b>Brush 2</b>	<b>Brush 3</b>
<b>Calculated Bacterial Capture Valency for 20K PLL patch</b>	13	18	20
<b>Bacterial interaction radius, <sup>note-1</sup> r<sub>s</sub>, nm</b>	84	117	124
<b>Bacterial interaction area, <sup>note-1</sup> nm<sup>2</sup></b>	7,000	13,700	15,400
<b>Fibrinogen interaction area, nm</b>	150-200	150-200	150-200
<b>PEG Content at Bacterial Threshold (20K patch), mg/m<sup>2</sup></b>	0.81	0.80	1.11
<b>Brush Height at Bacterial Threshold, nm (20K patch)</b>	7	13	16
<b>Brush Compression Energy, 2<sup>nd</sup> virial Relative to that of Brush 1<sup>note-2</sup></b>	---	0.98	1.88
<b>Brush Compression Energy, full osmotic expression, relative to Brush 1</b>	---	0.9	2.9
<b>PEG Content at Fibrinogen Threshold,<sup>32</sup> mg/m<sup>2</sup> (20K patch)</b>	0.57 ±0.12	0.6 ±0.04	0.80 ±0.13
<b>Brush Height at Fibrinogen Threshold, nm (20K patch)</b>	6	12	14
<b>Average Tether Spacing at Fibrinogen Threshold, nm (20K patch), σ<sup>-1/2</sup></b>	2.4±0.2	3.7±0.1	3.2±0.3
<b>Steric (Penetration) Repulsion, kT per Fibrinogen</b>	180	50	65
<b>Steric Compression Penalty, kT per Fibrinogen</b>	68	20	25

<sup>1</sup>. Assumes an ultimate gap separation of 2 nm for all brushes      <sup>2</sup>. Assumes similar brush compressions

Worth noting is that  $h$  and  $\sigma$ , along with the total tethered PEG, are preserved at the bacterial adhesion thresholds. That is, for a series of surfaces with increasing numbers of cationic patches at the base of a brush, the amount of brush needed to backfill the remaining surface decreases once the patch loading reaches a critical level, on the order of  $800 \text{ mg/m}^2$  for Brush 1,  $1200 \text{ mg/m}^2$  for Brush 2, and  $2200 \text{ mg/m}^2$  for Brush 3.<sup>32</sup> This decrease in backfill tends to compromise the brush, especially near the high protein adsorption thresholds in Figure 3B. However, the threshold patch densities for bacterial capture in Figures 6.1 and 6.2A occur at relatively low patch loadings and therefore correspond to negligible decreases in the PLL-PEG backfill relative to a brush containing no patches. The properties of the various brushes at the adhesion thresholds for bacteria and fibrinogen are summarized in Table 6.2, and for the bacterial adhesion are similar to the properties in Table 6.1.

With the properties of the brush determined at conditions where bacteria start to adhere, in Table 6.2, it becomes possible to estimate the steric cost of compression. Two approaches were considered for this calculation, both based on the Alexander DeGennes treatment of a Flory brush.<sup>37,38</sup> The Alexander-deGennes treatment, which neglects the real concentration profile in the brush in favor of a constant segmental concentration, is unrealistic. However, for uncompressed brushes, both osmotic and stretching energies are over estimated and errors cancel, so that estimates of brush height are often reasonable.<sup>18</sup> Additionally, for the large compressions in our work (starting with brushes on the order of 10 nm and compressing down to a thickness on the order of a Debye length), the structural features of the brush, for instance the tether spacing and segmental concentration profile, become relatively unimportant. Milner has demonstrated, for

instance, that the step function and parabolic brush forms give similar results for large compressions such as those in the current study.<sup>18</sup> The essential feature is that the compression is resisted by the osmotic pressure in the gap.

Assuming that the critical number of adhesive patches needed for capture is proportional to the steric repulsion, the ranking of the bacterial thresholds should follow similarly. This is the case qualitatively: In Figure 6.2A, though the ratios of the valencies for Brushes 2 and 3 relative to Brush 1 (18:13 and 20:13, respectively) are not exactly 1 and 3, respectively. One can explain this modest discrepancy, however, by relaxing the assumption that bacterial capture on the three brushes results in the exactly the same gap thickness (closest bacteria-surface contact) for all three brushes. The approximate agreement between these brush thresholds and the relative valencies for the bacterial capture supports the assumption of strong compression, providing insight into the nature and extent of bacterial-surface interactions.

### **6.4.3 Steric Interaction of brushes with proteins**

The large protein thresholds and sensitivity of protein capture to brush architecture suggest differences, relative to bacteria, in the steric interactions between brushes and fibrinogen. First, multivalent fibrinogen adsorption suggests a side-on protein orientation to the surface allowing the long fibrinogen molecule to bridge several patches. Protein approach to within a Debye length of the underlying substrate requires entry of the protein into the brush by compression or penetration. Thus the full side-on area, between 150 and 200 nm for fibrinogen independent of brush architecture,

comprises the area governing the steric interactions in Figure 6.4. This is much smaller than the bacterial contact areas in Figure 6.3.

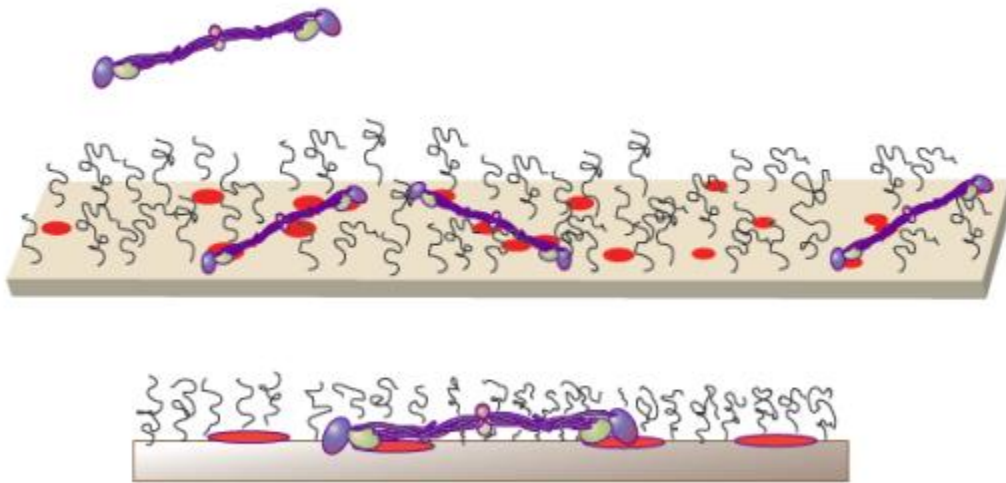


Figure 6.4 Side on fibrinogen adsorption, required for bridging multiple patches, likely requires brush penetration, especially because the narrow fibrinogen dimension is smaller than the brush height.

If fibrinogen penetrates a Flory brush in a side-on orientation, the entropic cost is the osmotic penalty associated with the protein excluded volume.<sup>7,51</sup> Estimating the excluded fibrinogen volume as  $4.5 \times 4.5 \times 45 = 900 \text{ nm}^3$ , and using second and third virial coefficients of  $0.0057 \text{ cm}^3 \text{ mol/g}^2$  and  $0.059 \text{ cm}^6 \text{ mol} / \text{g}^3$ , respectively, to estimate the osmotic pressure,<sup>39</sup> (also used to calculate the brush height), the results are summarized in Table 6.2.

The calculations raise two points: First, the calculated insertion costs suggest a ranking of the fibrinogen thresholds as Brush 1, Brush 3 and then Brush 2. While we do not observe this for  $\kappa^{-1}=2 \text{ nm}$ , we did report this trend at higher ionic strength,<sup>33</sup>

suggesting more extensive protein penetration at the smaller Debye length of  $\kappa^{-1} = 1$  nm into the same series of brushes. Second, the calculated steric insertion costs in Table 6.2 seem large: They represent an upper limit because the tether spacing in the calculation is an average value for the brush, not accounting for the greater tether spacing (order 10 nm) in the vicinity of the patches where the fibrinogen is actually located. Additionally, in the case of the thinner brush 1 at the fibrinogen threshold (around 6 nm), it may be that fibrinogen (4.5 nm high) need not insert fully, suggesting the insertion penalty could be reduced on the order of 50%. The dependence of the insertion cost on brush structure (with persistence lengths between 2 and 10 nm) could produce extreme sensitivity of fibrinogen interactions to local brush structure.

With side-on fibrinogen adsorption bridging multiple patches, the cost of brush compression is also worth estimating. First, the side-on contact area,  $4.5 \times 45 \sim 200 \text{ nm}^2$ , is estimated to be brush-independent, due to small fibrinogen dimensions perpendicular to the brush. Compressing this area of brush in a piston-like fashion (rather than applying Derjaguin, since fibrinogen is not a sphere), gives the results summarized in Table 6.2. Note that in obtaining these figures, the osmotic pressure is the resistance to compression, as described by Milner.<sup>18</sup> Rather than employing the second virial expression for osmotic pressure, a different expression as described by (Gon et al., 2012)<sup>1</sup>, with  $\chi = 0.4$ <sup>49</sup> was used, because of the elevated segmental concentrations in a gap whose thickness is the 2 nm Debye length. While the results appear slightly less costly than penetration, the sufficient uncertainty (the actual position of the protein within the brush, and the details of its surface contour) in the calculations precludes a firm argument for penetration or compression by protein. Penetration may be favorable only because it can exploit

structural details of the brush in the vicinity of the patches to further lower the energetic cost. Compression would tend to be sensitive average the local chain concentration in the vicinity of the patch and protein and therefore potentially sustain a higher steric penalty.

## 6.5 Conclusions

In the study of *S. aureus* interactions with flawed or patchy protein-resistant brushy surfaces, this study considered both the size (or binding energy) of the patches and the architecture of the brush. By varying the patch molecular weight, the numbers of cationic charges in localized surface regions were varied. Larger patches produced bacterial adhesion at lower patch loadings, and analysis confirmed the importance of both the patch size (numbers of charges) and the random patch arrangement. This reinforced the discrete, rather than mean field, nature of the bacteria-surface attractions.

Experiments provided an estimate of the relative brush compression penalty, ie the steric forces between *S. aureus* and surfaces containing different engineered brushes. Results were consistent with dramatic brush compression to heights on the order of the 2 nm Debye length. A treatment using the full Flory expression to estimate the osmotic pressure of a substantially compressed brush agreed reasonably with the estimates based on valency calculations. A simplified second virial expression for the osmotic pressure on compression was not inconsistent with the data. Both approaches, which were dominated by an osmotic term, reinforced a simple design rule for brushes, focusing on the amount of PEO tethered at the interface (assuming sufficient brush height and small persistence length relative to the protein size.) This further emphasized the relative

unimportance detailed brush structure (segmental concentration profile, tether density as long as it is smaller than the protein size). The consistency with large brush compressions explains observations in the literature concerning the important of overall brush mass.

Protein adhesion on the same series of brushes was found to require greater patch densities than those needed for bacterial capture. This observation carries scientific and practical weight. The greater patch density required for protein capture was a result of the localization of attractive interactions into patchy regions. With weakly attractive surface patches, a higher overall patch density is needed for protein capture because proteins must be able to bridge multiple patches in order to adsorb. Such bridging by larger bacteria can occur with smaller overall patchy loadings. Also observed, the threshold or patch loading for the onset of adsorption was much more sensitive, for proteins, to brush architecture than the thresholds for bacterial capture. This is thought to be a result of a protein's ability to penetrate the brush in a manner dependent on local brush structure. By contrast, bacterial adhesion requires a more uniform brush compression.

These observations imply that for brush-based protein resistant biomaterials, nanoscale flaws can induce bacterial fouling and cell adhesion long before protein adsorption occurs. This behavior differs markedly from classical understanding that protein adsorption precedes cell adhesion and explains why protein adsorption can sometimes be a poor predictor of cell-surface interactions.

## 6.6 References

- 1.) Gon, S., Kumar, K. N., Nusslein, K., & Santore, M. (2012). How bacteria adhere to brushy PEG surfaces: Clinging to flaws and compressing the brush. *Macromolecules*, 45(20), 8373-8381
- 2.) Kingshott, P., & Griesser, H. J. (1999). Surfaces that resist bioadhesion. *Current Opinion in Solid State & Materials Science*, 4(4), 403-412.
- 3.) Ratner, B. D., & Bryant, S. J. (2004). Biomaterials: Where we have been and where we are going. *Annual Review of Biomedical Engineering*, 6, 41-75.
- 4.) Ostuni, E., Chapman, R. G., Holmlin, R. E., Takayama, S., & Whitesides, G. M. (2001). A survey of structure-property relationships of surfaces that resist the adsorption of protein. *Langmuir*, 17(18), 5605-5620.
- 5.) Pasche, S., Textor, M., Meagher, L., Spencer, N. D., & Griesser, H. J. (2005). Relationship between interfacial forces measured by colloid-probe atomic force microscopy and protein resistance of poly(ethylene glycol)-grafted poly(L-lysine) adlayers on niobia surfaces. *Langmuir*, 21(14), 6508-6520.
- 6.) Currie, E. P. K., Norde, W., & Stuart, M. A. C. (2003). Tethered polymer chains: surface chemistry and their impact on colloidal and surface properties. *Advances in Colloid and Interface Science*, 100, 205-265.
- 7.) Halperin, A. (1999). Polymer brushes that resist adsorption of model proteins: Design parameters. *Langmuir*, 15(7), 2525-2533.
- 8.) Malmsten, M., Emoto, K., & Van Alstine, J. M. (1998). Effect of chain density on inhibition of protein adsorption by poly(ethylene glycol) based coatings. *Journal of Colloid and Interface Science*, 202(2), 507-517.
- 9.) Efremova, N. V., Bondurant, B., O'Brien, D. F., & Leckband, D. E. (2000). Measurements of interbilayer forces and protein adsorption on uncharged lipid bilayers displaying poly(ethylene glycol) chains. *Biochemistry*, 39(12), 3441-3451.



- 10.) Kelley, T. W., Schorr, P. A., Johnson, K. D., Tirrell, M., & Frisbie, C. D. (1998). Direct force measurements at polymer brush surfaces by atomic force microscopy. *Macromolecules*, 31(13), 4297-4300.
- 11.) Ruths, M., Johannsmann, D., Ruhe, J., & Knoll, W. (2000). Repulsive forces and relaxation on compression of entangled, polydisperse polystyrene brushes. *Macromolecules*, 33(10), 3860-3870.
- 12.) Martin, J. I., & Wang, Z. G. (1995). Polymer brushes - scaling, compression forces, interbrush penetration, and solvent size effects. *Journal of Physical Chemistry*, 99(9), 2833-2844.
- 13.) Yamamoto, S., Ejaz, M., Tsujii, Y., & Fukuda, T. (2000). Surface interaction forces of well-defined, high-density polymer brushes studied by atomic force microscopy. 2. Effect of graft density. *Macromolecules*, 33(15), 5608-5612.
- 14.) Yamamoto, S., Ejaz, M., Tsujii, Y., Matsumoto, M., & Fukuda, T. (2000). Surface interaction forces of well-defined, high-density polymer brushes studied by atomic force microscopy. 1. Effect of chain length. *Macromolecules*, 33(15), 5602-5607.
- 15.) Drobek, T., Spencer, N. D., & Heuberger, M. (2005). Compressing PEG brushes. *Macromolecules*, 38(12), 5254-5259.
- 16.) Heuberger, M., Drobek, T., & Spencer, N. D. (2005). Interaction forces and morphology of a protein-resistant poly(ethylene glycol) layer. *Biophysical Journal*, 88(1), 495-504.
- 17.) Pasche, S., Voros, J., Griesser, H. J., Spencer, N. D., & Textor, M. (2005). Effects of ionic strength and surface charge on protein adsorption at PEGylated surfaces. *Journal of Physical Chemistry B*, 109(37), 17545-17552.
- 18.) Milner, S. T. (1991). Polymer brushes. *Science*, 251(4996), 905-914.

- 19.) Kingshott, P., Thissen, H., & Griesser, H. J. (2002). Effects of cloud-point grafting, chain length, and density of PEG layers on competitive adsorption of ocular proteins. *Biomaterials*, 23(9), 2043-2056.
- 20.) McPherson, T., Kidane, A., Szleifer, I., & Park, K. (1998). Prevention of protein adsorption by tethered poly(ethylene oxide) layers: Experiments and single-chain mean-field analysis. *Langmuir*, 14(1), 176-186.
- 21.) Dalsin, J. L., Lin, L. J., Tosatti, S., Voros, J., Textor, M., & Messersmith, P. B. (2005). Protein resistance of titanium oxide surfaces modified by biologically inspired mPEG-DOPA. *Langmuir*, 21(2), 640-646.
- 22.) Sofia, S. J., Premnath, V., & Merrill, E. W. (1998). Poly(ethylene oxide) grafted to silicon surfaces: Grafting density and protein adsorption. *Macromolecules*, 31(15), 5059-5070.
- 23.) Wagner, V. E., Koberstein, J. T., & Bryers, J. D. (2004). Protein and bacterial fouling characteristics of peptide and antibody decorated surfaces of PEG-poly(acrylic acid) co-polymers. *Biomaterials*, 25(12), 2247-2263.
- 24.) Malmsten, M., & VanAlstine, J. M. (1996). Adsorption of poly(ethylene glycol) amphiphiles to form coatings which inhibit protein adsorption. *Journal of Colloid and Interface Science*, 177(2), 502-512.
- 25.) Wei, J., Ravn, D. B., Gram, L., & Kingshott, P. (2003). Stainless steel modified with poly(ethylene glycol) can prevent protein adsorption but not bacterial adhesion. *Colloids and Surfaces B-Biointerfaces*, 32(4), 275-291.
- 26.) Gon, S., Bendersky, M., Ross, J. L., & Santore, M. M. (2010). Manipulating Protein Adsorption using a Patchy Protein-Resistant Brush. *Langmuir*, 26(14), 12147-12154.
- 27.) Gon, S., & Santore, M. M. (2011). Single Component and Selective Competitive Protein Adsorption in a Patchy Polymer Brush: Opposition between Steric Repulsions and Electrostatic Attractions. *Langmuir*, 27(4), 1487-1493.

- 28.) Huang, N. P., Michel, R., Voros, J., Textor, M., Hofer, R., Rossi, A., Elbert, D. L., Hubbell, J. A., & Spencer, N. D. (2001). Poly(L-lysine)-g-poly(ethylene glycol) layers on metal oxide surfaces: Surface-analytical characterization and resistance to serum and fibrinogen adsorption. *Langmuir*, *17*(2), 489-498.
- 29.) Kenausis, G. L., Voros, J., Elbert, D. L., Huang, N. P., Hofer, R., Ruiz-Taylor, L., Textor, M., Hubbell, J. A., & Spencer, N. D. (2000). Poly(L-lysine)-g-poly(ethylene glycol) layers on metal oxide surfaces: Attachment mechanism and effects of polymer architecture on resistance to protein adsorption. *Journal of Physical Chemistry B*, *104*(14), 3298-3309.
- 30.) Gon, S., Fang, B., & Santore, M. M. (2011). Interaction of Cationic Proteins and Polypeptides with Biocompatible Cationically-Anchored PEG Brushes. *Macromolecules*, *44*(20), 8161-8168.
- 31.) Feuz, L., Leermakers, F. A. M., Textor, M., & Borisov, O. (2008). Adsorption of molecular brushes with polyelectrolyte backbones onto oppositely charged surfaces: A self-consistent field theory. *Langmuir*, *24*(14), 7232-7244.
- 32.) Halperin, A., & Kroger, M. (2009). Ternary Protein Adsorption onto Brushes: Strong versus Weak. *Langmuir*, *25*(19), 11621-11634.
- 33.) Gon, S., & Santore, M. M. (2011). Sensitivity of Protein Adsorption to Architectural Variations in a Protein-Resistant Polymer Brush Containing Engineered Nanoscale Adhesive Sites. *Langmuir*, *27*(24), 15083-15091.
- 34.) Watanabe, H., & Tirrell, M. (1993). Measurement of forces in symmetrical and asymmetric interactions between diblock copolymer layers adsorbed on mica. *Macromolecules*, *26*(24), 6455-6466.
- 35.) Harris, L. G., Tosatti, S., Wieland, M., Textor, M., & Richards, R. G. (2004). Staphylococcus aureus adhesion to titanium oxide surfaces coated with non-functionalized and peptide-functionalized poly(L-lysine)-grafted-poly(ethylene glycol) copolymers. *Biomaterials*, *25*(18), 4135-4148.

- 36.) Fu, Z. G., & Santore, M. M. (1998). Poly(ethylene oxide) adsorption onto chemically etched silicates by Brewster angle reflectivity. *Colloids and Surfaces a-Physicochemical and Engineering Aspects*, 135(1-3), 63-75.
- 37.) Alexander, S. (1977). Adsorption of chain molecules with a polar head a-scaling description. *Journal De Physique*, 38(8), 983-987.
- 38.) de Gennes, P. G. (1976). *J. Phys. (Paris)*, 38, 1443.
- 39.) Nam, J., & Santore, M. M. (2011). Depletion versus Deflection: How Membrane Bending Can Influence Adhesion. *Physical Review Letters*, 107(7).
- 40.) Fang, B., Gon, S., Park, M., Kumar, K. N., Rotello, V. M., Nusslein, K., & Santore, M. M. (2011). Bacterial adhesion on hybrid cationic nanoparticle-polymer brush surfaces: Ionic strength tunes capture from monovalent to multivalent binding. *Colloids and Surfaces B-Biointerfaces*, 87(1), 109-115.
- 41.) Fang, B., Gon, S., Park, M. H., Kumar, K. N., Rotello, V. M., Nusslein, K., & Santore, M. M. (2012). Using Flow to Switch the Valency of Bacterial Capture on Engineered Surfaces Containing Immobilized Nanoparticles. *Langmuir*, 28(20), 7803-7810.
- 42.) Kalasin, S., Dabkowski, J., Nusslein, K., & Santore, M. M. (2010). The role of nanoscale heterogeneous electrostatic interactions in initial bacterial adhesion from flow: A case study with *Staphylococcus aureus*. *Colloids and Surfaces B-Biointerfaces*, 76(2), 489-495.
- 43.) Duffadar, R., Kalasin, S., Davis, J. M., & Santore, M. M. (2009). The impact of nanoscale chemical features on micron-scale adhesion: Crossover from heterogeneity-dominated to mean-field behavior. *Journal of Colloid and Interface Science*, 337(2), 396-407.
- 44.) Kalasin, S., Martwiset, S., Coughlin, E. B., & Santore, M. M. (2010). Particle Capture via Discrete Binding Elements: Systematic Variations in Binding Energy for Randomly Distributed Nanoscale Surface Features. *Langmuir*, 26(22), 16865-16870.

- 45.) Bosker, W. T. E., Iakovlev, P. A., Norde, W., & Stuart, M. A. C. (2005). BSA adsorption on bimodal PEO brushes. *Journal of Colloid and Interface Science*, 286(2), 496-503.
- 46.) King, M. R., Rodgers, S. D., & Hammer, D. A. (2001). Hydrodynamic collisions suppress fluctuations in the rolling velocity of adhesive blood cells. *Langmuir*, 17(14), 4139-4143.
- 47.) Hammer, D. A., & Tirrell, M. (1996). Biological adhesion at interfaces. *Annual Review of Materials Science*, 26, 651-691.
- 48.) King, M. R., & Hammer, D. A. (2001). Multiparticle adhesive dynamics. Interactions between stably rolling cells. *Biophysical Journal*, 81(2), 799-813.
- 49.) Halperin, A., & Kroger, M. (2012). Theoretical considerations on mechanisms of harvesting cells cultured on thermoresponsive polymer brushes. *Biomaterials*, 33(20), 4975-4987.
- 50.) Pedersen, J. S., & Sommer, C. (2005). Temperature Dependence of the Virial Coefficients and the Chi Parameter in Semi-Dilute Solutions of PEG. *Progr. Colloid Polymer Sci.*, 130, 70-78.
- 51.) Halperin, A., Fragneto, G., Schollier, A., & Sferrazza, M. (2007). Primary versus ternary adsorption of proteins onto PEG brushes. *Langmuir*, 23(21), 10603-10617.

# CHAPTER 7

## CONCLUSIONS AND FUTURE DIRECTIONS OF RESEARCH

### 7.1 Conclusion

In this study a new class of biomaterials was developed and studied in the context of various applications. The program extended the classical construct of a sterically-repulsive PEG brush by embedding cationic patches at the base of the brush, setting up competition between the steric repulsion of the brush and electrostatic attractions to approaching molecules and cells. The interaction of these surfaces with different proteins and *S. aureus* bacteria was studied, using three different PEG brushes that systematically varied the PEG chain length, grafting density, and mass of PEG.

#### 7.1.1 New concept of patchy brush

The concept of a patchy brush is like putting selective imperfections within a polymer brush, providing insights into why some brushes fail while, at the same time, developing a novel and useful interfacial design strategy. Our study showed that cationic PLL patches adsorbed on silica are stable when exposed to buffer, protein solution, or an adsorbing copolymer that forms a polymer brush. Backfilling rest of the surface with the PEG brush then presents a surface with sparse cationic moieties separated by a bio-resistant stable PEG brush. As the size of these patches was a few nanometers (smaller

than the protein molecules in study) and as they tended to be weakly attracted towards negative objects in suspension, these nano-patterned PEG brushes showed unique bio-selective characteristics. The patches could interact, via electrostatic attractions, with negatively charged proteins or cells. Notably, the interactions between the individual patches and approaching objects are non-specific and non-selective. In this thesis, it was demonstrated that by tuning the average spacing between the adhesive patches, and ensuring a dominant repulsion between the brush on the remaining surface with approaching objects, one can achieve a remarkable control of sharp and specific bio-adhesion. Hence the main focus of this thesis was to produce sharp tunability of bio-adhesion without employing bio-specific target molecules like biotin, RGD or various cell adhesion molecules (CAMs).

### **7.1.2 Brush stability analysis with protein and polyelectrolyte addition**

The stability of three PEG brushes, varying molecular weight, tether spacing, and overall PEG content (but all strongly repellant to serum proteins) was studied by challenging the brushes with various proteins and a weak cationic polyelectrolyte, poly-L-lysine (PLL). The brush repelled all the anionic proteins, namely fibrinogen, albumin, alkaline phosphatase but retained the globular cationic protein lysozyme. Lysozyme adsorption increased with increasing PEG content in the brush, with the greatest lysozyme retention in brushes that were the most repellant to serum proteins. We therefore concluded that weak attractions between PEG and lysozyme were the cause. Separately, it was found that PLL challenge to adsorbed PLL-PEG brushes triggered complete brush desorption from the surface. This was expected, but the displacement was

found to take place on extremely rapid timescales, suggesting that PLL penetrates the PEG brush layers easily and that the PLL anchor onto the silica substrate is fundamentally dynamic.

### **7.1.3 Tuning size based protein adhesion**

Systematic variation of the number density of cationic PLL patches within a PEG brush revealed a series of sharp protein adhesion thresholds for fibrinogen, albumin, alkaline phosphatase and myoglobin. The threshold position (the density of patches at the threshold) increases as the protein size decreases, for fibrinogen, albumin, and alkaline phosphatase. While fibrinogen, albumin and alkaline phosphatase were all negatively charged at our operating condition (pH 7.4) and bigger than the patch size (10 nm), myoglobin's major dimension (4.4 nm) was smaller than the patch size and it is neutral at pH 7.4. The adhesion thresholds of the bigger proteins were found, in studies varying ionic strength, to be driven by electrostatic attraction between proteins. Protein adsorption occurred only when individual proteins were able to bridge the spacings between the patches, so that the surfaces acted like a molecular ruler.<sup>1,2</sup> In contrast, myoglobin showed a capability of binding onto single patches without bridging between patches, and the interaction of myoglobin with the patches was not electrostatic attraction. Sharp separation of fibrinogen and albumin was achieved at an intermediate surface in between the threshold points of the two proteins.



#### **7.1.4 Tuning protein adhesion by controlling brush height, density, and ionic strengths**

The effects of brush heights and ionic strength on protein adhesion were studied using fibrinogen as a model protein. It was found that adhesion thresholds for proteins can be tuned by changing the brush heights and ionic strengths of buffer solutions. The patchy brushes showed the ability to adsorb protein from a low ionic strength buffer and then release them at a higher ionic strength. Ionic strength was therefore demonstrated as a means of brush regeneration, with nearly reproducible cycles of protein adsorption and desorption, with changing ionic strength.

#### **7.1.5 Tuning bacterial adhesion**

Adhesion of *S. aureus* on the three patchy brushes was studied. Distinct adhesion thresholds for bacterial adhesion were observed for three brushes suggesting that such brushes can be used to tune bacterial adhesion and eventually separate different bacterial types. A distinct difference between protein and bacterial adhesion thresholds for all of the brushes was observed. This suggested that smart surfaces can be engineered to initiate separation of cells from its culture medium. The effect of fibrinogen on adhesion characteristics of *S. aureus* was studied and it was found that fibrinogen hampers capture of bacteria to due protein binding directly to the surface of *S. aureus*. This highly specific binding of fibrinogen on *S. aureus* was an unanticipated complication for this particular bacterium which has been found to present fibrinogen receptors.

## **7.2 Future directions**

The construct of patchy brush can be extended to diverse applications. Based on their unique bio-adhesive properties, the relatively simple and cost effective ways of surface preparation methodologies for such patchy brushes then can be useful in several bio-diagnostics and separation applications. A few of these potentially beneficial areas are highlighted below.

### **7.2.1 Generation of myoglobin sensor**

Myoglobin is among the smallest proteins which are not normally found in blood serum. During skeletal muscle injury myoglobin can secret into blood and urine and hence is commonly known as cardiac biomarker.<sup>3</sup> Common myoglobin detection kits that are commercially available give only qualitative information about myoglobin presence and can often give false signals.<sup>3-5</sup> Our experimental results showed that at surface conditions where fibrinogen, albumin, alkaline phosphatase do not adhere, myoglobin does adhere (near the onset of PEG threshold). Since fibrinogen and albumin are the major proteins present in serum, this observation suggests an application where these surfaces could be employed in the testing blood serum for trace myoglobin levels. The result can lead to an efficient myoglobin detector sensor.

### **7.2.2 Generation of smart surfaces to effectively capture and kill bacteria**

Precise tuning of bacterial adhesion leads to the possibility of producing smart systems that can effectively capture and kill bacteria. Besides synthetic polymers and

antimicrobial proteins for bacterial killing, other constructs have also been considered, for instance, recently bacteriophages been successfully attached to polymer materials and shown promise for bacterial manipulation.<sup>6</sup> Monoclonal antibodies have also been found to fill bacteria once it comes in contact with bacteria membrane.<sup>7</sup> The potential to immobilize such killer constructs within our patchy regions would enable sophisticated and achieve tunable bacteria capture and killing.

### **7.2.3 Capture of cells from media and complex biological fluids**

This thesis demonstrated that *S. aureus* adhesion precedes that of fibrinogen on series of brushy surfaces containing increasing densities of cationic patches. If this size effect can be extrapolated to other systems, it suggests that mammalian cell adhesion will precede protein adhesion in cell culture media. Hence patchy brushes could potentially be exploited to capture cells from the culture media and other complex biological fluids. A typical example is breast cancer cells which might be present in breast milk early on, or in blood during metastasis. Harvesting these epithelial cells from either complex fluid and discriminating them from other cells remains a challenge. Our research shows promise that such a surface can be engineered to efficiently capture cells of interest from complex fluids and culture media.

### **7.2.4 Separating different bacteria and cells**

Nano scale surface heterogeneity has been found to be effective in separating silica particles based on their sizes. The adhesion thresholds achieved in our patchy brushes for *S. aureus* shows promise that size based separation between different

bacterial strains or between different cell lines can be achieved by our patchy brushes in future.

In general the patchy brushes showed promise as a biologically compatible system and they present great promise in selective protein and cell detection, sorting, separation and for the development of biomedical devices in the future.

### 7.3 References

- 1.) Gon, S., Bendersky, M., Ross, J. L., & Santore, M. M. (2010). Manipulating Protein Adsorption using a Patchy Protein-Resistant Brush. *Langmuir*, 26(14), 12147-12154.
- 2.) Gon, S., & Santore, M. M. (2011). Single Component and Selective Competitive Protein Adsorption in a Patchy Polymer Brush: Opposition between Steric Repulsions and Electrostatic Attractions†. *Langmuir*, 27(4), 1487-1493.
- 3.) Suprun, E. V., Shilovskaya, A. L., Lisitsa, A. V., Bulko, T. V., Shumyantseva, V. V., & Archakov, A. I. (2011). Electrochemical Immunosensor Based on Metal Nanoparticles for Cardiac Myoglobin Detection in Human Blood Plasma. *Electroanalysis*, 23(5), 1051-1057.
- 4.) Grover, D. S., Atta, M. G., Eustace, J. A., Kickler, T. S., & Fine, D. M. (2004). Lack of clinical utility of urine myoglobin detection by microconcentrator ultrafiltration in the diagnosis of rhabdomyolysis. *Nephrology, Dialysis, Transplantation*, 19(10), 2634-2638.
- 5.) Almog, C., Isakov, A., Ayalon, D., Burke, M., & Shapira, I. (1987). Serum myoglobin in detection of myocardial necrosis in patients with “coronary insufficiency.” *Clinical Cardiology*, 10(5), 347-349.
- 6.) Applegate, B. M., Perry, L. L., Morgan, M. T., & Kothapalli, A. (2010, March 25). Methods for generation of reporter phages and immobilization of active bacteriophages on a polymer surface.
- 7.) Ronholm, J., Zhang, Z., Cao, X., & Lin, M. (2011). Monoclonal Antibodies to Lipopolysaccharide Antigens of *Salmonella enterica* serotype Typhimurium DT104. *Hybridoma*, 30(1), 43-52.

## APPENDIX A

### EFFECT OF GRAFTING RATIO ON PROTEIN ADHESION OVER BRUSH # 1

Different PLL-PEG brushes were synthesized with 2000 MW PEG tether attached to 20000 MW PLL backbone with varying grafting ratio. These experiments were done initially to find a suitable grafting ratio that would lead to best protein repellence characteristics for the brush. As shown in Figure A.1 PLL-PEG with grafting ratio 2.7 showed least amount of protein adhesion. A second batch of this polymer showed almost negligible protein adhesion and was selected for this study. This polymer was called Brush # 1 throughout this thesis.

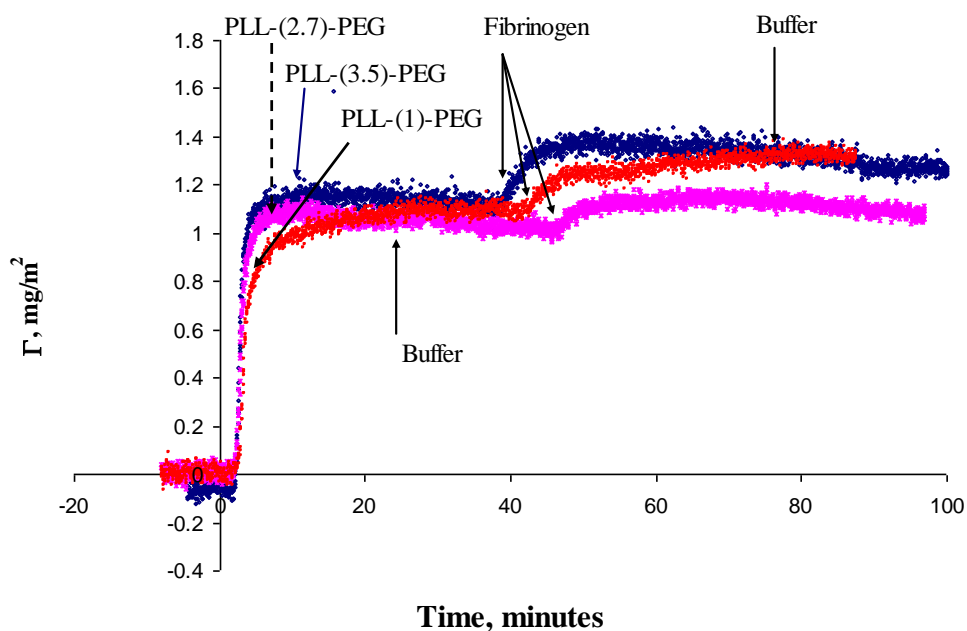


Figure A.1 Protein repellence for PLL-PEG with different grafting ratios

## APPENDIX B

### NMR DATA FOR BRUSH 1 2 AND 3

The PLL-PEG was characterized with  $^1\text{H}$  NMR using a  $\text{D}_2\text{O}$  solvent with a Bruker 400 MHz instrument. The areas of the lysine side chain peak ( $-\text{CH}_2-\text{N}-$ ) at 2.909 ppm highlighted in yellow and PEG peak ( $-\text{CH}_2-\text{CH}_2-$ ) at 3.615 ppm highlighted in light blue were compared to determine the grafting ratio for the three brushes.

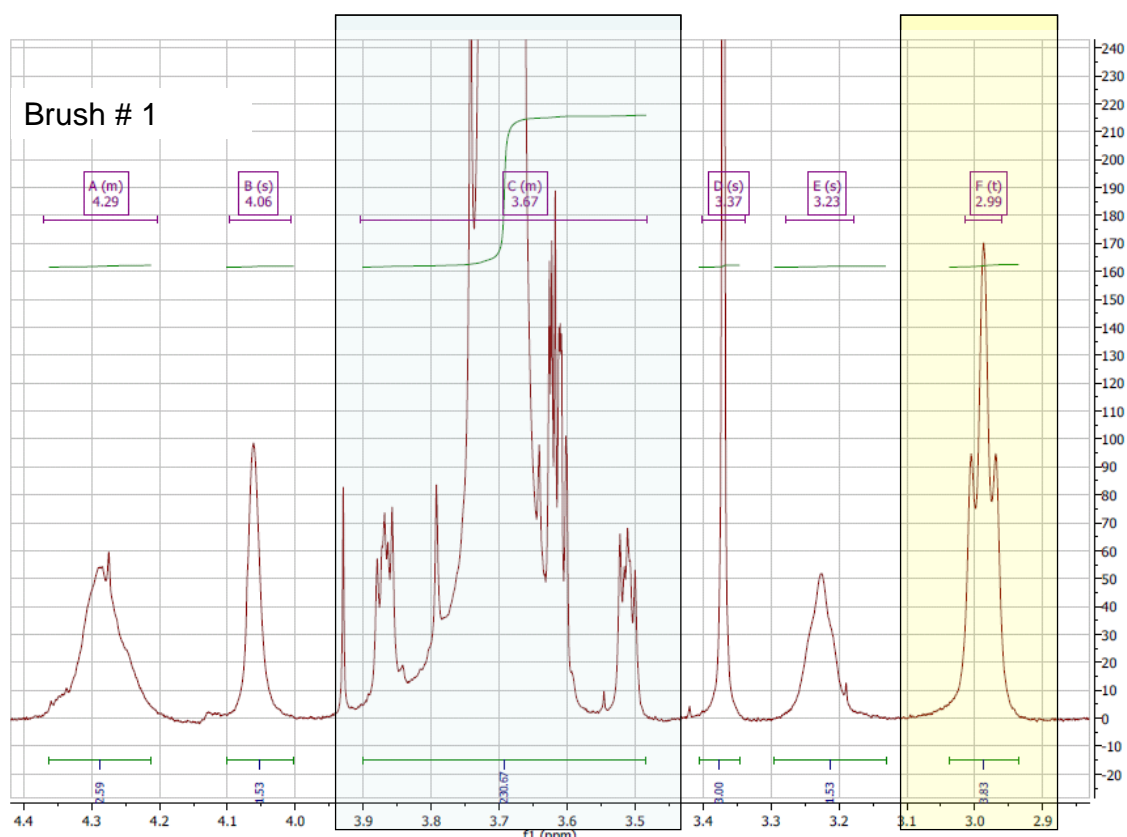


Figure B.1 NMR data for Brush # 1

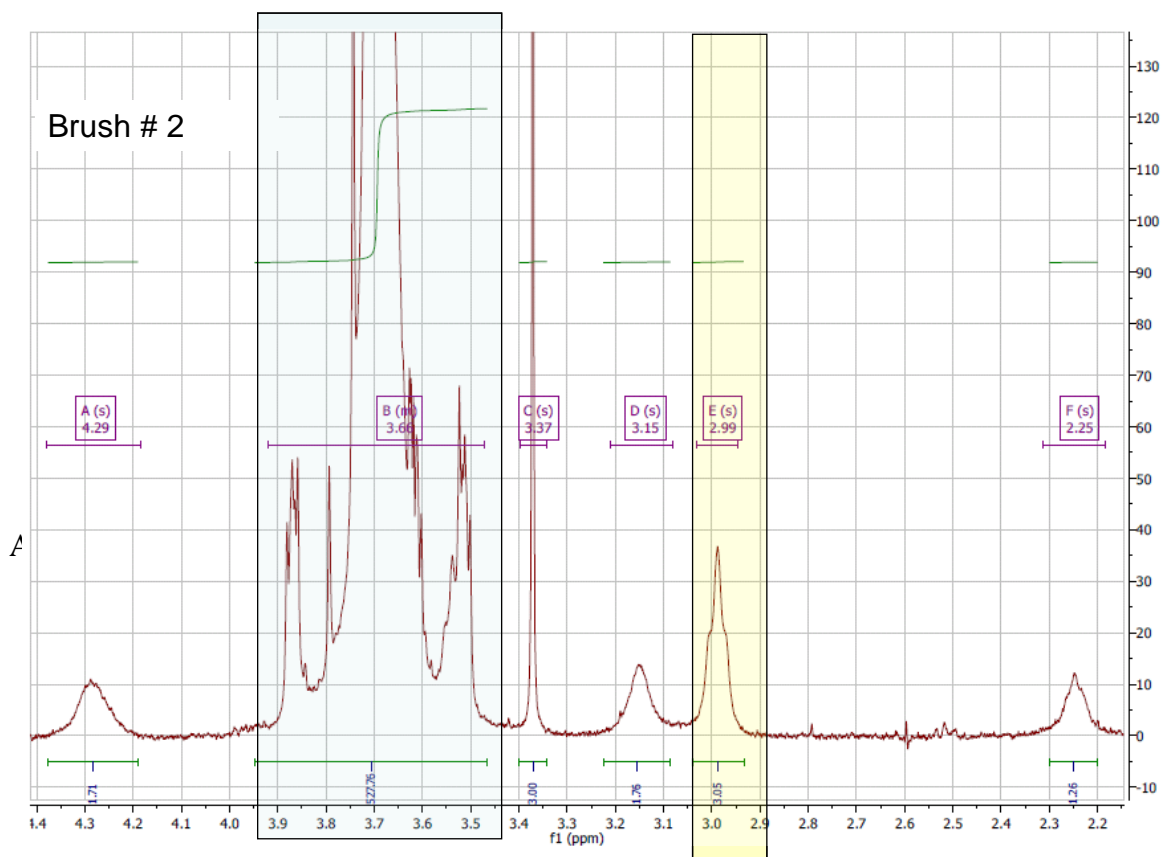


Figure B.2 NMR data for Brush # 2



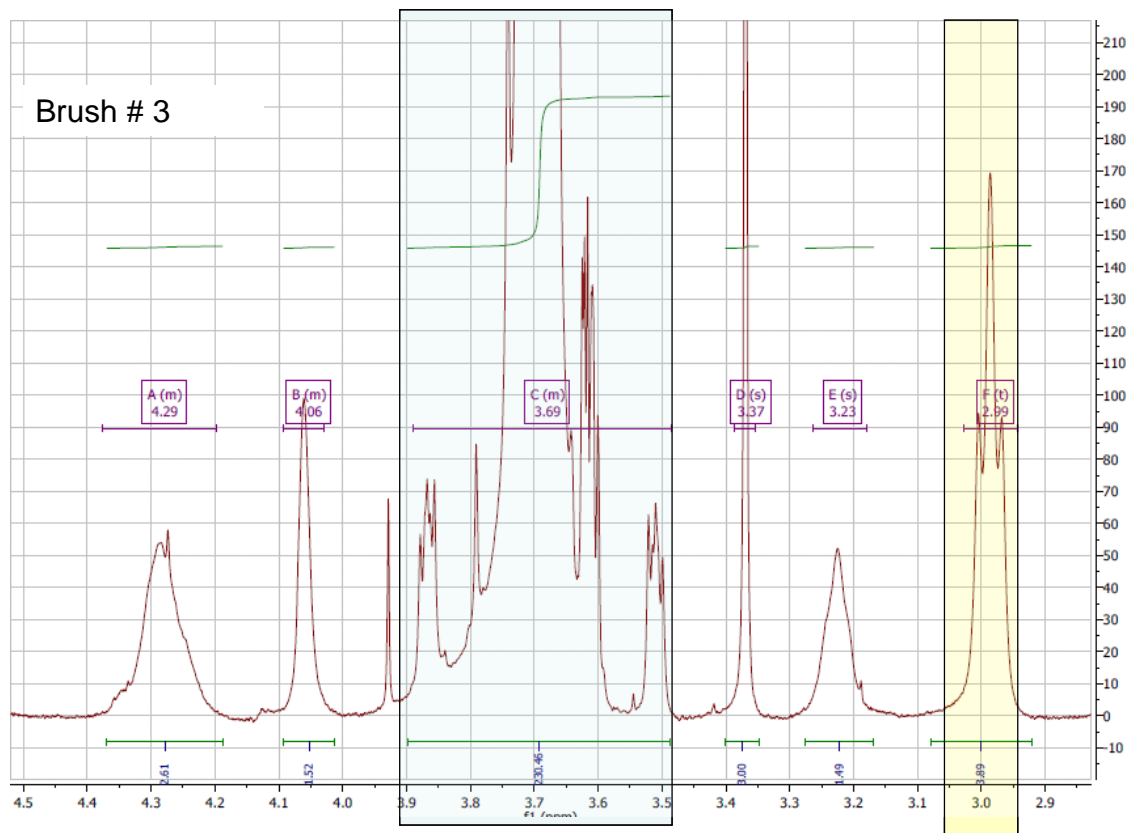


Figure B.3 NMR data for Brush # 3

## BIBLIOGRAPHY

- Adamczyk, Z, Nattich, M., Wasilewska, M, & Sadowska, M. (2011). Deposition of colloid particles on protein layers: fibrinogen on mica. *Journal of Colloid and Interface Science*, 356(2), 454-464.
- Agnihotri, A., & Siedlecki, C. A. (2004). Time-Dependent Conformational Changes in Fibrinogen Measured by Atomic Force Microscopy. *Langmuir*, 20(20), 8846-8852.
- Alang Ahmad, S., Hucknall, A., Chilkoti, A., & Leggett, G. J. (2010). Protein Patterning by UV-Induced Photodegradation of Poly(oligo(ethylene glycol) methacrylate) Brushes. *Langmuir*, 26(12), 9937-9942.
- Alexander, S. (1977). Adsorption of chain molecules with a polar head a scaling description. *Journal de Physique (Paris)*, 38(8), 983-7.
- Alexander, S. (1977). Polymer adsorption on small spheres. A scaling approach. *Journal de Physique (Paris)*, 38(8), 977-981.
- Almog, C., Isakov, A., Ayalon, D., Burke, M., & Shapira, I. (1987). Serum myoglobin in detection of myocardial necrosis in patients with "coronary insufficiency." *Clinical Cardiology*, 10(5), 347-349.
- Amanda, A., & Mallapragada, S. K. (2001). Comparison of protein fouling on heat-treated poly(vinyl alcohol), poly(ether sulfone) and regenerated cellulose membranes using diffuse reflectance infrared Fourier transform spectroscopy. *Biotechnology Progress*, 17(5), 917-923.
- Applegate, B. M., Perry, L. L., Morgan, M. T., & Kothapalli, A. (2010, March 25). Methods for generation of reporter phages and immobilization of active bacteriophages on a polymer surface.
- Arai, T., & Norde, W. (1990). The behavior of some model proteins at solid-liquid interfaces. 1. Adsorption from single protein solutions. *Colloids and Surfaces*, 51, 1-15.

- Asuri, P., Karajanagi, S. S., Vertegel, A. A., Dordick, J. S., & Kane, R. S. (2007). Enhanced stability of enzymes adsorbed onto nanoparticles. *Journal of Nanoscience and Nanotechnology*, 7(4-5), 1675-1678.
- Bartoli, F., Burtin, G., & Guerif, J. (1992). Influence of Organic-Matter on Aggregation in Oxisols Rich in Gibbsite or in Goethite .2. Clay Dispersion, Aggregate Strength and Water-Stability. *Geoderma*, 54(1-4), 259-274.
- Bartucci, R., Pantusa, M., Marsh, D., & Sportelli, L. (2002). Interaction of human serum albumin with membranes containing polymer-grafted lipids: spin-label ESR studies in the mushroom and brush regimes. *Biochimica et Biophysica Acta, Biomembranes*, 1564(1), 237-242.
- Bergstrand, A., Rahmani-Monfared, G., Ostlund, A., Nyden, M., & Holmberg, K. (2009). Comparison of PEI-PEG and PLL-PEG copolymer coatings on the prevention of protein fouling. *Journal of Biomedical Materials Research Part A*, 88A(3), 608-615.
- Billsten, P., Wahlgren, M., Arnebrant, T., McGuire, J., & Elwing, H. (1995). Structural changes of T4 lysozyme upon adsorption to silica nanoparticles measured by circular dichroism. *Journal of Colloid and Interface Science*, 175(1), 77-82.
- Böhme, U., & Scheler, U. (2007). Effective charge of bovine serum albumin determined by electrophoresis NMR. *Chemical Physics Letters*, 435(4-6), 342-345.
- Brant, J. A., Johnson, K. M., & Childress, A. E. (2006). Characterizing NF and RO membrane surface heterogeneity using chemical force microscopy. *Colloids and Surfaces a-Physicochemical and Engineering Aspects*, 280(1-3), 45-57.
- Brittain, W. J., & Minko, S. (2007). A structural definition of polymer brushes. *Journal of Polymer Science, Part A: Polymer Chemistry*, 45(16), 3505-3512.
- Blawas, A. S., & Reichert, W. M. (1998). Protein patterning. *Biomaterials*, 19(7-9), 595-609.

- Bloustine, J., Virmani, T., Thurston, G. M., & Fraden, S. (2006). Light Scattering and Phase Behavior of Lysozyme-Poly(Ethylene Glycol) Mixtures. *Physical Review Letters*, 96(8).
- Böhme, U., & Scheler, U. (2007). Effective charge of bovine serum albumin determined by electrophoresis NMR. *Chemical Physics Letters*, 435(4-6), 342-345.
- Bos, M. A., & van, V. T. (2001). Interfacial rheological properties of adsorbed protein layers and surfactants: a review. *Advances in colloid and interface science*, 91(3), 437-471.
- Bosker, W. T. E., Iakovlev, P. A., Norde, W., & Stuart, M. A. C. (2005). BSA adsorption on bimodal PEO brushes. *Journal of Colloid and Interface Science*, 286(2), 496-503.
- Bunt, C. R., Jones, D. S., & Tucker, I. G. (1993). The effects of pH, ionic-strength and organic-phase on the bacterial adhesion to hydrocarbons (bath) test. *International Journal of Pharmaceutics*, 99(2-3), 93-98.
- Chang, H. T., Rittmann, B. E., Amar, D., Heim, R., Ehlinger, O., & Lesty, Y. (1991). Biofilm detachment mechanisms in a liquid-fluidized bed. *Biotechnology and Bioengineering*, 38(5), 499-506.
- Camesano, T. A., & Abu-Lail, N. I. (2002). Heterogeneity in bacterial surface polysaccharides, probed on a single-molecule basis. *Biomacromolecules*, 3(4), 661-667.
- Casimirius, S., Flahaut, E., Laberty-Robert, C., Malaquin, L., Carcenac, F., Laurent, C., & Vieu, C. (2004). Microcontact printing process of individual for the patterned growth CNTs. *Microelectronic Engineering*, 73-4, 564-569.
- Cedervall, T., Lynch, I., Lindman, S., Berggard, T., Thulin, E., Nilsson, H., Dawson, K. A., & Linse, S. (2007). Understanding the nanoparticle-protein corona using methods to quantify exchange rates and affinities of proteins for nanoparticles. *Proceedings of the National Academy of Sciences of the United States of America*, 104(7), 2050-2055.

- Chang, B.S., Kendrick, B.S., & Carpenter, J.F. (1996). Surface-induced denaturation of proteins during freezing and its inhibition by surfactants. *Journal of pharmaceutical sciences*, 85(12), 1325-1330.
- Chen, H., Yuan, L., Song, W., Wu, Z. K., & Li, D. (2008). Biocompatible polymer materials: Role of protein-surface interactions. *Progress in Polymer Science*, 33(11), 1059-1087.
- Chen, S. F., Zheng, J., Li, L., & Jiang, S. (2005). Strong Resistance of Phosphorylcholine Self-Assembled Monolayers to Protein Adsorption: Insights into Nonfouling Properties of Zwitterionic Materials. *Journal of the American Chemical Society*, 127(41), 14473-14478.
- Collins, J. A., Xirouchaki, C., Palmer, R. E., Heath, J. K., & Jones, C. H. (2004). Clusters for biology: immobilization of proteins by size-selected metal clusters. *Applied Surface Science*, 226(1-3), 197-208.
- Cowan, S. E., Liepmann, D., & Keasling, J. D. (2001). Development of engineered biofilms on poly-L-lysine patterned surfaces. *Biotechnology Letters*, 23(15), 1235-1241.
- Currie, E. P. K., Norde, W., & Stuart, M. A. C. (2003). Tethered polymer chains: surface chemistry and their impact on colloidal and surface properties. *Advances in Colloid and Interface Science*, 100, 205-265.
- Dalsin, J. L., Hu, B. H., Lee, B. P., & Messersmith, P. B. (2003). Mussel adhesive protein mimetic polymers for the preparation of nonfouling surfaces. *Journal of the American Chemical Society*, 125(14), 4253-4258.
- Dalsin, J. L., Lin, L. J., Tosatti, S., Voros, J., Textor, M., & Messersmith, P. B. (2005). Protein resistance of titanium oxide surfaces modified by biologically inspired mPEG-DOPA. *Langmuir*, 21(2), 640-646.
- de, Backer, M., McSweeney, S., Rasmussen, H. B., Riise, B. W., Lindley, P., & Hough, E. (2002). The 1.9 Å crystal structure of heat-labile shrimp alkaline phosphatase. *Journal of Molecular Biology*, 318(5), 1265-1274.

- de Gennes, P. G. (1976). Scaling theory of polymer adsorption. *Journal de Physique (Paris)*, 37(12), 1445-1452.
- de Gennes, P. G. (1976). *J. Phys. (Paris)*, 38, 1443.
- de las Heras Alarcón, C., Farhan, T., Osborne, V. L., Huck, W. T. S., & Alexander, C. (2005). Bioadhesion at micro-patterned stimuli-responsive polymer brushes. *Journal of Materials Chemistry*, 15(21), 2089.
- de, V., Leermakers, F. A. M., de, K., Cohen, S., & Kleijn, J. M. (2010). Field Theoretical Analysis of Driving Forces for the Uptake of Proteins by Like-Charged Polyelectrolyte Brushes: Effects of Charge Regulation and Patchiness. *Langmuir*, 26(1), 249-259.
- Desfougeres, Y., Croguennec, T., Lechevalier, V., Bouhallab, S., & Nau, F. (2010). Charge and Size Drive Spontaneous Self-Assembly of Oppositely Charged Globular Proteins into Microspheres. *Journal of Physical Chemistry B*, 114(12), 4138-4144.
- Deshmukh, V., Britt, D. W., & Hlady, V. (2010). Excess fibrinogen adsorption to monolayers of mixed lipids. *Colloids and Surfaces. B, Biointerfaces*, 81(2), 607-613.
- Dickinson, E. (1999). Adsorbed protein layers at fluid interfaces: interactions, structure and surface rheology. *Colloids and Surfaces, B: Biointerfaces*, 15(2), 161-176.
- Dijt, J. C., Cohen, S., & Fleer, G. J. (1994). Competitive Adsorption Kinetics of Polymers Differing in Length Only. *Macromolecules*, 27(12), 3219-28.
- Dinçer, S., Türk, M., Karagöz, A., & Uzunalan, G. (2011). Potential c-myc antisense oligonucleotide carriers: PCI/PEG/PEI and PLL/PEG/PEI. *Artificial Cells, Blood Substitutes, and Immobilization Biotechnology*, 39(3), 143-154.
- Dorobantu, L. S., Bhattacharjee, S., Foght, J. M., & Gray, M. R. (2008). Atomic force microscopy measurement of heterogeneity in bacterial surface hydrophobicity. *Langmuir*, 24(9), 4944-4951.

- Draper, J., Luzinov, I., Minko, Sergiy, Tokarev, I., & Stamm, Manfred. (2004). Mixed Polymer Brushes by Sequential Polymer Addition: Anchoring Layer Effect. *Langmuir*, 20(10), 4064-4075.
- Drobek, T., Spencer, N. D., & Heuberger, M. (2005). Compressing PEG brushes. *Macromolecules*, 38(12), 5254-5259.
- Duffadar, R., Kalasin, S., Davis, J. M., & Santore, M. M. (2009). The impact of nanoscale chemical features on micron-scale adhesion: Crossover from heterogeneity-dominated to mean-field behavior. *Journal of Colloid and Interface Science*, 337(2), 396-407.
- Dufrene, Y. F. (2003). Recent progress in the application of atomic force microscopy imaging and force spectroscopy to microbiology. *Current Opinion in Microbiology*, 6(3), 317-323.
- Dutta, D., Sundaram, S. K., Teegarden, J. G., Riley, B. J., Fifield, L. S., Jacobs, J. M., Addleman, S. R., Kaysen, G. A., Moudgil, B. M., & Weber, T. J. (2007). Adsorbed proteins influence the biological activity and molecular targeting of nanomaterials. *Toxicological Sciences*, 100(1), 303-315.
- Efremova, N. V., Bondurant, B., O'Brien, D. F., & Leckband, D. E. (2000). Measurements of interbilayer forces and protein adsorption on uncharged lipid bilayers displaying poly(ethylene glycol) chains. *Biochemistry*, 39(12), 3441-3451.
- Elbert, D. L., & Hubbell, J. A. (1996). Surface treatments of polymers for biocompatibility. *Annual Review of Materials Science*, 26, 365-394.
- Fang, B., Gon, S., Park, M., Kumar, K. N., Rotello, V. M., Nusslein, K., & Santore, M. M. (2011). Bacterial adhesion on hybrid cationic nanoparticle-polymer brush surfaces: Ionic strength tunes capture from monovalent to multivalent binding. *Colloids and Surfaces B-Biointerfaces*, 87(1), 109-115.
- Fang, B., Gon, S., Park, M. H., Kumar, K. N., Rotello, V. M., Nusslein, K., & Santore, M. M. (2012). Using Flow to Switch the Valency of Bacterial Capture on Engineered Surfaces Containing Immobilized Nanoparticles. *Langmuir*, 28(20), 7803-7810.

- Fang, C. P., & Drelich, J. (2004). Theoretical contact angles on a nano-heterogeneous surface composed of parallel apolar and polar strips. *Langmuir*, 20(16), 6679-6684.
- Fang, J., & Knobler, C. M. (1996). Phase-separated two-component self-assembled organosilane monolayers and their use in selective adsorption of a protein. *Langmuir*, 12(5), 1368-1374.
- Falconnet, D., Csucs, G., Grandin, H. M., & Textor, M. (2006). Surface engineering approaches to micropattern surfaces for cell-based assays. *Biomaterials*, 27(16), 3044-3063.
- Falconnet, D., Pasqui, D., Park, S., Eckert, R., Schiff, H., Gobrecht, J., Barbucci, R., & Textor, M. (2004). A novel approach to produce protein nanopatterns by combining nanoimprint lithography and molecular self-assembly. *Nano Letters*, 4(10), 1909-1914.
- Feller, L. M., Cerritelli, S., Textor, M., Hubbell, J. A., & Tosatti, S. G. P. (2005). Influence of poly(propylene sulfide-block-ethylene glycol) di- and triblock copolymer architecture on the formation of molecular adlayers on gold surfaces and their effect on protein resistance: A candidate for surface modification in biosensor research. *Macromolecules*, 38(25), 10503-10510.
- Feng, L., & Andrade, J. D. (1994). *Proteins at Interfaces II: Fundamentals and Applications*. Horbett, T. A., Brash, J. L. Eds. American Chemical Society: Washington DC, 602, 66-79.
- Feuz, L., Leermakers, F. A. M., Textor, M., & Borisov, O. (2008). Adsorption of molecular brushes with polyelectrolyte backbones onto oppositely charged surfaces: A self-consistent field theory. *Langmuir*, 24(14), 7232-7244.
- Fischer, N. O., McIntosh, C. M., Simard, J. M., & Rotello, V. M. (2002). Inhibition of chymotrypsin through surface binding using nanoparticle-based receptors. *Proceedings of the National Academy of Sciences of the United States of America*, 99(8), 5018-5023.
- Fu, Z., & Santore, M. M. (1998). Kinetics of Competitive Adsorption of PEO Chains with Different Molecular Weights. *Macromolecules*, 31(20), 7014-7022.



- Fu, Z., & Santore, M. M. (1998). Poly(ethylene oxide) adsorption onto chemically etched silicates by Brewster angle reflectivity. *Colloids and Surfaces, A: Physicochemical and Engineering Aspects*, 135(1-3), 63-75.
- Gao, P., & Cai, Y. (2008). The Boundary Molecules in a Lysozyme Pattern Exhibit Preferential Antibody Binding. *Langmuir*, 24(18), 10334-10339.
- Gautrot, J. E., Huck, W. T. S., Welch, M., & Ramstedt, M. (2010). Protein-Resistant NTA-Functionalized Polymer Brushes for Selective and Stable Immobilization of Histidine-Tagged Proteins. *ACS Applied Materials & Interfaces*, 2(1), 193-202.
- Gon, S., Bendersky, M., Ross, J. L., & Santore, M. M. (2010). Manipulating Protein Adsorption using a Patchy Protein-Resistant Brush. *Langmuir*, 26(14), 12147-12154.
- Gon, S., Fang, B., & Santore, M. M. (2011). Interaction of Cationic Proteins and Polypeptides with Biocompatible Cationically-Anchored PEG Brushes. *Macromolecules*, 44(20), 8161-8168.
- Gon, S., & Santore, M. M. (2011). Single Component and Selective Competitive Protein Adsorption in a Patchy Polymer Brush: Opposition between Steric Repulsions and Electrostatic Attractions. *Langmuir*, 27(4), 1487-1493.
- Gon, S., & Santore, M. M. (2011). Sensitivity of Protein Adsorption to Architectural Variations in a Protein-Resistant Polymer Brush Containing Engineered Nanoscale Adhesive Sites. *Langmuir*, 27(24), 15083-15091.
- Gon, S., Kumar, K. N., Nusslein, K., & Santore, M. (2012). How bacteria adhere to brushy PEG surfaces: Clinging to flaws and compressing the brush. *Macromolecules*, 45(20), 8373-8381
- Graf, M., Galera, G. H., & Wätziq, M. (2005). Protein adsorption in fused-silica and polyacrylamide-coated capillaries. *Electrophoresis*, 26(12), 2409-2417.

- Grover, D. S., Atta, M. G., Eustace, J. A., Kickler, T. S., & Fine, D. M. (2004). Lack of clinical utility of urine myoglobin detection by microconcentrator ultrafiltration in the diagnosis of rhabdomyolysis. *Nephrology, Dialysis, Transplantation*, 19(10), 2634-2638.
- Gun'ko, V. M., Leboda, R., Turov, V. V., Villieras, F., Skubiszewska-Xieba, J., Chodorowski, S., & Marciniak, M. (2001). Structural and energetic nonuniformities of pyrocarbon-mineral adsorbents. *Journal of Colloid and Interface Science*, 238(2), 340-356.
- Gupta, R., & Kumar, A. (2008). Molecular imprinting in sol-gel matrix (Retracted article. See vol. 28, pg. 939, 2010). *Biotechnology Advances*, 26(6), 533-547.
- Halperin, A. (1999). Polymer brushes that resist adsorption of model proteins: Design parameters. *Langmuir*, 15(7), 2525-2533.
- Halperin, A., Buhot, A., & Zhulina, E. B. (2005). Brush effects on DNA chips: Thermodynamics, kinetics, and design guidelines. *Biophysical Journal*, 89(2), 796-811.
- Halperin, A., Fragneto, G., Schollier, A., & Sferrazza, M. (2007). Primary versus ternary adsorption of proteins onto PEG brushes. *Langmuir*, 23(21), 10603-10617.
- Halperin, A., & Kroger, M. (2009). Ternary Protein Adsorption onto Brushes: Strong versus Weak. *Langmuir*, 25(19), 11621-11634.
- Halperin, A., & Kroger, M. (2012). Theoretical considerations on mechanisms of harvesting cells cultured on thermoresponsive polymer brushes. *Biomaterials*, 33(20), 4975-4987.
- Hammer, D. A., & Tirrell, M. (1996). Biological adhesion at interfaces. *Annual Review of Materials Science*, 26, 651-691
- Hancock, J. F. (2006). Lipid rafts: contentious only from simplistic standpoints. *Nature Reviews Molecular Cell Biology*, 7(6), 456-462.

- Hansupalak, N., & Santore, Maria M. (2003). Sharp Polyelectrolyte Adsorption Cutoff Induced by a Monovalent Salt. *Langmuir*, 19(18), 7423-7426.
- Hansupalak, N., & Santore, M. M. (2004). Polyelectrolyte Desorption and Exchange Dynamics near the Sharp Adsorption Transition: Weakly Charged Chains. *Macromolecules*, 37(4), 1621-1629.
- Harris, L. G., Tosatti, S., Wieland, M., Textor, M., & Richards, R. G. (2004). Staphylococcus aureus adhesion to titanium oxide surfaces coated with non-functionalized and peptide-functionalized poly(L-lysine)-grafted-poly(ethylene glycol) copolymers. *Biomaterials*, 25(18), 4135-4148.
- Haynes, C. A., & Norde, W. (1995). Structures and stabilities of adsorbed proteins. *Journal of Colloid and Interface Science*, 169(2), 313-328.
- Heuberger, M., Drobek, T., & Spencer, N. D. (2005). Interaction forces and morphology of a protein-resistant poly(ethylene glycol) layer. *Biophysical Journal*, 88(1), 495-504.
- Hodgkinson, G., & Hlady, V. (2005). Relating material surface heterogeneity to protein adsorption: the effect of annealing of micro-contact-printed OTS patterns. *Journal of Adhesion Science and Technology*, 19(3-5), 235-255.
- Holland, N. B., Qiu, Y. X., Ruegsegger, M., & Marchant, R. E. (1998). Biomimetic engineering of non-adhesive glycocalyx-like surfaces using oligosaccharide surfactant polymers. *Nature*, 392(6678), 799-801.
- Holmberg, A., Blomstergren, A., Nord, O., Lukacs, M., Lundeberg, J., & Uhlen, M. (2005). The biotin-streptavidin interaction can be reversibly broken using water at elevated temperatures. *Electrophoresis*, 26(3), 501-510.
- Hong, R., Fischer, N. O., Verma, A., Goodman, C. M., Emrick, T., & Rotello, V. M. (2004). Control of protein structure and function through surface recognition by tailored nanoparticle scaffolds. *Journal of the American Chemical Society*, 126(3), 739-743.

- Huang, N. P., Michel, R., Voros, J., Textor, M., Hofer, R., Rossi, A., Elbert, D. L., Hubbell, J. A., & Spencer, N. D. (2001). Poly(L-lysine)-g-poly(ethylene glycol) layers on metal oxide surfaces: Surface-analytical characterization and resistance to serum and fibrinogen adsorption. *Langmuir*, 17(2), 489-498.
- Huang, Y.W., & Gupta, V. K. (2004). A SPR and AFM study of the effect of surface heterogeneity on adsorption of proteins. *Journal of Chemical Physics*, 121(5), 2264-2271.
- Jacobs, C., & Shapiro, L. (1999). Bacterial cell division: A moveable feast. *Proceedings of the National Academy of Sciences of the United States of America*, 96(11), 5891-5893.
- Jauneau, A., Quentin, M., & Driouich, A. (1997). Micro-heterogeneity of pectins and calcium distribution in the epidermal and cortical parenchyma cell walls of flax hypocotyl. *Protoplasma*, 198(1-2), 9-19.
- Jiang, M., Popa, I., Maroni, P., & Borkovec, M. (2010). Adsorption of poly(-lysine) on silica probed by optical reflectometry. *Colloids and Surfaces, A: Physicochemical and Engineering Aspects*, 360(1-3), 20-25.
- Jürgens, K. D., Peters, T., & Gros, G. (1994). Diffusivity of myoglobin in intact skeletal muscle cells. *Proceedings of the National Academy of Sciences of the United States of America*, 91(9), 3829-3833.
- Jones, J. F., Feick, J. D., Imoudu, D., Chukwumah, N., Vigeant, M., & Velegol, D. (2003). Oriented adhesion of Escherichia coli to polystyrene particles. *Applied and Environmental Microbiology*, 69(11), 6515-6519.
- Kalasin, S., Dabkowski, J., Nusslein, K., & Santore, M. M. (2010). The role of nanoscale heterogeneous electrostatic interactions in initial bacterial adhesion from flow: A case study with Staphylococcus aureus. *Colloids and Surfaces B-Biointerfaces*, 76(2), 489-495.
- Kalasin, S., Martwiset, S., Coughlin, E. B., & Santore, M. M. (2010). Particle Capture via Discrete Binding Elements: Systematic Variations in Binding Energy for Randomly Distributed Nanoscale Surface Features. *Langmuir*, 26(22), 16865-16870.

- Kalasin, S., & Santore, M. M. (2008). Hydrodynamic crossover in dynamic microparticle adhesion on surfaces of controlled nanoscale heterogeneity. *Langmuir*, 24(9), 4435-4438.
- Kalasin, S., & Santore, M. M. (2009). Non-specific adhesion on biomaterial surfaces driven by small amounts of protein adsorption. *Colloids and Surfaces B-Biointerfaces*, 73(2), 229-236.
- Kalasin, S., & Santore, M. M. (2010). Sustained Rolling of Microparticles in Shear Flow over an Electrostatically Patchy Surface. *Langmuir*, 26(4), 2317-2324.
- Kane, R. S., Takayama, S., Ostuni, E., Ingber, D. E., & Whitesides, G. M. (1999). Patterning proteins and cells using soft lithography. *Biomaterials*, 20(23-24), 2363-2376.
- Karajanagi, S. S., Vertegel, A. A., Kane, R. S., & Dordick, J. S. (2004). Structure and Function of Enzymes Adsorbed onto Single-Walled Carbon Nanotubes. *Langmuir*, 20(26), 11594-11599.
- Kasemo, B. (2002). Biological surface science. *Surface Science*, 500(1-3), 656-677.
- Katsikogianni, M., Amanatides, E., Mataras, D., & Missirlis, Y. F. (2008). Staphylococcus epidermidis adhesion to He, He/O-2 plasma treated PET films and aged materials: Contributions of surface free energy and shear rate. *Colloids and Surfaces B-Biointerfaces*, 65(2), 257-268.
- Katsikogianni, M. G., & Missirlis, Y. F. (2010). Interactions of bacteria with specific biomaterial surface chemistries under flow conditions. *Acta Biomaterialia*, 6(3), 1107-1118.
- Katsikogianni, M., Spiliopoulou, I., Dowling, D. P., & Missirlis, Y. F. (2006). Adhesion of slime producing Staphylococcus epidermidis strains to PVC and diamond-like carbon/silver/fluorinated coatings. *Journal of Materials Science-Materials in Medicine*, 17(8), 679-689.
- King, M. R., & Hammer, D. A. (2001). Multiparticle adhesive dynamics. Interactions between stably rolling cells. *Biophysical Journal*, 81(2), 799-813.

- King, M. R., Rodgers, S. D., & Hammer, D. A. (2001). Hydrodynamic collisions suppress fluctuations in the rolling velocity of adhesive blood cells. *Langmuir*, *17*(14), 4139-4143.
- Kingshott, P., & Griesser, H. J. (1999). Surfaces that resist bioadhesion. *Current Opinion in Solid State & Materials Science*, *4*(4), 403-412.
- Kingshott, P., Thissen, H., & Griesser, H. J. (2002). Effects of cloud-point grafting, chain length, and density of PEG layers on competitive adsorption of ocular proteins. *Biomaterials*, *23*(9), 2043-2056.
- Kelley, T. W., Schorr, P. A., Johnson, K. D., Tirrell, M., & Frisbie, C. D. (1998). Direct force measurements at polymer brush surfaces by atomic force microscopy. *Macromolecules*, *31*(13), 4297-4300.
- Kelly, M. S., & Santore, M. M. (1995). The role of a single end group in poly(ethylene oxide) adsorption on colloidal and film polystyrene: complimentary sedimentation and total internal reflectance fluorescence studies. *Colloids and Surfaces, A: Physicochemical and Engineering Aspects*, *96*(1/2), 199-215.
- Kenausis, G. L., Voros, J., Elbert, D. L., Huang, N. P., Hofer, R., Ruiz-Taylor, L., Textor, M., Hubbell, J. A., & Spencer, N. D. (2000). Poly(L-lysine)-g-poly(ethylene glycol) layers on metal oxide surfaces: Attachment mechanism and effects of polymer architecture on resistance to protein adsorption. *Journal of Physical Chemistry B*, *104*(14), 3298-3309.
- Kent, M. S. (2000). A quantitative study of tethered chains in various solution conditions using Langmuir diblock copolymer monolayers. *Macromolecular Rapid Communications*, *21*(6), 243-270.
- Kent, M. S., Lee, L. T., Factor, B. J., Rondelez, F., & Smith, G. S. (1995). Tethered chains in good solvent conditions: an experimental study involving Langmuir diblock copolymer monolayers. *Journal of Chemical Physics*, *103*(6), 2320-2342.
- Kerrigan, J. J., McGill, J. T., Davies, J. A., Andrews, L., & Sandy, J. R. (1998). The role of cell adhesion molecules in craniofacial development. *Journal of the Royal College of Surgeons of Edinburgh*, *43*(4), 223-229.

- Klapper, I., Rupp, C. J., Cargo, R., Purvedorj, B., & Stoodley, P. (2002). Viscoelastic fluid description of bacterial biofilm material properties. *Biotechnology and Bioengineering*, 80(3), 289-296.
- Kortright, J. B., Kim, S. K., Denbeaux, G. P., Zeltzer, G., Takano, K., & Fullerton, E. E. (2001). Soft-x-ray small-angle scattering as a sensitive probe of magnetic and charge heterogeneity. *Physical Review B*, 64(9), 2401-2404.
- Kozlova, N., & Santore, M. M. (2006). Manipulation of micrometer-scale adhesion by tuning nanometer-scale surface features. *Langmuir*, 22(3), 1135-1142.
- Kuehner, D. E., Engmann, J., Fergg, F., Wernick, M., Blanch, H. W., & Prausnitz, J. M. (1999). Lysozyme Net Charge and Ion Binding in Concentrated Aqueous Electrolyte Solutions. *Journal of Physical Chemistry B*, 103(8), 1368-1374.
- Ladd, J., Zhang, Z., Chen, S., Hower, J. C., & Jiang, S. (2008). Zwitterionic Polymers Exhibiting High Resistance to Nonspecific Protein Adsorption from Human Serum and Plasma. *Biomacromolecules*, 9(5), 1357-1361.
- Lau, K. H. A., Bang, J., Kim, D. H., & Knoll, W. (2008). Self-assembly of Protein Nanoarrays on Block Copolymer Templates. *Advanced Functional Materials*, 18(20), 3148-3157.
- Lin, J. J., Bates, F. S., Hammer, D. A., & Silas, J. A. (2005). Adhesion of polymer vesicles. *Physical Review Letters*, 95(2).
- Linse, S., Cabaleiro-Lago, C., Xue, W. F., Lynch, I., Lindman, S., Thulin, E., Radford, S. E., & Dawson, K. A. (2007). Nucleation of protein fibrillation by nanoparticles. *Proceedings of the National Academy of Sciences of the United States of America*, 104(21), 8691-8696.
- Lubarsky, G. V., Davidson, M. R., & Bradley, R. H. (2004). Elastic modulus, oxidation depth and adhesion force of surface modified polystyrene studied by AFM and XPS. *Surface Science*, 558, 135-144.

- Lundqvist, M., Stigler, J., Elia, G., Lynch, I., Cedervall, T., & Dawson, K. A. (2008). Nanoparticle size and surface properties determine the protein corona with possible implications for biological impacts. *Proceedings of the National Academy of Sciences of the United States of America*, 105(38), 14265-14270.
- Lutz, J. F. (2008). Polymerization of oligo(ethylene glycol) (meth)acrylates: Toward new generations of smart biocompatible materials. *Journal of Polymer Science Part a-Polymer Chemistry*, 46(11), 3459-3470.
- Mahmud, G., Huda, S., Yang, W., Kandere-Grzybowska, K., Pilans, D., Jiang, S. Y., & Grzybowski, B. A. (2011). Carboxybetaine Methacrylate Polymers Offer Robust, Long-Term Protection against Cell Adhesion. *Langmuir*, 27(17), 10800-10804.
- Mahnke, J., Stearnes, J., Hayes, R. A., Fornasiero, D., & Ralston, J. (1999). The influence of dissolved gas on the interactions between surfaces of different hydrophobicity in aqueous media Part I. Measurement of interaction forces. *Physical Chemistry Chemical Physics*, 1(11), 2793-2798.
- Malaquin, L., Carcenac, F., Vieu, C., & Mauzac, M. (2002). Using polydimethylsiloxane as a thermocurable resist for a soft imprint lithography process. *Microelectronic Engineering*, 61-2, 379-384.
- Malmsten, M., Emoto, K., & Van Alstine, J. M. (1998). Effect of chain density on inhibition of protein adsorption by poly(ethylene glycol) based coatings. *Journal of Colloid and Interface Science*, 202(2), 507-517.
- Martin, J. I., & Wang, Z. G. (1995). Polymer brushes - scaling, compression forces, interbrush penetration, and solvent size effects. *Journal of Physical Chemistry*, 99(9), 2833-2844.
- Matsuda, T., Moghaddam, M. J., Miwa, H., Sakurai, K., & Iida, F. (1992). Photoinduced prevention of tissue adhesion. *ASAIO journal (American Society for Artificial Internal Organs : 1992)*, 38(3), M154-157.
- Mayor, S., & Rao, M. (2004). Rafts: Scale-dependent, active lipid organization at the cell surface. *Traffic*, 5(4), 231-240.



- McCann, M. C., Wells, B., & Roberts, K. (1992). complexity in the spatial localization and length distribution of plant cell-wall matrix polysaccharides. *Journal of Microscopy-Oxford*, 166, 123-136.
- McPherson, T., Kidane, A., Szleifer, I., & Park, K. (1998). Prevention of Protein Adsorption by Tethered Poly(ethylene oxide) Layers: Experiments and Single-Chain Mean-Field Analysis. *Langmuir*, 14(1), 176-186.
- Mehta, P., Patel, K. D., Laue, T. M., Erickson, H. P., & McEver, R. P. (1997). Soluble monomeric P-selectin containing only the lectin and epidermal growth factor domains binds to P-selectin glycoprotein ligand-1 on leukocytes. *Blood*, 90(6), 2381-2389.
- Mendez-Vilas, A., Diaz, J., Donoso, M. G., Gallardo-Moreno, A. M., & Gonzalez-Martin, M. L. (2006). Ultrastructural and physico-chemical heterogeneities of yeast surfaces revealed by mapping lateral-friction and normal-adhesion forces using an atomic force microscope. *Antonie Van Leeuwenhoek International Journal of General and Molecular Microbiology*, 89(3-4), 495-509.
- Meyer, A., Auemheimer, J., Modlinger, A., & Kessler, H. (2006). Targeting RGD recognizing integrins: Drug development, biomaterial research, tumor imaging and targeting. *Current Pharmaceutical Design*, 12(22), 2723-2747.
- Michel, R., Pasche, Stephanie, Textor, Marcus, & Castner, D. G. (2005). Influence of PEG Architecture on Protein Adsorption and Conformation. *Langmuir*, 21(26), 12327-12332
- Miller, R., Guo, Z., Vogler, E. A., & Siedlecki, C. A. (2005). Plasma coagulation response to surfaces with nanoscale chemical heterogeneity. *Biomaterials*, 27(2), 208-215.
- Milner, S. T. (1991). Polymer brushes. *Science (New York, N.Y.)*, 251(4996), 905-914.
- Minko, S., Muller, M., Usov, D., Scholl, A., Froeck, C., & Stamm, M. (2002). Lateral versus perpendicular segregation in mixed polymer brushes. *Physical review letters*, 88(3), 035502.

- Mohamed, N., Rainier, T. R., & Ross, J. M. (2000). Novel experimental study of receptor-mediated bacterial adhesion under the influence of fluid shear. *Biotechnology and Bioengineering*, 68(6), 628-636.
- Mrksich, M., Chen, C. S., Xia, Y., Dike, L. E., Ingber, D. E., & Whitesides, G. M. (1996). Controlling cell attachment on contoured surfaces with self-assembled monolayers of alkanethiolates on gold. *Proceedings of the National Academy of Sciences of the United States of America*, 93(20), 10775-10778.
- Muller, B., Riedel, M., Michel, R., De Paul, S. M., Hofer, R., Heger, D., & Grutzmacher, D. (2001). Impact of nanometer-scale roughness on contact-angle hysteresis and globulin adsorption. *Journal of Vacuum Science & Technology B*, 19(5), 1715-1720.
- Nam, J., & Santore, M. M. (2011). Depletion versus Deflection: How Membrane Bending Can Influence Adhesion. *Physical Review Letters*, 107(7).
- Nilsson, L. M., Thomas, W. E., Sokurenko, E. V., & Vogel, V. (2006). Elevated shear stress protects *Escherichia coli* cells adhering to surfaces via catch bonds from detachment by soluble inhibitors. *Applied and Environmental Microbiology*, 72(4), 3005-3010.
- NopplSimson, D. A., & Needham, D. (1996). Avidin-biotin interactions at vesicle surfaces: Adsorption and binding, cross-bridge formation, and lateral interactions. *Biophysical Journal*, 70(3), 1391-1401.
- Norde, W. (1995). Adsorption of proteins at solid-liquid interfaces. *Cells and Materials*, 5(1), 97-112.
- Obel, N., Erben, V., Schwarz, T., Kuhnel, S., Fodor, A., & Pauly, M. (2009). Microanalysis of Plant Cell Wall Polysaccharides. *Molecular Plant*, 2(5), 922-932.
- Ortega-Vinuesa, J. L., Tengvall, P., & Lundstrom, I. (1998). Molecular packing of HSA, IgG, and fibrinogen adsorbed on silicon by AFM imaging. *Thin Solid Films*, 324(1,2), 257-273.

- Ostuni, E., Chapman, R. G., Holmlin, R. E., Takayama, S., & Whitesides, G. M. (2001). Survey of Structure-Property Relationships of Surfaces that Resist the Adsorption of Protein. *Langmuir*, *17*(18), 5605-5620.
- Park, S., Bearinger, J. P., Lautenschlager, E. P., Castner, D. G., & Healy, K. E. (2000). Surface modification of poly(ethylene terephthalate) angioplasty balloons with a hydrophilic poly(acrylamide-co-ethylene glycol) interpenetrating polymer network coating. *Journal of Biomedical Materials Research*, *53*(5), 568-576.
- Park, S., Kim, H. C., & Chung, T. D. (2007). Site-specific anti-adsorptive passivation in microchannels. *Biochip Journal*, *1*(2), 98-101.
- Pasche, Stephanie, De, P., Voeroes, J., Spencer, N. D., & Textor, Marcus. (2003). Poly(L-lysine)-graft-poly(ethylene glycol) assembled monolayers on Niobium Oxide surfaces: a quantitative study of the influence of polymer interfacial architecture on resistance to protein adsorption by ToF-SIMS and in situ OWLSu OWLS. *Langmuir*, *19*(22), 9216-9225.
- Pasche, S., Textor, M., Meagher, L., Spencer, N. D., & Griesser, H. J. (2005). Relationship between interfacial forces measured by colloid-probe atomic force microscopy and protein resistance of poly(ethylene glycol)-grafted poly(L-lysine) adlayers on niobia surfaces. *Langmuir*, *21*(14), 6508-6520.
- Pasche, Stéphanie, Vörös, J., Griesser, H. J., Spencer, N. D., & Textor, Marcus. (2005). Effects of Ionic Strength and Surface Charge on Protein Adsorption at PEGylated Surfaces. *The Journal of Physical Chemistry B*, *109*(37), 17545-17552.
- Pedersen, J. S., & Sommer, C. (2005). Temperature Dependence of the Virial Coefficients and the Chi Parameter in Semi-Dilute Solutions of PEG. *Progr. Colloid Polymer Sci.*, *130*, 70-78.
- Pike, L. J. (2004). Lipid rafts: heterogeneity on the high seas. *Biochemical Journal*, *378*, 281-292.

- Plaksin, I. N., & Shafeev, R. S. (1958). The Influence of the Electrochemical Heterogeneity of the Sulfide Mineral Surface on the Xanthate Distribution under the Conditions of Flotation. *Doklady Akademii Nauk Sssr*, 121(1), 145-148.
- Pluckthun, A., & Pack, P. (1997). New protein engineering approaches to multivalent and bispecific antibody fragments. *Immunotechnology*, 3(2), 83-105.
- Priest, C., Stevens, N., Sedev, R., Skinner, W., & Ralston, J. (2008). Inferring wettability of heterogeneous surfaces by ToF-SIMS. *Journal of Colloid and Interface Science*, 320(2), 563-568.
- Ratner, B. D., & Bryant, S. J. (2004). Biomaterials: Where we have been and where we are going. *Annual Review of Biomedical Engineering*, 6, 41-75.
- Rebar, V. A., & Santore, M. M. (1996a). A total internal reflectance fluorescence nanoscale probe of interfacial potential and ion screening in polyethylene oxide layers adsorbed onto silica. *Journal of Colloid and Interface Science*, 178(1), 29-41.
- Rebar, V. A., & Santore, M. M. (1996b). History-Dependent Isotherms and TIRF Calibrations for Homopolymer Adsorption. *Macromolecules*, 29(19), 6262-6272.
- Riedel, M., Muller, B., & Wintermantel, E. (2001). Protein adsorption and monocyte activation on germanium nanopyramids. *Biomaterials*, 22(16), 2307-2316.
- Ronholm, J., Zhang, Z., Cao, X., & Lin, M. (2011). Monoclonal Antibodies to Lipopolysaccharide Antigens of *Salmonella enterica* serotype Typhimurium DT104. *Hybridoma*, 30(1), 43-52.
- Ruoslahti, E. (1996). RGD and other recognition sequences for integrins. *Annual Review of Cell and Developmental Biology*, 12, 697-715.
- Ruths, M., Johannsmann, D., Ruhe, J., & Knoll, W. (2000). Repulsive forces and relaxation on compression of entangled, polydisperse polystyrene brushes. *Macromolecules*, 33(10), 3860-3870.

- Sanford, M. S., Charles, P. T., Commisso, S. M., Roberts, J. C., & Conrad, D. W. (1998). Photoactivatable Cross-Linked Polyacrylamide for the Site-Selective Immobilization of Antigens and Antibodies. *Chemistry of Materials*, 10(6), 1510-1520.
- Santore, M. M. (2005). Dynamics in adsorbed homopolymer layers: Understanding complexity from simple starting points. *Current Opinion in Colloid & Interface Science*, 10(3,4), 176-183.
- Santore, M. M., & Kozlova, N. (2007). Micrometer scale adhesion on nanometer-scale patchy surfaces: Adhesion rates, adhesion thresholds, and curvature-based selectivity. *Langmuir*, 23(9), 4782-4791.
- Santore, Maria M., & Wertz, C. F. (2005). Protein Spreading Kinetics at Liquid-Solid Interfaces via an Adsorption Probe Method. *Langmuir*, 21(22), 10172-10178.
- Santore, M. M., Zhang, J., Srivastava, S., & Rotello, V. M. (2009). Beyond Molecular Recognition: Using a Repulsive Field to Tune Interfacial Valency and Binding Specificity between Adhesive Surfaces. *Langmuir*, 25(1), 84-96.
- Sawhney, A. S., & Hubbell, J. A. (1992). Poly(ethylene oxide)-graft-poly(l-lysine) copolymers to enhance the biocompatibility of poly(l-lysine)-alginate microcapsule membranes. *Biomaterials*, 13(12), 863-870.
- Schillemans, J. P., Hennink, W. E., & van Nostrum, C. F. (2010). The effect of network charge on the immobilization and release of proteins from chemically crosslinked dextran hydrogels. *European Journal of Pharmaceutics and Biopharmaceutics*, 76(3), 329-335.
- Shang, L., Wang, Y., Jiang, J., & Dong, S. (2007). pH-Dependent Protein Conformational Changes in Albumin:Gold Nanoparticle Bioconjugates: A Spectroscopic Study. *Langmuir*, 23(5), 2714-2721.
- Sharma, A., Konnur, R., & Kargupta, K. (2003). Thin liquid films on chemically heterogeneous substrates: self-organization, dynamics and patterns in systems displaying a secondary minimum. *Physica a-Statistical Mechanics and Its Applications*, 318(1-2), 262-278.

- Shapiro, L., McAdams, H. H., & Losick, R. (2002). Generating and exploiting polarity in bacteria. *Science*, 298(5600), 1942-1946.
- Shibata, C. T., & Lenhoff, A. M. (1992). TIRF of salt and surface effects on protein adsorption. II. Kinetics. *Journal of Colloid and Interface Science*, 148(2), 485-507.
- Shin, Y., Roberts, J. E., & Santore, Maria M. (2002). Influence of charge density and coverage on bound fraction for a weakly cationic polyelectrolyte adsorbing onto silica. *Macromolecules*, 35(10), 4090-4095.
- Slater, J. H., & Frey, W. (2008). Nanopatterning of fibronectin and the influence of integrin clustering on endothelial cell spreading and proliferation. *Journal of Biomedical Materials Research. Part A*, 87(1), 176-195.
- Sofia, S. J., Premnath, V., & Merrill, E. W. (1998). Poly(ethylene oxide) Grafted to Silicon Surfaces: Grafting Density and Protein Adsorption. *Macromolecules*, 31(15), 5059-5070.
- Sofia, S. J., Premnath, V., & Merrill, E. W. (1998). Poly(ethylene oxide) grafted to silicon surfaces: Grafting density and protein adsorption. *Macromolecules*, 31(15), 5059-5070.
- Song, J., Duval, J. F. L., Stuart, M. A. C., Hillborg, H., Gunst, U., Arlinghaus, H. F., & Vancso, G. J. (2007). Surface ionization state and nanoscale chemical composition of UV-irradiated poly(dimethylsiloxane) probed by chemical force microscopy, force titration, and electrokinetic measurements. *Langmuir*, 23(10), 5430-5438.
- Stolnik, S., Illum, L., & Davis, S. S. (1995). Long circulating microparticulate drug carriers. *Advanced Drug Delivery Reviews*, 16(2,3), 195-214.
- Strobel, M., Jones, V., Lyons, C. S., Ulsh, M., Kushner, M. J., Dorai, R., & Branch, M. C. (2003). A comparison of corona-treated and flame-treated polypropylene films. *Plasmas and Polymers*, 8, 61-95.

- Sukhishvili, S. A., & Granick, S. (1998). Kinetic regimes of polyelectrolyte exchange between the adsorbed state and free solution. *Journal of Chemical Physics*, *109*(16), 6869-6878.
- Suprun, E. V., Shilovskaya, A. L., Lisitsa, A. V., Bulko, T. V., Shumyantseva, V. V., & Archakov, A. I. (2011). Electrochemical Immunosensor Based on Metal Nanoparticles for Cardiac Myoglobin Detection in Human Blood Plasma. *Electroanalysis*, *23*(5), 1051-1057.
- Sweryda-Krawiec, B., Devaraj, H., Jacob, G., & Hickman, J. J. (2004). A new interpretation of serum albumin surface passivation. *Langmuir*, *20*(6), 2054-2056.
- Szleifer, I. (1997). Polymers and proteins: Interactions at interfaces. *Current Opinion in Solid State & Materials Science*, *2*(3), 337-344.
- Teichroeb, J. H., Forrest, J. A., & Jones, L. W. (2008). Size-dependent denaturing kinetics of bovine serum albumin adsorbed onto gold nanospheres. *European Physical Journal E: Soft Matter*, *26*(4), 411-415.
- Teichroeb, J. H., Forrest, J. A., Ngai, V., & Jones, L. W. (2006). Anomalous thermal denaturing of proteins adsorbed to nanoparticles. *European Physical Journal E*, *21*(1), 19-24.
- Thibault, C., LeBerre, V., Casimirius, S., Trevisiol, E., Francois, J., & Vieu, C. (2005). Direct microcontact printing of oligonucleotides for biochip applications. *Journal of Nanobiotechnology*, *3*(1), 1-12.
- Thomas, W., Forero, M., Yakovenko, O., Nilsson, L., Vicini, P., Sokurenko, E., & Vogel, V. (2006). Catch-bond model derived from allostery explains force-activated bacterial adhesion. *Biophysical Journal*, *90*(3), 753-764.
- Tombacz, E., & Szekeres, M. (2006). Surface charge heterogeneity of kaolinite in aqueous suspension in comparison with montmorillonite. *Applied Clay Science*, *34*(1-4), 105-124.

- Tosatti, S., De, P., Askendal, A., VandeVondele, S., Hubbell, J. A., Tengvall, P., & Textor, M. (2003). Peptide functionalized poly(L-lysine)-g-poly(ethylene glycol) on titanium: resistance to protein adsorption in full heparinized human blood plasma. *Biomaterials*, 24(27), 4949-4958.
- Tosatti, S., Schwartz, Z., Campbell, C., Cochran, D. L., VandeVondele, S., Hubbell, J.A., Denzer, A., et al. (2004). RGD-containing peptide GCRGYGRGDSPG reduces enhancement of osteoblast differentiation by poly(L-lysine)-graft-poly(ethylene glycol)-coated titanium surfaces. *Journal of biomedical materials research. Part A*, 68(3), 458-472.
- Toscano, A., & Santore, Maria M. (2006). Fibrinogen Adsorption on Three Silica-Based Surfaces: Conformation and Kinetics. *Langmuir*, 22(6), 2588-2597.
- Tsapikouni, T. S., & Missirlis, Y. F. (2007). pH and ionic strength effect on single fibrinogen molecule adsorption on mica studied with AFM. *Colloids and Surfaces, B: Biointerfaces*, 57(1), 89-96.
- Tweedle, M. F. (2006). Adventures in multivalency the Harry S. Fischer Memorial Lecture CMR 2005; Evian, France. *Contrast Media & Molecular Imaging*, 1(1), 2-9.
- Uhlmann, P., Houbenov, N., Brenner, N., Grundke, K., Burkert, S., & Stamm, Manfred. (2007). In-Situ Investigation of the Adsorption of Globular Model Proteins on Stimuli-Responsive Binary Polyelectrolyte Brushes. *Langmuir*, 23(1), 57-64.
- Verschoor, J. A., Meiring, M. J., Vanwyngaardt, S., & Weyer, K. (1990). Polystyrene, poly-l-lysine and nylon as adsorptive surfaces for the binding of whole cells of mycobacterium-tuberculosis h37 rv to elisa plates. *Journal of Immunoassay*, 11(4), 413-428.
- VandeVondele, S., Voros, J., & Hubbell, J. A. (2003). RGD-Grafted poly-l-lysine-graft-(polyethylene glycol) copolymers block non-specific protein adsorption while promoting cell adhesion. *Biotechnology and Bioengineering*, 82(7), 784-790.
- Wagner, V. E., Koberstein, J. T., & Bryers, J. D. (2004). Protein and bacterial fouling characteristics of peptide and antibody decorated surfaces of PEG-poly(acrylic acid) co-polymers. *Biomaterials*, 25(12), 2247-2263.



- Wang, Z., Hemmer, S. L., Friedrich, D. M., & Joly, A. G. (2001). Anthracene as the origin of the red-shifted emission from commercial zone-refined phenanthrene sorbed on mineral surfaces. *Journal of Physical Chemistry A*, 105(25), 6020-6023.
- Wasilewska, Monika, Adamczyk, Zbigniew, & Jachimska, B. (2009). Structure of Fibrinogen in Electrolyte Solutions Derived from Dynamic Light Scattering (DLS) and Viscosity Measurements. *Langmuir*, 25(6), 3698-3704.
- Watanabe, H., & Tirrell, M. (1993). Measurement of forces in symmetrical and asymmetric interactions between diblock copolymer layers adsorbed on mica. *Macromolecules*, 26(24), 6455-6466.
- Wei, Y., Ji, Y., Xiao, L. L., & Jian, J. A. (2010). Construction of biomimetic polymer surface for endothelial cell selectivity. *Acta Polymerica Sinica*(12), 1474-1478.
- Wei, J., Ravn, D. B., Gram, L., & Kingshott, P. (2003). Stainless steel modified with poly(ethylene glycol) can prevent protein adsorption but not bacterial adhesion. *Colloids and Surfaces B-Biointerfaces*, 32(4), 275-291.
- Wertz, C. F., & Santore, M. M. (1999). Adsorption and Relaxation Kinetics of Albumin and Fibrinogen on Hydrophobic Surfaces: Single-Species and Competitive Behavior. *Langmuir*, 15(26), 8884-8894.
- Wertz, C. F., & Santore, Maria M. (2002). Fibrinogen Adsorption on Hydrophilic and Hydrophobic Surfaces: Geometrical and Energetic Aspects of Interfacial Relaxations. *Langmuir*, 18(3), 706-715.
- Wittmer, C. R., Phelps, J. A., Saltzman, W. M., & Van Tassel, P. R. (2007). Fibronectin terminated multilayer films: Protein adsorption and cell attachment studies. *Biomaterials*, 28(5), 851-860.
- Wolfram, T., Belz, F., Schoen, T., & Spatz, J. P. (2007). Site-specific presentation of single recombinant proteins in defined nanoarrays. *Biointerphases*, 2(1), 44-48.

- Wright, A. T., & Anslyn, E. V. (2006). Differential receptor arrays and assays for solution-based molecular recognition. *Chemical Society Reviews*, 35(1), 14-28.
- Yamakawa, H. (1971). *Modern Theory of Polymer Solutions*. Harper and Row. New York
- Yamamoto, S., Ejaz, M., Tsujii, Y., & Fukuda, T. (2000). Surface interaction forces of well-defined, high-density polymer brushes studied by atomic force microscopy. 2. Effect of graft density. *Macromolecules*, 33(15), 5608-5612.
- Yamamoto, S., Ejaz, M., Tsujii, Y., Matsumoto, M., & Fukuda, T. (2000). Surface interaction forces of well-defined, high-density polymer brushes studied by atomic force microscopy. 1. Effect of chain length. *Macromolecules*, 33(15), 5602-5607.
- Yang, Z., Zhou, F., Yuan, J., Ma, L., Zhai, C., & Cheng, S. (2006). Preparation of PLL-PEG-PLL and its application to DNA encapsulation. *Science in China Series B: Chemistry*, 49(4), 357-362.
- Zalipsky, S. (1995). Chemistry of polyethylene-glycol conjugates with biologically-active molecules. *Advanced Drug Delivery Reviews*, 16(2-3), 157-182.
- Zhang, J., Srivastava, S., Duffadar, R., Davis, J. M., Rotello, V. M., & Santore, Maria M. (2008). Manipulating Microparticles with Single Surface-Immobilized Nanoparticles. *Langmuir*, 24(13), 6404-6408.